

**BUBBLE DISPERSION AND COALESCENCE  
IN TURBULENT PIPE FLOW**

by

Jianjun Luo

Submitted  
in partial fulfilment of the requirements  
for the degree of

DOCTOR OF PHILOSOPHY

Major Subject: Chemical Engineering

at

DALHOUSIE UNIVERSITY

Halifax, Nova Scotia

March, 2002

© Copyright by Jianjun Luo, 2002



National Library  
of Canada

Acquisitions and  
Bibliographic Services

395 Wellington Street  
Ottawa ON K1A 0N4  
Canada

Bibliothèque nationale  
du Canada

Acquisitions et  
services bibliographiques

395, rue Wellington  
Ottawa ON K1A 0N4  
Canada

*Your file Votre référence*

*Our file Notre référence*

The author has granted a non-exclusive licence allowing the National Library of Canada to reproduce, loan, distribute or sell copies of this thesis in microform, paper or electronic formats.

The author retains ownership of the copyright in this thesis. Neither the thesis nor substantial extracts from it may be printed or otherwise reproduced without the author's permission.

L'auteur a accordé une licence non exclusive permettant à la Bibliothèque nationale du Canada de reproduire, prêter, distribuer ou vendre des copies de cette thèse sous la forme de microfiche/film, de reproduction sur papier ou sur format électronique.

L'auteur conserve la propriété du droit d'auteur qui protège cette thèse. Ni la thèse ni des extraits substantiels de celle-ci ne doivent être imprimés ou autrement reproduits sans son autorisation.

0-612-77597-6

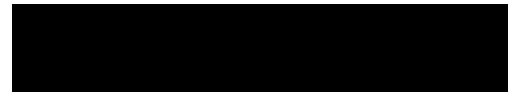
Canada

**Dalhousie University**  
**Faculty of Engineering**

The undersigned hereby certify that they have examined, and recommend to the Faculty of Graduate Studies for acceptance, the thesis entitled “Bubble Dispersion and Coalescence in Turbulent Pipe Flow” by Jianjun Luo in partial fulfilment of the requirement for the degree of Doctor of Philosophy.

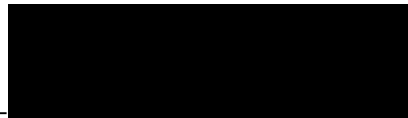
Dated: March 8, 2002

Supervisor:



Adel M. Al Taweel

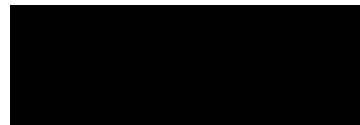
External Examiner:



Jan Czarniecki

Syncrude Canada Ltd.

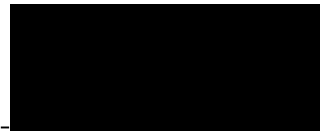
Examiner:



Feridun Hamdullahpur

Carleton University

Examiner:



Mort Fels

**Dalhousie University**  
**Faculty of Engineering**

DATE: March, 2002

**AUTHOR:** Jianjun Luo  
**TITLE:** Bubble Dispersion and Coalescence in Turbulent Pipe Flow  
**MAJOR SUBJECT:** Chemical Engineering  
**DEGREE:** Doctor of Philosophy  
**CONVOCATION:** May, 2002

Permission is herewith granted to Dalhousie University to circulate and to have copied for non-commercial purposes, at its discretion, the above title upon the request of individuals or institutions.

A solid black rectangular box redacting the author's signature.

\_\_\_\_\_  
Signature of Author

The author reserves other publication rights, and neither the thesis nor extensive extracts from it may be printed or otherwise reproduced without the author's written permission.

The author attests that permission has been obtained for the use of any copyrighted material appearing in the thesis (other than the brief excerpts requiring only proper acknowledgement in scholarly writing), and that all such use is clearly acknowledged.

IN MEMORY OF MY DEAR SISTER, CHUNHUA LUO.

# TABLE OF CONTENTS

<b>TABLE OF CONTENTS.....</b>	<b>v</b>
<b>LIST OF TABLES.....</b>	<b>viii</b>
<b>LIST OF FIGURES.....</b>	<b>ix</b>
<b>NOMENCLATURES.....</b>	<b>xv</b>
<b>ACKNOWLEDGMENT.....</b>	<b>xxii</b>
<b>ABSTRACT.....</b>	<b>xxiii</b>
<b>CHAPTER 1 INTRODUCTION.....</b>	<b>1</b>
<b>CHAPTER 2 LITERATURE REVIEW.....</b>	<b>4</b>
2.1 Hydrodynamics of Gas-Liquid Pipe Flow and Gas Distributors.....	4
2.2 Mechanism of Bubble Breakage.....	7
2.2.1 Bubble Breakage.....	7
2.2.2 Expressions of Bubble Break-up.....	10
2.2.2.1 Taylor Instability.....	11
2.2.2.2 Bubble Break-up in Isotropic Turbulence.....	12
2.3 Phenomena and Mechanisms of Bubble Coalescence.....	17
2.3.1 Bubble Coalescence Process.....	17
2.3.2 Experimental Investigation of Bubble Coalescence.....	18
2.3.3 Coalescence Models.....	22
2.3.3.1 Bubble Collision.....	22
2.3.3.2 Collision Efficiency.....	26
2.4 Effect of Interfacial Characteristic on Bubble Break-up and Coalescence.....	35
2.4.1 Interfacial Characteristics.....	35
2.4.1.1 Static Interfacial Properties.....	35
2.4.1.2 Dynamic Interfacial Properties.....	37
2.4.1.3 Models of SAA Adsorption.....	42
2.4.2 Effect of Interfacial Characteristic on Bubble Breakup.....	43
2.4.3 Effect of Interfacial Characteristic on Bubble Coalescence.....	45

<b>CHAPTER 3 EXPERIMENTAL.....</b>	<b>51</b>
3.1 Experimental Setup.....	51
3.2 Sources of Error.....	58
3.3 Systems Investigated.....	58
3.4. Methods of Parameter Computation and Turbulence Validation.....	60
3.5 Experimental Conditions .....	64
<b>CHAPTER 4 INTERFACIAL CHARACTERISTICS OF THE SYSTEMS STUDIED.....</b>	<b>66</b>
4.1 Background.....	66
4.1.1 Static Interfacial Characteristics.....	66
4.1.2 Modeling Dynamics Interfacial Diffusion / Adsorption.....	68
4.1.2.1 Short-term Approximation.....	70
4.1.2.2 Long-term Approximation.....	71
4.1.2.3 Apparent Effective Diffusivity.....	73
4.2 Selection of System.....	74
4.3 Results and Discussions .....	74
4.3.1 Static Properties of SDS and MIBC Aqueous Solutions.....	74
4.3.2 Dynamic Surface Tension of SDS Aquous Solutions.....	79
4.3.3 Parameters Derived from Diffusion/Adsorption Models.....	85
4.3.3.1 Diffusion Coefficient.....	85
4.3.3.2 Surface Excess Based on Long-term Approximation.....	87
4.4 Conclusions .....	92
<b>CHAPTER 5 BUBBLE COALESCENCE IN TURBULENT PIPE FLOW.....</b>	<b>94</b>
5.1 Theoretical Coalescence Model.....	94
5.1.1 Modeling Bubble Coalescence Rate.....	96
5.1.1.1 Turbulent Collision Frequency.....	98
5.1.1.2 Collision Efficiency.....	99
5.1.2 Normalization of Bubble Coalescence Rates.....	102
5.2 Results And Discussion.....	104
5.2.1 Effects of Hydrodynamic Factors on Bubble Coalescence Rates.....	104

5.2.1.1 Effect of Gas-up on Bubble Coalescence.....	105
5.2.1.2 Effect of Local Energy Dissipation Rate on Bubble Coalescence.....	110
5.2.1.3 Effect of Bubble Size on Coalescence Rate.....	113
5.2.2 Effect of Interfacial Characteristics on Bubble Coalescence Rate.....	120
5.2.2.1 Bubble Coalescence Retardation.....	120
5.2.2.2 Effects of Interfacial Characteristics on Bubble .....	122
5.2.3 Modeling Bubble Coalescence Rate in Industrial Systems.....	131
5.3. Conclusions.....	138
<b>CHAPTER 6 BUBBLE DISPERSION AND PERFORMANCE OF A NOVEL DYNAMIC SPARGER.....</b>	<b>140</b>
6.1 Introduction.....	140
6.2 Results and Discussions.....	142
6.2.1 Effect of Gas Hold-up.....	143
6.2.2 Effect of Local Energy Dissipation Rate.....	149
6.2.3 Effect of Interfacial Characteristics.....	156
6.2.4 Energy Consumption in Dynamic Sparger.....	165
6.2.5 Correlation of Experimental Data.....	176
6.3. Conclusions .....	112
<b>CHAPTER 7 OVERALL CONCLUSIONS AND RECOMMENDATION .....</b>	<b>178</b>
<b>REFERENCES.....</b>	<b>181</b>
<b>APPENDIX MEASURED PARAMETERS AND CALCULATED VARIABLES .....</b>	<b>223</b>



## LIST OF TABLES

Table 2.1 Critical Weber number for bubble or drop breakup in turbulent flow.....	16
Table 2.2 Comparison of the dependence of surface excess concentration and coalescence time on solute concentration (Drogaris and Weiland, 1983) .....	49
Table 4.1. Interfacial Characteristics of aqueous SDS solutions.....	79
Table 4.2 Summary of interfacial properties of SDS aqueous solutions presently investigated .....	91

## LIST OF FIGURES

Fig. 3.1 Experimental set-up.....	52
Fig. 3.2 Diagram of dynamic sparger and its installation.....	55
Fig. 3.3 Geometry of the sparger head.....	56
Fig. 3.4 Two-phase jet formed from the sparger mixes with the surrounding pipe flow stream.....	57
Fig. 3.5 Static surface tension of SDS and MIBC systems.....	59
Fig. 4.1 Schematic representation of SAA adsorbing upon gas/liquid interface.....	69
Fig. 4.2 Effect of SDS concentration on the static surface tension (obtained by extrapolating the dynamic surface tension data) (25 °C) .....	75
Fig. 4.3 Effect of bulk concentration on surface excess of MIBC aqueous solutions (25°C, data from Rajafarla, 1983) .....	78
Fig. 4.4 Applicability of the Langmuir adsorption isotherm to aqueous SDS solutions .....	78
Fig. 4.5 Dynamic surface tension of SDS aqueous solution at a low concentration range (25 °C, adapted from Yang, 1996) .....	80
Fig. 4.6 Ability of the effective diffusivity concept (Eq. 4 -14) to the model the dynamic surface tension of aq. SDS solution ( $C_0=0.0173$ mM).....	81
Fig. 4.7 Ability of the short-term approximation (Eq. 4 -8) to model the dynamic surface tension of aq. SDS solution ( $C_0=0.0173$ mM).....	82
Fig. 4.8 Ability of the long-term approximation (Eq. 4-10) to model the dynamic surface tension of aq. SDS solution (0.0173 mM) .....	83
Fig. 4.9 Dynamic surface tension of SDS aqueous solution vs $t^{-1/2}$ with a broad range of concentration (25°C).....	84
Fig. 4.10 Determining SDS diffusivity by the Fang and Joos (1996) method.....	86
Fig. 4.11 Effect of bulk concentration on the surface excess value of aqueous SDS solutions (determined using the long-term approximation).....	89
Fig. 4.12 Effect of bubble generation time on the absorption-to-diffusion characteristic time ratio for very dilute aqueous SDS solutions.....	90
Fig. 5.1 Schematic representation of bubble coalescence.....	115
Fig. 5.2a Effect of gas hold-up on bubble dispersion characteristics (20 ppm SDS, $U_L = 1.2$ m/s, $U_{LS} = 0.2$ m/s, $\epsilon_s \approx 17$ w/kg) : specific interfacial area.....	106
Fig. 5.2b Effect of gas hold-up on bubble dispersion characteristics (20 ppm SDS, $U_L = 1.2$ m/s, $U_{LS} = 0.2$ m/s, $\epsilon_s \approx 17$ w/kg) : Sauter mean bubble diameter.....	106
Fig. 5.2c Effect of gas hold-up on bubble dispersion characteristics (20 ppm SDS, $U_L = 1.2$ m/s, $U_{LS} = 0.2$ m/s, $\epsilon_s \approx 17$ w/kg) : bubble population density.....	107

Fig. 5.3a Effect of gas hold-up on bubble coalescence rate (20 ppm SDS, $U_L = 1.2$ m/s, $U_{LS} = 0.2$ m/s, $\varepsilon_s \approx 17$ w/kg) expressed by differential coefficient of specific interfacial area.....	107
Fig. 5.3b Effect of gas hold-up on bubble coalescence rate (20 ppm SDS, $U_L = 1.2$ m/s, $U_{LS} = 0.2$ m/s, $\varepsilon_s \approx 17$ w/kg) expressed by differential coefficient of Sauter mean bubble diameter.....	108
Fig. 5.3c Effect of gas hold-up on bubble coalescence rate (20 ppm SDS, $U_L = 1.2$ m/s, $U_{LS} = 0.2$ m/s, $\varepsilon_s \approx 17$ w/kg) expressed by differential coefficient of bubble population density.....	108
Fig. 5.4a Effect of gas hold-up on coalescence rate with the same initial bubble size expressed by differential coefficient of specific interfacial area (10 ppm SDS, $U_L = 1.2$ m/s, $U_{LS} = 0.2$ m/s, $\varepsilon_s \approx 17$ w/kg, $d_i = 500$ $\mu$ m).....	109
Fig. 5.4b Effect of gas hold-up on coalescence rate with the same initial bubble size expressed by differential coefficient of Sauter mean bubble diameter (10 ppm SDS, $U_L = 1.2$ m/s, $U_{LS} = 0.2$ m/s, $\varepsilon_s \approx 17$ w/kg, $d_i = 500$ $\mu$ m).....	109
Fig. 5.4c Effect of gas hold-up on coalescence rate with the same initial bubble size expressed by differential coefficient of bubble population density (10 ppm SDS, $U_L = 1.2$ m/s, $U_{LS} = 0.2$ m/s, $\varepsilon_s \approx 17$ w/kg, $d_i = 500$ $\mu$ m).....	110
Fig. 5.5a Effect of energy dissipation rate in pipe on bubble dispersion characteristics (water, $\Phi_P \approx 0.07$ ) : specific interfacial area.....	111
Fig. 5.5b Effect of energy dissipation rate in pipe on bubble dispersion characteristics (water, $\Phi_P \approx 0.07$ ) : Sauter mean bubble diameter.....	112
Fig. 5.5c Effect of energy dissipation rate in pipe on bubble dispersion characteristics (water, $\Phi_P \approx 0.07$ ) : bubble population density.....	112
Fig. 5.6 Effect of energy dissipation rate in pipe on normalized bubble coalescence rate (water, $\Phi_P \approx 0.07$ ), a) specific interfacial area, b) Sauter mean bubble diameter, c) bubble population density.....	113
Fig. 5.7a Effect of bubble size on gas/liquid dispersion characteristics (water, $U_L = 1.8$ m/s, $\Phi_P = 0.07$ , $\varepsilon_s = 25$ w/kg) : interfacial area.....	114
Fig. 5.7b Effect of bubble size on gas/liquid dispersion characteristics (water, $U_L = 1.8$ m/s, $\Phi_P = 0.07$ , $\varepsilon_s = 25$ w/kg) : bubble size.....	115
Fig. 5.7c Effect of bubble size on gas/liquid dispersion characteristics (water, $U_L = 1.8$ m/s, $\Phi_P = 0.07$ , $\varepsilon_s = 25$ w/kg) : bubble population density.....	115
Fig. 5.8 Effect of bubble size on normalized coalescence rate characteristics (water, $U_L = 1.8$ m/s, $\Phi_P = 0.07$ , $\varepsilon_s = 25$ w/kg), a) interfacial area, b) bubble diameter, c) bubble population density.....	116
Fig. 5.9a Effect of bubble size on gas/liquid dispersion characteristics (2 ppm, $U_L = 1.2$ m/s, $\Phi_P = 0.08$ , $\varepsilon_s = 16$ w/kg) : interfacial area.....	136

Fig. 5.9b Effect of bubble size on gas/liquid dispersion characteristics (2 ppm, $U_L=1.2$ m/s, $\Phi_P=0.08$ , $\epsilon_S=16$ w/kg) : bubble size.....	117
Fig. 5.9c Effect of bubble size on gas/liquid dispersion characteristics (2 ppm, $U_L=1.2$ m/s, $\Phi_P=0.08$ , $\epsilon_S=16$ w/kg) : bubble population density.....	117
Fig. 5.10 Effect of bubble size on normalized coalescence rate characteristics (2 ppm, $U_L=1.2$ m/s, $\Phi_P=0.08$ , $\epsilon_S=16$ w/kg) a) interfacial area b) bubble size c) bubble population density.....	118
Fig. 5.11 Comparison of experimental bubble coalescence rate in tap water with model predictions (Eq. 5-30). ....	119
Fig. 5.12a Effect of SDS concentration on normalized bubble coalescence rate (0, 2, 5, 10, 50 ppm, $\Phi_P=0.08$ , $\epsilon_P=16$ w/kg) : interfacial area.....	121
Fig. 5.12b Effect of SDS concentration on normalized bubble coalescence rate (0, 2, 5, 10, 50 ppm, $\Phi_P=0.08$ , $\epsilon_P=16$ w/kg) : bubble size.....	121
Fig. 5.12c Effect of SDS concentration on normalized bubble coalescence rate (0, 2, 5, 10, 50 ppm, $\Phi_P=0.08$ , $\epsilon_P=16$ w/kg) : bubble population density.....	123
Fig. 5.13a Effect of SDS bulk concentration on the gas/liquid contacting characteristics ( $\Phi_P=0.2$ , $\epsilon_P=16$ w/kg, $d_l \approx 1000$ $\mu\text{m}$ ) : interfacial area.....	123
Fig. 5.13b Effect of SDS bulk concentration on the gas/liquid contacting characteristics ( $\Phi_P=0.2$ , $\epsilon_P=16$ w/kg, $d_l \approx 1000$ $\mu\text{m}$ ) : bubble size.....	124
Fig. 5.13c Effect of SDS bulk concentration on the gas/liquid contacting characteristics ( $\Phi_P=0.2$ , $\epsilon_P=16$ w/kg, $d_l \approx 1000$ $\mu\text{m}$ ) : bubble population density.....	124
Fig. 5.14 Effect of bulk concentration on bubble coalescence rates ( $\Phi_P=0.2$ , $\epsilon_P=16$ w/kg, $d_l \approx 1,000$ $\mu\text{m}$ ) .....	126
Fig. 5.15 Effect of static surface tension on bubble coalescence ( $\Phi_P=0.2$ , $\epsilon_P=16$ w/kg, $d_l \approx 1000$ $\mu\text{m}$ ) .....	127
Fig. 5.16 Effect of surface pressure on bubble coalescence ( $\Phi_P=0.2$ , $\epsilon_P=16$ w/kg, $d_l \approx 1000$ $\mu\text{m}$ ) .....	127
Fig. 5.17 Effect of Gibbs surface excess on bubble coalescence ( $\Phi_P=0.2$ , $\epsilon_P=16$ w/kg, $d_l \approx 1000$ $\mu\text{m}$ ) .....	128
Fig. 5.18 Effect of surface excess based on long-term approximation of diffusion model on bubble coalescence ( $\Phi_P=0.2$ , $\epsilon_P=16$ w/kg, $d_l \approx 1000$ $\mu\text{m}$ ).....	128
Fig. 5.19 .Comparison of bubble coalescence rate between experiment and model by Eq.(5-37).....	135
Fig. 5.20 Comparison of bubble coalescence rate among three surface active agents (For SDS:1 mm bubble in pipeline flow, $U_{LS}=1$ m/s; for $\text{Na}_2\text{SO}_4$ and $\text{NaCl}$ : 3.8 mm bubble in bubble column, $U_{GS}=0.05$ m/s).....	137

Fig. 6.1a Effect of gas-to-liquid volumetric flow ratio on performance of two-phase dynamic sparger in MIBC solutions ( $U_L = 1.4$ m/s, $\Delta p_{\text{Sparger}} = 30$ psi) : interfacial area.....	144
Fig. 6.1b Effect of gas-to-liquid volumetric flow ratio on performance of two-phase dynamic sparger in MIBC solutions ( $U_L = 1.4$ m/s, $\Delta p_{\text{Sparger}} = 30$ psi) : bubble size.....	144
Fig. 6.1c Effect of gas-to-liquid volumetric flow ratio on performance of two-phase dynamic sparger in MIBC solutions ( $U_L = 1.4$ m/s, $\Delta p_{\text{Sparger}} = 30$ psi) : bubble population density.....	146
Fig. 6.2a Effect of gas holdup on performance of two-phase dynamic sparger with various concentrations of SDS solution ( $U_L = 1.1$ m/s, $U_{LS} = 0.1$ m/s) : interfacial area.....	146
Fig. 6.2b Effect of gas holdup on performance of two-phase dynamic sparger with various concentrations of SDS solution ( $U_L = 1.1$ m/s, $U_{LS} = 0.1$ m/s) : bubble size .....	147
Fig. 6.2c Effect of gas holdup on performance of two-phase dynamic sparger with various concentrations of SDS solution ( $U_L = 1.1$ m/s, $U_{LS} = 0.1$ m/s) : bubble population density .....	147
Figs. 6.3 Performance comparison between static and dynamic spargers ( $U_L = 1$ m/s, $Q_G/Q_L = 0.3$ , 20 ppm MIBC) .....	149
I: Bubble produced by static sparger: $d_{32} = 2,000$ $\mu\text{m}$	
II: Bubble produced by dynamic sparger: $d_{32} = 300$ $\mu\text{m}$	
Fig. 6.4a Effect of pressure drop on performance of two-phase dynamic sparger ( $U_L = 1.1$ m/s, $\Phi_G = 0.27$ , 20 ppm MIBC ) : interfacial area.....	150
Fig. 6.4b Effect of pressure drop on performance of two-phase dynamic sparger ( $U_L = 1.1$ m/s, $\Phi_G = 0.27$ , 20 ppm MIBC ) : bubble size.....	150
Fig. 6.4c Effect of pressure drop on performance of two-phase dynamic sparger ( $U_L = 1.1$ m/s, $\Phi_G = 0.27$ , 20 ppm MIBC ) : bubble population density.....	151
Fig. 6.5a Effect of pressure drop on performance of two-phase dynamic sparger in various concentrations of SDS solution ( $U_L = 1.2$ m/s, $U_{LS} = 0.2$ m/s, $\Phi_G = 0.08$ ) : interfacial area.....	151
Fig. 6.5b Effect of pressure drop on performance of two-phase dynamic sparger in various concentrations of SDS solution ( $U_L = 1.2$ m/s, $U_{LS} = 0.2$ m/s, $\Phi_G = 0.08$ ) : bubble size.....	152
Fig. 6.5c Effect of pressure drop on performance of two-phase dynamic sparger in various concentrations of SDS solution ( $U_L = 1.2$ m/s, $U_{LS} = 0.2$ m/s, $\Phi_G = 0.08$ ) : bubble population density.....	152
Fig. 6.6 Dynamic equilibrium between bubble dispersion and coalescence processes...	153

Fig. 6.7a Effect of local energy dissipation ratio $\epsilon_{\text{sparger}}/\epsilon_{\text{pipe}}$ on performance of two-phase dynamic sparger ( $U_L = 1.2$ m/s, $U_{LS} = 0.2$ m/s, $\Phi_G = 0.08$ , 20 ppm MIBC): interfacial area.....	153
Fig. 6.7b Effect of local energy dissipation ratio $\epsilon_{\text{sparger}}/\epsilon_{\text{pipe}}$ on performance of two-phase dynamic sparger ( $U_L = 1.2$ m/s, $U_{LS} = 0.2$ m/s, $\Phi_G = 0.08$ , 20 ppm MIBC) : bubble size.....	155
Fig. 6.7c Effect of local energy dissipation ratio $\epsilon_{\text{sparger}}/\epsilon_{\text{pipe}}$ on performance of two-phase dynamic sparger ( $U_L = 1.2$ m/s, $U_{LS} = 0.2$ m/s, $\Phi_G = 0.08$ , 20 ppm MIBC) : bubble population density.....	156
Fig. 6.8a Effect of MIBC concentration on performance of two-phase dynamic sparger ( $U_L=1.6$ m/s, $U_{LS} = 0.14$ m/s, $\Delta p_{\text{sparger}} = 30$ psi) : interfacial area.....	158
Fig. 6.8b Effect of MIBC concentration on performance of two-phase dynamic sparger ( $U_L=1.6$ m/s, $U_{LS} = 0.14$ m/s, $\Delta p_{\text{sparger}} = 30$ psi) : bubble size.....	158
Fig. 6.8c Effect of MIBC concentration on performance of two-phase dynamic sparger ( $U_L=1.6$ m/s, $U_{LS} = 0.14$ m/s, $\Delta p_{\text{sparger}} = 30$ psi) : bubble population density.....	159
Fig. 6.9a Effect of SDS concentration on performance of two-phase dynamic sparger ( $U_L=1.2$ m/s, $U_{LS} = 0.2$ m/s, $\Phi_G = 0.08$ , $\Delta p_{\text{sparger}} = 20$ psi ) : interfacial area.....	159
Fig. 6.9b Effect of SDS concentration on performance of two-phase dynamic sparger ( $U_L=1.2$ m/s, $U_{LS} = 0.2$ m/s, $\Phi_G = 0.08$ , $\Delta p_{\text{sparger}} = 20$ psi ) : bubble size.....	160
Fig. 6.9c Effect of SDS concentration on performance of two-phase dynamic sparger ( $U_L=1.2$ m/s, $U_{LS} = 0.2$ m/s, $\Phi_G = 0.08$ , $\Delta p_{\text{sparger}} = 20$ psi ) : bubble population density.....	160
Figs. 6.10a Effect of static surface tension on performance of two-phase dynamic sparger in comparison between SDS and MIBC solutions at the similar operation conditions ( $U_L=1.2$ m/s, $U_{LS} = 0.2$ m/s, $\Phi_G = 0.08$ , $\Delta p_{\text{sparger}} = 20$ psi ) : interfacial area.....	162
Fig. 6.10b Effect of static surface tension on performance of two-phase dynamic sparger in comparison between SDS and MIBC solutions at the similar operation conditions ( $U_L=1.2$ m/s, $U_{LS} = 0.2$ m/s, $\Phi_G = 0.08$ , $\Delta p_{\text{sparger}} = 20$ psi ) : bubble size.....	162
Fig. 6.10c Effect of static surface tension on performance of two-phase dynamic sparger in comparison between SDS and MIBC solutions at the similar operation conditions ( $U_L=1.2$ m/s, $U_{LS} = 0.2$ m/s, $\Phi_G = 0.08$ , $\Delta p_{\text{sparger}} = 20$ psi ) : bubble population density.....	163
Fig. 6.11a Effect of Gibbs surface excess on performance of two-phase dynamic sparger in comparison between SDS and MIBC solutions at the similar operation conditions ( $U_L=1.2$ m/s, $U_{LS} = 0.2$ m/s, $\Phi_G = 0.08$ , $\Delta p_{\text{sparger}} = 20$ psi ) : interfacial area.....	163
Fig. 6.11b Effect of Gibbs surface excess on performance of two-phase dynamic sparger in comparison between SDS and MIBC solutions at the similar operation conditions ( $U_L=1.2$ m/s, $U_{LS} = 0.2$ m/s, $\Phi_G = 0.08$ , $\Delta p_{\text{sparger}} = 20$ psi ) : bubble size.....	164

Fig. 6.11c Effect of Gibbs surface excess on performance of two-phase dynamic sparger in comparison between SDS and MIBC solutions at the similar operation conditions ( $U_L=1.2$ m/s, $U_{LS} = 0.2$ m/s, $\Phi_G = 0.08$ , $\Delta p_{\text{sparger}} = 20$ psi ) : bubble population density.....	164
Fig. 6.12 Comparative evaluation of the performance of various gas/liquid contactors.....	168
Fig. 6.13 Comparison of dimensionless bubble size between experiment and model by Eq.(6-14) for air-SDS aq. solutions.....	174
Fig. 6.14 Comparison of dimensionless bubble size between experiment and model by Eq.(6-21) for air-MIBC aq. solutions.....	174
Fig. 6.15 Comparison of dimensionless bubble size between experiment and correlated equation by Eq.(6-22) for both air-SDS and air-MIBC aq. solutions.....	175

## NOMENCLATURES

a	Specific interfacial area of contact	[m <sup>2</sup> /m <sup>3</sup> ]
A	Cross-sectional area of duct	[m <sup>2</sup> ]
a <sub>L</sub>	Langmuir-Von Szyszkowski constant	[mol/L]
b	Screen thickness (wire diameter)	[m]
B	Retarded van der Waals coefficient	[N.m]
c <sub>1</sub> – c <sub>2</sub>	Empirical constants	[-]
C	Bulk concentration, C <sub>MIBC</sub> for MIBC, C <sub>SDS</sub> for SDS	[mM or ppm]
C <sub>0</sub>	Concentration in bulk	[mol/m <sup>3</sup> = mM]
C <sub>a</sub>	Concentration of additive	[ppm]
C <sub>f</sub>	Frictional factor	[-]
C <sub>S</sub> (t)	Surfactant concentration at the surface at time t	[Mol/m <sup>3</sup> ]
C <sub>t</sub>	Transition concentration of electrolyte solutions	[mol/m <sup>3</sup> = mM]
D	Diameter of pipeline	[m]
d	Bubble size	[m]
d <sub>32</sub>	Sauter mean bubble diameter, $\frac{\sum n_i d_i^3}{\sum n_i d_i^2}$	[m]
d <sub>max</sub>	Maximum stable bubble diameter	[m]
dq <sub>c</sub> /dz:	Heat transfer per unit length of duct	[J/m]
D <sub>T</sub> :	Diameter of duct	[m]
E	Total energy dissipated per unit fluid mass	



E	Energy consumption	[W]
$E_{spm}$	Specific energy consumption rate per unit mass of processed stream	[J/kg]
$E_{spv}$	Specific energy consumption rate per unit volume of processed stream	[J/m <sup>3</sup> ]
f	Collision frequency	[Hz]
F	Interaction force exerted by one bubble to another	[N]
G	Mass flow rate per unit cross-sectional area (=ρu)	[kg/m <sup>2</sup> ]
$h_c$	Critical (rupture) film thickness	[m]
$h_i$	Initial film thickness	[m]
I	Intensity of scattered light beam	[μA]
$I_o$	Intensity of unscattered light beam	[μA]
$k_1, k_2$	Proportionality constants	[-]
L	Length of the pipe section in which the contacting is undertaken	[m]
$L_{12}$	Distance between two measuring points	[m]
$L_e$	Length scale of the energy-containing eddies	[m]
$L_f$	Longitudinal scale	[m]
$L_k$	Kolmogoroff length scale of turbulence	[m]
$L_p$	Optical path length	[m]
M	Surface immobility	[-]
$M_w$	Molecular weight	[g/mol]
n	Bubble population density	[1/m <sup>3</sup> ]
N	Sum of bubbles in the selected volume	[-]
$N_{TURN}$	Turns of the sparger	[-]

P	Static pressure	[psi]
P <sub>0</sub>	Pressure in the atmosphere	[psi]
P <sub>1</sub>	Pressure at the location 1 (i.e. 0.46 m after the tip of the sparger)	[psi]
P <sub>2</sub>	Pressure at the location 2 (i.e. 2.2 m after the tip of the sparger)	[psi]
P <sub>Pipe</sub>	Average pressure in the pipe (from location 1 to location 2)	[psi]
P <sub>Sparger</sub>	Pressure just before the sparger	[psi]
ΔP <sub>S</sub>	Pressure Drop across the sparger	[Pa]
Δp/ΔL	Average pressure differential	[psi/m]
Δp <sub>sparger</sub>	Pressure drop across the sparger (= P <sub>0</sub> - P <sub>1</sub> )	[psi]
Q	Volumetric flow rate	[m <sup>3</sup> /s]
Q <sub>G</sub>	Gas flow rate	[m <sup>3</sup> /s]
Q <sub>GS</sub> /Q <sub>LP</sub>	Flow ratio of gas to liquid in the pipeline	[-]
Q <sub>L</sub>	Total liquid flow rate (= Q <sub>LS</sub> + Q <sub>LP</sub> )	[m <sup>3</sup> /s]
Q <sub>LP</sub>	Liquid flow rate of main stream in the pipeline	[m <sup>3</sup> /s]
Q <sub>LS</sub>	Liquid flow rate across the sparger,	[m <sup>3</sup> /s]
Q <sub>LS</sub> /Q <sub>LP</sub>	Flow ratio of liquid in the sparger to liquid in the pipeline	[-]
Q <sub>Mix</sub>	Volumetric flow rate of gas-liquid mixture	[m <sup>3</sup> /s]
R <sub>g</sub>	Universal gas constant (8,314 J/kmol.K)	[J/kmol.K]
Re	Reynolds number, $\frac{\rho VD}{\mu}$	[-]
R <sub>cqu</sub>	Equivalent radius of annular gap inside of the sparger	[m]
R <sub>f</sub>	Film radius	[m]
S	Collision cross-sectional area	[m <sup>2</sup> ]
t <sub>c</sub>	Coalescence time	[s]

$t_{rup}$	Rupture time	[s]
$t_{th}$	Thinning time	[s]
$u_t$	Turbulent velocity	[m/s]
$U$	Superficial velocity	[m/s]
$U_{GS}/U_{LP}$	Flow ratio of gas to liquid in pipeline	[-]
$U_{LP}$	Superficial velocity of main stream in the pipeline	[m/s]
$U_{LP}$	Superficial velocity of liquid across the sparger	[m/s]
$U_{rel}$	Relative velocity of phases	[m/s]
$U_r'$	Root mean square relative velocity of two particles	[m/s]
$V$	Volume of the pipe section in which the contacting is undertaken	[m <sup>3</sup> ]
$W$	Mass flow rate	[kg/s]
$W_G$	Gas mass flow rate	[kg/s]
$W_{Pipe}$	Mass flow rate in the pipeline	[kg/s]
$W_{Sparger}$	Mass flow rate in the sparger	[kg/s]
$We$	Weber number ( $We = \frac{\rho u^2 d}{\sigma}$ )	[-]
$We_{Crit}$	Critical Weber number (around 1 for most cases)	[-]
$x$	Gas/Liquid mass flow ratio	[-]
$X$	Correction factor for coalescence time, defined in Eq. (5-32)	[-]
$z$	Coordinate along the axis of the sparger	[m]

### **GREEK SYMBOLS**

$\varepsilon$	Energy dissipation rate per unit mass	[w/kg]
$\varepsilon_p$	Energy dissipation rate in the pipe	[w/kg]

$\varepsilon_s$	Energy dissipation rate in the sparger,	[w/kg]
$\Phi_G$	Gas holdup [= $Q_G / (Q_G + Q_L)$ , in homogeneous flow]	[-]
$\Phi_{G1}$	Gas holdup at point 1	[-]
$\Phi_{G2}$	Gas holdup at point 2	[-]
$\Phi_{GS}$	Gas holdup inside of the sparger	[-]
$\Phi_{S\_STP}$	Gas hold-up in the sparger under the standard conditions	[-]
$\Phi_P$	Gas holdup in the pipeline	[-]
$\Gamma_G$	Gibbs surface excess	[mol/m <sup>2</sup> ]
$\Gamma_L$	Surface excess based on long-term approximation	[mol/m <sup>2</sup> ]
$\Gamma_\infty$	Maximum surface excess	[mol/m <sup>2</sup> ]
$\Pi_{hyd}$	Hydrophobic force	[N/m <sup>2</sup> ]
$\Pi_e$	Electrostatic force	[N/m <sup>2</sup> ]
$\Pi_{vdw}$	van der Waal force	[N/m <sup>2</sup> ]
$\kappa$	von Karman constant	[-]
$\kappa_b$	Wave number corresponding to the bubble/drop size	[m]
$\kappa_d$	Wave number of the eddies of viscous dissipation	[m]
$\kappa_e$	Wave number of the large energy containing eddies	[m]
$\lambda$	Coalescence efficiency	[-]
$\lambda_{Eff}$	Effective coalescence efficiency for contaminated systems,	

	defined in Eq. (6-31)	[-]
$\mu$	Absolute viscosity	[Pa.s]
$\mu_d, \mu_c$	Absolute viscosity of dispersed and continuous phase	[Pa.s]
$\nu_c$	Kinematic viscosity of continuous phase	[m <sup>2</sup> /s]
$\theta$	Residence time in mixer	[s]
$\vartheta$	Dimensionless relaxation time	[-]
$\rho_{G0}$	Gas density at atmosphere and room temperature (25°C)	[kg/m <sup>3</sup> ]
$\rho_d, \rho_c$	Density of dispersed and continuous phases	[kg/m <sup>3</sup> ]
$\rho_G$	Gas density	[kg/m <sup>3</sup> ]
$\rho_{GL}$	Density of gas-liquid mixture	[kg/m <sup>3</sup> ]
$\rho_L$	Liquid density	[kg/m <sup>3</sup> ]
$\rho_M$	Density of mixture	[kg/m <sup>3</sup> ]
$\sigma_0$	Surface tension in the absence of surfactant	[N/m]
$\sigma(C_S)$	Interfacial tension at surface concentration $C_S$	[N/m]
$\sigma_{sta}$ or $\sigma_{\infty}$	Static surface tension or equilibrium surface tension	[N/m]
$\sigma_t$ or $\sigma_{dyn}$	Dynamic surface tension	[N/m]
$\tau_w$	Shear rate on the wall	[N/m <sup>2</sup> ]

### **Subscripts**

0	Stagnation condition in the chamber
1	Located at point 1

2	Located at point 2
c	Continuous phase
d	Dispersed phase
e	Eddy
G	Gas
GS	Gas in the sparger
i, j	Bubble i and bubble j
L	Liquid
LP	Liquid in the pipeline
LS	Liquid in the sparger
m	Mixture of two phase
Pipe	Pipeline
S	Surface
Sparger	Sparger

**Superscripts:**

B	Bubble
t	Turbulence

## ACKNOWLEDGMENT

The author likes to express deep appreciation to the following individuals and institutions for their support in this work:

Dr. A.M. Al Taweel, for his wealth of knowledge, inspiration and constructive criticism. His guidance is not limited to academic aspect; particularly his personality and positive attitude approaching matters influence me so much. Dr. J. Czarnecki, acceptance of being my external examiner. Dr. F. Hamdullphur and Dr. M. Fels, for serving on the guiding committee and their helpful comments.

Mr. R. Dube and Mr. J. Kozel, for the technical support they provided and all my friends, for the support and friendship.

The financial support provided by Natural Sciences and Engineering Research Council, Syncrude Canada Ltd. and Dalhousie University is greatly appreciated.

A special thank is expressed to my girlfriend Haiyi Lu for her care and inspiration that torch a path for me to go forward at the last stage of my thesis writing. Thanks to my parents Yuanyu Luo and Jiuxiang Zeng and my elder brother Yijun Luo for their constant support and understanding throughout the course of this work.

## ABSTRACT

Operations involving gas phase dispersed into a liquid phase are frequently encountered in many industries such as hydrogenation, chlorination, oxygenation, ozonation, fermentation, absorption, distillation and flotation, etc., in which either gas-liquid contacting or dispensability of the gas phase play a major role. Unfortunately, the rational design of gas-liquid contactors or bubble generators is restricted by the limited understanding of the factors governing the evolution of bubble size, number, and specific interfacial area particularly in the case of industrial systems where the presence of multi-components strongly affects bubble breakage, coalescence and their equilibrium. These crucial issues are believed to control the final values of the bubble size, the specific interfacial area and the bubble population density.

The parameters used to represent interfacial characteristics, and the models used to describe the adsorption of surface active agent (SAA) were analyzed to obtain an insight into what the presence of extra-additives would do in industrial streams. By taking sodium dodecyl sulfate (SDS) as an example, its static and dynamic interfacial properties were evaluated and it was found that its adsorption dynamics closely follow the long-term approximation of diffusion-controlled model. A general method was developed to determine the static and dynamic interfacial characteristics of various streams.

An experiment for investigating bubble coalescence rate in turbulent pipe flow was designed based on measuring evolution of the specific interfacial area at two locations along the pipeline. A broad range of operating conditions (i.e.  $0.008 < \Phi_G < 0.5$ ,  $4 < \epsilon_p < 26$  w/kg,  $25 \mu\text{m} < d_{32} < 8,700 \mu\text{m}$ , and SDS concentration range of 0 - 50 ppm) were investigated. Three bubble coalescence rates were developed based on the temporal rate of variation of Sauter mean diameter, specific interfacial area, and bubble population density and the resulting findings were discussed in terms of hydrodynamic factors (including gas hold-up, energy dissipation rate and bubble size) and interfacial properties. The bubble coalescence rate was found to increase as the gas hold-up and the energy dissipation rate increase, and decrease as the bubble size and SAA concentration increase. Compared to tap water, the normalized coalescence rates were found to decrease radically by the presence of minute dosage of SAA due to the decisive role interfacial characteristics play. The exponential format of interfacial parameters can be used to characterize their effect on bubble coalescence processes, which implies that the interfacial characteristics affect the bubble coalescence through influencing coalescence efficiency which leads to decreasing bubble coalescence rate in gas/liquid turbulent flow. A theoretical collision model was adapted to the case of bubble coalescence rate in turbulent two-phase flow in pipes, and the resulting expression was found to apply not only to pure water system but also to contaminated streams displaying surface activity. The use of different interfacial parameters (such as the static surface tension, surface pressure, Gibbs surface excess and surface excess based on long-term approximation) to explain how SAA retards bubble coalescence rate was evaluated and it was found although the dimensionless forms of these interfacial parameters are correlated with bubble coalescence rate for SDS aqueous solutions to the similar degrees, the surface excess based on the long-term approximation could prevail due to its revealing the underlying mechanism of coalescence hindrance.



Factors affecting bubble dispersion and sparger performance were systematically investigated through the use of a 25.4 mm pipe loop in which liquid velocities of up to 3.2 m/s, and gas holdup varying between 0.008 and 0.5 were tested. Trace dosage of either MIBC or SDS was added to simulate the industrial streams. The use of novel dynamic spargers results in the formation of large interfacial area of contact (up to 5,400 m<sup>2</sup>/m<sup>3</sup>) and small bubbles ( $d_{32}$  down to 25  $\mu$ m). The efficiency by which dynamic spargers utilize energy for the formation of interfacial area was found to be one order of magnitude higher than that obtained in mechanically-agitated tanks and traditional pipe nozzles, and more efficient than some of the commonly used static mixers operating at the same power input per unit mass of the stream processed. The interfacial area and the Sauter mean bubble size can be predicted by using correlation equations for MIBC and SDS aqueous solutions.

## CHAPTER 1 INTRODUCTION

Many industrial processes include operations in which gas phase is dispersed in a liquid phase with or without suspended solids. Such multiphase contacting apparatuses have great applications as reactors in chemical and biochemical processes including hydrogenation, chlorination, oxygenation, ozonation, fermentation, etc., and in separation processes such as absorption, distillation and flotation. In many cases, the overall performance of such units is limited by the rate of mass transfer between the phases, which is strongly dependent on the interfacial area of contact. The interfacial area is, in turn, determined by the volume fraction of the gas phase and by the bubble size and its distribution, both of which are strongly influenced by the hydrodynamic and interfacial characteristics of the multi-phase system.

The importance of bubble breakup is obvious since the breakup of the gas into smaller bubbles results in the formation of larger interfacial area between the phases. However, bubble coalescence emerges as a determining factor that controls the evolution of bubble size and size distribution in naturally occurring and man-made gas-liquid dispersions. Coalescence is strongly influenced by the presence of electrolytes, surfactants, or any other third that exhibits surface activity. The bubble size, the interfacial area and the bubble population density are therefore strongly influenced by system properties, particularly by its interfacial characteristics. Although extensive studies on the hydrodynamics and mass transfer in multiphase reaction have been reported in the literature, variations of bubble size and size distributions due to varying system properties cannot be easily predicted. This is mainly due to the limited understanding of the mechanism of bubble break-up and coalescence in impure systems.

There are a number of investigations that deal with gas-liquid contacting in which bubble coalescence takes an important role, however this role hasn't clearly been stated. However, the effect of additive concentration, or interfacial tension, on the coalescence time is well investigated for the interaction between two adjacent bubbles as well as in the case of foam formation and destruction. Obviously the hydrodynamics of those two

cases are so different from industrial processes such as the bubble evolution occurring in bubble columns, mechanically agitated tank or turbulent pipelines but the insight they provide may be used as a first approximation. It is not clear how the interfacial properties except the concentration and the surface tension of contaminated streams influence the bubble coalescence, which interfacial parameters are responsible for this influence. There is no general agreement concerning the mechanism by which these phenomena are influenced. A significant part of the uncertainty associated with the design and scale-up of gas/liquid contactors arises from a lack of fundamental understanding of these counteracting processes and how they behave in industrial situations where the presence of third components can strongly affect the overall behavior of the system. Better understanding of the role surfactants play in bubble dispersion/coalescence could lead not only to improved process efficiencies, but can also provide a more rational basis for contactor design.

This thesis was therefore undertaken with the objectives of determining the factors that influence bubble dispersion and coalescence in turbulent pipe flow and characterizing the role of interfacial properties in bubble coalescence process.

The state of the knowledge concerning the factors affecting bubble breakage and coalescence are reviewed in Chapter 2 (Literature review) whereas details concerning the experimental setup, systems used and methodology of computing relevant parameters are presented in Chapter 3 (Experimental). Knowledge concerning the kinetics of diffusion/adsorption of surface activate agent (SAA) on gas/liquid interfaces is needed in order to understand the hydrodynamic and interfacial factors affecting film drainage/stability and bubble rupture/coalescence. An in depth analysis of the static and dynamic interfacial characteristics of dilute aqueous SDS solutions (the system used in the present investigation) was undertaken in Chapter 4. This knowledge was used to develop reliable values for static surface tension, surface pressure, Gibbs surface excess, dynamic surface tension, diffusivity, surface excess based on long-term approximation, that are able to well describe the data generated in this investigation, as well as those reported by other investigators.

Using the experimental data of the specific interfacial area, as well as the Sauter mean diameter and bubble population density derived from such measurements, the bubble coalescence rates were computed and the effect of various hydrodynamic and interfacial parameters were analyzed in Chapter 5. A theoretical collision model was adapted to the case of bubble coalescence in turbulent two-phase pipe flow. It takes into account the effect of hydrodynamic factors (gas holdup, turbulent energy dissipation rate, and bubble size) as well as the effect of interfacial characteristics that were obtained in Chapter 4. This model was obtained by incorporating the factors affecting coalescence efficiency and was found capable of correlating bubble coalescence rather well over a five order of magnitudes.

In Chapter 6, the factors affecting bubble dispersion and the performance of dynamic spargers are analyzed. It was found to be capable of generating large interfacial area of contact, and very small bubbles, when bubble coalescence is hindered by the presence of SAA. It was also found to be more efficient than some of the commonly used static mixers operating at the same power input per unit mass of the stream processed. The interfacial area and the Sauter mean bubble size can be predicted by using correlation equations for MIBC and SDS aqueous solutions respectively. Finally, overall conclusions are drawn in Chapter 7.

## CHAPTER 2 LITERATURE REVIEW

### 2.1 Hydrodynamics of Gas-Liquid Pipe Flow and Gas Distributors

#### 2.1.1 Gas-Liquid Pipe Flow

The problem of two-phase concurrent gas-liquid flow in pipelines has become of great concern to engineers in recent years. This type of flow is encountered in an increasing number of important situations, and a clear understanding of the rates of transfer of momentum, heat, and material in such systems is required for proper design and operation of a wide variety of chemical engineering equipment and processes. Two-phase pipeline flow is commonly encountered in the production and transport of crude petroleum and petroleum products. It is also encountered in the operation of many heat transfer equipment such as steam generators, refrigeration equipment, evaporators, and partial condensers. A growing number of such potential applications can also be found in the wastewater, metallurgical and mining processing industries.

Most of the investigations dealing with concurrent gas/liquid two-phase flow focused on the hydrodynamic conditions and the ability to predict flow patterns, pressure drop, and volume fractions of the phases. Mass, momentum, mechanical energy, and total energy balance equations are usually considered first and used as a framework in which to interpret experimental data. The most reliable prediction of multiphase behaviors generally requires the use of experimental data or correlations. Mechanistic models were developed by Barnea, et al. (1985, 1993) and Taiteland, et al. (1980, 1997) and used to predict flow pattern. For fully developed incompressible co-current flow of gases and liquids in vertical pipes, it showed a reasonable agreement with experimental flow patterns.

Detailed studies of void fraction and velocity profiles were performed by Ganchev and Peresadko (1985) and Wang, et al. (1987). Nakoryakov, et al. (1996) studied gas-liquid bubbly flow in vertical pipes and found that all the velocity profiles were deformed to be more blunter as compared to a single phase parabolic profiles. Many investigations dealing with the flow behavior of gas-liquid mixtures are based on the use of the

Lockhart-Martinelli parameter (Lockhart and Martinelli, 1949) which is essentially expressed as the ratio of the two-phase pressure drop to that obtained in the case of single phase (the continuous liquid phase) flow. This approach was successful for many conditions, as discussed by Barocsy (1966), Chisholm (1978), Chen and Spedding (1981) and Marie (1987). In contrast to the case of a liquid flow, the flow of gas-liquid mixtures under bubbly flow conditions undergoes significant acceleration along the tube as the critical choking point is approached. This has been discussed in detail by Davis (1974) and Herringe and Davis (1978).

Whilst the application of mixing length considerations to two-phase flow has been discussed by Beattie and Whalley (1982), the main body of experimental observations relating to two-phase pressure drop and wall friction has been obtained for flow in smooth tubes. The experiments with rough and smooth pipes by Jensen et al. (1985) and Davis (1990) have shown generally similar increases in the wall friction factor due to bubble addition, and the wall friction was found to increase with increasing void fraction in the mixture. The smallest bubble size was less than the turbulent buffer layer thickness for both rough and smooth wall tubes, and it was therefore to be expected that the wall friction would be modified to some extent by the presence of the gas phase.

### **2.1.2 Gas Distribution**

In general, gases are introduced through distributors where bubbles are generated to form gas-liquid two-phase flow. Characterization of sparger performance is thus of concern to many fields, such as chemical engineering, mineral processing and agriculture engineering (Mikekiilineni and Kinickle, 1985; Xu and Finch, 1989; Al Taweel et al., 1995). In the case of spargers used for flotation columns, several empirical and analytical relationships, relating the bubble size generated to the operational variables, have been reported by several investigators (Ahmed and Jameson, 1985; Szatkowski and Freyberger, 1985; Szatkowski, 1987; and Ramadan, 1996). The behavior of gas-liquid turbulent jets received considerable attention with the early work being reviewed by Abdel-Aal et al. (1966) and Goldschmidt et al. (1971). Past analysis of gas/liquid jets was based on the classical integral models of single-phase flow, e.g. Turner (1969), Chesters

et al. (1980) and McDougall (1978), this was efficient for gaining a general understanding of bubbly jets.

The purpose of using spargers is to generate fine bubbles which provide large interfacial area of contact and/or provide liquid agitation within the vessel. Spargers are usually divided into two main categories namely, static and dynamic. The former includes perforated plates, porous plates and simple tubes, whereas the latter, in which gas is dispersed by the kinetic energy of a liquid stream, includes jet ejectors, venturi jets, two-phase venturis, and slot jet spargers (Ramadan, 1996). The perforated plates provide high gas throughputs but generate relatively large bubble sizes that, in turn, produce small gas holdups and interfacial areas of contact. Porous spargers may be made of glass, ceramics, metal, and plastics and produce small bubbles with a narrow bubble size distribution. Unfortunately, they have limited gas throughputs and tend to plug when used in conjunction with slurries. In the case of simple tube spargers, the bubbles are formed as soon as the gas jet begins to break up and the ascending bubbles are exposed to the mechanical shear action present in the bulk of the liquid. They are, however, not as effective as perforated and sintered plate alternatives, as both gas holdup and interfacial area were rather low (Deckwer, 1992).

A dynamic sparger system can be used to obtain a high level of gas dispersion. The motive jets create a high-energy dissipation zone in which the gas breaks up into small entities. The use of jet ejector offers the advantage of being able to simultaneously suck the gas into the system as well as dispersing it in the liquid. As a result of a large amount of motive liquid being used for mixing and distribution of gas, the injector-type spargers provide a bigger total exchange surface for the same level of energy input.

Two phase gas-liquid ejectors were used for gas distribution in many gas-liquid operations such as: processing of natural gas to remove H<sub>2</sub>S or CO<sub>2</sub>, hydrogenation, chlorination, direct-contact heat exchangers, pressure-suppression devices, gas mixing and dissolution systems, wastewater treatment, bubble breakwaters, ice prevention systems in harbors, oil-well blowout, reservoir destratification and the confinement of

spills (Grosz-Roll, 1972; Mutsakis, et al., 1986; Rader, et al., 1989; Zahradnik et al., 1997).

Spargers have been proposed for generating small bubbles that can enhance performance of flotation devices. In this case, it is important for the sparger used to be able to provide bubbles of the desired size (and size distribution) in order to meet changing processing requirements. In addition, they should also be robust, easily maintained, exhibit little tendency to be plugged. Unfortunately, little information is available concerning sparger performance and most of the data reported in the literature were obtained using pure liquids, although it is known that up to 15-fold increase in interfacial area can be obtained in the presence of coalescence-hindering material (Cheng, 1994; Al Taweel et al., 1995).

The benefits obtained by using better gas dispersion devices were exemplified by the findings of Fregapane, et al. (1999) who reported significant improvement in acetic acid fermentation rate using a novel type of gas-liquid dynamic sparger in conjunction with a 100-L industrial scale bubble column reactor. A linear relationship was obtained between overall productivity and  $k_La$  with different operating conditions and fermentation scales.

## **2.2 Mechanism of Bubble Breakage**

The gas-liquid contacting devices have major applications as reactors in chemical and biochemical processes (Ramachandran and Chaudhari, 1983; Schugerl et al., 1977; Doraiswamy and Sharma, 1984), as well as in separation processes like absorption and distillation. The performance of the reactors is often dependent on the rate of gas-liquid mass transfer in addition to other mass transfer steps and reaction kinetics. The former is controlled by the interfacial area in the reactor and the mass transfer coefficient. One of the most important parameters influencing the interfacial area of contact in multiphase systems is the frequency of bubble breakup and coalescence; hence, proper understanding these phenomena is necessary.

### **2.2.1 Bubble Breakage**

The phenomenon of bubble breakage plays an important role in determining the performance of gas liquid contactors. This topic has been reviewed by Levich (1962),



Walter and Blanch (1986), Hesketh, et al. (1991), Wilkinson, et al. (1993), Zahradnik, et al. (1997), and Hibiki and Ishii (2000).

Experimental research dealing with bubble breakup can be categorized into three main groups:

- Breakup of single bubbles (2-7 mm) in a turbulent shear field (Levich, 1962; Arndt, 1987; Dodd et al., 1988; Frizell and Arndt, 1987; Hesketh et al., 1987; Killen, 1981; Lewis and Davidson, 1982; Pandit and Davidson, 1986; Sevik and Park, 1973; Walter and Blanch, 1986; Wilkinson and van Dierendonck, 1990; Janssen, et al. 1994; Uchida, T. and Iguchi, 2001).
- Breakup of spherical cap bubbles rising in a stagnant liquid (Levich, 1962; Batchelor, 1987; Grace et al., 1978; Walter, 1983). Breakup of spherical cap bubbles due to collision with a sphere (Levich, 1962; Frijlink, 1987; Henriksen and Ostergaard, 1974; Chen and Fan, 1989; Kim and Kim, 1990; Tsuchiya, et al., 1996; Hibiki and Ishii, 2000).
- Breakup of bubbles in the presence of other bubbles such as those encountered in bubble columns (Levich, 1962; Otalce et al., 1977; Walter, 1983; Prince and Blanch, 1990; Zakharov, et al., 1993; Tsuchiya, et al., 1996; Zahradnik, et al., 1997).

As observed by Walter (1983), a single mechanism of breakup was observed in the experiments, and most of the breakup events occurred in the isotropic core of the tube. This mechanism could be modeled by three stages: oscillation, dumbbell stretching, and pinching off. As a bubble larger than the maximum stable size traveled down the center of the tube, its surface oscillated and rippled due to the fluctuating pressure forces. The bubble then stretched into the shape of a dumbbell with two large centers of mass connected by a thin strand of fluid. This strand was pinched off and two independent bubbles were formed. The dumbbell-stretching step seemed to be the controlling step and breakup required a total time of about 25 ms in the case of low flow rates.

Walter and Blanch (1986) further reported that bubble breakup was controlled by hydrodynamic conditions for the following three cases:

- Turbulent Flow: Bubble breakup is caused by fluctuating eddies that tear up the bubble surface.
- Laminar Flow: Viscous shear at the bubble surface will elongate the bubble and ultimately cause breakup.
- Stagnant Liquid: Bubble break-up was caused by surface instabilities and wake vortices.

Hesketh, et al. (1991), found two types of bubble breakage mechanisms in turbulent pipe flow,

- The most prevalent type of breakage was a result of a bubble undergoing large-scale deformations,
- The second type of breakage appeared to be caused by some type of tearing mechanism and resulted in a very small volume of gas being torn from the original bubble.

Bubble breakage was also found to typically result in the formation of two unequal-sized bubbles. This observation is significant since most theoretical investigators assume that the sizes formed from bubble breakage were either equal volume or normally distributed (Tavlarides and Stamatoudis, 1981).

Wilkinson et al. (1993) characterized the bubble breakage in two-phase pipe flow and their findings can be summarized as follows:

- Bubble velocities in horizontal flow were found to be almost equal to the average liquid velocity, and in vertical pipe flow, the bubble velocity was only slightly larger,
- In vertical pipe flow the bubbles rose into spiral motion from the pipe center to the wall and back. Presumably, this spiral motion is similar to the spiral motion that ellipsoidal bubbles show when they rise in a stagnant liquid,

- High-speed films revealed that the bubble surface oscillated and rippled while the bubbles were constantly being deformed. Surprisingly, the extremely gross deformations did not necessarily lead to immediate bubble breakup,
- A part of the bubble lagged behind at the pipe wall causing a deformation of the bubble, eventually bubble breakup occurred relatively frequently. This was caused by the shear forces associated with the high velocity gradients and associated high turbulent energy dissipation rates near the wall,
- Most bubbles consisted of two parts connected by a relatively thin neck. The "bubble neck" decreased in size as bubble break-up progressed. Furthermore, the two parts of the bubbles that were connected by the bubble neck did not remain equal in size. The smaller half progressively decreased in size, implying that gas was flowing through the bubble neck during the breakup stage.

Their main conclusion that could be drawn from these observations is that bubble breakup always proceeded through a mechanism in which a neck connects between two parts of the bubble, but that the formation of a bubble neck is not a sufficient condition for bubble breakup to occur.

In addition, Miyahara et al. (1991), Stewart (1995) and Tsuchiya, et al. (1996) observed that the wake could also be considered to be responsible for bubble breakage.

In a summary, the popularly accepted mechanism of bubble breakage in turbulent flow is caused by bubble-eddy collisions. The second theory is that bubble breakage is essentially due to instabilities of the bubbles --- the bubbles larger than a critical size are subjected to breakup and they break all with the same velocity. The third interpretation is wake effect, i.e. the wake-driven collisions lead to the bubble breakage. The last two are often applied to laminar flows.

### **2.2.2 Expressions of Bubble Break-up**

Available mathematic description of the bubble breakage is discussed in this section, such as bubble breakage due to instability, bubble-eddy collision, and also some empirical correlations.

### 2.2.2.1 Taylor Instability

For large spherical cap bubbles, Wilkinson, et al. (1993) showed that bubble breakup would occur only when a destabilizing force that acted on the bubble was larger than the capillary force that tended to oppose bubble deformations. The major destabilizing force was gravity force acting on the bubble interface at the roof of the bubble, which could lead to the so-called Taylor instabilities. Many photographs that showed large bubbles splitting due to the formation of a growing indentation at the roof of the bubble had been published to support this mechanism (Levich, 1962; Clift and Grace, 1972; Rowe and Partridge, 1964; and Walter, 1983). Mathematical descriptions for this type of bubble breakup have been suggested by a number of authors (Levich, 1962; Grace, et al, 1978; Batchelor, 1987; Walter, 1983) based on linear perturbation analyses similar to the one originally proposed by Taylor (1950), and the results of these analyses generally express the maximum bubble diameter as,

$$d_{\max} = C \sqrt{\frac{\sigma}{gd\rho_l}} \quad (2-1)$$

where C is a constant, d is the bubble diameter,  $\rho_l$  is the density of continuous liquid phase while  $\sigma$  is the static/equilibrium surface tension. For small bubbles, the gravitational forces are usually neglected in comparison with the surface tension force. Breakup of these small bubbles is generally expected to occur due to shear stresses in the liquid, which are generated by velocity gradients. A mathematical description of this process is extremely complex due to the fact that the dynamic deformation of the bubble has an influence on the liquid shear flow around it, and the surface tension force depends on the shape of the bubble and will, thus, also change during bubble breakup and bubble deformations.

The instability was originally derived from big cap bubbles, but it is one of the mechanism for small bubble breakage too (Hesketh, et al., 1991a).

### 2.2.2.2 Bubble Breakup in Isotropic Turbulence

The most commonly used models of bubble break-up in turbulent flow are based on the descriptions of Kolmogoroff (1949) and Hinze (1955) but different authors adapted or extended them to their particular cases. Hinze (1955) suggested that a bubble would break up if the ratio of the inertial and surface tension forces, expressed in the form of a Weber number, exceeded a critical value. The critical Weber number is given as,

$$We_c = \frac{\rho_l \overline{u^2} d_{max}}{\sigma} \quad (2-2)$$

Since  $\overline{u^2}$  is mean-square fluctuating velocity term,  $We_c$  is obviously a function of the local flow pattern responsible for the deformation of the bubble. An expression for mean square velocity can be obtained by considering Kolmogoroff's theory of local isotropic turbulence (Kolmogoroff, 1949). According to this theory, the primary eddies, of scale similar in magnitude to the turbulence generating element (for example, the impeller diameter in stirred tanks, duct diameter in pipe flow) are anisotropic. However, they lose their directional nature rapidly as they disintegrate into smaller ones in a cascade fashion. The smallest eddies are statistically independent of the main flow and are responsible for energy dissipation by viscous effects. In this range of eddies the flow can be considered to be locally isotropic. Kolmogoroff's analysis suggests that the eddies in the inertial sub-range are the main contributors to the kinetic energy responsible for bubble breakup, and that the energy contained in the inertial sub-range of the spectrum is solely determined by the rate of energy dissipation per unit mass,  $\varepsilon$ . Batchelor (1951) has given an expression for  $\overline{u^2}$  in this region in terms of  $\varepsilon$  as,

$$\overline{u^2} = C(\varepsilon d_{max})^{2/3} \quad (2-3)$$

The following equation can thus be used to estimate  $d_{max}$ ,

$$d_{max} = C \frac{\sigma^{3/5}}{\varepsilon^{2/5} \rho_l^{3/5}} \quad (2-4)$$

A critical Weber number would exist at the point where cohesive and disruptive forces are balanced, resulting in a maximum stable bubble size. Levich (1962) postulated this force balance, but he also considered the balance of the internal pressure of the bubble with the capillary pressure of the deformed bubble. The dispersed-phase density was included through the internal pressure force term, and the capillary pressure was determined from the shape of the deformed bubble rather than the spherical bubble. Levich's critical Weber number was thus given as,

$$We'_{crit} = \frac{\tau}{\sigma/d_{max}} \left( \frac{\rho_g}{\rho_l} \right)^{1/3} \quad (2-5)$$

The dynamic pressure force of the continuous phase acting on the dispersed phase was characterized by Hinze (1955) as,

$$\tau = \rho_l \overline{u^2} \quad (2-6)$$

As is the case in Eq.(2-3), the mean-square spatial fluctuating velocity term,  $\overline{u^2}$ , describes the turbulent pressure forces of eddies sized  $d$  and is defined as the average of the square of the differences in velocity over a distance equaling to the bubble or drop diameter.

Therefore, Levich's  $d_{max}$  can be expressed as:

$$d_{max} = \left[ \left( \frac{We'_{crit}}{2} \right)^{0.6} \right] \left[ \frac{\sigma^{0.6}}{(\rho_l^2 \rho_g)^{0.2}} \right] \epsilon^{-0.4} \quad (2-7)$$

These theories predict a maximum stable bubble size for a given turbulent flow field and fluid physical properties. However, the time required for a bubble to reach its stable bubble size for a given level of turbulence has not been considered in the development of gas/liquid dispersion units. As a result, many equipment specific equations have been obtained by correlating bubble or drop size data without regard for the time that the bubble or drop have spent in the pertinent turbulent flow field.

For instance, if a large bubble is placed in a turbulent flow field for an infinite time, it will break up to bubble sizes smaller than or equal to the maximum stable bubble size for that particular turbulence level. If the same bubbles were in a turbulent flow field for a time shorter than that required to break to its stable size then some of the resulting bubble sizes will be larger than the maximum stable size. In two-phase contactors, there are active zones in which bubbles will break up, and inactive zones in which the turbulence level was too low for breakup. In designing two-phase contactors, one must take into account that bubble residence times in the equipment are of the order of seconds. Bubbles may only be in the active zone for a fraction of the residence time, and some of the resulting bubbles will be larger than the maximum stable bubble size.

The first condition for application of the theory of bubble breakage in isotropic turbulence is that the Reynolds number of the main flow should be sufficiently high that the flow is fully turbulent; the second one was that,

$$L_e > d > L_k \quad (2-8)$$

where  $L_e$  is the scale of the primary eddies and  $L_k$  is the scale of energy dissipating eddies of the viscous sub-range. As an order of magnitude, the dimension  $L_e$  is usually taken to be equal to the impeller blade width for stirring tanks (Shinnar and Church, 1960) and sometimes the diameter of pipes or vessels is chosen for  $L_e$  in regard to pipes or columns (Prince and Blanch, 1990; Kawase and Moo-Young, 1990). The energy dissipating length scale,  $L_k$ , is Kolmogoroff length scale, and is approximated by the relation (Hinze, 1975 and Baldyga and Bourne, 1999),

$$L_k = \nu^{3/4} \varepsilon^{-1/4} \quad (2-9)$$

where  $\nu$  is the kinematic viscosity of the continuous phase and  $\varepsilon$  is the energy dissipation rate per unit mass in the region surrounding the bubbles.

Clift, Grace and Weber (1971) reviewed Hinze's theory and concluded that,

- The total local shear stress imposed by the continuous phase acted to deform a drop or bubble, and to break it if the counterbalancing surface tension forces and viscous stresses inside the fluid particle were overcome,
- Due to the ability of bubbles and drops to follow the motion of large and slow turbulent eddies, only the energy associated with eddies of length scales smaller than a critical size was available to cause bubble splitting.
- Moo-Young and Blanch (1981) as well as Parthasarathy, et al. (1991) found that the forces controlling bubble size in stirred vessels are the inertial forces due to dynamic pressure fluctuations and the surface tension forces. The inertial forces tended to deform the bubbles but the surface tension forces resist the deformation. Prince and Blanch (1990) findings for air-water in bubble column also suggested that bubble breakup occurred through bubble interactions with turbulent eddies. It is believed that eddies responsible for breakup were those equal to or marginally smaller than the bubble size. Larger eddies simply transported the bubble without causing breakup, while very small eddies did not contain sufficient energy to affect breakage.

Experimental studies to determine the breakage time of a bubble in a turbulent flow field have not been conducted, but an estimate can be made using bubble and drop size data from pipeline flow. A bubble or drop formed in the introduction zone in a pipeline and passing in an active zone near the wall (where turbulent energy dissipation is concentrated) would undergo a series of breakages until the resulting bubble or drop sizes were less than or equal to the maximum stable bubble size for the active zone (Hesketh, 1987). The time required to achieve the maximum stable bubble size could be estimated by visual or photographic observations and had been found to range from 1.5 to 11 seconds or even longer depending on bubble size, bubble concentration and dynamics of fluid flow (Sleicher, 1962; Collins and Knudsen, 1970; Kubie and Gardner, 1977).

The concept of bubble breakage in turbulent flow determined by bubble-eddy collision has been widely accepted (Lee, et al., 1987; Prince and Blanch, 1990; Grienberger, 1992;



Wilkinson et al., 1993). However, it appears that the critical Weber number varied among different authors (Table 2.1).

Table 2.1 Critical Weber number for bubble or drop breakup in turbulent flow

Reference	Method	We <sub>c</sub>
Hinze (1955)	Drop breakup	0.6
Sevik and Park (1973)	Bubble breakup in liquid jet	1.2
Lewis and Davidson (1982)	Bubble breakup in liquid jet	4.7
Kang and Leal (1989)	Theoretical	> 6*

\* The exact value was found to depend on the type of shear flow

Recently, Risso (2000) summarized the critical Weber number that is applied to the breakup of either bubbles or drops in his review.

Chen and Al Taweel (1995) used the Weber number to correlate to Sauter mean diameter instead of the maximum bubble size. It was found to fit the experimental data of bubble breakage downstream from static mixer (i.e. screen) rather well in the case of gas/liquid turbulent flow in pipelines.

$$d_{32} = 0.577We^{-0.672}\Phi^{0.667}\left(\frac{b}{M}\right)^{-0.263} \quad (2-10)$$

where  $b$  is bar diameter and  $M$  is wire mesh size.

Many other mathematical models either incorporate one or some of the other affecting factors into their expressions such as, wake interactions, bubble swarm velocity and the shape of the bubbles, etc. (Grienberger, 1992; Wilkinson, et al., 1993; Colella, et al.,

1999), or applies statistic analysis to obtain a sophisticated stochastic model, such as bubble population balance model (Hesketh, 1987; Colella, et al., 1999; Sirijeerachai, 2002). However, they will not provide any insights of bubble breakage.

## **2.3 Phenomena and Mechanisms of Bubble Coalescence**

In this section, the mechanism of bubble coalescence will be discussed, particular attention will be given to the process of bubble coalescence, factors that influence coalescence processes, and the methods used to model bubble coalescence.

### **2.3.1 Bubble Coalescence Processes**

A very limited number of papers addressed bubble coalescence under turbulent hydrodynamic conditions, instead most papers studied bubble coalescence under limited agitation conditions. These will be reviewed here,

Although bubble coalescence in turbulent flow is not clear, based on previous investigation of adjacent two bubble and de-foaming process, the bubble coalescence is believed to occur in three steps:

1. The approach of two bubbles within a distance of 10-100  $\mu\text{m}$  from each other and the formation of a thin film between them (usually referred to as the quasi equilibrium film thickness). The initial thickness of such a film is typically 1 ~ 10  $\mu\text{m}$  (Lee et al. 1987). This step is controlled by the hydrodynamics of the bulk liquid phase particularly the extent of energy dissipation (Oolman and Blanch, 1986).
2. In the second step, the thickness of quasi equilibrium liquid film present between the bubbles is reduced to 0.01-0.1  $\mu\text{m}$  (Lee et al. 1987). The existence of capillary force (due to varying interface curvature), hydrostatic force and disjoining force leads to bubble deformation and causes liquid drainage at plateau borders. The process of film thinning is strongly influenced by the interfacial characteristics of the system such as interfacial tension, viscosity and elasticity as well as the morphology and properties of the film formed. When the thickness of the film is

reduced to about 0.1  $\mu\text{m}$ , van der Waals attraction increases the draining rate, while the electrostatic double layer repulsive force decreases it (Vrij, 1966).

3. On further thinning, the films become metastable and collapse when they reach a thickness between 0.05-0.01  $\mu\text{m}$  (Bhakta and Ruckenstein, 1997). Unstable films (often called transient films) rupture spontaneously at a characteristic "critical thickness" of 0.01  $\mu\text{m}$  (Mobius and Miller, 1998).

In the process of bubble coalescence, the rate of drainage of the thin liquid film is believed to be the main controlling step since the rupturing step was very rapid. When the contact time between the bubbles is less than the film thinning time, coalescence would not occur and the two bubbles will rebound as separate entities. Therefore, primary attention has been focused on the analysis of the rate of thinning of the liquid film in an attempt to understand bubble coalescence behavior.

### **2.3.2 Experimental Investigation of Bubble Coalescence**

Only a limited number of experimental investigations have been reported and the progress achieved in understanding bubble coalescence behavior is rather inadequate.

The experimental techniques used for measuring the coalescence times are:

- High-speed photographic method
- Zoom stereo microscope technique
- Optical probe/electronic method
- High-speed video technique
- Dynamic disengagement technique.

While the high-speed photographic method has been popularly used for measuring both the bubble size and coalescence time, the other techniques have been mainly used for measurement of coalescence times.

Allan et al. (1961) were one of the first to report experimental data on coalescence of nitrogen bubbles in various liquids by using a zoom microscope. Marrucci et al. (1969) and Nicodemo et al. (1972) measured the coalescence time for two adjacent bubbles, which is popular cited results for coalescence studies. Their technique is able to measure

coalescence times in the range of 1 to 500 ms. Marrucci and Nicodemo (1967) also determined bubble size in a column by means of a photographic method. They found the coalescence occurs mainly in the region near the distributor, and the uniform bubble size is in the rest of the column. Grienberger and Hofmann (1991) also proved that the mean bubble size increases with increasing distance from the distributor due to coalescence. The coalescence is also intensified as the gas hold-up increases.

Sagert and Quinn (1976) measured the coalescence time for bubbles of H<sub>2</sub>S and CO<sub>2</sub> formed on adjacent nozzles in water by photographic method. They observed that liquid film between two bubbles were stabilized due to immobility of the interfaces.

Drogaris and Weiland (1983) studied coalescence time for aqueous solutions of alcohols and acids, and the coalescence time was measured by visual observation. A wide range of bubbling frequency (0.01 to 5 s<sup>-1</sup>) was measured for different bubble size. It seems coalescence frequency decreased dramatically with an increase of surfactant concentration.

Yang and Maa (1984) took pictures for N<sub>2</sub>-aqueous surfactant solutions to study the stretching behavior of a gas-liquid interface. They found the stretching time was from 1 to 500 ms depending on surfactant concentration.

Li and Slattery (1988) detected coalescence times as a function of NaCl concentration in SDS solutions. Furthermore, they developed models to predict coalescence time and coalescence efficiency (Li 1990; Liu and Li, 1999).

Rode (1990) measured the gas hold-up in a bubble column, and he found that the gas hold-up increased substantially in the presence of additives. None of the previous correlations could predict that change.

Prince and Blanch (1990) have studied the critical concentration of electrolyte beyond which the liquid film between two adjacent bubbles became immobile. They developed a theoretical analysis based on their data incorporating Marrucci's model by taking effect of inertia and retardation in London attraction between two surfaces of film into account. The transition concentration that the interface is immobilized is obtained. They also proposed a phenomenological model for bubble coalescence in turbulent gas-liquid

dispersions. The predictions of model agreed to the experimental data on air-aqueous NaCl and Na<sub>2</sub>SO<sub>4</sub> solutions. The results indicated that Na<sub>2</sub>SO<sub>4</sub> is more effective in reducing coalescence than that of NaCl, but at high salt concentration, the model does not predict them well.

An in-depth review of the experimental data of the coalescence time data and bubble size, the theory and mechanism of bubble coalescence was provided by Chaudhari and Hofmann (1994). The various physical processes involved in bubble coalescence are identified and their contributions in the case of pure liquids, electrolytes and surfactants solutions are discussed.

Since then, Chen et al. (1995) studied the effect of SDS concentration on bubble dispersion and coalescence. They found that the coalescence rate was well correlated by the following equation,

$$\frac{\partial d_{32}}{\partial t} = m_1 m_2 e^{-m_2 t} \quad (2-11)$$

where  $m_1 = (d_{32\infty} - d_{320})$ ,  $m_2$  is a constant that depends on the hydrodynamic conditions,  $d_{32\infty}$  is the Sauter mean diameter at equilibrium state, and  $d_{320}$  is the Sauter mean diameter at initial state.

Gao et al. (1996) carried out an experimental studies on bubble coalescence in a stirred tank with circulating zone at various vessel diameter of 0.287, 0.495 and 1.1 m respectively. Bubble size was measured with a dual electrode conductive probe placed in the tanks. Gas holdup was measured by spillover method. Taking into account the equilibrium between the surface energy of the bubbles and the energy supplied by agitation, the model could well predict bubble size and gas holdup.

Weissenborn and Pugh (1995), Pashley and Craig (1997) examined bubble coalescence behavior in electrolytes and found that the parameter  $(d\sigma/dc)^2$  gave a reasonable correlation with coalescence behavior.

Yuan et al. (1997) found there existed a bubble distribution zone (BDZ) in bubble columns and air-lift loop reactors located above the gas spargers, which was characterized as a zone with dynamics of bubble coalescence-breakup and enhanced mass transfer. Kolmogoroff's theory of isotropic turbulence was applied to simulate bubble coalescence-breakup behavior and the mass transfer coefficient was correlated with operation conditions.

Zahradnik, et al. (1999) conducted an experimental study aimed at examining the coalescence phenomena in aqueous solutions of aliphatic alcohols and electrolytes and at determining the effect of these surface-active compounds on bubble coalescence in viscous aqueous media with Newtonian and non-Newtonian behavior respectively. Bubble coalescence in aqueous solutions of alcohols and electrolytes was significantly hindered by increasing solute concentration

A controlled flow-induced vibration was introduced to investigate the two-phase flow structure and bubble breakup and coalescence (Hibiki and Ishii, 1999). In case of low superficial liquid velocity, flow-induced vibration promoted the bubble coalescence but liquid turbulence energy enhanced by the vibration might not be enough to break up the bubble. This led to the marked increase of bubble size, and the marked decrease of specific interfacial area. Accordingly, flow-induced vibration changed the void fraction profile from 'wall peak' to 'core peak' or 'transition', which increased distribution parameter in the drift-flux model. For high superficial liquid velocity, shear-induced liquid turbulence generated by two-phase flow itself might be dominant for liquid turbulence enhanced by flow-induced vibration. Therefore, the effect of flow-induced vibration on local flow parameters was not marked as compared with that for low superficial liquid velocity.

Most recently, the bubble coalescence studies on bubble size evolution along a pipe under microgravity conditions have been carried out during parabolic flights in aircraft (Kamp, et al., 2001). Bubble diameter and its distribution in turbulent pipe flow had been determined from high-speed video recording and image processing. In the absence of gravity, collisions between bubbles smaller than the integral length scale of turbulence

are primary caused by turbulence. The model can well predict the experimental data in terms of the effects of the gas hold-up, the bubble size at the pipe inlet and the liquid mean velocity on coalescence rate.

### 2.3.3 Coalescence Models

In most literature, the bubble coalescence rate is studied separately as the collision frequency and the collision efficiency of which involves two characteristic times, contact time and coalescence time (Levich, 1962; Ross, 1976; Coulaloglou, 1975; Coulaloglou and Tavlarides, 1977; Thomas, 1981; Lee, et al., 1987; Prince and Blanch, 1990; Chesters, 1991; Liu and Li, 1999; Kamp, et al., 2001). The coalescence rate will be the production of the collision frequency and collision efficiency.

$$\text{Coalescence rate} = \text{Collision frequency} \times \text{collision efficiency}$$

The following sections will discuss those individual collision characteristics in details.

#### 2.3.3.1 Bubble Collision

Bubble collisions might occur due to a variety of mechanisms such as turbulence, buoyancy, laminar shear (in the case of laminar flow), or Brownian motion (in the case of bubble size less than 1 microns).

##### **Buoyancy-driven collision**

Collisions can result from the difference in rise velocities of bubbles/drops of different sizes. The buoyant collision rate was given by Friedlander (1977) as,

$$f = n_i n_j S_{ij} (u_{ri} - u_{rj}) \quad (2-12)$$

The rise velocity could be expressed as a function of size. Clift et al.(1978) provided the following expression that covers the size range typical of gas-liquid contactors operating in the turbulent flow regime:

$$u_r = [(2.14\sigma)/\rho_c d + 0.505 g d]^{1/2} \quad (2-13)$$

Tavlarides and Stamatoudis (1981) pointed out that it should be noted that gravity could play an important role in collision rates for systems with large differences in density between the dispersed and continuous phases. For example, Bhavaraju et al. (1978) developed an expression for the power input to gas-sparged vessels which results from the expansion of bubbles as they ascend the column from pressure  $P_2$  to  $P_1$  at a volumetric gas flow rate  $Q$ :

$$\Psi = QP_2 \frac{\ln(P_1 / P_2)}{P_1 - P_2} \rho_l g H_T \quad (2-14)$$

where,

$$P_1 = P_2 + \rho_l g H_T \quad (2-15)$$

The following expression for  $\varepsilon$  was obtained by gravitational driven flows,

$$\varepsilon = \frac{Qg}{\pi R_T^2} \frac{P_2 \ln(P_1 / P_2)}{(P_1 - P_2)} \quad (2-16)$$

On the other hand, in turbulent liquid-liquid dispersions with small fluid density differences, gravity was not an important factor in the collision rate model.

### **Laminar shear collision**

It is well recognized that bubbles preferentially rise through the center of the bubble column and flow downwards in the outer annular region near the wall. This results in the formation of high rise velocities in the center and relative low velocities around the wall. The resulting collision rate (driven by differentia of velocities between bubbles due to laminar shear) is given by Friedlander (1977) as,

$$f_{ij} = n_i n_j \frac{4}{3} (r_{bi} + r_{bj})^3 \left( \frac{dU_l}{dR} \right) \quad (2-17)$$

where  $U_l$  is the liquid circulation velocity and  $R$  is the radial coordinate of the column.



### **Brownian motion collision**

The collision caused by Brownian motion has nothing to do with hydrodynamics of the fluids, and its collision rate is given by (Ulrich and Riehl, 1982).

$$f_{ij} = \frac{2\kappa_B T}{3\mu} (d_i - d_j) \left( \frac{1}{d_i} - \frac{1}{d_j} \right) n_i n_j \quad (2-18)$$

where  $\kappa_B$  is the Boltzman constant, and T is an absolute temperature. Brownian motion contributes insignificantly to the collision process due to large bubble or drop sizes in actual industrial operations (Tavlarides and Stamatoudis, 1981).

### **Turbulent collision**

The primary cause of bubble collisions in turbulent flows is the fluctuating turbulent velocity present in the liquid phase. Several expressions have been developed to predict collision rates in multi-phase systems (Abrahamson, 1975; Lee et al., 1987; Prince and Blanch, 1990; Chesters, 1991; Kamp, et al., 2001) with some of the most common being derived in a fashion analogous to particle collisions in an idea gas -- kinetic theory of gases (Kennard, 1938).

Abrahamson (1975) derived collision frequency models based on the kinetic theory of gas and extended to solid-air dispersion system resulting from: (i) turbulent motion, (ii) gravity force acting on the particles, and (iii) centrifugal force. Equation Eq. (2-19) was obtained in the absence of gravitational and centrifugal accelerations

$$f_{ij} = 1.25(0.50d_i + 0.50d_j)^2 (\overline{u_i'^2} + \overline{u_j'^2})^{1/2} \quad (2-19)$$

where  $\overline{u_i'^2}$  is the mean squared particle velocity that is related to the mean squared fluid velocity in term of integral time scale.

William and Crane (1983) presented the collision frequency for intermediate energy dissipation rate, between particles of water droplets dispersed in air phase in pipe flow. A series of assumptions were made such as, Stoke's flow around the particles, no strong

acceleration due to external force, and isotropic turbulence, the collision rate was derived as,

$$f_{ij} = \left[ (8\pi)^{1/2} \frac{18}{4} \nu L_f \frac{\rho_c}{\rho_d} \frac{U_r'}{u_i'} (\mathcal{G}_i^{1/2} + \mathcal{G}_j^{1/2})^2 \right] \times \frac{2}{\pi} \tan^{-1} \left[ \frac{1}{3} \frac{\rho_c}{\rho_d} \frac{u_i' L_f}{\nu} \left( \frac{U_r'}{2} \right)^{1/2} \frac{\mathcal{G}_i \mathcal{G}_j}{(\mathcal{G}_i^{1/2} + \mathcal{G}_j^{1/2})^2} \right] \quad (2-20)$$

where  $U_r'$  is the root mean square relative velocity of two particles,  $L_f$  is the longitudinal scale, and  $\mathcal{G}$  is the dimensionless relaxation time. This model is valid for particles with velocities which are neither well-correlated not totally independent of each other. The relative velocity between two particles depends on particle relaxation time.

The problem of using Abrahamson, William and Crane collision frequency model comes from their expression in term of integral length scale ( $L_f$ ) that is not well defined, which restrains their popularity.

Similar to Coulaloglou and Tavlarides' methodology (1977) of applying Kennard's concepts to drop-drop collision in liquid, Lee, et al. (1987) and Prince and Blanch (1990) derived the collision frequency,  $f$ , for non-equal size bubble-bubble collision in liquid case as,

$$f = n_i n_j S_{ij} (\bar{u}_{ii}^2 + \bar{u}_{jj}^2)^{1/2} \quad (2-21)$$

where  $n_i$  and  $n_j$  are the number concentrations of bubbles of radii of  $r_{bi}$  and  $r_{bj}$ , respectively,  $\bar{u}_i$  is the average turbulent fluctuating velocity of the bubble, and  $S_{ij}$  is the collision cross-sectional area of the bubbles defined by,

$$S_{ij} = \frac{\pi}{4} (r_{bi} + r_{bj})^2 \quad (2-22)$$

Expression for the collision frequency,  $f$ , per unit time and volume could be derived if dispersed bubbles are assumed spherical equal-size and flow in the continuous phase as (Chesters, 1991),

$$f = k_1 u_t n^2 d^2 \quad (2-23)$$

where  $k_1$  is proportion constant and  $u_t$  is characteristic velocity.

In bubble collision analysis it is customary to assume that the turbulence is isotropic. The velocity of fluid particles is assumed to be comparable to the turbulent velocity of eddies having the same length scale of the fluid particle. Eddy motion of this scale is primarily responsible for the relative motion between fluid particles. Very small eddies do not contain sufficient energy to significantly affect fluid particle motion, while eddies much larger than the fluid particles size transport groups of fluid particles without leading to significant relative motion. The turbulent velocity in the inertial sub-range of isotropic turbulence is given by (Rotta, 1972),

$$u_t = 1.4 \varepsilon^{1/3} d^{1/3} \quad (2-24)$$

In general, flow field in the multi phase system is mostly turbulent, in which turbulent collision frequency models is focus on. Most models are expressed in terms of two colliding bubble or drop size diameters and energy dissipation rate. Densities and viscosities of dispersed and continuous phases, and bubble/drop relaxation time have been expressed in some models.

### 2.3.3.2 Collision Efficiency

Not all bubble collisions lead to bubble coalescence. When the contact time is less than the time needed for coalescence to take place, coalescence will not happen. To determine what fraction of bubble collision leads to coalescence events, it is necessary to determine the value of the collision efficiency. A commonly used expression was developed by Coualaloglou and Tavlarides (1977),

$$\lambda = e^{-t_c/t_i} \quad (2-25)$$

where,

$t_c$  : Coalescence time [s]

$t_i$ : Contact time [s]

The competition of those two characteristic times is crucial in order for two bubbles to coalesce to each other.  $\lambda$  tends to zero for large  $t_c/t_i$ , which indicates that the coalescence takes too long to make film rupture, and to unity for small  $t_c/t_i$ , which indicates that the coalescence takes place easily.

### 2.3.3.2.1 Bubble Contact Time in Turbulent Flows

The time that equal-sized bubbles remain in contact with each other under the action of turbulence is controlled by the hydrodynamics of the bulk liquid phase (Coulaloglou and Tavlarides, 1977; Oolman and Blanch, 1986) particularly the turbulent intensity and the bubble size. High turbulent intensities generate rapid eddies that cause the bubbles to bounce from each other faster, while large bubbles offer large contact area and stay longer in contact. Levich (1962) estimated the contact time between bubbles suspended in turbulent flows to be given by,

$$t_i = \frac{(d/2)^{2/3}}{\varepsilon^{1/3}} \quad (2-26)$$

Consequently, big bubbles present in low levels of turbulence will exhibit long contact times that favor bubble coalescence.

Coulaloglou (1975) took the contact time as a value that is proportional to the lifetime or period of an eddy of size  $(d_i+d_j) < L_k$ , resulting in.,

$$t_i \propto \left( \frac{\nu_c}{\varepsilon} \right)^{1/2} \quad (2-27)$$

where  $\nu_c$  is a kinetic viscosity of continue-phase. However, it is physically unreasonable for large bubbles and small bubbles to have the same contact time.

Recently, based on that increase of surface free energy due to bubble deformation is made up by reduction of kinetic energy when ratio of radius of flatter dick over bubble radius is much less than unity corresponding to small Weber number, Chesters (1991)

derived the following expression for  $t_i$ , i.e. time from onset of flattening up to the point at which bubble motion was arrested,

$$t_i = \left[ (4\rho_G / 3\rho_L + 1) \rho_L (d/2)^3 / 2\sigma \right]^{1/2} \quad (2-28)$$

This expression is similar to that for the period of oscillation of a single drop or bubble and is likewise independent of the amplitude of the deformation. However, it does not show any dependence on turbulence intensity.

### 2.3.3.2.2 Coalescence Time

The coalescence time includes time spent for thinning the liquid film and the film rupturing time, i.e.

$$t_c = t_{th} + t_{rup} \quad (2-29)$$

Because the rate of thinning of liquid film or film drainage is believed to be the main controlling step as the rupturing step is very rapid (Hartland, 1967; Chesters, 1991), most investigators focused on the film drainage or thinning ( $t_{th}$ ) which is often referred to as the coalescence time. The expressions used to estimate it are quite complicated and differ significantly based on the various assumptions used.

#### a) Film Characteristics and Interactions Between Two Bubbles

In order to understand the thinning process of the liquid film, the forces acting on the film have to be stated clearly. The thickness of the thin aqueous film between two bubbles is determined by the balance amongst the following forces: sum of the various components of the disjoining pressure ( $\sum \Pi$ ), hydrostatic pressure ( $P_h$ ), and capillary pressure ( $P_c$ ) of the film (Pugh and Yoon, 1994), i.e.,

$$P_h + P_c + \sum \Pi = 0 \quad (2-30)$$

The film capillary pressure,  $P_c$ , is generated by the curvature difference between the curved interface and the flat region. The hydrostatic pressure,  $P_h$ , is caused by gravity and may be neglected for horizontal thin films. The classical Derjaguin and Landau (1941) and Verwey and Overbeek (1948) (DLVO) theory used for describing the disjoining

pressure between approaching interfaces can be formulated as the competition of van der Waal force  $\Pi_{vdw}$  and electrostatic force  $\Pi_e$ ,

$$\sum \Pi = \Pi_{vdw} + \Pi_e \quad (2-31)$$

Only in the case of thin films does  $\Pi_{vdw}$  become significant. It can be calculated from the following expression,

$$\Pi_{vdw} = -\frac{A}{6\pi h^3} \quad (2-32)$$

where A is the Hamaker function of the molecular interactions, weakly dependent on the film thickness. The value of A is of the order of  $10^{-20}$  J (Israelachvili, 1988).

The widely used approximation for the electrostatic force is (Dukhin, 1995),

$$\Pi_e = 64C_e RT \tanh^2 \phi_0 \exp(-\kappa h) \quad (2-33)$$

where  $\phi_0 = ze_0\psi_0 / 4kT$ ,  $z$  is ion valency,  $e_0$  is elementary charge and  $\kappa$  is Debye-Hückel parameter and  $C_e$  is electrolyte concentration.

In most cases, when only the electrostatic and van der Waal components were taken into consideration, the stability of common films in weak electrolyte could be satisfactorily explained (Möbius and Miller, 1998).

However, DLVO theory is only an approximation even in simple systems, for instance, if there exists strongly hydrophobic interfaces or moderately hydrophilic interacting interfaces, the theory loses its accuracy. It is therefore necessary to modify the Eq. (2-31) as,

$$\sum \Pi = \Pi_{vdw} + \Pi_e + \Pi_{hyd} \quad (2-34)$$

where the hydrophobic interaction,  $\Pi_{hyd}$ , for two parallel interfaces is described as (Israelachvili and Pashley, 1983),

$$\Pi_{hyd} = -\frac{Ce^{-h/D_0}}{2\pi D_0} \quad (2-35)$$

This expression shows that the hydrophobic interaction decays exponentially with increasing of the distance of the two surfaces ( $h$ ). For the same reason, if there existed any other forces, Eq. (2-34) would be modified to fit the specific situation.

In terms of the liquid drainage in bubble coalescence process, it is reported that the main force responsible for drainage of thin liquid film between static bubbles is the influence of capillary force, van der Waals attraction and electrostatic double layer repulsive, gravity and also inertial force caused by virtual mass attached with the bubble of high Reynolds number (Marrucci, 1967; Sagert and Quinn, 1978; Chaudhari and Hofmann, 1994; Kamp, et al., 2001). This process is influenced by the mobility of the bubble surfaces and the physical properties of the fluid phases (such as viscosity, surface viscosity, surface tension gradients and differences between density of gas and liquid phases). Bubble deformation is increasingly resisted at higher interfacial tensions, a factor that leads to a reduction in the film area to be drained, and hence to faster coalescence (Pugh, et al, 1997; Liu and Li, 1999). The presence of electrolytes can lead to the formation of electrical double layer at the interfaces between two bubbles and thus influence the film draining process. Once electrical double layer is built, the interface of the film become immobile and the flow of draining film is retarded by the force of opposite charges attached to the interfaces (the electroviscous effect, Elton and Pickness, 1957). Drainage rate could also be influenced by diffusion processes such as the diffusion of solutes from the bulk of the liquid to the film as well as from the film to the G/L interface (Marrucci, 1969). Vrij (1966) observed that when the film thinned drainage rate slowed down and stable fluctuations grew faster and faster until a critical thickness,  $h_c$ , is reached where one of the fluctuations grew so fast that film broke (Mobius and Miller, 1998).

#### **b) Film Thinning by Drainage**

Liem and Woods (1974) and Sagert and Quinn (1976) examined the process of film thinning by assuming the surfaces of coalescing bubbles to deform into parallel plates and they modeled the coalescence process as a film being squeezed from between two parallel plates. The parallel disc model includes two important film-thinning mechanisms that will be discussed in detail, i.e. film thinning controlled by inertial forces and film

thinning controlled by viscous forces (McBride, et al., 1980; Oolman and Blanch, 1986a, 1986b; Lee, et al., 1987; Prince and Blanch, 1990),

### **Inertial Thinning**

When inertial forces are significant, as in the case of turbulent flows, the film drainage is inertially controlled and the liquid film can be considered to be inviscid. The Bernoulli equation can therefore be used to obtain a thinning rate equation. It could predict the inertial thinning time of a liquid film with totally mobile surfaces from an initial thickness,  $h_i$ , up to a final thickness,  $h_c$  (Sagert and Quinn, 1976).

$$t_{th} = (R/4)(\rho_c d / 2\sigma)^{1/2} \ln(h_i / h_c) \quad (2-36)$$

where  $R$  is radius of disc that two equal-size bubbles collide and flatten into. It is not a function of time but proportional of the bubble diameter.

### **Viscous Thinning**

For more viscous continuous systems, the film surfaces are essentially immobile, so liquid must be expelled from between these rigid surfaces by laminar flow. The thinning time in the case of immobile film is consequently much longer than that for a mobile film. The rate of thinning for a flat disc of liquid with partially immobile interfaces was given by Sagert and Quinn (1976) as,

$$\int_0^{t_{th}} dt / 3M\mu R^2 = - \int_{h_i}^{h_f} dh / [8h^3 (4\sigma / d + A_h / 6\pi h^3)] \quad (2-37)$$

where  $M$  is the surface immobility parameter and  $A_h$  is the Hamaker constant.

Due to the simple geometry of parallel plate, the thinning and stability of films with uniform thickness have received much attention in the literature (Ivanov and Dimitrov, 1974; Zapryanov, et al., 1983; Malhotra and Wasan, 1987; Jeelani and Hartland, 1994; Li, 1994 and 1996). Since such a film remains intact and does not break up during liquid drainage, the coalescence time was obtained for a film to drain between assumed values



of initial and final film thickness (Zapryanov et al; 1983; Malhotra and Wasan, 1987; Jeelani and Hartland, 1994; Li, 1994).

However, for deformable surfaces, Ivanov et al. (1985) discussed the effects of mass transfer on thinning rate of films for the limiting cases of small and large surface deformations. The minimum film thickness is initially at the center of the film and then moves to the rim as drainage proceeds, so that a dimple is formed due to the radial pressure gradient in the film. Recently, dimple formation between bubbles was investigated by taking into account of effects of dimpling and surface mobility (Joye et al., 1992; Li, 1994 and 1996). As the dimple develops, the thinning rate decays at one-tenth of the initial value predicted by no-dimple model (Chesters, 1991). It is therefore necessary to consider the different drainage modes depending on the rigidity and mobility of the interfaces.

For drainage between rigid Colliding particles, the thinning time is given by (Chesters, 1991),

$$t_{th} = \frac{3}{8F} \pi d^2 \mu_c \quad (2-38)$$

where F is interaction force exerted by one to another. If an approach velocity is given as  $(-dh/dt)$ , then the interaction force will be (Chesters, 1991),

$$F = \frac{3}{8h} \pi \mu d^2 \left(-\frac{dh}{dt}\right) \quad (2-39)$$

Film immobility is applicable when the dispersed phase is highly viscous or when high concentrated surfactant is dissolved in the continue phase thus the dispersed phase is attached with the surfactant.

For drainage between deformable immobile interfaces, if the deformed portion of the film is assumed parallel-sided, a similar approach to the above case is applied to yield (Mackay and Mason, 1963)

$$-\frac{dh}{dt} \approx \frac{32\pi\sigma^2 h^3}{3\mu_c dF} \quad (2-40)$$

It implies that increasing of the interaction force decreases the thinning rate, which is why the coalescence is favored by gentle collisions. If the gravity is dominant, the interaction force is given by,

$$F = \frac{1}{6} \pi d^3 \Lambda \rho g \quad (2-41)$$

However, the gravity is not dominant in the case of bubbles suspended in turbulent flows.

For drainage between deformable partially-mobile interfaces, the drainage is controlled by the motion of film surface that results from the shear stress on the film by the adjacent liquid. An approximation of quasi-steady creeping flow is applied to yield the relation between the thinning rate and the pressure variation in the film as (Chesters, 1991),

$$-\frac{dh}{dt} \approx 2 \frac{(4\pi\sigma / d)^{3/2}}{\pi\mu_c F^{1/2}} h^2 \quad (2-42)$$

For drainage between deformable fully mobile interfaces, the drainage is no longer controlled by the dispersed phase due to its sufficiently small viscosity, but by the film due to its deformation and acceleration. The parallel film model for fully-mobile interfaces, including both viscous and inertial sub-ranges, was solved by Chesters (1975) as,

$$\frac{dH}{dt} = \frac{2\sigma}{3\mu d} \left( \frac{dH}{dt} \right)_0 e^{-12\mu d / \rho \alpha^2} - \frac{2\sigma}{3\mu d} \quad (2-43)$$

where

$$H = \frac{1}{2} \ln h \quad (2-44)$$

In the case of bubbles suspended in turbulent flows, the closest drainage case for air-pure water system would be characterized as fully interfacial mobility and inertial control, to

which either Eq. (2-42) or Eq. (2-43) can apply. For air-impure solutions, it is arbitrary to choose one of above equations. Moreover, most of mentioned models do not have analytic solutions.

Most of coalescence efficiency models also do not include the effect of the drop surface charge, which has been reported to play an important role Tobin et al. (1990). In a word, the film thinning is far more sophisticated than what was expected. A comparative analysis of the various coalescence models was recently completed by Sirijeerachai (2002).

### **c) Film Rupturing Process**

Using the hydrodynamic stability theory, the rupture of a free liquid film has been studied by Ruckenstein and Jain (1974), Sagert et al. (1976), Chesters and Hoffman (1982) and Chesters (1991). Assuming the lubrication approximation of the Navier-Stokes equations can be used to describe the motion when small perturbations were applied to the gas-liquid interfaces, they established a wave-motion equation that allowed one to calculate the critical wavelength of the perturbations and the time of rupture. If the perturbations exceed this critical wavelength, the film will burst and the coalescence will take place. Concerning the rupture of a free thin film, it is important to stress that in real systems the presence of polar impurities act as surface active agents the presence of which, even in minute quantities, has a strong stabilizing effect by virtue of the ability to dampen the waves that occur at a free surface. For this reason, the film rupture time in a pure liquid was found to be the lower bound value in the case of real systems. In the presence of surface-active impurities, the time of rupture depends strongly on the surface concentration of surfactants.

In a summary, when the film is still thick, the thinning usually proceeds rapidly and the surface fluctuations grow slowly or do not grow at all. When the film becomes thinner, however, the rate of thinning slows down, whereas the stable fluctuations (if present) grow faster and faster until a critical thickness  $h_c$  is reached at which one of the fluctuations grows so fast that the film breaks.

As it is shown that the bubble coalescence rate is the production of the collision frequency and the collision efficiency, there is not much different for the expression of the collision frequency in turbulent flow, however, the time ratio of coalescence characteristic time against contacting characteristic time is different from case to case. For example, recently Kamp, et al. (2001) developed an equation that includes Weber number to express the time ratio; their model works well for their experimental data. As discussed above, there are so many expressions for the coalescence time although that for contacting time is essentially the same in most situations. This manifests that there is inconsistency or even conflict for the expressions of bubble coalescence time.

## **2.4 Effect of Interfacial Characteristic on Bubble Break-up and Coalescence**

In this section, the various interfacial characteristics affecting bubble breakage and coalescence are briefly introduced and their role in bubble breakage and coalescence discussed.

### **2.4.1 Interfacial Characteristics**

Generally speaking, the interfacial characteristics are classified into two major groupings: static, or equilibrium, interfacial properties and dynamic interfacial properties. In the case of pure systems, there is no significant difference between the two but the importance of dynamic interfacial parameters have recently gained more attention because of their ability to account of the presence of impurities present in most industrial processing streams.

#### **2.4.1.1 Static Interfacial Properties**

It is well known that some organic and inorganic substances when dissolved in water are strongly adsorbed at the interface. As a consequence, the static/equilibrium surface tension of the solution decreases rapidly with increasing concentration of organic solutes. The extent of this adsorption is determined mostly by the polarity and asymmetry of the solute molecule (Myers, 1999). Thus, if the solute is weakly surface active at the air/water interface, its effect on the surface tension of the water is very limited. Examples of such solutes are KOH and alkyl xanthates. Other surfactants such as fatty acids,

alcohols, ethers, etc., lower the surface tension of their aqueous solutions much more strongly than xanthates. The change in interfacial tension with SAA concentration continues but the rate of change decreases with increasing concentration until the saturation points is reached. The concentration for which surface tension levels off and attains a constant value is defined as the critical micelle concentration (CMC). When a solution becomes supersaturated (concentration higher than CMC), it no longer represents a homogeneous system but forms micelles. Because of its simplicity, the static/equilibrium surface tension is the most popular parameter to represent the interfacial property of systems in the majority of published literature.

Gas-liquid contacting experiments with fluids having clean interfaces are relatively rare. There is evidence of the presence of minute amounts of surface-active agents in all systems but those purified with the most extraordinary care. These agents can have an effect on the hydrodynamics indirectly for multi-phase flow and rates of mass or heat transfer in dispersions. Many unsuspected impurities in a system can have surface-active characteristics, and even the equipment itself can supply enough such contamination to affect the results.

Direct determination of the amount of surfactant adsorbed per unit area of a liquid-gas dispersion, although possible, was not undertaken generally because of the difficulty of isolating the region around the interface from the bulk phases including both gas and liquid (Myers, 1999). Instead, the amount of material adsorbed per unit area of interface was calculated indirectly from surface tension measurement. As a result, a plot of surface tension as a function of surfactant concentration is generally used to describe adsorption at these interfaces. From such a plot the amount of surfactant adsorbed per unit area of interface can readily be calculated by applying the Gibbs isotherm adsorption equation that reflects the thermodynamics of adsorption.

In its general form, the Gibbs adsorption equation is given by:

$$\Gamma_G = -\frac{1}{RT} \frac{\partial \sigma}{\partial \ln C_0} \quad (2-45)$$

Sircar (1999) found that the Gibbs Surface Excess (GSE), i.e.  $\Gamma_G$ , could be used as primary variable to formulate the general thermodynamic and kinetic models for the adsorption of components, and adsorption related processes.

There are very limited correlations that can be used to predict a general surface tension for various surfactants. Reid and Prausnitz (1977) suggested the use of the MacLeod-Sugden correlation that is based on a homogeneous distribution of the solute. However, when Jamialahmadi et al. (1992) compared their measured values of surface tension for alcohol and organic acid solutions to the values predicted using the MacLeod-Sugden correlation. The deviations between calculated and experimental surface tensions, which exhibit a maximum around 10% solute concentration depending on the type of alcohol or acid used, clearly demonstrates that the solute was not homogeneously distributed.

#### **2.4.1.2 Dynamic Interfacial Properties**

The equilibrium in which the static surface properties of a surfactant solution exhibits are not completed instantaneously, the surfactant molecules have to first diffuse from the bulk to the interface, then adsorb, whilst also achieving the correct orientation. Some time-related parameters will be discussed in the following section.

##### **a) Dynamic Surface Tension**

In many processing applications, the time scale of the process does not allow for surfactant molecules to reach equilibrium at an interface. Therefore, it is not appropriate to model such dynamic processes using the equilibrium surface tension. Consequently, it is important to understand the effect of additives on dynamic surface tension and to test the possibility of using dynamic surface tension characteristics to accurately predict the behaviour of gas-liquid contacting processes. The dynamic surface tension of any particular system describes the variation of a freshly created interface with time, which results from the diffusion of the SAA molecules from the bulk of the liquid, and their subsequent adsorption at the interface. It, therefore, represents a non-equilibrium state. Depending on the nature of the system, equilibrium may be reached within a fraction of a second, in several seconds, or in hours. Different surfactants exhibit fairly wide variations in the kinetics of adsorption; for example, short-chain alcohols adsorb at the air/water

interface in fractions of a second, while alkyl amines require several seconds, and long-chain sulfates require several hours (Leja, 1982).

Several experimental techniques can be used to determine the dynamic interfacial characteristics of solutions and its variation with surface age. One of the most commonly used effective technique is the maximum bubble pressure method in which the variation of the pressure within a bubble is monitored, by electrical pressure transducers, from the point of inception until the bubble is detached. The advantages of this approach are high sensitivity and the low inertia of the pressure transducers (Miller and Fainerman, 1998). The bubble is formed at the tip of a capillary placed within the liquid system and the maximum pressure is obtained at the point when the bubble reaches the hemispherical shape with a radius equal to the radius of the capillary  $r$ . The dynamic interfacial tension at this point can be determined by using the Young-Laplace equation as follows (Kao, 1992; Xue, 1999),

$$\Delta P_{max} = 2\sigma/r_{cap} + \Delta\rho gh \quad (2-46)$$

Hua and Rosen (1988) investigated the effect of surfactant concentration and electrolyte on dynamic surface tension and found that the dynamic surface tension is clearly reduced with increasing surfactant concentration. They attributed this reduction to the electrolyte encouraging the migration of the surfactant species to the air/liquid interface.

The reduction of interfacial tension is related to the adsorption/desorption of surface-active agents at the interface. The kinetics of interfacial tension can therefore be described in terms of adsorption kinetics. Many kinetic adsorption models based on diffusion-controlled processes have been used for description of adsorption at the interface. Vogler (1989) proposed that the time-dependent interfacial tension  $\sigma(t)$  is a composite function of  $\sigma(C_S) \cdot C_S(t)$  where  $\sigma(C_S)$  is interfacial tension at surface concentration  $C_S$ , while  $C_S(t)$  is the surface concentration at time  $t$ . The value of  $\sigma(t)$  was obtained by solving the differential equation,

$$d[\sigma(t)]/dt = \{d\sigma(C_S)/dC_S\} \cdot \{dC_S(t)/dt\} \quad (2-47)$$

Vogler (1989) introduced an empirical test function for concentration-dependent interfacial tension,

$$\sigma(C_s) = \sigma^E . e^{-(AR)} \quad (2-48)$$

where A is a constant and R is a relative surface concentration which is calculated from surface concentration  $C_s(t)$  and equilibrium surface concentration  $C_s^E$  using  $R = [C_s(t) - C_s^E] / C_s^E$ . Vogler (1989) applied four different theoretical kinetic models to describe surface concentration as a function of time and obtained four different kinetic models for dynamic interfacial tension  $\sigma(t)$  as a function of time. Of these kinetic models, Xu (1994) reported that the model, which is based on the Langmuir formulation, could be successfully applied to their bitumen-caustic solution systems. The resulting kinetic equation for his case reads,

$$\sigma(t) = \sigma^E \exp(A \exp(-k_L t)) \quad (2-49)$$

where A is an empirical constant and  $k_L$  is the Langmuir constant.

In the study of the dynamic interfacial tension between asphaltene-toluene solutions and caustic solutions, Sheu et al. (1992) used the following dynamic model:

$$\sigma(t) = \gamma_0 \exp[-(\beta * t)^{1/2}] + \sigma_\infty \quad (2-50)$$

where  $\gamma_0$  is a proportionality constant, and  $\beta$  is a kinetic parameter similar to the diffusion constant. Equation (2-50) is based on an approach similar to Vogler's, but Gibbs's isotherm is applied.

Xu (1994) reported that the two equations were suitable models for the interface adsorption between bitumen in toluene solutions and caustic solutions, but the model with the Gibbs isotherm was slightly better than the Langmuir model for representing the dynamic interfacial tension data for this specific system. Therefore, these two adsorption models can be used to characterize the adsorption kinetics quantitatively. However, at longer elapsed times, the experimental data points deviated slightly from the kinetic



model, indicating that at longer elapsed times, when the interface has nearly equilibrated, the diffusion-controlled mechanism changed to another controlling mechanism.

Hua and Rosen (1988) suggested the following empirical equation to fit the dynamic surface tension data,

$$\sigma_t - \sigma_m = \frac{\sigma_0 - \sigma_m}{1 + (t/t^*)^n} \quad (2-51)$$

where  $\sigma_0$  is the surface tension of the pure solvent and  $\sigma_t$  is the surface tension at time  $t$ ,  $\sigma_m$  is the meso-equilibrium surface tension,  $t^*$  is time for reaching the meso-equilibrium and  $n$  is empirical constant.

Little information is available concerning the dynamic surface tension of SDS solutions. For example, Woolfrey et al. (1986) obtained the dynamic surface tension of SDS in the absence and presence of 0.5M sodium chloride. Garrett and Ward (1989) and Fang and Joos (1996) similarly acquired some experimental results. A bubble pressure tensiometer based on the principle of maximum bubble pressure (Kruss, Germany) was recently used to measure the dynamic surface tension of SDS by Hsu et al. (2000). The concentration range was from 0.4 mM to 10 mM. The relaxation rate of the surface tension was from 72 to 40 mN/s. Under those conditions, the dynamic surface tension was expressed in the form,

$$\sigma = \sigma_w - \frac{at^c}{1 + bt^c} \quad (2-52)$$

where  $\sigma_w$  is the surface tension of water,  $t$  is the bubble generation interval time and  $c$  is empirical constant. The constants  $a$ ,  $b$  and  $c$  were found to vary with the concentration of the SDS solution.

### **b) Gibbs-Maragoni Elasticity**

Since there is limited investigation regarding film thinning in turbulent flows, the analogous theory of foam deformation and collapse is presumed to apply to bubble coalescence under intensive agitation conditions. If a foam film undergoes a sudden

expansion in a surfactant-containing system, the expanded portion of the film has a lower surfactant concentration than the unexpanded portion due to the increase of interface area. The adsorbed surfactant layer at the interface would then require some time to restore its equilibrium interfacial concentration. This takes place by diffusion of the surfactant from the bulk of the liquid as well as along the interface from the surfactant rich regions to the surfactant deficient ones. Thus, the interface has regions in which the interfacial tension has changed. The existence of an interfacial tension gradient creates a force that resists further expansion or contraction. This effect is so called the Gibbs-Marangoni effect and it imparts an elastic property to the interface (Rosen, 1988).

Following a rapid expansion of a film element, the elasticity of each interface will have an initial value given by the limiting value for an insoluble monolayer (Lucassen-Reynders, 1996). After equilibration by diffusion, the final adsorbed concentration is slightly lower, because the constant total amount of material is now distributed over a larger interfacial area. The first effect (i.e. the change in interfacial tension with change in the concentration of the surface-active solute) is known as the Gibbs effect. If the number of molecules is so low that the surfactant cannot restore the equilibrium interfacial concentration after deformation, that is Gibbs elasticity (Rosen, 1988; Schramm and Wassmuth, 1994). The elasticity determined from isothermal equilibrium measurements, such as the spreading pressure-area method, is a thermodynamic property.

The change in interfacial tension with time during the rapid rate of change of the interfacial area is known as the Marangoni effect (Marangoni, 1872; Bohm and Lyklema, 1974; Isaacs and Chow, 1992). The elasticity, determined from dynamic measurements, depends upon the stresses applied to a particular system, and can be much more significant than the Gibbs elasticity. This is termed the Marangoni surface elasticity (Malysa, 1981; Perez De Ortiz, 1992; Schramm and Wassmuth, 1994; Lyford et al., 1998). The Marangoni elasticity is significant in dilute solutions, and within a limited concentration range provided the diffusion time of the solute is not very short.

### **c) Interfacial Viscoelasticity**

In the case of interfacial compression/expansion, the presence of an adsorbed layer of surfactant results in the formation of a gradient in interfacial tension that can slow down the movement of the interface and the adjoining bulk liquid. There are some interfaces that show neither pure interfacial elasticity nor pure interfacial viscosity. For example, when subjected to a force they deform continuously, but when the force is removed they return spontaneously, though not completely, towards the original shape. Such viscoelastic behavior was observed by Mysels (1959). The viscoelasticity depends on the interfacial concentration of adsorbed surfactant and also on the rate of change of interfacial area (Lucassen-Reynders, 1996). When the interfacial expansion rate greatly exceeds the rate of surfactant adsorption, the elasticity is known as the Marangoni elasticity (Edwards, 1991).

#### **2.4.1.3 Models of SAA adsorption**

Broadly speaking there are three major models for molecular transport and adsorption: diffusion controlled, kinetic controlled and mixed kinetic-diffusion models. The diffusion-controlled model assumes that the process of diffusion from the bulk to subsurface is the rate-controlling step, and that the adsorption from the subsurface to the interface is very fast. The kinetic model assumes that once the molecule has moved to the subsurface, there may be an adsorption barrier present which retards molecular adsorption. This barrier may be due to increased surface pressure, limited empty space at the interface, steric restraint due to the proximity of other molecules, or re-orientation of molecules. All those will increase the timescale of the dynamic surface tension decay. The mixed kinetic-diffusion model reflects the equal weight to the processes of diffusion and adsorption in the overall transfer of molecules to the interface (Bonfillon et al., 1994; Ravera et al., 1994; Miller, et al., 1994; Dukhin, et al., 1995; Rosen and Gao, 1995; Campanelli and Wang, 1998).

The most influential theoretical work was conducted by Ward and Tordai (1946) who accounted for the diffusion of monomers from the bulk to the interface, and for the back diffusion into the bulk as the interface becomes more crowded. Both processes are treated using Fick's diffusion equation. In the early stages of diffusion, it has been found that the

back diffusion is not important, and the short-time approximation can be made (Miller and Kretzschmar, 1991; Joos et al., 1992; Miller et al., 1994; Dukhin et al., 1995; Campanelli and Wang, 1998). When the diffusion process is near equilibrium, the subsurface concentration will be closed to the bulk concentration, the long-time approximation of the general diffusion equation is applicable (Rosen et al., 1995; Garrett and Ward, 1995; Joos et al., 1996; Joos et al., 1992; Fang and Joos, 1996; Mobius and Miller, 1998). It is thus possible to obtain values for the surface tension gradient and surfactant diffusion coefficient from dynamic interfacial tension measurements. A more detailed analysis and explanation of these phenomena is given in Chapter 4.

In addition to the above mentioned models, some empirical models have been used to fit the experimental data (Lin, et al., 1996; Steytler, et al., 1998) but they provide little physical insight into what is really happening. Recent advances in the understanding the dynamic surface tension and SAA adsorption models are comprehensively review by Eastoe and Dalton (2000).

#### **2.4.2 Effect of Interfacial Characteristic on Bubble Breakup**

Tavlarides, et al. as early as 1970, reviewed the phenomena of bubble breakup. Wilkinson et al. (1993) and Risso (2000) summarized recent advances in the understanding of bubble deformation and breakage behavior under the influence of various flow conditions, fluid viscosities and densities. However, very limited effort was dedicated to investigating the effect of interfacial characteristics on bubble breakage.

The use of Taylor instabilities to describe bubble breakup have been suggested by a number of authors (Grace et al., 1978; Batchelor, 1987; Walter, 1983). This concept is based on the application of linear perturbation analyses similar to the one originally proposed by Taylor (1950) and the results of all these analyses are generally in a form similar to Eq. (2-1). According to this result, the bubble stability (or the maximum stable bubble diameter) would decrease as the surface tension decreases, a conclusion, which is in good agreement with the experimental data for bubbles in pure liquids.

Walter and Blanch (1986) found that reducing the liquid surface tension by 50% reduces the maximum stable bubble size by 34% and, correspondingly, increases the interfacial

area per unit volume. The time required for breakup was found to vary slightly between bubbles in the same flow field, but the general trend indicated an increase in breakup time with increasing surface tension. Similarly, Wilkinson et al. (1993) reported that a higher surface tension hindered bubble breakup for small as well as large bubbles.

Al Taweel and Cheng (1996) studied the effect of interfacial properties on the characteristics of gas/liquid contacting achieved in tanks agitated by self-aerating Rushton-type impellers surrounded by a stator. As a consequence of focusing energy dissipation rate in the small gap between the impeller and stator, large gas holdups (up to  $\phi = 0.19$ ) and interfacial areas as high as  $4,160 \text{ m}^2/\text{m}^3$  were obtained in slowly coalescent systems. The results obtained also suggested that surface tension inadequately characterizes the effect additives had on the dynamic equilibrium between the individual processes of dispersion and coalescence. Better correlation was obtained by using the Gibbs surface excess value.

In order to determine the effect of surface characteristics on bubble breakup, a series of alcohol surfactants were examined by Walter and Blanch (1986). The maximum stable bubble size decreases as predicted by isotropic turbulence theory ( $d_{\text{max}} \propto \sigma^{0.6}$ ) (Levich, 1969) in the case of aqueous solutions containing short carbon chain-length surfactants (up to octanol). In the case of higher molecular weight and long-chain surfactants (such as dodecanol, antifoam, sodium lauryl sulfate, and Tween 80) maximum stable bubble sizes which are much larger than those predicted by Eq. (2-4) were observed. This was attributed to the fact that Eq.(2-4) ignores the influence of the surface excess and surface elasticity on the mechanism of bubble breakup. Their results also showed that solutions having similar surface tensions could have significantly different maximum bubble sizes. This suggested that factors other than the surface tension (such as surface elasticity) could play an important role in stabilizing the bubble.

The Surface elasticity can be described as,

$$E = \frac{\partial \sigma}{\partial \ln A} = -RT \frac{\partial \Gamma}{\partial \ln A} \quad (2-53)$$

Two important factors might influence the generation of elastic forces during bubble breakup; the magnitude of the surface excess limited by the rate of surfactant mass transfer and the rate of surface replenishment. Since the diffusivities of the surfactants used by Walter and Blanch were of the same magnitude and all the surface excesses measured were of the same order of magnitude, it appeared that surface replenishment might control the surface elasticity. The results also suggest that the surface of the bubble was rapidly replenished by low molecular weight surfactants ( $< C_8$ ) and more slowly by longer chain length surfactants ( $> C_8$ ). Surface tension gradients might thus be created on the surface. However, in a turbulent system the surface region would be well mixed, resulting in very little mass transfer resistance. A similar observation has been reported in stagnant systems by Kimizuka et al. (1972) where the interfacial tension of the solution was found to be time dependent. In a word, short chain molecules are expected to be more easily adsorbed onto the surface, and thus depict no elastic effects, while long chain molecules would take longer to properly orient themselves and adsorb at a much slower rate.

#### **2.4.3 Effect of Interfacial Characteristic on Bubble Coalescence**

Although knowledge concerning the effect of interfacial characteristics on bubble coalescence is rather limited, several reviews addressed the effect of interfacial characteristics on bubble coalescence and collapse in foam (Aveyard and Clint, 1996; Bhakta and Ruckenstein, 1997). One of the most comprehensive reviews on bubble coalescence was made by Chaudhari and Hofmann (1994). They gave the current status of the theory and mechanisms of bubble coalescence as well as experimental data on coalescence time and bubble sizes. The various physical processes involved in bubble coalescence were identified and the roles of electrolytes and surfactants are discussed. The theoretical models proposed on the basis of different mechanisms were reviewed and their utility in application to practical systems critically discussed. Hereafter, most work on SAA influencing bubble coalescence have been done by Zahradnik et al. (1995), Weissenborn and Pugh (1996), Pugh et al. (1997), Pashley and Craig (1997), and Zahradnik et al. (1999a, 1999b).

### **Influence of SAA Concentration and Surface Tension**

Although the static surface tension is popularly used in analyzing several interfacial phenomena, such as foam stability, collapse and coalescence, film drainage, etc., the concentration of the surface-active agents was adapted by many researchers to express the effect of SAAs on bubble coalescence (Marrucci, et al., 1967, 1972; Drogaris and Weiland, 1983; Prince and Blanch 1990; Zahradnik et al., 1999a, 1999b).

The results of Sagert and Quinn (1978) demonstrated the influence of the alcohol concentration on coalescence time. The coalescence time was found to be proportional to the alcohol concentration for low molecular weight alcohols, but proportional to the square of the concentration in the case of n-hexanol. Their results also showed that the coalescence time, at a given concentration, increased as the chain length of the solute increases. Ueyama et al. (1993) investigated the bubble coalescence time as a function of alcohol concentration (methanol, ethanol, propanol, and amyl alcohol). Their results were in good agreement with the data of Sagert and Quinn (1978).

The earliest model accounting mass diffusion coalescence time,  $t_s$ , was proposed by Marrucci (1969) and Sagert and Quinn (1978). The coalescence time depends mainly on a dimensionless term ( $cdk_2^2/2\sigma$ ), where  $d$  is bubble diameter;  $\sigma$  is the surface tension, while both  $c$  and  $k_2$  are quite complicated parameters that reflect the system properties. The importance concept introduced is that the ratio of coalescence time to the diffusion time of liquid film is proportional to this term ( $cdk_2^2/2\sigma$ ). High value of parameter indicates diffusion control while, on the other hand, low value of this term indicates that film thinning is controlling step.

Similar to SAAs, salts in the solutions is able to inhibit bubble coalescence by retarding the thinning of liquid film between bubble pairs (Marrucci, 1967; Nicodemo et al., 1969; Jamialahmadi and Muller-Steinhagen, 1990; Prince and Blanch, 1990; Cralg, et al., 1993; Zahradnik, et al., 1995; Weissenborn and Pugh, 1996; Pashley and Craig, 1997). It is found that at sufficiently high salt concentrations, the gas-liquid interface between coalescing bubbles is immobilized by the surface tension gradient resulting from thinning, which slows down the drainage process dramatically (Marrucci, 1967; Prince

and Blanch, 1990). The critical concentration of electrolyte required to immobilize the gas-liquid interface of coalescing bubbles is given by Prince and Blanch (1990),

$$C_t = 1.18 \left( \frac{2B\sigma}{d} \right)^{1/2} R_g T \left( \frac{\partial \sigma}{\partial t} \right)^{-2} \quad (2-54)$$

where  $C_t$  is transition concentration,  $B$  is retarded van der Waals coefficient. Film thinning time for stagnant bubbles with immobile interface is the order of seconds and partial mobility to the gas-liquid interface still results in coalescence times of the order of hundreds of milliseconds (Nicodemo et al., 1969). For salt concentrations lower than the transition value, thinning times can be calculated by the following thinning equation (Oolman and Blanch, 1986a),

$$-\frac{dh}{dt} = \left\{ \frac{8}{R_f \rho_L} \left[ -\frac{4M}{RT} \left( \frac{d\sigma}{dC} \right)^2 + h^2 \left( \frac{4\sigma}{d} + \frac{A}{6\pi h^3} \right) \right] \right\}^{1/2} \quad (2-55)$$

It has been numerically integrated for various bubble sizes with the initial and final film thicknesses. This model can well predict bubble coalescence time in either NaCl or Na<sub>2</sub>SO<sub>3</sub> solution with a low concentration range. Therefore the coalescence rate can be obtained by using the coalescence time. However, it may not be applicable in turbulent systems where the turbulent contacting time is much short, and the hydrodynamics affect surface properties and the energy of bubble collisions.

Zahradnik et al. (1999a, 1999b) conducted an experimental study aimed at examining the coalescence phenomena in aqueous solutions of aliphatic alcohols and electrolytes and at determining the effect of these surface-active compounds on bubble coalescence in viscous aqueous media with Newtonian and non-Newtonian behavior. Bubble coalescence in aqueous solutions of alcohols and electrolytes was significantly hindered by increasing solute concentration and the coalescence percentage exhibited sharp transition from 100% of bubble pairs coalescing to very low values (less than or equal to 10%) over a narrow concentration range. The transition concentrations of the surface-active additives, characterizing suppression of coalescence in their aqueous solutions, were successfully correlated as a function of the surface tension, e.g. the term



$[\sigma^n(\delta\sigma/\delta c)^2]$ , with exponent values  $n = 1/3$  or  $1/4$  (sometimes  $1/6$ ) for solutions of alcohols and electrolytes respectively.

### **Influence of Surface Excess Concentration**

A very limited number of investigators attempted to use the surface excess to describe bubble coalescence. Sagert and Quinn (1978) found the bubble coalescence time to be almost proportional to the surface excess concentration of the surfactants, such as n-butane, propane, ethane and ethylene. Drogaris and Weiland (1983) also found the coalescence time, and the coalescence frequency, could be correlated with the degree of surface coverage from solute molecule.

According to Gibbs adsorption equation, the surface excess concentration could be calculated from the change of surface tension with solute concentration ( $d\sigma/d\ln c$ ). For dilute solutions, the surface tension fell almost linearly with the bulk concentration and hence, surface concentration can be considered to be proportional to the bulk concentration. However, as the bulk concentration increases, the surface excess concentration increases but in a non-linear fashion due to the fact that the adsorbed molecules come close together and "condensed" films can be created. At a definite concentration a saturated monolayer appears and the surface excess concentration remains unaffected by further increase in solute concentration. The resulting dependence of bubble coalescence time on the solute concentration is compared with the dependence of surface excess concentration on bulk concentration in Table 2.2 for the three different film states.

The common feature of all cases was that coalescence time was proportional to surface excess concentration. It could therefore be concluded that coalescence times of bubbles of a defined size present in an aqueous solutions of a given substance were mainly determined by the surface excess concentration and not the bulk concentration (Drogaris and Weiland, 1983). It has been also demonstrated by Zlokarnik (1985) that the coalescence behavior of some aqueous systems can be clearly correlated with the corresponding  $d\sigma/dc$  values corresponding to the surface excess value.

Table 2.2 Comparison of the dependence of surface excess concentration and coalescence time on solute concentration (Drogaris and Weiland, 1983)

State of surface film	Surface excess concentration	Coalescence time
low degree of surface coverage	$\Gamma = \Gamma_{\infty} C_0$	$t_c \propto C_0, t_c \propto C_0^2$
condensed	$\Gamma = \Gamma_{\infty} \frac{C_0}{1 + C_0}$	$t_c \propto C_0^{0.5}$
saturated	$\Gamma = \Gamma_{\infty}$	$t_c = \text{const.}$

Weissenborn and Pugh (1995) assessed the inhibition of bubble coalescence by electrolytes beyond a critical transition concentration by the relation between transition concentration and surface tension gradients of electrolytes  $[d(\Delta\sigma)/dc]$ , but the correlation between transition concentration and the parameter  $[\delta(\Delta\sigma)/\delta c]^{-2}$  was mediocre ( $R^2 = 0.74$ ).

Recently, Zahradnik et al. (1999a, 1999b) studied the effect of surface-active additives on bubble coalescence in aqueous media. The solutes include organic solvent such as ethanol, propanol, butanol, pentanol, hexanol, and octanol, and also up to seven different electrolytes. The suppression of bubble coalescence in their aqueous solutions was successfully correlated as a function of the term  $[\sigma''(\partial\sigma/\partial c)^{-2}]$  for solutions of alcohols and electrolytes.

In a summary, it can be said that several investigators reach the conclusion that bubble coalescence time is related to the surface excess within the range of operating conditions they investigated. Unfortunately, all these investigations were carried out using a pair of bubbles coalescing in either stagnant fluids or in bubble columns where the hydrodynamic turbulence is not known and could not be controlled.

### **Influence of Surface Charge**

For solutions of ionic surfactants an additional resistance to film thinning exists. The surface active ions are usually concentrated on the bubble surface due to the electrolyte adsorption and a surface electrical double layer (with a thickness of 10-100 nm) is formed. This leads to reducing the coalescence rate due to the introduction of charge repulsion forces. The fact that coalescence was inhibited by the development of electrostatic charges on the dispersed bubbles had been verified by several experiments (Zieminski and Whittemore, 1971; Zlokarnik, 1985; Vrtovsek et al., 1989; Prince and Blanch, 1990; Pashley and Craig, 1997).

Based on drainage time measurements, Pashley and Craig (1997) developed the following simple expression for calculating the thickness of the thinning film,  $h$ , as a function of time ( $t-t_0$ ). They considered the case of parallel disks of radius  $r$ , with zero slip condition at the liquid-wall interfaces and obtained,

$$h = \{[4P(t-t_0)/(3\mu r^2)] + 1/h_0^2\}^{-1/2} \quad (2-56)$$

where  $h_0$  is the initial film thickness at time  $t_0$ ,  $P$  is the drainage pressure,  $\mu$  is the viscosity of the fluid. This equation is able to predict film thinning in pure water systems well.

## CHAPTER 3 EXPERIMENTAL

This chapter addresses the experimental set-up, details concerning the construction and operation of the dynamic sparger, the methods used for measuring and calculating the various parameters, sources of error, and the systems investigated.

### 3.1 Experimental Setup

The experimental setup used in this investigation is schematically depicted in Fig. 3.1. It consists of a 9 m pipe loop constructed from transparent polycarbonate piping (25.4 mm i.d.) that can be used to investigate once-through and recirculating pipeline operations. The loop contains a vertical section 2.2 m high that was used to study the effect of various design and operating conditions on gas/liquid contacting but neglecting effect of gravity. An agitated 1,000 liter polyethylene tank was used to prepare and store the liquid used in this investigation. This liquid was fed at a controlled rate to the pipeline by means of a centrifugal pump and its flow rate was measured by a paddle-wheel flow meter (SIGNET model: MK 309). Superficial liquid velocities as high as 3.2 m/s could thus be achieved in the main pipeline.

Compressed air was introduced to the flowing liquid stream through a novel dynamic sparger (the TUNS sparger) located at the bottom of the vertical section. The amount of compressed air passing through the sparger was measured and controlled using a mass flow PID controller (MKS1151 supplied by MKS Technology). A small part of the solution from the tank was branched for dispersion purpose in the two-phase spargers and was adjusted by a manual valve to maintain the desired pressure drop between the sparger's inlet and the point of discharge or to keep the flow rate constant.

The interfacial area of contact was measured at a point where the two-phase jet is fully mixed with the main flow (0.46 m downstream from the sparger tip). The results reported here may thus be considered as conservative estimates since some coalescence took place before the measurement point was reached. A laser-based light attenuation technique (Kasireddy and Al Taweel, 1990) was used to measure the average interfacial area of

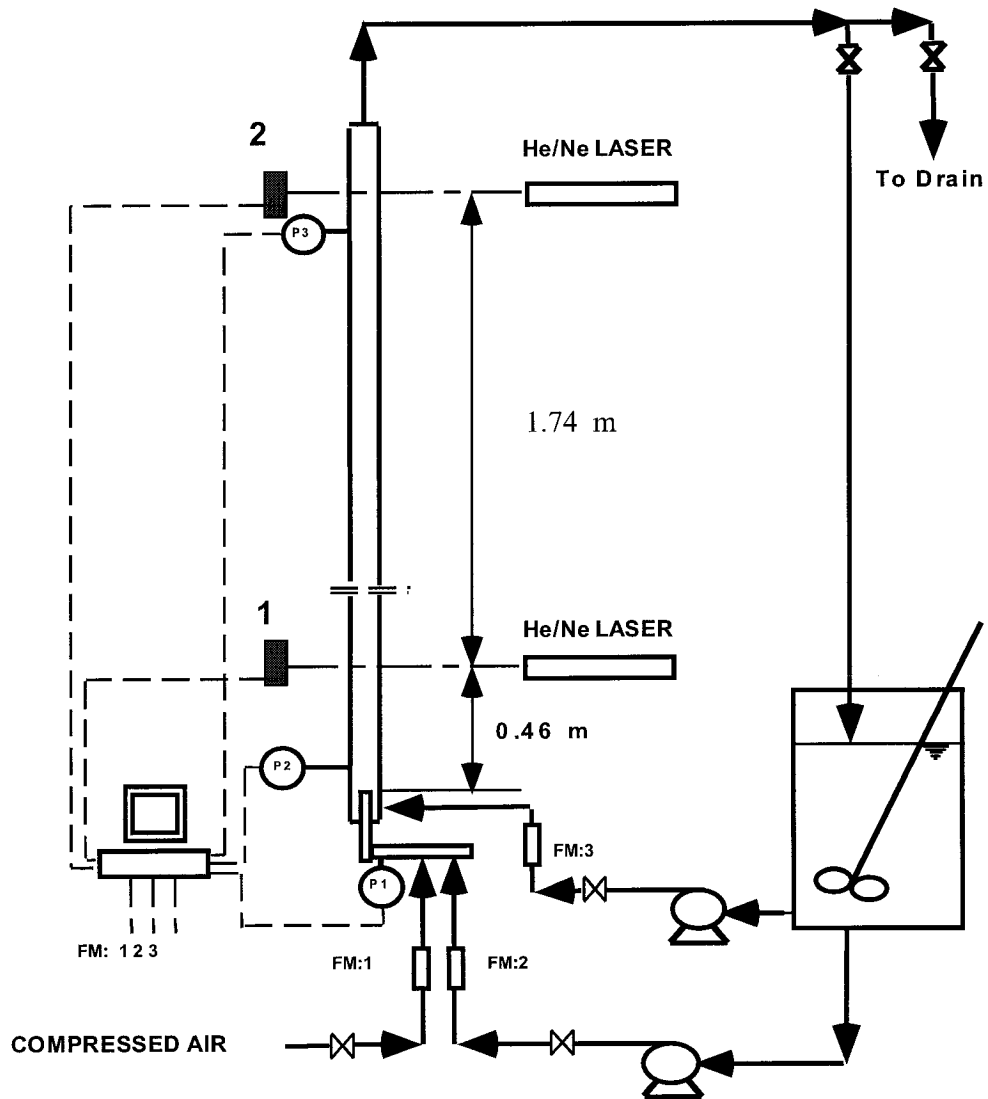


Fig. 3.1 Experimental set-up

contact along the path of the light beam (i.e. across the pipe's diameter). This technique accounts for the multiple scattering encountered at high interfacial areas, and as such is capable of measuring interfacial areas as high as  $7,000 \text{ m}^2/\text{m}^3$ .

On-line specific interfacial area measurement were conducted at a second point (1.74 m downstream from the first one) in order to provide information that can be used for calculating coalescence rates in the pipeline under the different experimental conditions investigated. No detectable bubble segregation was detected in the horizontal or vertical runs of the flow loop. This can be attributed to the formation of very small bubbles that exhibit low segregation tendencies.

Centrifugal force was used to facilitate separation of the gas bubbles from the recycled streams at the main tank (the mixture stream was introduced tangentially). Pressures were measured at three different locations, at the inlet and outlet of the sparger, and at the top of the vertical pipeline by means of pressure transducer (OMEGA Eng. Model PX26).

A data acquisition/control system was used to monitor several experimental parameters (temperature, pressures, pressure drop across the sparger, liquid flow rate, and interfacial area of contact) and to control the main operational parameter (the gas to liquid flow ratio in the pipe flow). It consists of a National Instruments data acquisition board (AT-MIO-16E-10) with 16 analog input channels and 2 analog output channel. A special program was developed using LabVIEW version 3.0 and LabVIEW PID to calculate the Sauter mean bubble diameter and allow all monitoring and control processes to be conducted in a user-friendly fashion.

The dynamic sparger used, and its installation in the pipeline, are shown in Fig. 3.2. The sparger head is detailed in Fig. 3.3. The sparger is based on the concept of the Venturi-tube (converging section, throat, and divergent section) in which the cross section of the circumferential throat can be adjusted by means of a regulating spindle the position of which can be adjusted along the sparger's axis. The cross sectional area of the throat decreases as the conical spindle moves further into the Venturi, and decreases as it is pulled away from the throat.

The gas and liquid streams are introduced at the bottom of the sparger and move along the annular gap between a rod and the inner walls of the sparger tube. The two-phase flow passes through a packed mixing section that pre-disperses the gas phase into small bubbles. It then passes through the convergent section where it is accelerated to the velocity at the entrance to the throat section where most of the pressure drop takes place. The finely-dispersed gas liquid stream emerging from the throat de-accelerates as it progresses through the divergent section and ultimately mixes with the main stream flowing through the pipe as shown in Fig. 3.2. That two-phase jet formed as the jet coming out from the sparger mixes with the surrounding pipe flow stream is shown in Fig. 3.4.

The mechanism responsible for the formation of finely-divided bubbles in the two-phase sparger depends on the operating conditions used. Turbulent breakage in the regions of high energy dissipation rates encountered in the throat is thus expected to dominate under conditions where bubble coalescence plays a relatively small role. Cavitation and the presence of a standing sonic wave are expected to play a role when the two-phase sonic velocities are exceeded in the throat (large gas flowrates, high pressure-drops across the sparger, and small cross sectional areas in the throat).

After the extreme small bubbles are formed in the throat, the small bubble could start to coalesce when they flow through the expanding portion of the sparger. Once the bubbles produced move out of the tip of the sparger, they will coalesce and grow large dramatically.

One of the advantages of using this dynamic sparger design is the possibility of adjusting the size of the gas dispersion generated without interrupting the process operation. This can be achieved by adjusting the gas to liquid ratio and/or the pressure drop across the sparger (i.e. the cross sectional area of the throat). However, since the dispersion of the gas phase takes place mostly in the throat, the size of bubbles generated by the sparger is strongly influenced by the interfacial characteristics of the stream since the fine bubbles formed in the region of high energy-dissipation coalesce into large entities as they move

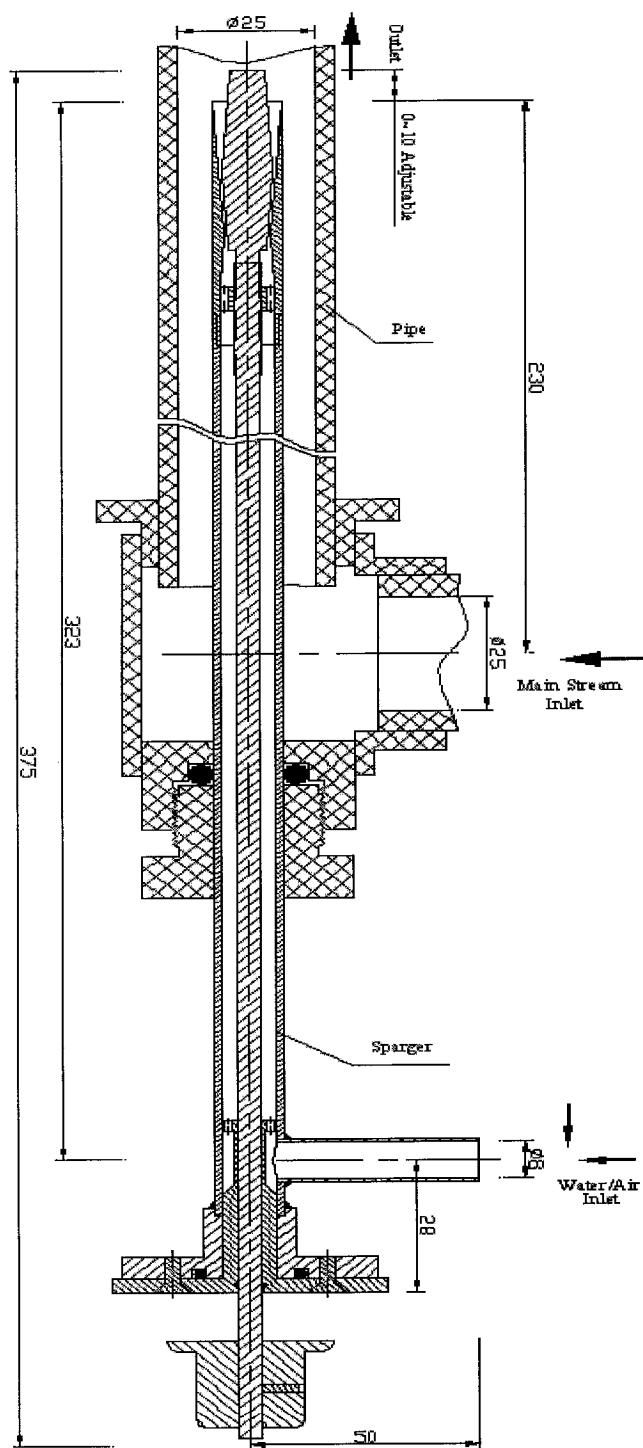


Fig. 3.2 Diagram of dynamic sparger and its installation



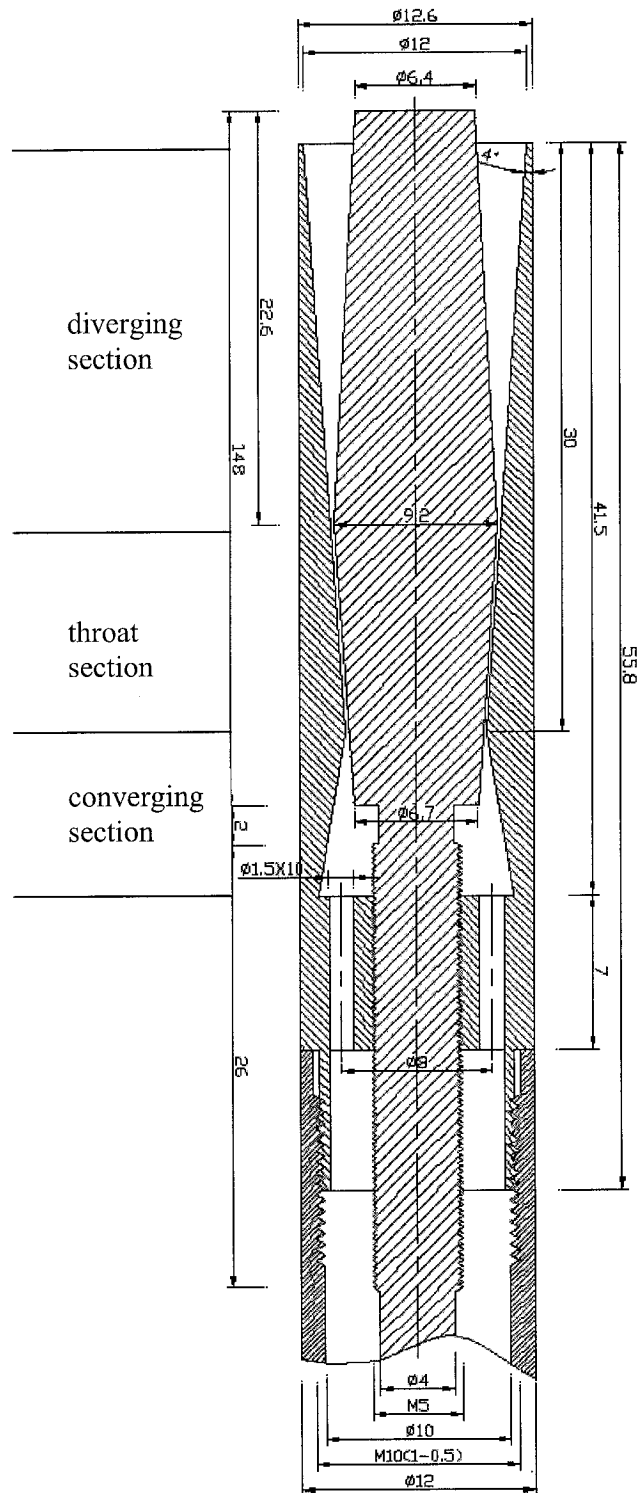


Fig. 3.3 Geometry of the sparger head

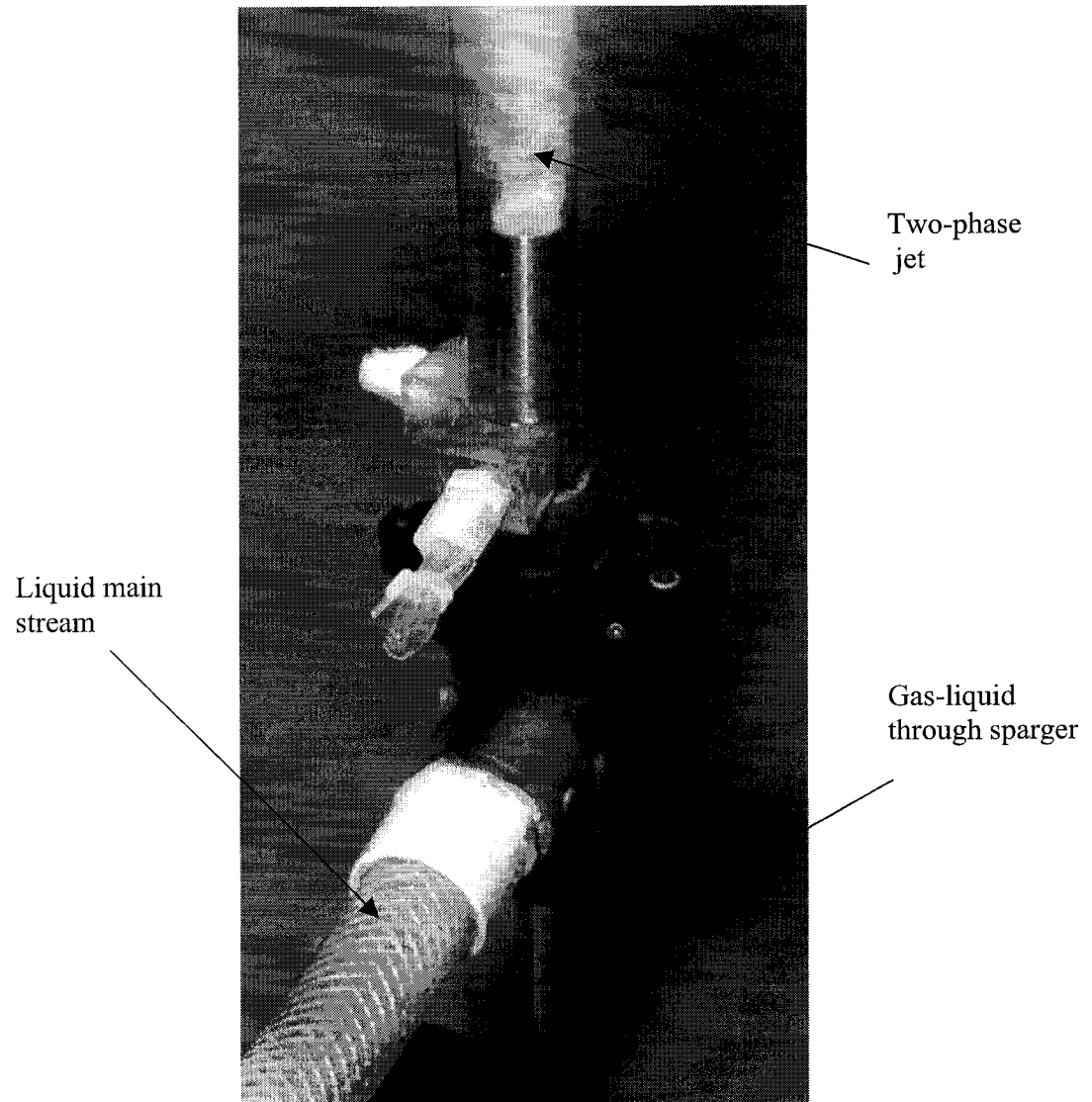


Fig. 3.4 Two-phase jet formed from the sparger mixes with the surrounding pipe flow stream

into regions of significantly lower energy dissipation rates (such as the divergent section and in the pipeline).

### **3.2 Sources of Error**

By using the laser attenuation technique, a part of discrepancy is due to non-uniform bubble size; particularly bubble dispersion with wide size distribution would cause more deviation. The gas holdup is assumed as gas-liquid flow ratio for current investigation, then the Sauter mean diameter is calculated will produce error too. The statistical bias stems from the limited bubble number detected through a narrow light path across the pipe diameter to represent that of the whole cross-sectional area. Those error analysis were well reviewed by Al Taweel, etc. (1984) and Kasireddy and Al Taweel (1990).

In addition, it is a good practice for two laser sensors to obtain almost the same initial signals at two locations in order to eliminate the error caused by age difference of the sensor or illuminators.

The mass flow controller and the pressure sensor would also bring 0.1 and 1% separately.

### **3.3 Systems Investigated**

In order to simulate the coalescence retardation phenomena encountered in most industrial streams, additives (such as MIBC and SDS ) were intentionally added to the tap water. MIBC (methyl-iso-butyl carbinol) is a nonionic surface active agent (SAA) composed of a mixed 6-carbon alcohol. The material supplied by Allied Colloids Ltd. (as Procol F937) contains about 20% methyl isobutyl carbinol in other organic solvents including MIBK (methyl isobutyl ketone) and mesityl oxide, the rest being inert components. The shortcoming of choosing MIBC is not only that the components in MIBC solution can change from one supplier to another but also the paucity of information concerning the dynamic interfacial properties of this system (Johansson and Pugh, 1990; Zhou, et al., 1993).

Therefore, another well-known surface-active agent, SDS (Product No. L5750, made by Sigma Chemical Co., containing approximately 95% Sodium Dodecyl Sulfate,  $C_{12}H_{25}SO_4Na$ , based on alkyl sulfate content) whose interfacial characteristics are well-known

was also used in this investigation in order to enable a better understanding of the role interfacial characteristics play in gas/liquid dispersion/coalescence processes.

The static surface tension of MIBC aqueous solutions was measured by Rajasekhar (1983) and its presence in the concentration range of 0 - 100 ppm (i.e.  $0 - 9.8 \times 10^{-4}$  mol/L) was found to reduce the static surface tension from 72.8 to 32.5 mN/m. The static and dynamic surface tension of SDS aqueous solutions currently used were measured by (Chen, 1996) and Yang (1996). Its presence in distilled water was found to reduce the static surface tension from 72.8 mN/m to 44.1 mN/m when its concentration range is changed from 0 to 50 ppm ( $0 - 3.12 \times 10^{-6}$  mol/L). The effect of SAA concentration on the static surface tensions is shown in Fig.3.5 for SDS and MIBC.

The static surface tensions were found to decrease with increasing SAA concentrations, but the trends appear to be different. The aqueous SDS solution exhibits the normal pattern where its surface tension undergoes rapid reduction in the presence of small SDS concentration but approaches an asymptote at high concentrations. This follows the

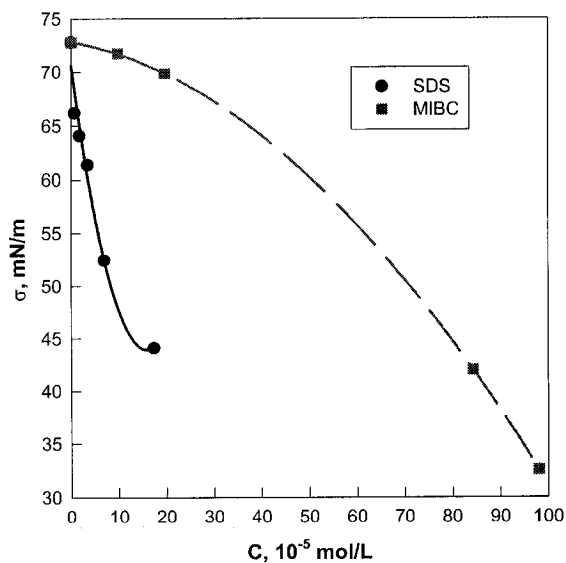


Fig. 3.5 Static surface tension of SDS and MIBC systems

trends identified by Mysels (1986) over a decade ago. On the other hand, the experimentally observed behavior of MIBC solution does not show similar tendencies, the surface tension decreases slowly as the concentration of MIBC increases, which agrees to the findings by Johansson and Pugh (1990), Zhou, et al. (1993). It indicates that different types of SAA exhibit dissimilar interfacial properties. An in depth analysis of the static and dynamic properties of the aq. SDS solutions is presented in Chapter 4.

### 3.4 Methods of Parameter Computation and Turbulence Validation

The variables involved and their computation methodology will be discussed in this section. The measured parameters and computational results are listed in a CD-ROM attached.

The Sauter mean bubble diameter was calculated from a knowledge of the interfacial area of contact and the gas holdup at the point of measurement using the following equation,

$$d_{32} = \frac{6\Phi}{a} \quad (3-1)$$

and the bubble population density was calculated from,

$$n = \frac{\Phi}{\frac{1}{6}\pi d_{32}^3} \quad (3-2)$$

Because of the compressibility of the gas fed to the sparger, the volumetric flow rates passing through the sparger were not directly measured but calculated from a knowledge of the mass flow rate of each phase and the pressures at the entrance and exit of the sparger. The total mass flow rate passing through the sparger,  $W_{\text{sparger}}$ , is thus given by,

$$W_{\text{sparger}} = A \times (Q_{\text{GS}}/Q_{\text{LP}} \times U_{\text{LP}} \times 1.293 + U_{\text{LS}} \times 998.2) \quad (3-3)$$

where  $A$  is the cross-sectional area of the pipe on which the superficial velocities are based,  $Q_{\text{GS}}/Q_{\text{LP}}$  is volumetric flow ratio of gas in the sparger over liquid in the pipeline,  $U_{\text{LP}}$  and  $U_{\text{LS}}$  are superficial liquid velocities in the pipe and the sparger measured at standard conditions. The densities for air and water at standard conditions are 1.293 and

998.2 kg/m<sup>3</sup> respectively. To add the mass flow rate of main liquid stream in Eq.(3-3), it will be the mass flow rate in the pipeline, which is given by,

$$W_{Pipe} = A \times [Q_{GS}/Q_{LP} \times U_{LP} \times 1.293 + (U_{LS} + U_{LP}) \times 998.2] \quad (3-4)$$

The gas mass flow rate is given as,

$$W_G = A \times Q_{GS}/Q_{LP} \times U_{LP} \times 1.293 \quad (3-5)$$

The mass fraction of air in the two-phase flow thus becomes,

$$x = W_G/W \quad (3-6)$$

In general, the gas holdup for dispersed bubbly flow is given by,

$$\Phi = Q_G / (Q_G + Q_L) = \frac{x / \rho_g}{x / \rho_g + (1-x) / \rho_L} = \frac{1}{1 + \frac{(1-x) / \rho_L}{x / \rho_g}} \quad (3-7)$$

This is a universal equation that can be applied to different locations, such as in the sparger or in the pipeline, but the gas density,  $\rho_g$ , will change accordingly as the pressure in various locations, whereas, the liquid density,  $\rho_L$ , remains practically constant. For instance, the gas holdup in location 1 is,

$$\Phi_{G1} = \frac{1}{1 + \frac{(1-x) / \rho_L}{x / (\rho_g P_1 / P_0)}} \quad (3-8)$$

whereas the average gas holdup in the pipeline will be,

$$\Phi_{Pipe} = \frac{1}{1 + \frac{(1-x) / \rho_L}{x / (\rho_g P_{Pipe} / P_0)}} \quad (3-9)$$

For homogeneous flow, the mixture density can be expressed in terms of gas holdup as,

$$\rho_m = \Phi \rho_g + (1 - \Phi) \rho_L \quad (3-10)$$

Study of bubble dispersion and coalescence requires knowledge of several parameters (such as local energy dissipation rate, scales of energy-containing eddies and energy-

dissipating eddies) besides the value of Reynolds number that characterize the overall turbulent flow conditions.

Turbulent velocity fluctuations ultimately dissipate their kinetic energy through viscous effects. From the macro-scale point of view, energy dissipation requires pressure gradient or velocity decrease. If a small volume,  $V$ , is selected for study, the volumetric flow rate of fluids is,  $Q$ , and the pressure gradient is,  $dP$ , the local energy dissipation rate per unit mass of the continuous phase is given by (Levich, 1962; Walker, 1984 and Zahradnik, et al., 1991),

$$\varepsilon = -\frac{dE}{dt} = -\frac{dP / \rho_L}{V / Q} \quad (3-11)$$

The average local energy dissipation rate per unit mass from location 1 (static pressure as  $P_1$ ) to location 2 (static pressure as  $P_2$ ) is calculated as,

$$\begin{aligned} \varepsilon &= -\int \frac{Q dP}{\rho_L V} = -\int \frac{\rho_m dP}{\rho_L V} = -\frac{W}{\rho_L V} \int_{P_1}^{P_2} \frac{dP}{\rho_m} \\ &= -\frac{W}{\rho_L V} \int_{P_1}^{P_2} \left( \frac{x}{\rho_g} + \frac{1-x}{\rho_L} \right) dP = -\frac{W}{\rho_L V} \int_{P_1}^{P_2} \left( \frac{x}{\rho_{g0} \frac{P}{P_0}} + \frac{1-x}{\rho_L} \right) dP \\ &= -\frac{W}{\rho_L V} \left[ \frac{x P_0}{\rho_{g0}} \int_{P_1}^{P_2} \frac{dP}{P} + \frac{1-x}{\rho_L} (P_2 - P_1) \right] \\ &= \frac{W}{\rho_L V} \left[ \frac{x P_0}{\rho_{g0}} \ln \frac{P_1}{P_2} + \frac{1-x}{\rho_L} (P_1 - P_2) \right] \end{aligned} \quad (3-12)$$

where  $\rho_m$  is the density of the mixture,  $\rho_{g0}$  is air density at 25°C,  $p_0$  is standard atmosphere pressure. The first term is the contribution made by gas phase whereas the second term represents the contribution of the liquid phase. As shown by Ramadan (1996), the relative importance of the first term is small at small gas holdups and low pressure drops. It was therefore decided to retain both terms while calculating  $\varepsilon$  since gas holdups as large as 0.5 were encountered in this work. This expression can, therefore, be applied to the case either in the pipe or in the sparger.

In turbulent flow, primary eddies which have scales similar to the dimensions of the main flow stream are produced by mechanical and/or pneumatic forces. These large primary eddies are not isotropic and are unstable, disintegrating into smaller eddies of intermediate size. The intermediate-size eddies contain the bulk of the turbulent kinetic energy and are usually referred to as the energy-containing eddies. The scale of these energy containing eddies is approximated by (Hinze, 1975),

$$L_e = \frac{\kappa D}{2} \quad (3-13)$$

where,

$\kappa$  is von Karman constant = 0.41 (Kamp, et al., 2001).

D is pipe diameter [m]

For the pipeline used in the current investigation, the scale of the energy-containing eddies is therefore 5.2 mm which is larger than most bubble (typical bubble size is 1.3 mm) encountered in the present investigation. Some investigators such as Prince and Blanch (1990) and Kawase and Moo-Young (1990) assumed that the size of the energy-containing eddies to be equal to the vessel diameter, which would be 25.4 mm for the current investigation and is much larger than the largest bubble (8.7 mm) formed in current research.

These intermediate eddies eventually break up into smallest eddies and finally into the energy-dissipating eddies (i.e. Kolmogoroff eddies) which have completely lost their directional nature and are isotropic. The size of the Kolmogoroff eddies was thus determined using Eq. (2-9) from which it was found that  $L_k = 12 - 22 \mu\text{m}$  in the pipeline for the range of experimental conditions investigated.

To validate the bubble collision model in turbulent flow and determine the turbulent velocity, it is necessary to assume that the turbulence is isotropic and the bubble size lies in the inertial range. This criterion is typically examined in terms of three scales as,

$$L_k \leq d_b \leq L_e \quad (3-14)$$

The bubble size range for the current investigation is of 25  $\mu\text{m}$  - 8.7 mm for the combined system of air pure water and air-SDS aqueous solutions (which has a typical



bubble size of 1.3 mm) whereas it varied between 25  $\mu\text{m}$  and 4.0 mm for the air- aqueous SDS solutions (with a typical bubble size of less than 1 mm). These sizes are, therefore, larger than the Kolmogoroff scale (12 or 22  $\mu\text{m}$ ) and smaller than scale of the energy containing eddy (5.2 mm or 25.4 mm).

Generally, in turbulent pipe flow with high Reynolds number, the velocity profile in radial coordinator appears as low velocity near the wall and almost uniform high value of the velocity around the core. The radial profile of the local energy dissipation rate is opposite, which there is high value of the local energy dissipation rate near the wall but homogeneous low value in the rest and also most of cross-sectional area (Hinze, 1975). Therefore it is homogeneous in almost all over the cross-sectional area in terms of the energy dissipation rate, even in anisotropic turbulent flow, those small bubbles just like the small eddies often behave in an isotropic manner locally.

### 3.5 Experimental Conditions

The performance of dynamic spargers is strongly influenced by bubble breakage and coalescence rates which, in turn, are influenced by four main operating parameters:

- gas to liquid flow ratio in the sparger,
- pressure drop across the sparger,
- liquid flow rates in the sparger, and
- the coalescence tendencies of the system which, in turn, are influenced by the SAA concentration (Luo et al., 1998).

The pressure drop across the sparger is controlled by both the cross section area of the throat in the sparger and by the liquid and gas flow rates passing through it. The ranges of experimental conditions investigated are summarized as follows:

Superficial liquid velocity in pipeline( $U_L$ )	0.2 – 3.2 m/s
Gas holdup in pipeline (mean value of 0.14)	0.008 – 0.50
Sparger to pipeline liquid flow ratio	0.05 – 0.27
Reynolds number in pipeline	5,000 – 80,000
Energy dissipation rate in pipeline	4.5 – 48 W/kg

Kolmogoroff scale in pipeline ( $L_k$ )	12 – 22 $\mu\text{m}$
Scale of energy containing eddies ( $L_e$ )	5.2 – 25.4 mm
Bubble size in pipeline ( $d_{32}$ )	25 – 8,700 $\mu\text{m}$
Average energy dissipation rate in sparger	8.4 – $1,900 \times 10^3$ W/kg
Average Kolmogoroff scale in sparger	1.5 – 3.3 $\mu\text{m}$
Cross-sectional area of annual channel in sparger throat	1.5 – 17.7 $\text{mm}^2$
Gas holdup at sparger tip (mean value of 0.56)	0.08 – 0.93
MIBC concentration in the tap water tested	0 – 100 ppm
SDS concentration in the tap water tested	0 – 50 ppm
Static surface tension in the aqueous MIBC solutions	32.5 – 72.8 mN/m
Static surface tension in the aqueous SDS solutions	44.1– 72.8 mN/m
Weber number (mean value of 2.0)	0.003 – 29

The performance of the sparger was evaluated using both MIBC and SDS aqueous solutions whereas the effect of hydrodynamic and interfacial characteristics on bubble coalescence process was evaluated using the well-known SDS system.

In order to test the effect of every individual parameter (such as the gas-liquid flow ratio, or the pressure drop between the sparger, etc.), different operating combinations were selected. The sparger performance tests for MIBC solutions (108 Runs) were conducted while maintaining a constant pressure drop across the sparger, whereas constant gas-to-liquid flow ratio was maintained throughout the sparger performance tests for SDS solution (388 Runs). The latter, were also used to investigate the role of interfacial characteristics in bubble breakage and coalescence processes.

## CHAPTER 4 INTERFACIAL CHARACTERISTICS OF THE SYSTEMS STUDIED

The presence of minor quantities of impurities in processing streams is known to strongly influence multiphase contacting with up to 80-fold increase in interfacial area being observed in gas-liquid contactors (Zlokarnik, 1985; Jamialahmadi and Muller-Steinhagen, 1992; Al Taweel and Cheng, 1996; Zahradnik et al., 1999). This is mostly due to the ability of these impurities to significantly affect the interfacial characteristics of the system which are very important factors governing bubble breakage and coalescence rates. However, identification of the role these interfacial characteristics plays remains a challenge particularly in the case of industrial streams that contain a multitude of polar surface-active ingredients.

This chapter attempts to systematically characterize the interfacial properties of the streams used in this investigation (very dilute aqueous solutions of SDS or MIBC) as a means of simulating the interfacial behaviour of industrial systems.

### 4.1 Background

In this section, the theories used to interpret the interfacial properties will be summarized and the approaches used to analyze the adsorption of surfactant onto the interface will be discussed. Practically both static and dynamic parameters commonly used to express the interfacial characteristics will thus be covered.

#### 4.1.1 Static Interfacial Characteristics

The interfacial properties of gas/liquid systems are usually characterized using equilibrium, or thermodynamic, properties such as the static surface tension,  $\sigma_{sta}$ , surface pressure,  $\Pi$ , or the Gibbs surface excess,  $\Gamma_G$ . The value of the static surface tension is a reflection of the fact that the attractive van der Waals forces between molecules in a liquid are felt equally by all molecules except those in the interfacial region between the dispersed and continuous phases. This imbalance pulls the molecules of the interfacial region toward the interior of the liquid and the resulting contracting force at the surface is known as the surface tension. The static surface tension,  $\sigma_{sta}$ , is thus defined thermodynamically as the free surface energy per unit area when equilibrium is reached.

It is also defined as the force per unit length (measured at equilibrium) trying to minimize the interfacial area of contact, an approach that illustrates the fact that area expansion of the surface requires energy input.

The value of the surface pressure,  $\Pi$ , is a reflection of the fact that the free surface energy per unit interfacial area (measured under equilibrium conditions) is generally reduced when surface-active agents are present in solution. It is, therefore, defined as the surface tension of the pure solvent minus that of the surfactant solution measured at equilibrium.

$$\Pi = \sigma_0 - \sigma_\infty \quad (4-1)$$

It yields information about the tendency of the surface-active molecules to adsorb at the interface as well as the ability of these adsorbed molecules to reduce the free surface energy of the interface.

The amount of SAA species adsorbed per unit area of the interface can be calculated indirectly from equilibrium measurements of the effect SAA bulk concentration has on the value of the static surface tension. This parameter is usually referred to as the surface excess,  $\Gamma$ , which can readily be calculated by using the Gibbs isothermal adsorption equation,

$$\Gamma = -\frac{C_0}{RT} \left( \frac{\partial \sigma_{sta}}{\partial C_0} \right) \quad (4-2)$$

If the surfactant is ionized, both the anions and cations of the surfactant will adsorb to the interface to maintain the local electrical neutrality even though not all of these ions are surface-active. A factor of 2 is required to allow for this simultaneous adsorption of cations and anions, and the Gibbs equation has to be modified as (Shaw, 1988),

$$\Gamma = -\frac{C_0}{2RT} \left( \frac{\partial \sigma_{sta}}{\partial C_0} \right) \quad (4-3)$$

As the SAA concentration increases the value of the surface excess increases as a result of more surfactant molecules moving onto the surface. This process continues until a plateau is reached at which the interface is saturated by the surfactant molecules. The value of the surface excess under such conditions is called the maximum or saturation

surface excess,  $\Gamma_{\infty}$ . The Langmuir Adsorption law can be used to correlate the surface excess at any concentration to the saturation surface excess as follows,

$$\Gamma_{sta} = \Gamma_{\infty} \frac{C_0}{a_L + C_0} \quad (4-4)$$

The above-mentioned static interfacial characteristics ( $\sigma_{sta}$ ,  $\Pi$ ,  $\Gamma_{sta}$ ) are commonly used to describe and correlate the performance of gas/liquid contacting operations. Whereas this may be acceptable in the case of pure and uncontaminated systems (where the value of the surface tension does not vary with time), it should be born in mind that the time scales encountered in many processing applications do not allow for the surfactant molecules to reach equilibrium at the interface. For example, whereas bubble breakage and coalescence in turbulent flows usually take place within milli-seconds (Oolman & Blanch, 1986), the time required for most SAA species to approach equilibrium at the interface is in the order of seconds or minutes. The use of equilibrium interfacial characteristics, for example the static interfacial tension, to describe such a highly dynamic processes is most probably one of the main reasons behind the proliferation of system specific correlation. It is also the main reason behind the difficulties while correlating gas/liquid contacting in complex systems (Walter and Blanch, 1986; Zahradnik et al., 1995; Al Taweel and Cheng, 1996). Better understanding of the effect SAA have on the dynamic interfacial characteristics is therefore necessary for the development of more effective gas/liquid contactors and predicting their behaviour when used in conjunction with industrial streams that usually incorporate a wide range of constituents.

#### 4.1.2 Modeling Dynamics of Interfacial Diffusion/Adsorption

The dynamics of SAA diffusion/adsorption at the gas/liquid interface is usually considered as a two-step process (Ward and Torda, 1946; Borwankar and Wasan, 1983; Joos and Serrien, 1989; Garrett and Ward, 1989 and Fang and Joos, 1996) in which the SAA molecules are first transferred from the bulk of the liquid to the subsurface (a thin liquid layer immediately below to the interface) then the molecules are adsorbed from the subsurface onto the interface (Fig. 4.1). The speed at which each of these steps takes

place will determine whether the overall diffusion/adsorption kinetics are diffusion-controlled, adsorption barrier-controlled or mixer mode.

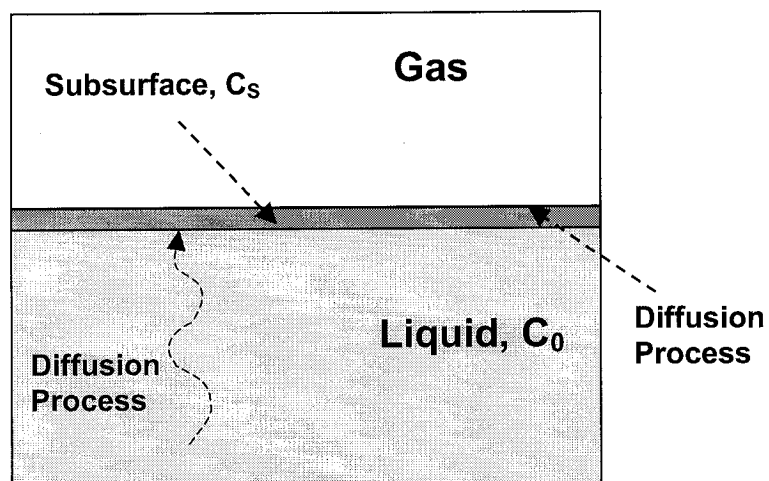


Fig. 4.1 Schematic representation of SAA dynamic adsorption on gas/liquid interfaces

Few models have been proposed in the literature to characterize the dynamics of adsorption processes involving SAA at gas-liquid or liquid-liquid interfaces. In most cases, the overall rate of adsorption has been found to be controlled by the diffusion of a SAA from the bulk phase to the subsurface (Garrett and Ward, 1989; Joos and Serrien, 1989; Bonfillon et al., 1994; Ravera, et al., 1994; Rosen, 1996; Fang and Joos, 1996; Campanelli and Wang, 1998). In few cases, the transport of the SAA from the subsurface to the interface plays a role that is almost equally important to the molecular diffusion in the bulk of the liquid (Miller et al., 1994; Dukhin, et al., 1995; Campanelli and Wang, 1998). In such cases, the condition becomes that of mixed diffusion-kinetic adsorption, a situation that is beyond the scope of the present investigation.

The adsorption dynamics of most SAA studied in the literatures can thus be adequately described by considering the diffusion-controlled models alone (Garrett and Ward, 1989; Joos and Serrien, 1989; Fang and Joos, 1996; Mobius and Miller, 1998). The classical form of the diffusion controlled adsorption equation was derived by Ward and Tordai

(1946). It is based on the assumption that the interfacial concentration of surface active molecules,  $\Gamma(t)$ , is limited by diffusion of the surfactant from the bulk phase to a clean interface. The resulting mathematical expression has the following form:

$$\Gamma(t) = 2\sqrt{\frac{D}{\pi}} \left\{ C_0\sqrt{t} - \int_0^t C_s(0, t-\tau) d\sqrt{\tau} \right\} \quad (4-5)$$

where,

$\Gamma(t)$	is the surfactant excess of SAA molecules	[mol/m <sup>2</sup> ]
$C_0$	is the bulk SAA concentration	[mol/m <sup>3</sup> ]
$C_s(0, t-\tau)$	is the subsurface concentration	[mol/m <sup>3</sup> ]
$\tau$	is a dummy variable of integration	[s]

The first term accounts for the SAA diffusion in the bulk of the solution while the second term accounts for the molecular transport/adsorption near the subsurface. The application of such complex equation to dynamic surface tension is not practicable since it contains two independent functions  $\Gamma(t)$  and  $C_s(0, t-\tau)$ . The convolution integral makes the exact solution of Eq. (4-5) difficult. Only recently, when Fainerman et al. (1994) derived asymptotic solutions to the Ward and Tordai equation (Short-term and long-term approximations) was it possible to apply Eq. (4-5) to the case of interfacial surfactant diffusion/adsorption.

#### 4.1.2.1 Short-term Approximation

In the early stages of an adsorption process, i.e. as  $t \rightarrow 0$ , there is little back diffusion into the bulk of the solution, and the second term in Eq. (4-5) can be neglected yielding,

$$\Gamma(t) = 2C_0\sqrt{\frac{Dt}{\pi}} \quad (4-6)$$

Similarly, at the start of the adsorption process when  $\sigma \rightarrow \sigma_0$ , the surfactant solution in the subsurface is dilute and Henry's isotherm can be used to relate  $\Gamma$  and  $\sigma$ , yielding,

$$\sigma - \sigma_0 = -2RT\Gamma \quad (4-7)$$

The short-term approximation can thus be expressed as (Miller and Fainerman, 1994),

$$\frac{d\sigma_t}{dt^{1/2}} = -2RTC_0\sqrt{\frac{D}{\pi}} \quad (4-8)$$

If the relationship between the dynamic surface tension,  $\sigma_t$ , and  $t^{1/2}$  is a linear one, an accurate value of  $\frac{d\sigma_t}{dt^{1/2}}$  can be obtained by plotting  $\sigma_t$  vs.  $t^{1/2}$  and determining the slope of the straight line fitting the experimental data. Using this information, and the value of the surfactant bulk concentration at which the data were obtained, it is possible to determine the surfactant diffusion coefficient from dynamic interfacial tension measurements through the application of Eq. (4-8).

#### 4.1.2.2 Long-term Approximation

When the adsorption process is far from the initial state, i.e. as  $t \rightarrow \infty$ , the subsurface concentration will be close to that present in the bulk of the liquid, and

$C_s$  can therefore be eliminated out from the integral in Eq.(4-5), and the following expression will be acquired,

$$\Delta C_{t \rightarrow \infty} = C_0 - C_s = \Gamma \sqrt{\frac{\pi}{4Dt}} \quad (4-9)$$

Combining Eq. (4-9) with the Gibbs isotherm equation, the long time approximation can be expressed as,

$$\frac{d\sigma_t}{d(t^{-1/2})} = \frac{RT\Gamma^2}{C_0} \sqrt{\frac{\pi}{D}} \quad (4-10)$$

Fang and Joos (1996) proposed a method to directly calculate SAA diffusivity from its dynamic interfacial tension data. They reorganized Eq. (4-10) into,

$$\left[ \frac{d\sigma_t}{d(t^{-1/2})} C_0 \right]^{-1/2} = \frac{1}{\Gamma} \left[ \frac{1}{RT} \left( \frac{D}{\pi} \right)^{1/2} \right]^{1/2} \quad (4-11)$$



which yields a linear relationship when  $\left[ \frac{d\sigma_t}{d(t^{-1/2})} C_0 \right]^{-1/2}$  is plotted vs.  $1/C_0$ .

When  $1/C_0$  approaches 0, i.e. as  $C_0 \rightarrow \infty$ , the interface would be saturated by SDS species and the maximum surface excess,  $\Gamma_\infty$ , is reached at the interface. This is expressed as,

$$\left[ \frac{d\sigma_t}{d(t^{-1/2})} C_0 \right]^{-1/2} \Big|_{1/C_0 \rightarrow 0} = \frac{1}{\Gamma_\infty} \left[ \frac{1}{RT} \left( \frac{D}{\pi} \right)^{1/2} \right]^{1/2} \quad (4-12)$$

Accordingly, a value for  $\frac{1}{\Gamma_\infty} \left[ \frac{1}{RT} \left( \frac{D}{\pi} \right)^{1/2} \right]^{1/2}$  can be obtained from the zero intercept of

the linear plot of  $\left[ \frac{d\sigma_t}{d(t^{-1/2})} C_0 \right]^{-1/2}$  vs.  $1/C_0$ . This information can then be used to determine the mean diffusivity,  $D$ , for the SDS solutions using a value of  $\Gamma_\infty$  determined through other means.

#### 4.1.2.3 Apparent Effective Diffusivity

Besides the above-mentioned approaches for analyzing diffusion-controlled surfactant adsorption, Vogler (1989) developed a simple method for analyzing the data by assuming that the concentration of surface active agent at the interface is controlled by the effective rate of diffusion of the species to the interface (a parameter that reflects the combined effect of both diffusion and adsorption). The diffusion equation can then be solved to obtain a surface concentration as a function of time. Sheu et al. (1992) assumed that Gibbs isotherm is applicable under such non-equilibrium condition and obtained the following analytical expression for the dynamic interfacial tension as a function of time,

$$\sigma_t - \sigma_\infty = \gamma_0 e^{-(\beta t)^{0.5}} \quad (4-13)$$

where  $\gamma_0$  is a proportionality constant,  $\beta$  is a kinetic parameter characterizing the ability of the surface active species to diffuse and adsorb on the surface (i.e. an effective diffusivity). If the dynamic surface tension at the zero time can be considered as the solvent surface tension,  $\gamma_0$  becomes the surface tension difference between the solvent and the solution and Eq. (4-13) becomes,

$$\sigma_t - \sigma_\infty = (\sigma_0 - \sigma_\infty) e^{-(\beta t)^{0.5}} \quad (4-14)$$

If a plot of  $(\ln \frac{\sigma_t - \sigma_\infty}{\sigma_0 - \sigma_\infty})^2$  vs.  $t$  is linear, the value of  $\beta$  can be calculated by fitting the experimental data. Sheu et al.(1992) successfully used this model to the study of the dynamic interfacial tension between asphaltene-containing toluene solutions and caustic solutions. Later, Xu and Finch (1994) reported that their experimental data for the surface tension of bitumen systems fitted Eq. (4-14) quite well.

#### 4.2 Selection of System

Aqueous solutions were prepared using deionized water and unpurified sodium dodecyl sulfate supplied by SIGMA Chemical Co. (St. Louis, USA). It contains approximately 95% SDS based on total alkyl sulfate content. This system was selected because it is commonly used to study the effect of interfacial characteristics on gas liquid contacting (Sagert, et al, 1976; Rosen, et al., 1990; Malysa, 1991; Chen, 1996; Yang, 1995; Djuve, et al., 2001).

Although the interfacial properties of SDS aqueous solution have been well investigated, the experimental results differ significantly from one investigator to the other. For example, the static surface tension for a 4 mM aqueous SDS solution ranged from 48.4 to 52.5 mN/m although the experimental error of such measurements does not exceed  $\pm 0.2$  mN/m (Mysels, 1986). This discrepancy can be mainly attributed to the extreme sensitivity of the interfacial measurements to the presence of trace impurities in both the solute and solvent. One can thus imagine how difficult it is to obtain accurate dynamic surface tension values, which in addition to the previously mentioned problem varies with time and is sensitive to the measurement methods and type of gas phase used.

Since the experimental data obtained in the present investigation focused on a rather limited concentration range, additional data recently reported in the literature were included in the following data interpretation in order to expand the range of applicability of the findings. The data set used in following analysis covers a wide concentration range (from 0.0173 to 10 mM) and includes the commercial SDS system used in the present

investigation as well as popularly accepted data by Garrett and Ward (1989) and Mysels (1989) as well as the recent data obtained by Hsu et al. (2000).

Whereas SDS is a relatively pure compound, commercially supplied MIBC is a mixture of highly polar organic compounds (MIBC, MIBK, mesityl oxide) and inert diluents. Moreover the exact components and their proportions can vary from one vendor to another rendering it difficult to undertake a comparative evaluation of the data. Furthermore, no dynamic surface tension data have been reported in the literature. Consequently, only the static surface tension and its derived surface excess were determined in the case of MIBC solutions.

### **4.3 Results and Discussion**

#### **4.3.1 Static Properties of SDS and MIBC Aqueous Solutions**

The dynamic interfacial tension is a function of the exposure time (surface age). When the exposure time is sufficiently long, i.e. approaches infinity, the adsorption of surfactant molecules onto the surface reaches equilibrium and the surface tension approaches the so-called equilibrium surface tension. The interfacial properties at equilibrium are also often referred to as static or thermodynamic interfacial properties. Following this principle, the static surface tensions of SDS system can be obtained from dynamic measurements by extrapolating the bubble interval to infinity, i.e. as  $t \rightarrow \infty$ .

The static surface tension results for aqueous SDS solutions (obtained by extrapolating the dynamic surface tension results obtained in the present investigation, as well as those reported by Garrett & Ward (1989), Mysels (1989), Yang (1995) and Hsu, et al. (2000)) are presented in Fig. 4.2. It clearly shows that the static surface tension of aqueous SDS solutions was decreases with increasing bulk concentration with the effect being most pronounced at low concentrations.

The lower static values obtained by extrapolating the data obtained in the present investigation can be attributed to the fact that the SDS surfactant used in preparing the aqueous solutions was not as pure as those in the other investigations where the SDS was further purified. These results were, therefore, not included in the correlation derived using the Szyszkowski equation (Mysels, 1986),

$$\sigma_{sta} = \sigma_0 - m \ln(1 + C_0 / n) \quad (4-15)$$

where  $m$  and  $n$ : are empirically determined constants.

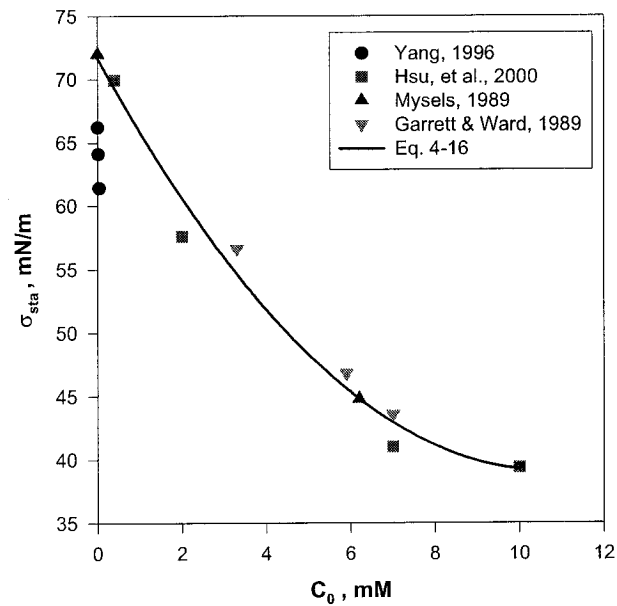


Fig. 4.2 Effect of SDS concentration on the static surface tension (obtained by extrapolating the dynamic surface tension data) (25°C)

As can be seen from Fig. 4.2, the effect of SDS bulk concentration on the static surface tension can be accurately predicted ( $R^2 = 0.96$ ) using the following equation, which is applicable over a broad concentration range ( $0 < C_0 < 10$  mM),

$$\sigma_{sta} = 0.072 - 0.02071 \ln(1 + C_0 / 2.403) \quad (4-16)$$

where,

$\sigma_{sta}$  is the static surface tension, [N/m]

$C_0$  is the bulk SDS concentration [mM]

Eq. (4-16) can thus be considered to be a better representation of the SDS static interfacial characteristics since it incorporates a broad set of dependable data from many

investigators (Mysels, 1986 and 1989; Garrett and Ward, 1989; Hsu, et al., 2000; and the present investigation).

The Szyszkowski expression (Eq. 4-15) could not fit the static surface tension of aqueous MIBC solution over the concentration range measured by Davakarla (1983). A simple polynomial equation was therefore used to correlate the experimental data. The following expression was found to correlate the static surface tension of MIBC solution rather well ( $R^2=0.94$ ),

$$\sigma_{sta} = 0.072 - 4.9C_0 - 3.7 \times 10^4 C_0^2 \quad (4-17)$$

where,

$$C_0 \quad \text{is bulk concentration of MIBC} \quad [\text{mM}]$$

As shown in Fig. 3.3, the effect of bulk concentration on the static surface tension shows different patterns for SDS and MIBC. Although in both cases the surface tension was found to decrease as the bulk concentration increases. The static surface activity of the short-chain molecule of MIBC ( $C_6$ -chain) is relatively low and high bulk concentrations are required in order to yield substantial depression of surface tension. On the other hand, the long-chain polar molecule of SDS ( $C_{12}$ -chain) exhibit strong static surface activity and much lower bulk concentrations are needed to achieve significant reduction in surface tension.

The value of the equilibrium surface excess,  $\Gamma_{sta}$ , provides an indication of how many SAA molecules are present at the interface between the gas and liquid phases. A general expression for the value of  $\Gamma_{sta}$ , in the case of SDS and MIBC, can be obtained by applying the Gibbs adsorption equation to Eq. (4-16) and (4-17) respectively. Since MIBC is non-ionized, the Gibbs equation can apply to it directly whereas a factor of 2 is required in the case of the ionic SDS system (Shaw, 1988). The effect of bulk concentrations on the surface excesses in aqueous MIBC solutions based on Davakarla's measurement is depicted in Fig. 4.3 and does not show the existence of a maximum value within the concentration range investigated. However, the existence of the so-called

maximum surface excess,  $\Gamma_{\infty}$ , is clearly evident in the case of SDS solutions (Fig. 4.4). When  $\Gamma_{\infty}$  is reached, it means that the gas-liquid interface is saturated with the SDS molecules and cannot be loaded with any extra SDS molecules although the SDS concentration in the bulk is further increased.

As shown in Fig.4.4, the SDS surface excess data follow the Langmuir adsorption isotherm law very well yielding the following expression ,

$$\Gamma_{sta} = 4.18 \times 10^{-6} \frac{C_0}{2.40 + C_0} \quad (4-18)$$

where,

$\Gamma_{\infty}$  is the saturated surface excess [mol/m<sup>2</sup>]

$C_0$ : is the bulk concentration [mM]

Over the concentration range studied in the present investigation ( $0 < C_0 < 10$  mM), the value of the Langmuir-Von Szyszkowski constant  $a_L$  was thus found to be equal to 2.40 mM whereas the value of the saturated surface excess  $\Gamma_{\infty}$  equals  $4.18 \pm 0.02 \times 10^{-6}$  mol/m<sup>2</sup>. This value compares rather well with other SDS saturation surface excess values reported in the literature (Table 4.1) but it has the advantage of being applicable over a very wide concentration range. By integrating the set of data reported in the literature, it was possible to overcome the problem of having a 4-fold variation in the value of the maximum surface excess values has been reported in the literature ( $1.95$  to  $7.64 \times 10^{-6}$  mol/m<sup>2</sup>). The projected areas per molecule, (obtained by assuming the saturation surface excesses value to correspond to a monomolecular layer of the solute on the interface, i.e. Gibbs monolayer) was found to depict similar trends (Table 4.1) and the value developed in the present investigation ( $0.663 \text{ nm}^2$ ) offers similar advantages.

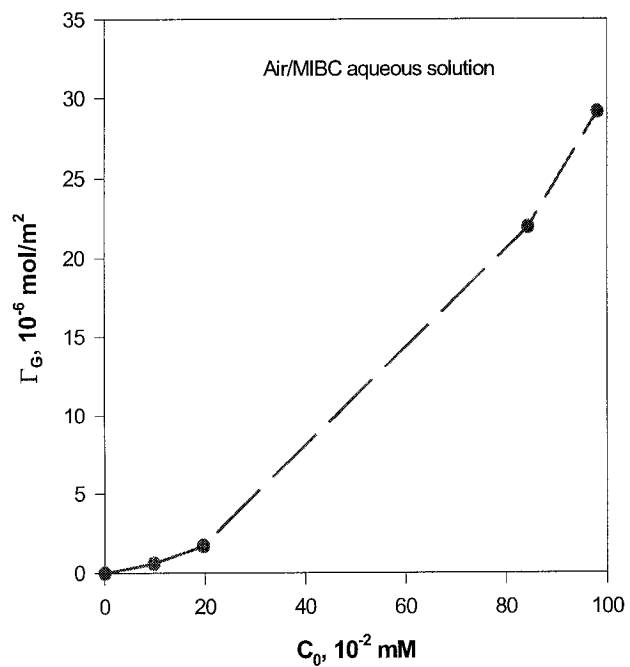


Fig. 4.3 Effect of bulk concentration on surface excess of MIBC aqueous solutions (25°C, data from Rajasekhar, 1983)

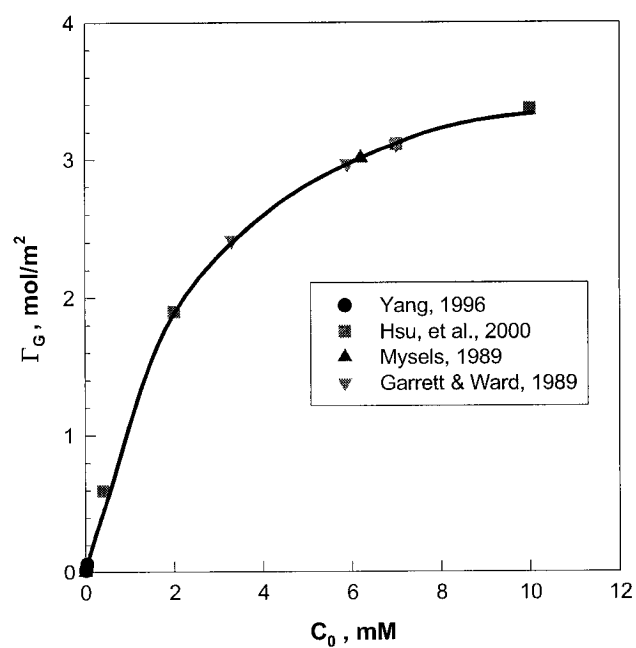


Fig. 4.4 Applicability of the Langmuir adsorption isotherm to aqueous SDS solutions (25°C)

Table 4.1 Interfacial characteristics of aqueous SDS solutions (25° C)

Investigator	Systems	$\Gamma_{\infty}$ , $10^{-6} \text{ mol/m}^2$	SAA molecular area, $\text{nm}^2$	Diffusivity, $10^{-10} \text{ m}^2/\text{s}$
Mukerjee et al. 1958.	Air-water-SDS	n/a		7
Matuura et al. 1959; Fainerman, 1978; Mysels, 1986.	Air-water-SDS	4.5	0.37	n/a
Sasaki et al., 1975	Air-water-SDS	3.1	0.536	n/a
Garrett & Ward, 1989	Air-water-SDS (3.3-7 mM)	7.64	0.218	6
Rosen, 1989	Air-water-SDS	3.1	0.536	n/a
Fang & Joos, 1996	Hexane-water-SDS (0.05-0.2 mM)	1.95	0.852	4.6
Vanýsek, 1997 (Perry's handbook)	Air-water (infinite dilution)	n/a		6.4
Present investigation	Air-water-SDS (0.0069-10 mM)	4.18	0.397	8.4

#### 4.3.2 Dynamic Surface Tension of SDS Aqueous Solutions

Dynamic surface tension is the surface tension of a freshly created surface measured after a given time has transpired, thus allowing a certain amount of the SAA molecules to diffuse and adsorb on the freshly created surface. It thus represents a non-equilibrium state the value of which is a strong function of the surface age. Data concerning the dynamic surface tension of various systems are rather limited and are mostly measured using the Maximum Bubble Pressure method (MBPM) (Woolfrey, 1986; Mysel, 1986



and 1989; Garrett and Ward, 1989; Hirt et al., 1990; Varadaraj et al., 1991; Joos, et al., 1992; Fainerman, et al., 1994; Miller, et al., 1996 and Hsu, et al., 2000).

Fig. 4.5 is a typical example of how the dynamic surface tension,  $\sigma_t$ , changes with the bubble generation interval for dilute SDS aqueous solutions. The dynamic surface tension was found to decrease monotonously with the bubble generation time (surface age) with the rate of change being most pronounced at very short surface ages. An equilibrium surface tension value is approached at very large bubble generation times. That is the reason why the equilibrium surface tension can be obtained by extrapolating the bubble generation interval to  $t \rightarrow \infty$ .

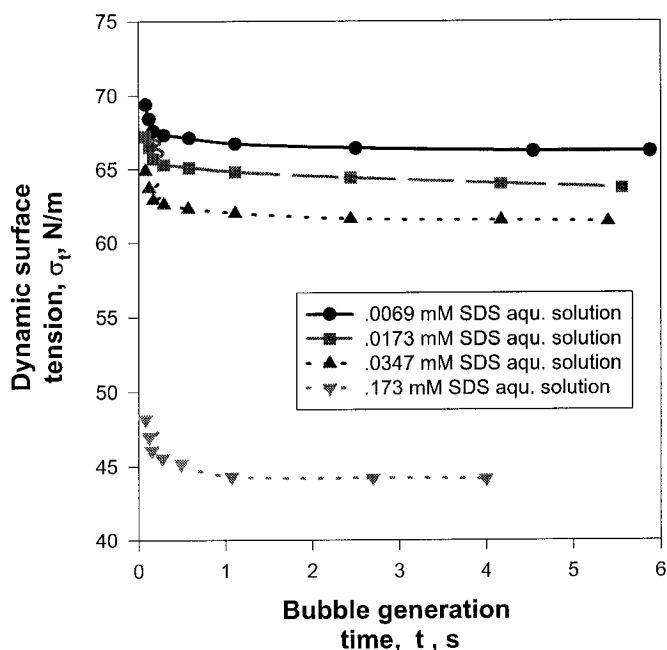


Fig. 4.5 Dynamic surface tension of SDS aqueous solution at a low concentration range (25°C, Adapted from Yang, 1996)

Attempts were undertaken to identify the mechanism controlling SDS diffusion/adsorption on freshly generated interfaces. The possibility of explaining the overall SDS diffusion/adsorption process using the relatively simple concept of effective

diffusivity (Vogler, 1989; Sheu et al., 1992; Xu and Finch, 1994) was first investigated. If this was the case, the dynamic surface tension would obey Eq.(4-14) and a linear relationship would be obtained between  $(\ln \frac{\sigma_t - \sigma_e}{\sigma_0 - \sigma_e})^2$  and  $t$ . However, as can be seen from Fig. 4.6 the data show systematic deviations from the linear relationship. It can, therefore, be concluded that the rate of SDS molecular adsorption onto the gas/liquid interface cannot be adequately modeled using the effective diffusivity approach.

In the case of slowly diffusing SAA, the characteristic diffusion time can be much larger than the characteristic adsorption time. Under such conditions, the short time approximation to the diffusion equation (Eq. 8) is expected to be applicable and a linear relationship would exist between  $\sigma_t$  vs.  $t^{1/2}$ . However, as can be seen from Fig. 4.7, the short-term approximation of the diffusion controlled does not apply to the case of very dilute SDS solutions (0 - 100 ppm SDS) present experimental data. This observation is in line with the findings of Garrett and Ward (1989) and Fang and Joos (1996) who report that, in the case of aqueous SDS solutions, diffusion in the bulk of the solution is relatively fast but slows down near the subsurface.

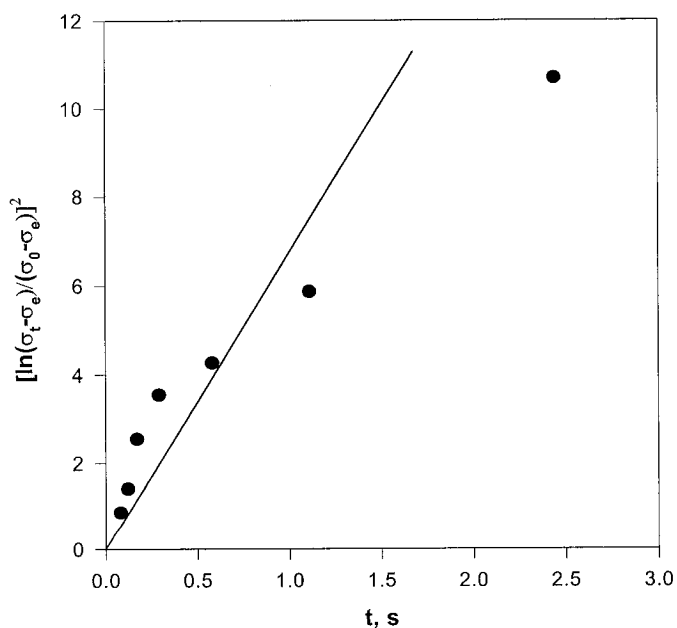


Fig. 4.6 Ability of the effective diffusivity concept (Eq. 4 -14) to model the dynamic surface tension of aq. SDS solution ( $C_0 = 0.0173$  mM)

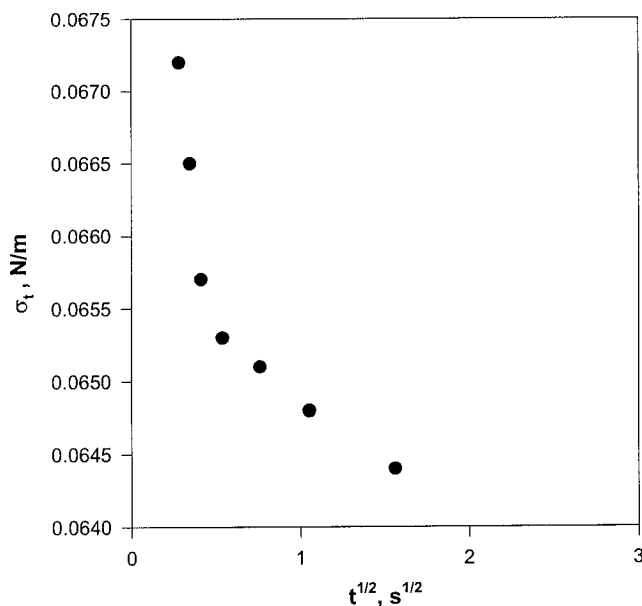


Fig. 4.7 Ability of the short-term approximation (Eq. 4 - 8) to model the dynamic SDS surface tension data of aq. SDS solution ( $C_0 = 0.0173$  mM)

As shown in Fig. 4.6, the dynamic surface tension of the dilute SDS solutions was found to be linearly proportional to  $t^{-1/2}$  for any particular SDS concentration. Similar trends were observed when the data obtained by previous investigators were plotted in a similar fashion (Fig. 4.7). At any particular time interval, the dynamic surface tension was found to increase as the SDS bulk concentration is reduced but the slope of the  $\sigma_t$  vs.  $t^{-1/2}$  straight line was found to be steeper as the bulk concentration increased. These observations indicate that the SDS molecules diffuse faster to the interface at higher bulk concentration (due to the generation of larger concentration gradients).

The fact that a linear relationship exists between  $\sigma_t$  and  $t^{-1/2}$  suggests that, in the case of aqueous SDS solutions, the overall process of diffusion/adsorption of freshly generated surfaces (or surfaces in which the SAA concentration has been reduced due to sudden stretching) can be modeled by the long-term approximation of the diffusion-controlled adsorption equation (Eq. 4-10). That is to say that the characteristic adsorption time,  $t_a$ , is

much greater than the characteristic diffusion time,  $t_d$ , and the concentration in the sublayer will be essentially equal to that in the bulk of the solution.

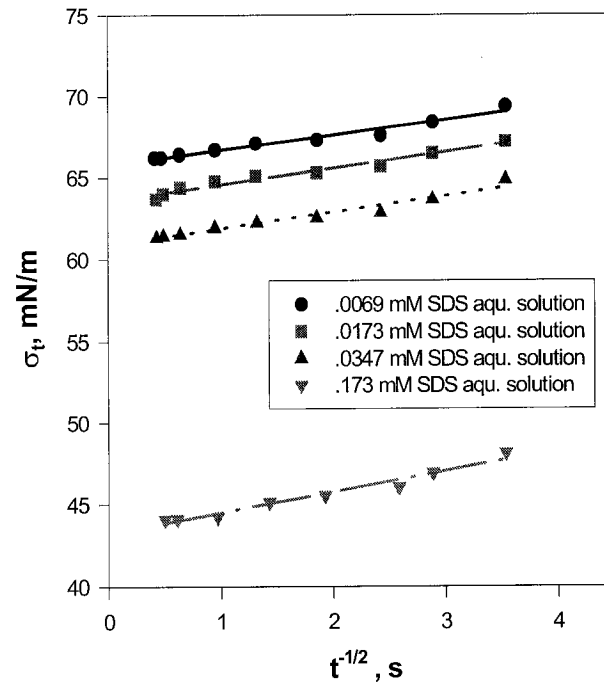


Fig. 4.8 Ability of the long-term approximation (Eq. 4-10) to model the dynamic surface tension of aq. SDS solution (0.0173 mM)

A regression analysis of the data obtained in the present investigation was conducted using the following linear relationship and the ensuing values of the parameters  $a$  and  $b$  are listed in Table 4.2 for the different concentrations investigated (an average value of  $R^2 = 0.97$  was obtained),

$$\sigma_t = a + b t^{-1/2} \quad (4-19)$$

Similar results were obtained when the data reported by various other investigators covering a concentration range of 0.4 mM to 10 mM were analyzed (Fig. 4.9).

The above mentioned finding agrees well with the observations reported by many investigators (Fang and Joos, 1996; Woolfrey, et al., 1986; Mysels, 1986; Garrette and Ward, 1989; and Hsu et al., 2000) namely that SDS molecules can easily diffuse into the

aqueous subsurface and that the controlling step is their migration from the subsurface onto the interface between the gas and liquid phases.

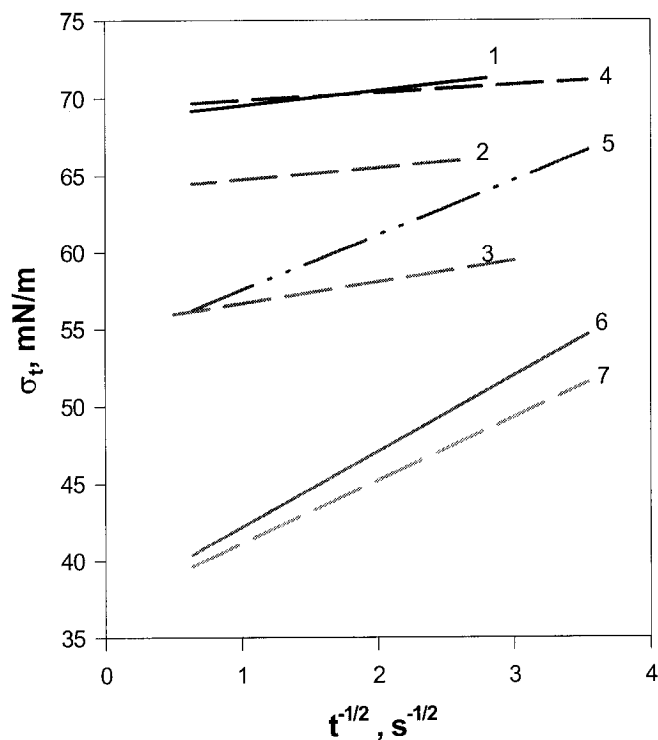


Fig. 4.9 Dynamic surface tension of SDS aqueous solution vs  $t^{-1/2}$  with a broad range of concentration (25°C)

—	1: .52 mM SDS aqu. solution (Woolfred, 1986)
—	2: 1.73 mM SDS aqu. solution (Woolfred, 1986)
—	3: 3.3 mM SDS aqu. solution (Garrett & Ward, 1989)
—	4: .4 mM SDS aqu. solution (Hsu, et al., 2000)
—	5: 2.0 mM SDS aqu. solution (Hsu, et al., 2000)
—	6: 7.0 mM SDS aqu. solution (Hsu, et al., 2000)
—	7: 10.0 mM SDS aqu. solution (Hsu, et al., 2000)

If the interfacial tensions are extrapolated to  $t^{-1/2} \rightarrow 0$  (i.e. as  $t \rightarrow \infty$ ) the resulting surface tension corresponds to a region where equilibrium is established. As shown in Fig. 4.2, the equilibrium surface tensions obtained by extrapolating experimental data match quite well with the static surface tension values measured by Mysels (1986). This further

confirms the validity of using the long-term approximation model to represent the diffusion of SDS entities in aqueous solutions.

### 4.3.3 Parameters Derived from Diffusion/Adsorption Models

#### 4.3.3.1 Diffusion Coefficient

The diffusion coefficient represents a quantitative measure of the ability of surfactants to diffuse to the interface. In general, there is only a 10-fold difference of diffusivity between the fastest diffusing  $H^+$  to the worst diffusible ion at infinite dilution. Unfortunately, most measurements reported in the literature are in poor agreement and most diffusivity values reported in chemical handbooks cannot be relied upon to better than  $\pm 10\%$  (Vanýsek, 1997).

As shown in Table 4.1, all reported SDS diffusivities are of the same order of magnitude but differ significantly depending on concentration range investigated and the purity of the SAA used. Garrett and Ward (1989) even thought the diffusion coefficients were only weakly dependent upon molecular structure (measured values being in the region of  $2 - 6 \times 10^{-10} \text{ m}^2/\text{s}$ ) and they somehow arbitrarily selected a value from those range as a diffusivity of SDS. In a word, no generally acceptable SDS diffusivity value has emerged that can be applied to a broad range of experimental conditions. The experimental data of the dynamic surface tension obtained by Woolfred, et al. (1986), Garrett & Ward (1989), Yang (1995) and Hsu, et al. (2000) cover a concentration range of 0.0069 mM to 10 mM and were therefore used to obtain a more accurate and more representative mean diffusion coefficient for aqueous SDS systems.

The diffusivity was determined from the dynamic surface tension data using Eq. (4 - 12),

where the value of the right hand side parameter,  $\left[ \frac{d\sigma_t}{d(t^{-1/2})} C_0 \right]^{-1/2}$  at infinite concentration, was obtained by extrapolating the data shown in Fig. 4 - 10 to the value

$1/C_0 = 0$ ,  $\frac{1}{\Gamma_\infty} \left[ \frac{1}{RT} \left( \frac{D}{\pi} \right)^{1/2} \right]^{1/2} = 19.4$ . The value of the diffusivity,  $D$ , was then calculated

from this parameter using the previously obtained value of the saturated surface excess ( $\Gamma_{\infty} = 4.18 \times 10^{-6} \text{ mol/m}^2$ ). This approach yielded a single value of the diffusivity ( $D = 8.4 \pm 0.5 \times 10^{-10} \text{ m}^2/\text{s}$ ) that fits a broad range SDS concentration ( $0 < C_0 < 10 \text{ mM}$ ).

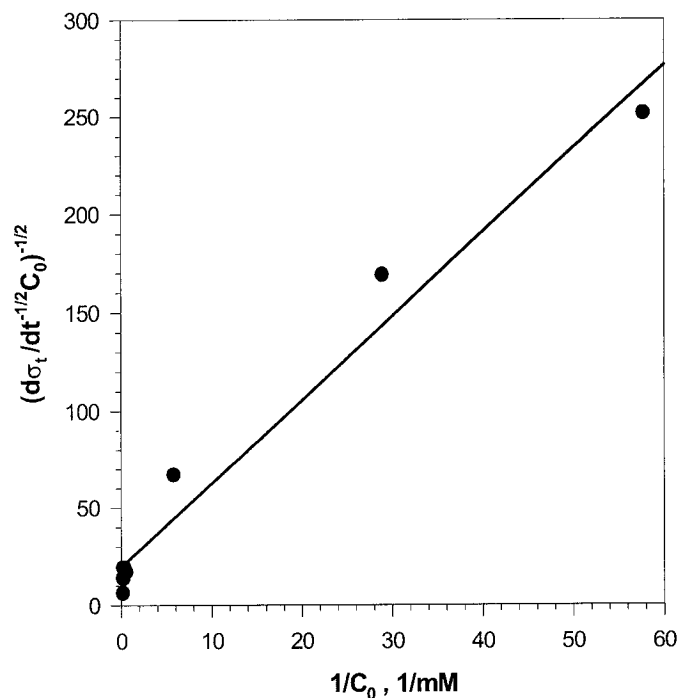


Fig. 4.10 Determining SDS diffusivity by the Fang and Joos (1996) method.

The value of SDS diffusivity developed in this investigation is expected to be more reliable than previously derived ones since it is based on a large data base covering a wide concentration range ( $0.0069 \text{ mM} < C < 10 \text{ mM}$ ). Although the value of current diffusivity is of the same order as that from the literatures, it is slightly higher than most previously reported ones. Part of this difference could be attributed to the inclusion of the data generated in the present investigation which were obtained using commercially

purified SDS. The residual isomers and contaminants appear to exhibit synergetic effects that accelerate the adsorption of SDS ions at the interface.

The concept of a diffusivity value that is independent of concentration (at least within the relatively low concentration range considered in this investigation) is in agreement with the recent findings of Fang and Joos (1996) where only one diffusivity value is reported for different concentrations of the same type of surfactant. However, this average diffusivity value developed in the present investigation is almost double the corresponding value determined for SDS diffusing through aqueous solutions to the interface with Hexane ( $D = 4.6 \times 10^{-10} \text{ m}^2/\text{s}$ ). This suggests that the rate of adsorption of SDS entities from the sublayer is faster in the case of air/water interface.

#### **4.3.3.2 Surface Excess Based on Long-term Approximation**

It is well known that the presence of surfactants significantly alters the properties of the interface with the extent of change being a function of how many molecules are adsorbed onto the interface. The value of the maximum surface excess shown in Table 4.1 yields an indication of the level that can be reached when the surfactant species are present in very high concentrations and are given enough time to adsorb onto the interface until the interface is packed by the species to the maximum extent. However, dynamic bubble breakage and coalescence in turbulent flows typically happen within milliseconds, a time scale which is insufficient for the SDS species to diffuse and adsorb onto the interface and reach equilibrium.

The concept of dynamic surface excess was introduced by Fordham (1959) and Borwankar and Wasan (1983). The dynamic surface excess is the quantity of surfactant molecules adsorbed upon the surface per unit area of interface and is, therefore, a function of the time elapsed before equilibrium is reached. It may therefore be possible that the dynamic surface excess can yield an indication of the interfacial characteristics relevant to dynamic processes such as bubble breakage and coalescence in turbulent flow. However, the difficulty associated with this approach is the need to identify a characteristic time value at which the dynamic surface excess is to be calculated,



particularly when the characteristic bubble breakup and coalescence times can vary from milliseconds to seconds.

Under conditions where the long-term approximation applies, the value of the surface excess can be determined at any particular time provided that both the diffusivity and the derivative of the dynamic surface tension with respect to  $t^{-1/2}$  are known. Under such conditions, Eq. 4-10 can be rearranged to yield,

$$\Gamma_L = \left[ \frac{C_0}{RT} \sqrt{\frac{D}{\pi}} \frac{d\sigma}{d(t^{-1/2})} \right]^{1/2} \quad (4-20)$$

As shown in Fig. 4.8 and 4.9, the value of  $\frac{d\sigma}{d(t^{-1/2})}$  is a constant for each SDS concentrations, and the range of surface ages, studied in the present experimental investigation ( $0.0069 < C_0 < 10$  mM,  $0.08 \text{ s} < t < 6$  s). Since the value of the diffusivity is also independent of SDS concentration and time, the value of  $\Gamma_L$  can be considered to be a linear function of production of  $C_0$  and  $\frac{d\sigma}{d(t^{-1/2})}$  that is independent of contact time.

The result is present in Fig. 4.11. It is however important to recall that these dynamic surface excess values are derived from the long-term approximation which implies that the characteristic adsorption time,  $t_a$ , is much greater than the characteristic diffusion time,  $t_d$ , and that the concentration in the sublayer will be essentially equal to that in the bulk of the solution.

To test the validity of this assumption, the value of  $t_a/t_D$  was calculated using the approach proposed by Campanelli and Wang (1998) where,

$$t_a = 3/7 t \quad (4-21)$$

and,

$$t_d = 1/D \left[ \Gamma_\infty a_L / (a_L + C_0) \right]^2 \quad (4-22)$$

Eq. (4-21) was developed for the case of expanding drops and can be considered as a first approximation for the case of expanding bubbles encountered in this investigation. However, high-speed camera investigation of the bubble formation process suggests that the proportionality constant is closer to 0.95 in the case of the Synsadyne 6000 setup.

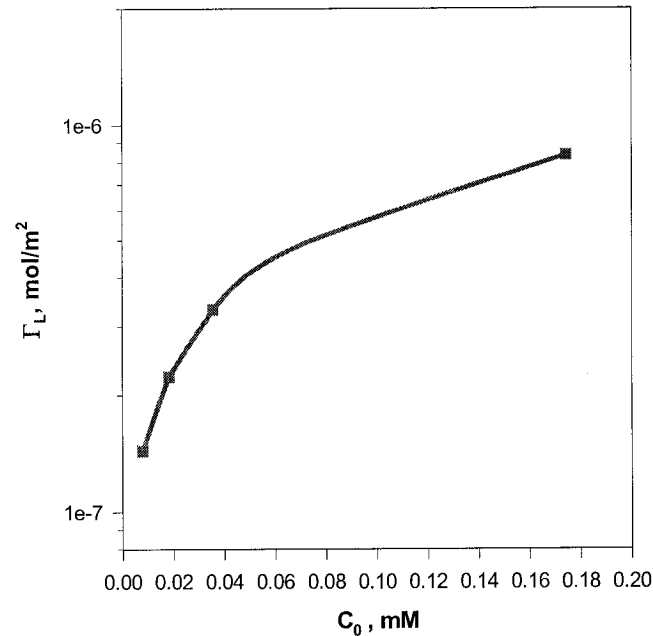


Fig. 4.11 Effect of bulk concentration on the surface excess value of aqueous SDS solutions (determined using the long-term approximation)

For the current investigation of concentration range from 0.0069 to 0.173 mM aq. SDS solutions, the characteristic diffusion times are found to vary from  $5.1 \times 10^{-6}$  to  $3.6 \times 10^{-3}$  s whereas the absorption times vary from 0.07 to about 5.3 s. The combined effect of these two times yields the characteristic time ratio,  $t_a/t_D$ , varying from 20 to 1500 (see Fig. 4.12), which are significantly larger than unity, it suggests the long-term approximation is valid for the adsorption of aq. SDS solutions in the concentration range of 0.0069 to 0.173 mM. However, most of other investigators (Mysels, 1989; Garrett and

Ward, 1989 and Hsu, et al., 2000) used even higher concentration range, e.g. from 0.4 to 10 mM. As Eq. (4-22) shows that the higher concentration, and the faster diffusion time,

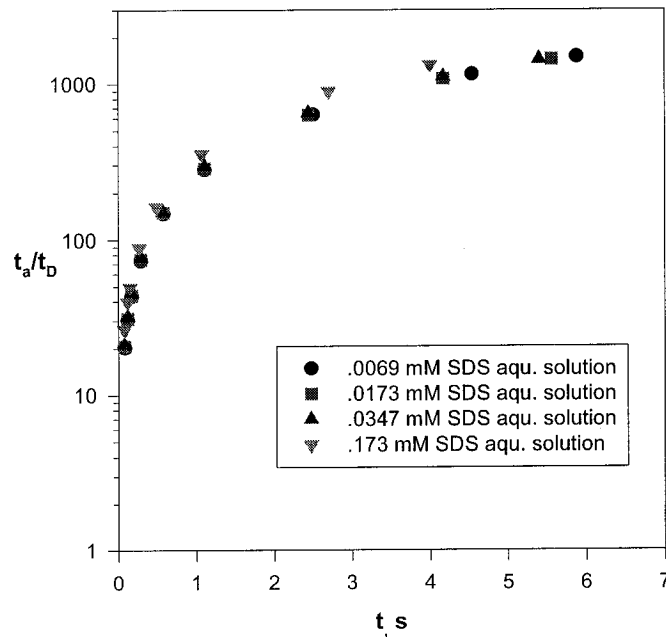


Fig. 4.12 Effect of bubble generation time on the absorption-to-diffusion characteristic time ratio for very dilute aqueous SDS solutions.

therefore the characteristic time ratio,  $t_a/t_d$ , will be much bigger than this reported range, It implies that the long-term approximation is also valid for extended concentration range of 0.0069 to 10 mM.

Because of the relatively short characteristic diffusion times encountered in the case of SDS solutions, the value of  $\Gamma_L$  (determined from the long-term approximation) was found to be smaller than the Gibbs surface excess values,  $\Gamma_G$ , obtained using static surface tension data (subscript G is hereby assigned for distinction) which is based on the assumption that Gibbs isotherm applies under equilibrium conditions. This is proved by comparing Fig. 4.4 to Fig. 4.11 and also shown in Table 4.2.

From the above, it is obvious that there is substantial evidence that the long-term approximation of diffusion-controlled adsorption properly describes the situation in relatively dilute aqueous SDS solutions. This can be attributed to its ability to account for the diffusivity of the surface-active species, the concentration gradient of the dynamic surface tension, as well as for the bulk concentration of that species given in Eq. (4-20). The surface excess,  $\Gamma_L$ , could, thereby, be more justifiable than Gibbs surface excess,  $\Gamma_G$ , to represent the SDS adsorption in current time and concentration ranges.

Table 4.2 Summary of interfacial properties of SDS aqueous solutions presently investigated

SDS Conc., ppm	0	2	5	10	20	50
$C_0$ , mM	0	0.00694	0.0173	0.0347	0.0694	0.173
$\sigma_\infty$ , mN/m	72.0	66.2	64.1	61.4	52.4	44.1
$\Pi$ , mN/m	0	5.8	7.9	10.6	19.6	27.9
$\Gamma_G$ , $10^{-6}$ mol/m <sup>2</sup>	0	0.506	1.01	1.50	1.94	2.25
$\Gamma_\infty$ , mol/m <sup>2</sup>	$4.18 \times 10^{-6}$					
Expression for $\sigma_t$ , N/m (0.08 s < t < 6 s)	0.072	$\sigma_t =$ 0.0657 + $9.50 \times 10^{-4}$ $t^{-0.5}$	$\sigma_t =$ 0.0638 + $9.10 \times 10^{-4}$ $t^{-0.5}$	$\sigma_t =$ 0.0609 + $10.1 \times 10^{-4}$ $t^{-0.5}$	n/a	$\sigma_t =$ 0.0433 + $12.8 \times 10^{-4}$ $t^{-0.5}$
$d\sigma_t/dt^{1/2}$	0	$9.50 \times 10^{-4}$	$9.10 \times 10^{-4}$	$10.1 \times 10^{-4}$	n/a	$12.8 \times 10^{-4}$
$D_{mean}$ , m <sup>2</sup> /s	$8.42 \times 10^{-10}$					
$\Gamma_L$ , $10^{-6}$ mol/m <sup>2</sup>	0	0.208	0.323	0.480	0.663 (interpolation)	1.21

The dynamic surface tension data obtained in this investigation, as well as those reported by several other investigators, can be well represented by the diffusion-controlled model of surfactant adsorption. The analytical solution obtained using long-term approximations was found to fit the data very well. This can be attributed to the characteristic adsorption time,  $t_a$ , being much greater than the characteristic diffusion time,  $t_D$  ( $t_a/t_D$  varying between  $4.35 \times 10^3$  and  $3.06 \times 10^6$ , for the range of concentrations and bubble formation times analyzed).

This diffusion model was then used to estimate several equilibrium and dynamic interfacial characteristics. An accurate correlation of the static surface tension, and Gibbs surface excess of aqueous SDS solutions was developed. Within the range of SDS concentrations analyzed (0.0069 – 10 mM), a single value for the SDS diffusion coefficient and saturated surface excess were found to fit the data well. Furthermore, the SDS surface excess data were found to follow the Langmuir adsorption isotherm law. This information can be used to analyze the complex behaviour of gas liquid contactors where SDS is used to modify the coalescence behaviour of the system.

For SDS systems, the value of the dynamic surface excess,  $\Gamma_L$ , at any particular concentration was found to be independent of the surface age over the range of 0.08 – 6 s. This is mainly due to the fact that the characteristic adsorption time is much greater than the characteristic diffusion time in the case of aqueous SDS solutions.

#### 4.4 Conclusions

1. The dynamic surface tension data for aqueous SDS solutions obtained in this investigation, as well as those reported by several other investigators, can be well represented by the diffusion-controlled model of surfactant. The analytical solution obtained using long-term approximations was found to fit the data very well.
2. An accurate correlation of the static surface tension, and Gibbs surface excess of aqueous SDS solutions was developed in a quite wide concentration range of 0 – 10 mM. The static surface tension for aqueous MIBC solutions is also correlated.

3. A single value for the SDS diffusion coefficient and saturated surface excess were found to fit the data well. The SDS surface excess data were found to follow the Langmuir adsorption isotherm law in a broad concentration range.
4. For SDS systems, the value of the dynamic surface excess,  $\Gamma_L$ , at any particular concentration was found to be independent of the surface age over the range of 0.08 – 6 s. This is mainly due to the fact that the characteristic adsorption time is much greater than the characteristic diffusion time in the case of aqueous SDS solutions.

## **CHAPTER 5 BUBBLE COALESCENCE IN TURBULENT PIPE FLOW**

In the process of bubble coalescence, several physical phenomena occur simultaneously. These have been discussed by some authors (Overbeek, 1960; Calderbank et al., 1964; Vrij, 1966; Shah et al., 1982; Deckwer, 1986; Prince and Blanch, 1990; Chaudhari and Hofman, 1994). However, due to lack of understanding of the mechanism of bubble coalescence, the design of multiphase reactors has been so far based on empirical methods. The major reason for the empirical analysis is the inability to describe dispersion properties (such as bubble size and its distribution, turbulence structure, interfacial area and gas hold-up) as a function of operating conditions and system properties. In particular, it is not clear how the interfacial characteristics influence bubble breakage and coalescence processes. It is well known that in pure liquids, bubbles tend to coalesce faster, while the addition of a SAA leads to retardation of bubble coalescence which, in turn, leads to a smaller average bubble size, higher gas hold-up and larger interfacial area of contact. This results in the inability of most correlations reported in the literature (which are usually related to pure systems) to accurately predict the performance under conditions where a secondary component is present (Shah et al., 1982; Lee et al., 1987; Prince and Blanch, 1990; Tjaberinga and Chesters, 1993). The simple use of surface tension to characterize the interfacial properties of complex systems is therefore not suitable, since it does not explain the observed variation in the parameters.

In this Chapter, theoretical coalescence models are evaluated, chosen and applied to the case of bubble coalescence in turbulent pipe flow. The results obtained from the comprehensive experimental investigation are then used to determine the factors affecting coalescence rate and to test how the theoretical model fits the data obtained. The role of interfacial characteristics responsible for retarding bubble coalescence rate in gas/liquid turbulent flows is further discussed.

### **5.1 Theoretical Coalescence Model**

Knowledge concerning bubble coalescence originates mainly from two disciplines: namely chemistry and chemical engineering. The former focuses mostly on foaming,

foam breaking, and foam coalescence/stability whereas the latter addresses issues such as bubble generation and coalescence in mixing tanks, bubble columns and turbulent pipe flow. The model developed in this section (which attempts to describe bubble coalescence phenomena in turbulently flowing industrial streams) is based on the knowledge gained from both fields.

As summarized in Chapter 2, the process of bubble coalescence in turbulent flows is believed to occur in three steps in series, first of all, two bubbles approach each other and form a thin film between them (Fig. 5.1), then the liquid layer between the bubbles thins down due to liquid drainage under the capillary force, and inertial forces due turbulent flows. When the thickness of the film is reduced to about  $0.1\ \mu\text{m}$ , the van der Waals attraction forces promote film-draining rate while the electrostatic double layer repulsive force decreases it. As the thickness of the film is reduced to its critical thickness (about  $0.01\ \mu\text{m}$ ), it ruptures leading to bubble coalescence. In the process of bubble coalescence, the rate of thinning of liquid film is believed to be the main controlling step since the rupturing step is very rapid. The contact time of the bubbles thus plays an important since if the contact time of bubbles is less than the time of thinning; coalescence will not occur (Chesters, 1991). Attention has, therefore, been focused on analyzing the rate of thinning of the thin liquid film in an attempt to understand coalescence behavior.

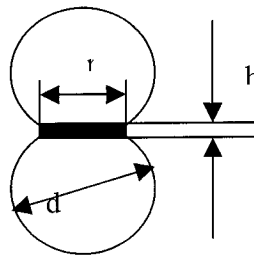


Fig. 5.1 Schematic representation of bubble coalescence



### 5.1.1 Modeling Bubble Coalescence Rates

The bubble coalescence model developed below is analogous to that developed by Prince and Blanch (1990) but applied to turbulent pipe flow instead of the bubble column. It is based on the following assumptions:

1. The behavior of the dispersed bubbles is coalescence dominated (i.e. bubble breakage can be neglected);
2. The primary cause of bubble collisions is the turbulent fluctuations in the continuous phase, where the turbulence is locally isotropic and the bubble size falls in the inertial sub-range;
3. No net slip velocity exists between the dispersed phase and the continuous phase. This is expected to prevail when the turbulent flow velocity is much larger than the relative slip velocity (i.e. small bubbles).
4. Coalescence involves two equally-sized spherical bubbles;
5. Bubble coalescence rate is controlled by the rate of bubble collision and the likelihood of such collisions resulting in coalescence.

The bubble coalescence rate, expressed as the temporal rate of change of bubble number density, can therefore be expressed as,

$$\frac{\partial n}{\partial t} \propto f \lambda \quad (5-1)$$

where,

n	bubble population density	[-]
f	Collision rate	[1/s.m <sup>3</sup> ]
λ	Collision efficiency	[-]

In order to clarify the derivation of the mathematic model, some equations will be re-stated although they appeared in the Chapter 2. Whereas collision rate is mainly dominated by hydrodynamic factors, collision efficiency is determined by the time required for coalescence to take place and the time during which the two bubbles are in close in contact in the turbulent flow.

For any particular gas holdup, coalescence rate can be expressed in different forms. As the bubble number density decreases from  $n_1$  to  $n_2$ , the specific interfacial area of contact decreases from  $a_1$  to  $a_2$  while the bubble size increases from  $d_1$  to  $d_2$ . Consequently, the coalescence rate can be expressed in different forms such as:

Interfacial area shrinking rate,

$$-\frac{\partial a}{\partial t} = -\frac{a_2 - a_1}{\Delta t} \quad [m^2/m^3.s] \quad (5-2)$$

Bubble diameter growth rate,

$$\frac{\partial d}{\partial t} = \frac{d_2 - d_1}{\Delta t} \quad [1/m.s] \quad (5-3)$$

Rate of change of bubble population density,

$$-\frac{1}{V} \frac{\partial N}{\partial t} = -\frac{\partial n}{\partial t} = -\frac{n_2 - n_1}{\Delta t} \quad [1/m^3.s] \quad (5-4)$$

where  $N$  is sum of bubbles in selected volume  $V$ . Based on the assumption that the dispersed bubbles are uniformly sized spherical entities, the Sauter mean bubble diameter can be used to correlate the various expressions as follows,

$$d_{32} = \frac{6\Phi}{a} \quad (5-5)$$

$$n = \frac{\Phi}{\frac{\pi}{6} d_{32}^3} \quad (5-6)$$

The various expressions of coalescence rate are thus inter-related by,

$$-\frac{\partial n}{\partial t} = -\frac{6\Phi}{\pi} (-3) d_{32}^{-4} \frac{\partial d_{32}}{\partial t} = \frac{18\Phi}{\pi d_{32}^4} \frac{\partial d_{32}}{\partial t} \quad (5-7)$$

$$-\frac{\partial a}{\partial t} = \frac{6\Phi}{d_{32}^2} \frac{\partial d_{32}}{\partial t} \quad (5-8)$$

### 5.1.1.1 Turbulent Collision Frequency

In turbulent flow, eddies impact on the bubbles at all directions causing them to move in a random fashion, a situation that lead researchers to assume that the collisions were analogous to the collisions of molecules in the gas kinetic theory or analogous to particle collisions in an ideal gas.

Following Kennard (1938) theory, the collision frequency resulting from turbulent motion can be expressed as a function of bubble size, bubble concentration and relative velocity. So the collision rate per unit time and volume,  $f$ , can be derived if the bubbles are assumed as equal-sized spheres and to follow the basic continuous-phase flow (Lee, et al., 1987; Prince and Blanch, 1990; Chesters, 1991),

$$f = k_1 u_r n^2 d^2 \quad (5-9)$$

One of reason why Eq. (5-9) is chosen by most researchers is that its physical meaning is obvious and the format is quite simple. Other complicated expressions of collision rate don't really improve the accuracy much (William & Crane, 1980) and are limited in their application range.

The turbulent fluctuating velocity in the inertial sub-range of isotropic turbulence can be expressed as (Rotta, 1972),

$$u_t = 1.4 \varepsilon^{1/3} d^{1/3} \quad (5-10)$$

Substituting Eq. (5-10) into Eq. (5-9), the turbulent collision rate can therefore be expressed as,

$$f = k_2 n^2 d^2 (\varepsilon d)^{1/3} \quad (5-11)$$

Using Eq. (5-6) to describe  $n$  and substituting in Eq. (5-11), the collision frequency can be expressed as,

$$f = k_2 \Phi^2 \varepsilon^{1/3} / d^{11/3} \quad (5-12)$$

Combining Eq. (5-1), (5-12), (5-7) and (5-8), the various bubble coalescence rate equations can be expressed as a function of variations in interfacial area, bubble size, or the bubble population density,

$$-\frac{\partial n}{\partial t} = k_2 \lambda \Phi^2 \varepsilon^{1/3} / d^{11/3} \quad (5-13)$$

$$\frac{\partial d_{32}}{\partial t} = \frac{\pi k_2}{18} \lambda \Phi \varepsilon^{1/3} d^{1/3} \quad (5-14)$$

$$-\frac{\partial a}{\partial t} = \frac{\pi k_2}{3} \lambda \Phi^2 \varepsilon^{1/3} / d^{5/3} \quad (5-15)$$

### 5.1.1.2 Collision Efficiency

As previously mentioned, coalescence will happen only if the contact time is longer than the time needed for coalescence to take place. Consequently, the most widely accepted expression for the collision efficiency is given by (Coulaloglou and Tavlarides, 1977),

$$\lambda = e^{-t_c/t_i} \quad (5-16)$$

Substituting Eq. (5-16) in Eq. (5-13), the rate of change of bubble population by coalescence can be expressed as,

$$-\frac{\partial n}{\partial t} = k_2 \Phi^2 \varepsilon^{1/3} e^{-t_c/t_i} / d^{11/3} \quad (5-17)$$

where the proportional constant  $k_2$ , can best be determined through the use of carefully designed experimental data.

Similarly, the bubble size growth rate by coalescence is expressed as,

$$\frac{\partial d_{32}}{\partial t} = k_2 \Phi \varepsilon^{1/3} e^{-t_c/t_i} d^{1/3} \quad (5-18)$$

while the interfacial area shrinking rate is given by,

$$-\frac{\partial a}{\partial t} = k_2 \Phi^2 \varepsilon^{1/3} e^{-t_c/t_i} / d^{5/3} \quad (5-19)$$

### **Bubble Contact Time in Turbulent Flows**

The overwhelming majority of investigators (Ross, 1971; Coualoglou and Tavlarides, 1977; Oolman and Blanch, 1986; Lee, et al., 1987; Chesters, 1991; Li, 1996) chose Levich's equation to predict the value of contact time in turbulent flows,

$$t_i = \frac{(d/2)^{2/3}}{\varepsilon^{1/3}} \quad (5-20)$$

This equation shows a dependence of the contact time with the turbulent characteristics (such as the local energy dissipation rate,  $\varepsilon$ ), an observation which agrees with the concept that the contact time is determined by the bulk hydrodynamics. This compares favorably with Eq. (2-25) in which the contact time is independent of the continuous phase hydrodynamics. Based on Eq. (5-20), small bubbles present in high levels of turbulence will exhibit short contact times, a fact that does not favor bubble coalescence.

### **Film Thinning Time**

In the process of bubble coalescence, the rate of thinning of liquid film is believed to be the rate-controlling step as the rupturing step is very rapid. Rupture most likely occurs due to the contact of the peaks of capillary waves formed at each of the two facing surfaces. Several studies show films formed from water and electrolyte solution rupture suddenly at thickness in the range  $5-11 \times 10^{-8}$  m (Pashley and Craig, 1996). Consequently, the film thinning time is usually taken to represent the coalescence time.

The main factors responsible for drainage of the liquid film are controlled by the hydrodynamics and interfacial characteristics of the system. The coalescence time has been successfully modeled in stagnant fluid by examining the time needed for the liquid film to thin from an initial thickness to a critical thickness where the rupture occurs (Marrucci, 1967; Sagert and Quinn, 1978; Ivanov et al., 1985; Li and Slattery, 1989).

As discussed in Chapter 2, there are various drainage modes depending on the rigidity of the bubble and mobility of the interfaces. In the present investigation, the size of the bubbles suspended in the turbulent pipe flow is larger than the Kolmogorov eddies due to the high Reynolds number encountered. The drainage modes of partially interface mobile or fully interfacial mobility and inertial control should therefore be applicable. For example,

in the case of air-pure water system with large bubble size, the closest drainage mode would be characterized as deformable bubbles and fully interface mobility. For air-impure solutions with small bubble, since the additives adsorbed onto the bubble interface result in interface immobility and also by which the small bubbles resist deformation, the drainage mode could be partially or fully mobile without evident deformation.

An expression for the thinning of liquid film between two equal-sized bubbles was derived by (Oolman and Blanch, 1988; Prince and Blanch, 1990),

$$-\frac{dh}{dt} = \left\{ \frac{8}{R_f \rho_L} \left[ -\frac{4M}{RT} \left( \frac{d\sigma}{dC} \right)^2 + h^2 \left( \frac{4\sigma}{d} + \frac{A}{6\pi h^3} \right) \right] \right\}^{1/2} \quad (5-21)$$

where  $R_f$  is radius of liquid disk between the contacting bubbles,  $M$  is the surface immobility the value of which varies between 0 and 4. For distilled water, the gas-liquid interface is assumed to be fully mobile (that results in  $M = 0$ ) whereas the value of  $M$  can take any values between 0 and 4 in the presence of surfactants.

This equation is derived based on consideration of the flow rate of fluid film by the capillary pressure, enlarged by the Hamaker force (one kind of van der Waals force) which only become appreciable at very low film thickness (i.e. just prior to rupture). This term demands a numerical solution for the coalescence time and renders the current model cumbersome. This difficulty may be overcome by neglecting the Hamaker contribution but the results obtained may overestimate the coalescence time. The effect of bubble deformation by turbulence eddies on the coalescence rate is also disregarded since the influence of the bubble deformation, and the subsequent increase in coalescence time, by turbulent eddies is not well understood. The radius of the liquid disk between the coalescing bubbles (Fig. 5.1) can be assumed to be a constant fraction of the bubble radius (Prince and Blanch, 1990). Hence Eq.(5-21) can be simplified by integration as,

$$t_c = \left[ \frac{(d/2)^3 \rho_L}{16\sigma} \right]^{1/2} \ln \frac{h_i}{h_c} \quad (5-22)$$

This equation is consistent with the expression of the coalescence time obtained by Sagert and Quinn (1976) and Lee, et al. (1987). Big bubble moving in low surface tension systems are thus expected to exhibit long coalescence times and result, therefore, in low coalescence efficiencies.

When two bubbles approach each other they form a thin film between them that is usually referred to as the quasi equilibrium film. The initial thickness of this film,  $h_i$ , has been well investigated for a wide range of systems (Ivanov and Dimitrov, 1974; Prince and Blanch, 1990; Möbius and Miller, 1998). For the case of air-water systems it is typically estimated to be,

$$h_i = 1 \times 10^{-5} \text{ m} \quad (5-23)$$

When the film is very thin, van der Waals attraction forces increase the draining rate, while the electrostatic double layer repulsive force decreases it. During the process of bubble coalescence the thinning of the liquid film reaches a stage at which the film become metastable and spontaneous rupture occurs. The thickness at this stage is defined as the critical thickness of the film  $h_c$  and is typically considered to be around  $1 \times 10^{-8}$  m (Kim and Lee, 1988), a value that was used by Prince and Blanche (1990) in their analysis of bubble coalescence rates. On the other hand, Chesters and Hoffman (1982) and Chesters (1991) used a simple expression to estimate the value of the critical film thickness,

$$h_c = \left( \frac{A_H d / 2}{8\pi\sigma} \right)^{1/3} \quad (5-24)$$

This expression is used in the coalescence model because of its ability to accounts for variation in the physical properties of the system.

### 5.1.2 Normalization of Bubble Coalescence Rates

In situations where a wide range of experimental conditions are encountered, the use of the absolute differential rate of a variable (e.g.  $(d_2 - d_1)/\Delta t$ ) can often fail to yield a good indicator of the true variation of that parameter. Better sensitivity is achieved by normalizing the parameter through the use of its initial value (e.g.  $(d_2 - d_1)/d_1 \Delta t$ ). This

point will be delineated in the results and discussions section. Hence, Eq. (5-13) – (5-15) can be expressed in the following normalized forms,

$$\text{Normalized interfacial area shrinking rate:} \quad -\frac{1}{a} \frac{\partial a}{\partial t} \quad [1/s]$$

$$\text{Normalized bubble diameter growth rate:} \quad \frac{1}{d_{32}} \frac{\partial d_{32}}{\partial t} \quad [1/s]$$

$$\text{Normalized bubble population decrease rate:} \quad -\frac{1}{n} \frac{\partial n}{\partial t} \quad [1/s]$$

and the bubble coalescence rate equations (Eq. 5-13 to 5-15) can be replaced by the following expressions,

$$-\frac{1}{a} \frac{\partial a}{\partial t} = \frac{\pi k}{18} \lambda \Phi_p \varepsilon_p^{1/3} / d^{2/3} \quad (5-25)$$

$$\frac{1}{d} \frac{\partial d}{\partial t} = \frac{\pi k}{18} \lambda \Phi_p \varepsilon_p^{1/3} / d^{2/3} \quad (5-26)$$

$$-\frac{1}{n} \frac{\partial n}{\partial t} = \frac{\pi k}{6} \lambda \Phi_p \varepsilon_p^{1/3} / d^{2/3} \quad (5-27)$$

All the above bubble coalescence rate expressions predict an increase in with increasing gas holdup, turbulent energy dissipation rate, and collision efficiency but a decreased coalescence rate with increasing of bubble size. All these trends conform to the extensive experimental database developed by a large number of investigators. The most interesting is that although bubble coalescence rate can be expressed in three different ways, the resulting expressions are interrelated. The normalized coalescence rate expressed as the rate of change in the interfacial area is thus equal to that expressed as the rate of change in bubble size while the normalized coalescence rate expressed as the rate of change in bubble population density is 3 times of that given by the interfacial area or bubble size,

$$-\frac{1}{a} \frac{\partial a}{\partial t} = \frac{1}{d} \frac{\partial d_{32}}{\partial t} \quad (5-28)$$



$$-\frac{1}{n} \frac{dn}{dt} = 3\left(-\frac{1}{a} \frac{da}{dt}\right) = 3\left(\frac{1}{d} \frac{dd_{32}}{dt}\right) \quad (5-29)$$

This suggests that if one expression of coalescence rate is available, the other two would be calculated from such value.

## 5.2 Results And Discussion

Factors influencing bubble coalescence rate will hereby be presented including the effect of various hydrodynamic and interfacial characteristics factors. The theoretical coalescence model developed above will be adapted to fit the experimental results and the role of interfacial parameters in the models will be discussed.

### 5.2.1 Effects of Hydrodynamic Factors on Bubble Coalescence Rates

Previous experimental studies on bubble coalescence can be categorized in two groups:

- the measurement of bubble coalescence time in stagnant liquids (e.g. Marrucci, 1969, Kim and Lee, 1987; Zahradnik, et al., 1995), and
- bubble coalescence rates calculated from the variation of bubble size in particular pieces of equipment such as mechanically agitated tanks and bubble columns (Calderbank et al., 1964; Lee et al., 1987; Prince and Blanch, 1990). Unfortunately, the hydrodynamic conditions encountered in these units are very complex and the simplifying assumptions of uniform conditions throughout the vessel does not take into account the complex interaction between bubble dispersion and coalescence taking place.

Both approaches can, therefore, not be used to determine bubble coalescence rates under the wide range of hydrodynamic conditions encountered in various parts of a processing unit. The present experimental investigation therefore focused on the use of well understood hydrodynamic regime which approximates isotropic turbulent plug flow (Pipe flow) in which coalescence is dominant. This, in turn, enabled the development of a better understanding of the hydrodynamic factors affecting bubble coalescence (gas holdup, bubble size, and local energy dissipation rate) which can be used to for the purpose of equipment design and simulation

### 5.2.1.1 Effect of Gas Hold-up on Bubble Coalescence

Due to the tendency of bubbles to coalesce as they move further away from the sparger (i.e. from location 1 to location 2 in Fig.3.1), the Sauter mean bubble size was found to increase with the consequent reduction in the specific interfacial area and bubble population density (Fig. 5.2 a, b and c). As shown in Fig. 5.2 the difference between the two locations is strongly influenced by the gas holdup in the system. This effect is clearly depicted in Fig 5.3 where the specific interfacial area reduction rates, as well as the bubble size growth rates, were found to increase with increasing gas holdup. This is caused by the greater coalescence tendencies obtained at larger gas holdups (greater collision frequency). On the other hand, the rate of change of bubble population density was found to decrease with increasing gas holdup. This apparent anomaly is caused by the tendency of the average bubble size, at any particular point, to increase with increasing gas holdup, a factor that strongly affects the bubble population density ( $n \propto 1/d_{32}^3$ ). As shown in Fig. 5.2b, the bubble size increased by more than two times when the gas hold-up was doubled. This causes an 8-fold decrease in bubble population density, a factor that can not be compensated for by the increased coalescence rate. The importance of this point is clearly shown in the results depicted in Fig. 5.4 a, b and c where only the data having a consistent initial bubble size ( $d_{32} \approx 500 \mu\text{m}$ ) are shown. Under those conditions, the rate of change of bubble population density (Fig. 5.4c) was found to behave in a fashion that is consistent with those of the interfacial area reduction rates, as well as the bubble size growth rates (Fig. 5.4 a and b), i.e. it increases with increasing gas holdup. This example serves to illustrate the importance of incorporating all pertinent parameters that affect bubble coalescence in order to develop a physically consistent understanding of the phenomenon.

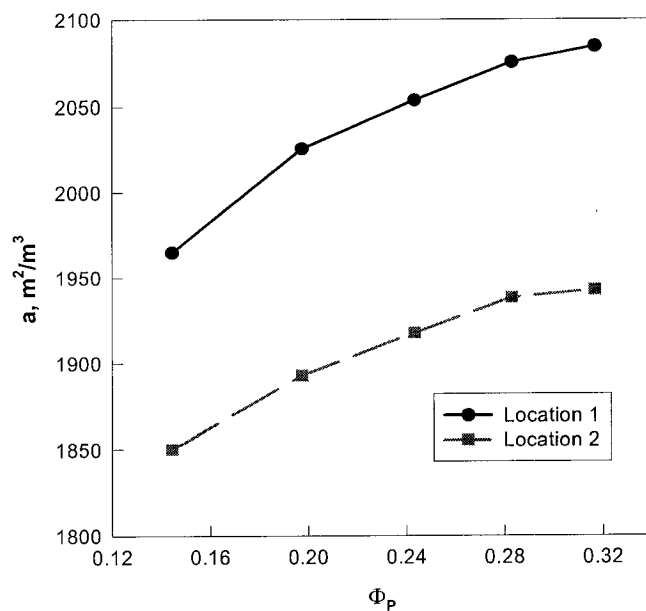


Fig. 5.2a Effect of gas hold-up on bubble dispersion characteristics : specific interfacial area (20 ppm SDS,  $U_L = 1.2$  m/s,  $U_{LS} = 0.2$  m/s,  $\epsilon_s \approx 17$  w/kg)

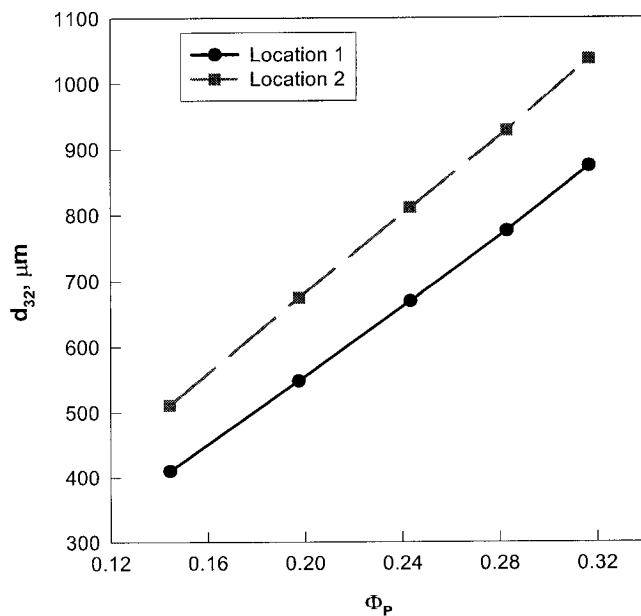


Fig. 5.2b Effect of gas hold-up on bubble dispersion characteristics : bubble size (20 ppm SDS,  $U_L = 1.2$  m/s,  $U_{LS} = 0.2$  m/s,  $\epsilon_s \approx 17$  w/kg)

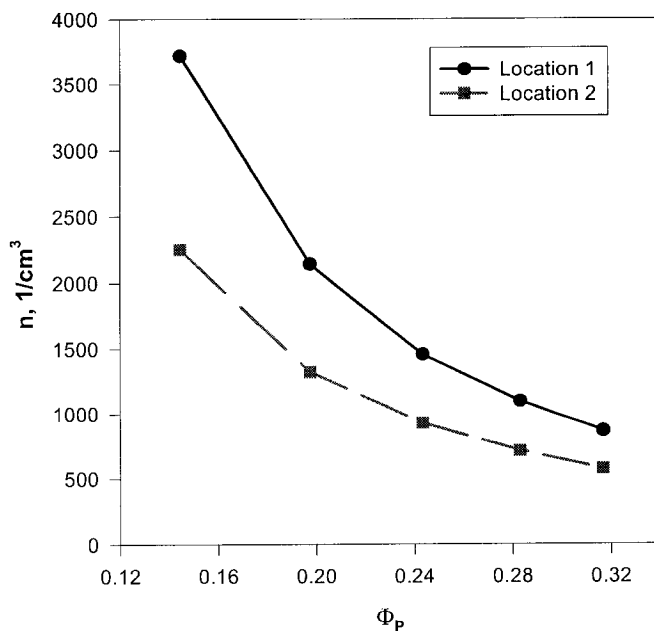


Fig. 5.2c Effect of gas hold-up on bubble dispersion characteristics: bubble population density (20 ppm SDS,  $U_L = 1.2$  m/s,  $U_{LS} = 0.2$  m/s,  $\epsilon_s \approx 17$  w/kg)

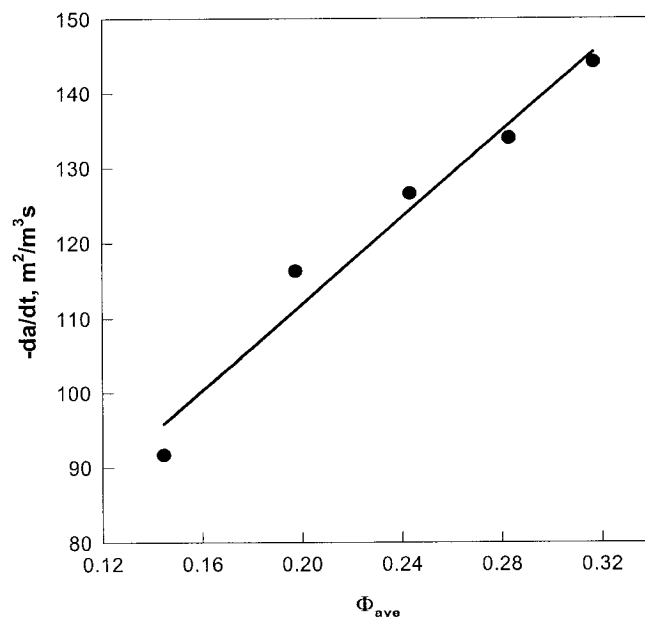


Fig. 5.3a Effect of gas hold-up on bubble coalescence rate (20 ppm SDS,  $U_L = 1.2$  m/s,  $U_{LS} = 0.2$  m/s,  $\epsilon_s \approx 17$  w/kg) expressed by differential coefficient of specific interfacial area

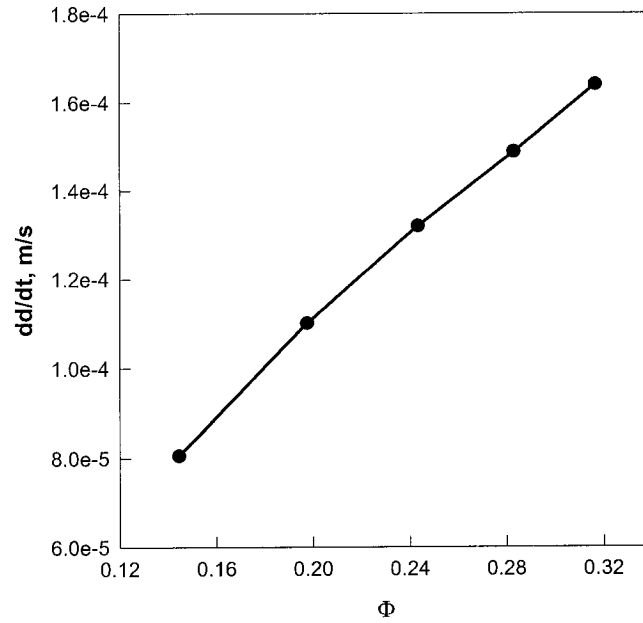


Fig. 5.3b Effect of gas hold-up on bubble coalescence rate (20 ppm SDS,  $U_L = 1.2$  m/s,  $U_{LS} = 0.2$  m/s,  $\epsilon_s \approx 17$  w/kg) expressed by differential coefficient of bubble size

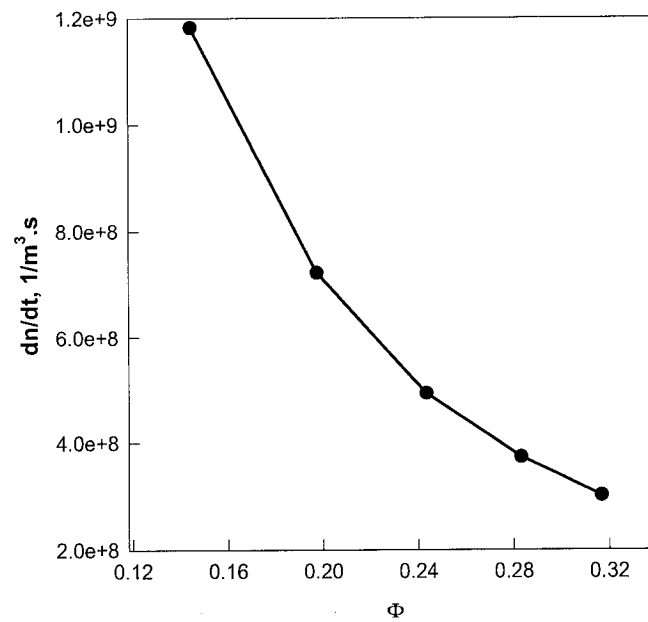


Fig. 5.3c Effect of gas hold-up on bubble coalescence rate (20 ppm SDS,  $U_L = 1.2$  m/s,  $U_{LS} = 0.2$  m/s,  $\epsilon_s \approx 17$  w/kg) expressed by differential coefficient of bubble population density

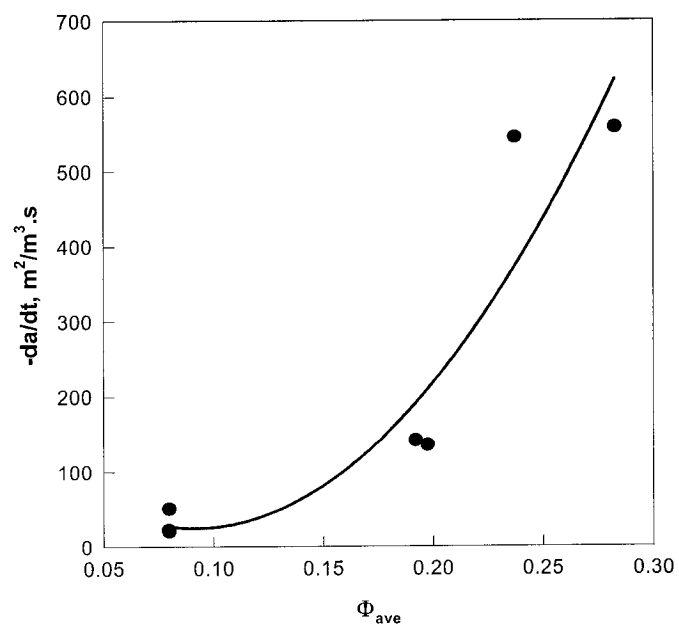


Fig. 5.4a Effect of gas hold-up on coalescence rate with the same initial bubble size expressed by differential coefficient of specific interfacial area (10 ppm SDS,  $U_L = 1.2$  m/s,  $U_{LS} = 0.2$  m/s,  $\epsilon_S \approx 17$  w/kg,  $d_i = 500 \mu\text{m}$ )

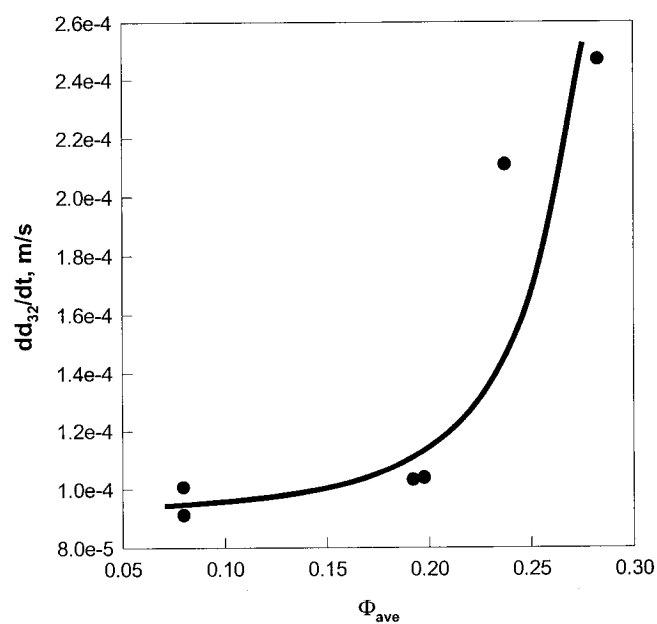


Fig. 5.4b Effect of gas hold-up on coalescence rate with the same initial bubble size expressed by differential coefficient of Sauter mean bubble diameter (10 ppm SDS,  $U_L = 1.2$  m/s,  $U_{LS} = 0.2$  m/s,  $\epsilon_S \approx 17$  w/kg,  $d_i = 500 \mu\text{m}$ )

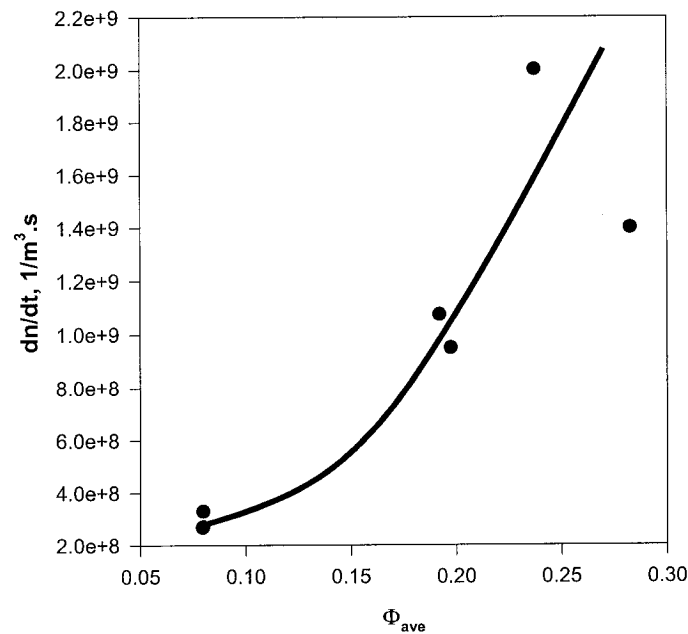


Fig. 5.4c Effect of gas hold-up on coalescence rate with the same initial bubble size expressed by differential coefficient of bubble population density (10 ppm SDS,  $U_L = 1.2$  m/s,  $U_{LS} = 0.2$  m/s,  $\epsilon_S \approx 17$  w/kg,  $d_1 = 500 \mu\text{m}$ )

### 5.2.1.2 Effect of Local Energy Dissipation Rate on Bubble Coalescence

The local energy dissipation rate in the pipeline was changed by adjusting the velocity of main liquid stream passing through the pipeline. The effect of this parameter on the interfacial area, bubble size and bubble population density is presented in Fig. 5.5 a, b and c. The specific interfacial areas of contact and the bubble population densities at both locations 1 and 2 were found to increase and the bubble size to decrease with increasing local energy dissipation rate in the pipeline. These observations stem from the fact that an increase in the local energy dissipation rate will result in more frequent bubble break-ups.

On the other hand, an increase in the local energy dissipation rate will also increase the frequency of bubble collision in which the bubbles have more possibility to contact and coalescence with each other. As shown in Fig. 5.5 a and c, the lines representing conditions at point 1 consistently deviate from those at location 2 as the local energy

dissipation rate is increased. This suggests that the bubble coalescence rate is enhanced by increasing the local energy dissipation rate. However, judging from Fig. 5.5 b, one can draw an opposite conclusion due to the fact that the two lines at location 1 and 2 approach each other. This is an excellent example to demonstrate that the absolute differential rate of a variable can fail to predict the true variation of this parameter. As mentioned above, the use of normalized coalescence rate yields better indication of what is actually happening. This is clearly shown in Fig. 5.6 where all normalized coalescence rates, no matter whether expressed by the interfacial area, the bubble size or the bubble population density, show a consistent increase with increasing local energy dissipation rates.

All these trends agree with Eq. (5-13 to 5-15), the predictions of Lee et al. (1987), Prince and Blanch (1990) and Chesters (1991) and the experimental findings of Prince and Blanch where the superficial gas velocity is related to the local turbulent energy dissipation rate.

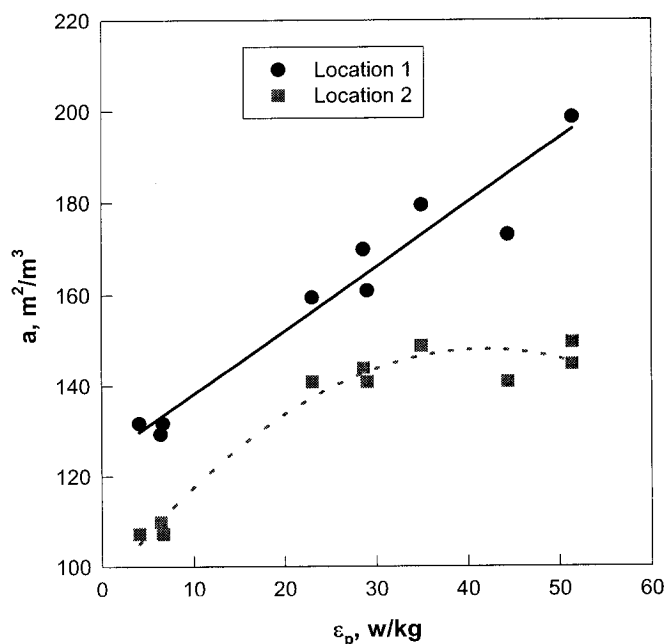


Fig. 5.5a Effect of energy dissipation rate in pipe on bubble dispersion characteristics : specific interfacial area (water,  $\Phi_p \approx 0.07$ )



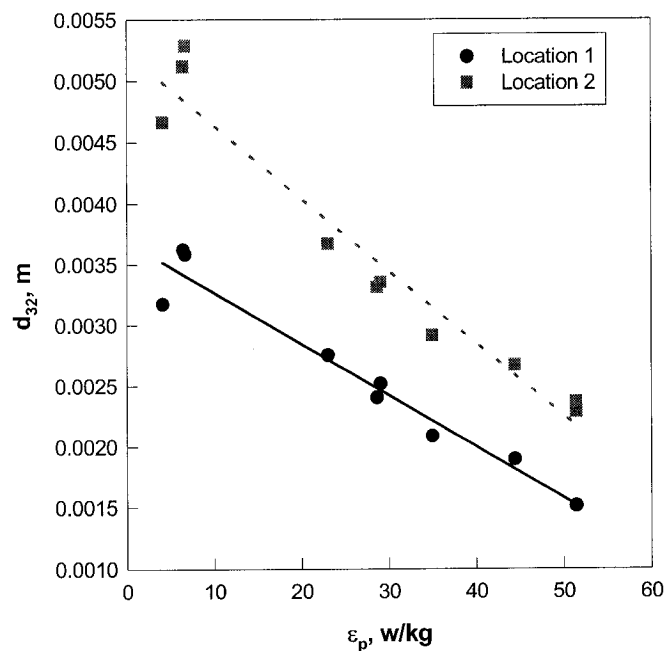


Fig. 5.5b Effect of energy dissipation rate in pipe on bubble dispersion characteristics : Sauter mean bubble diameter (water,  $\Phi_P \approx 0.07$ )

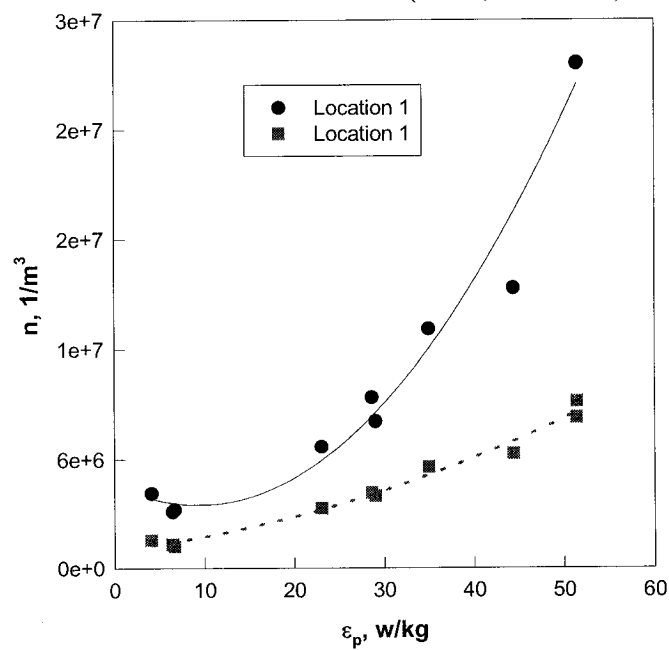


Fig. 5.5c Effect of energy dissipation rate in pipe on bubble dispersion characteristics : bubble population density (water,  $\Phi_P \approx 0.07$ )

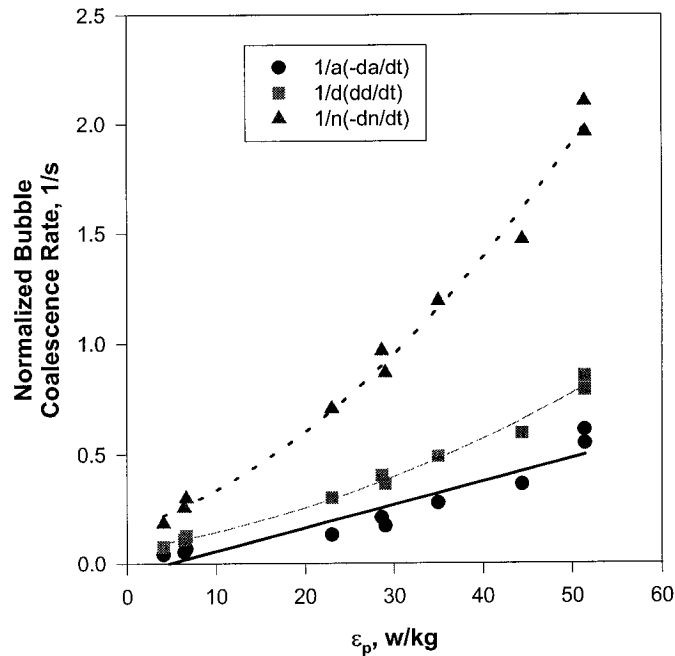


Fig. 5.6 Effect of energy dissipation rate in pipe on normalized bubble coalescence rate (water,  $\Phi_p \approx 0.07$ ), a) specific interfacial area, b) Sauter mean bubble diameter, c) bubble population density

### 5.2.1.3 Effects of Bubble Size on Coalescence Rate

When both the liquid velocity of the main stream and the gas/liquid flow ratio are kept constant, the bubble sizes generated by the sparger can be adjusted by varying the local rate of energy dissipation in the throat. This, in turn, can be accomplished by either changing the volumetric flow rate of the liquid passing through the sparger, or by altering the cross sectional area of the throat through which that liquid has to pass, or by a combination of both actions. The operational flexibility of this sparger was taken advantage of to generate gas/liquid dispersions, having a wide range of initial bubble size under essentially the same pipeline conditions (47 points). This approach was necessary in order to accurately identify the effect of bubble size on coalescence rate, and to separate this effect from others.

The results obtained using tap water are presented in Fig. 5.7 a, b and c for a constant liquid superficial velocity of 1.8 m/s. The variation of interfacial area and bubble population density clearly show that bubble coalescence rate is faster for small bubbles and decreases as the initial bubble size increases. This is clearly depicted in Fig. 5.8 for the three formats of normalized coalescence rates.

The fact that the specific interfacial area and the bubble population density at point 2 is essentially independent from the initial conditions (Fig. 5.7 a and c) suggest that bubble breakage/coalescence essentially reached equilibrium at point 2 in the case of tap water. This is clearly shown in Fig. 5.7 b where the final bubble size is independent of  $d_{32}$  at point 1. This behaviour is significantly different from the observations obtained using 2 ppm SDS (Fig. 5.9 a, b and c) where the interfacial area, the bubble size and the bubble population density at point 2 vary as the initial bubble size increases. It implies that the bubble breakage and coalescence at point 2 have not yet reached equilibrium conditions.

As shown in Fig. 5.10, all expressions of the coalescence rates were found to decrease

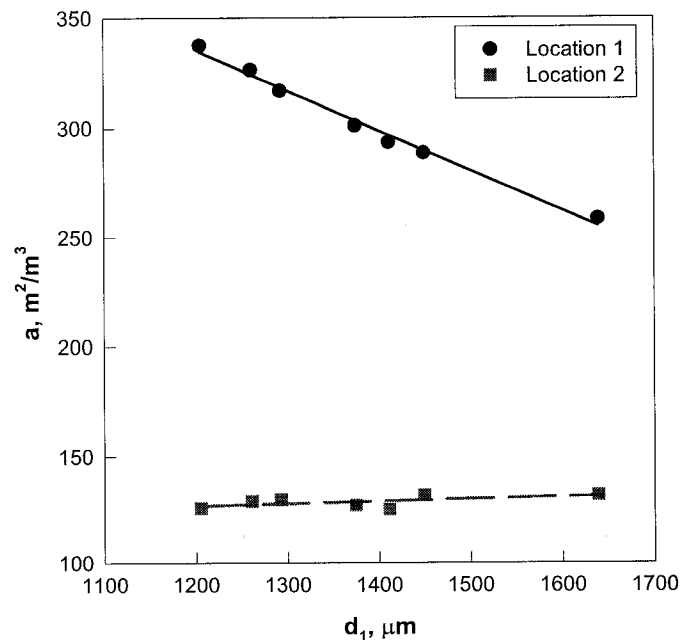


Fig. 5.7a Effect of bubble size on gas/liquid dispersion characteristics : interfacial area (water,  $U_L = 1.8$  m/s,  $\Phi_P = 0.07$ ,  $\varepsilon_s = 25$  w/kg)

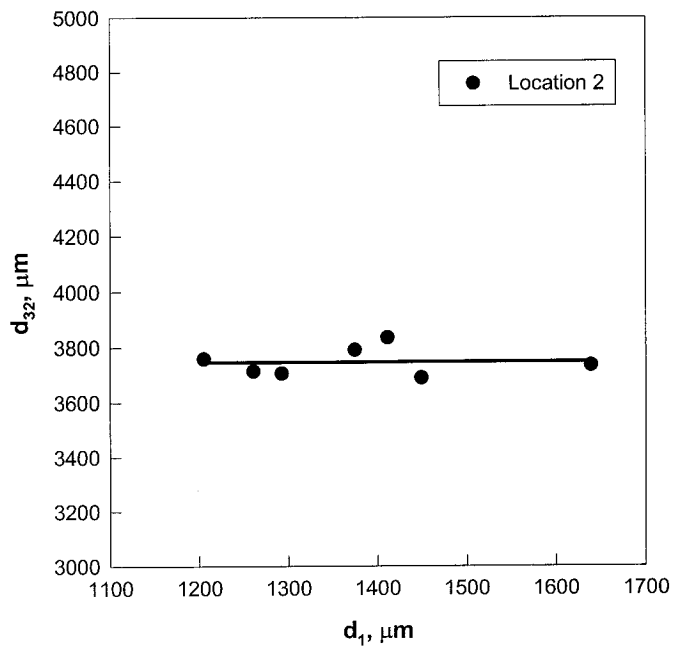


Fig. 5.7b Effect of bubble size on gas/liquid dispersion characteristics : bubble size (water,  $U_L = 1.8$  m/s,  $\Phi_P = 0.07$ ,  $\epsilon_s = 25$  w/kg)

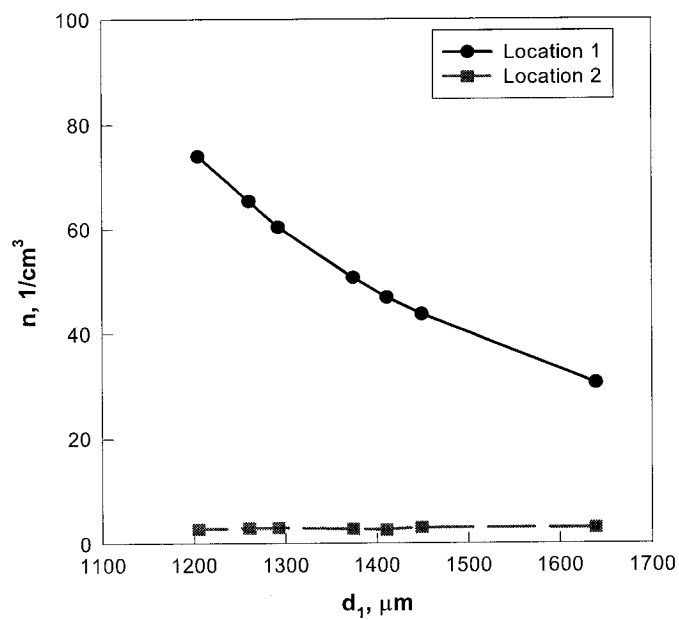


Fig. 5.7c Effect of bubble size on gas/liquid dispersion characteristics : bubble population density (water,  $U_L = 1.8$  m/s,  $\Phi_P = 0.07$ ,  $\epsilon_s = 25$  w/kg)

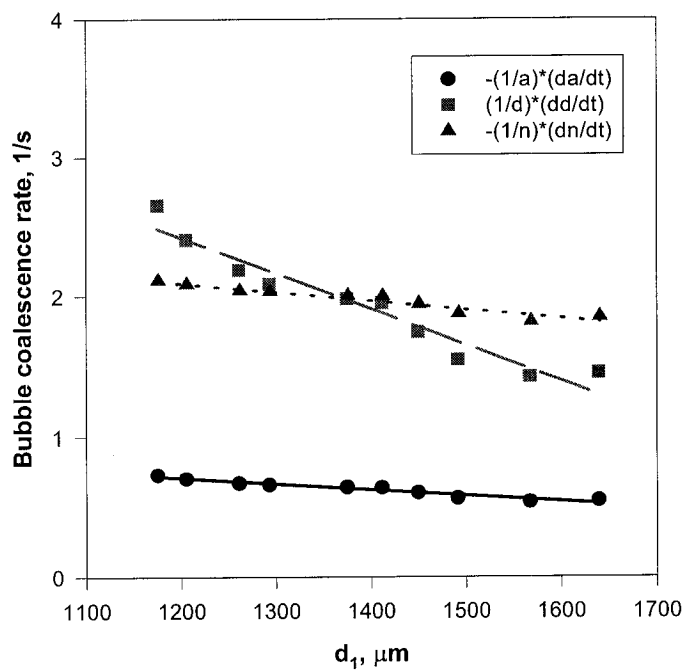


Fig. 5.8 Effect of bubble size on normalized coalescence rate characteristics (water,  $U_L = 1.8$  m/s,  $0.07$ ,  $\epsilon_s = 25$  w/kg)

a) interfacial area, b) bubble diameter, c) bubble population density

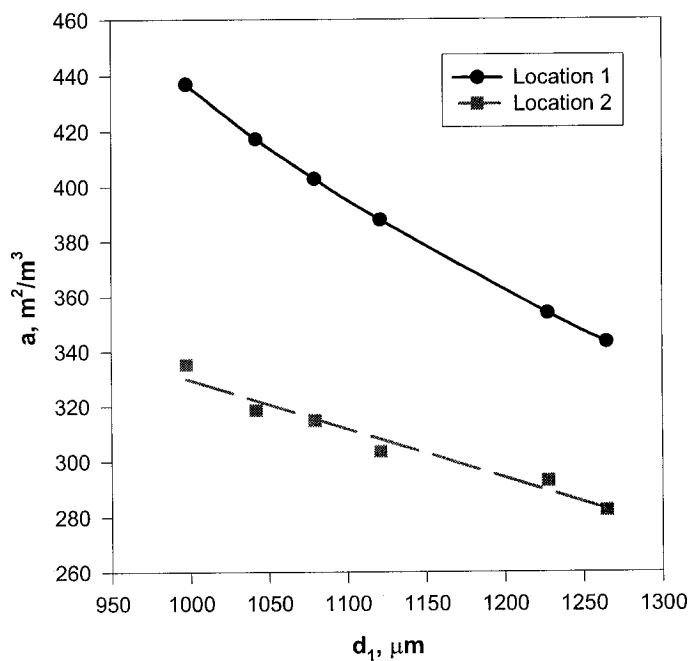


Fig. 5.9a Effect of bubble size on gas/liquid dispersion characteristics : interfacial area (2 ppm,  $U_L = 1.2$  m/s,  $\Phi_P = 0.08$ ,  $\epsilon_s = 16$  w/kg)

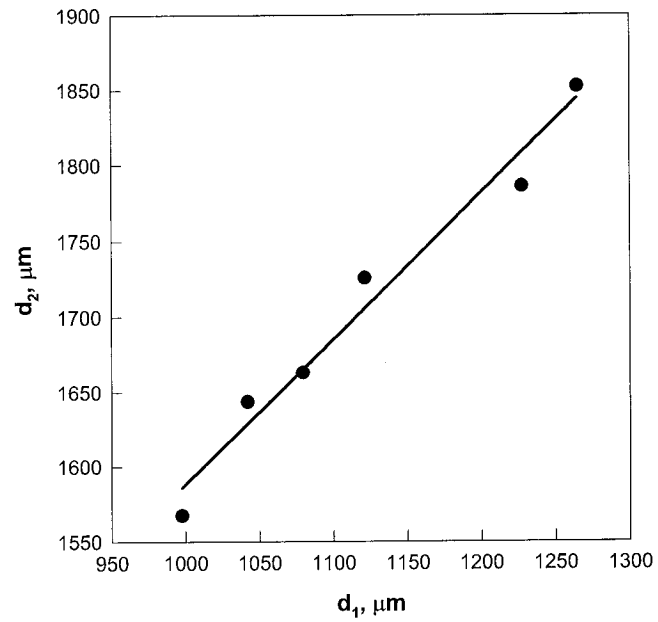


Fig. 5.9b Effect of bubble size on gas/liquid dispersion characteristics : bubble size (2 ppm,  $U_L=1.2$  m/s,  $\Phi_P=0.08$ ,  $\epsilon_S=16$  w/kg)

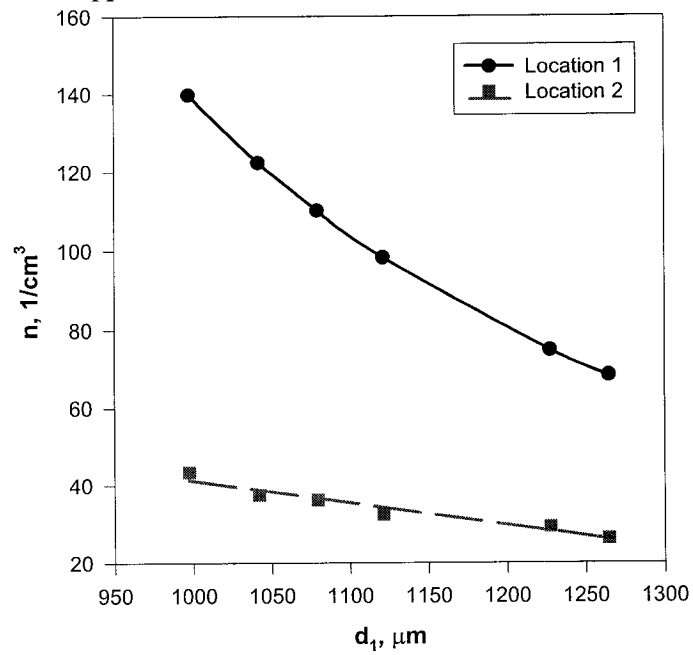


Fig. 5.9c Effect of bubble size on gas/liquid dispersion characteristics : bubble population density (2 ppm,  $U_L=1.2$  m/s,  $\Phi_P=0.08$ ,  $\epsilon_S=16$  w/kg)

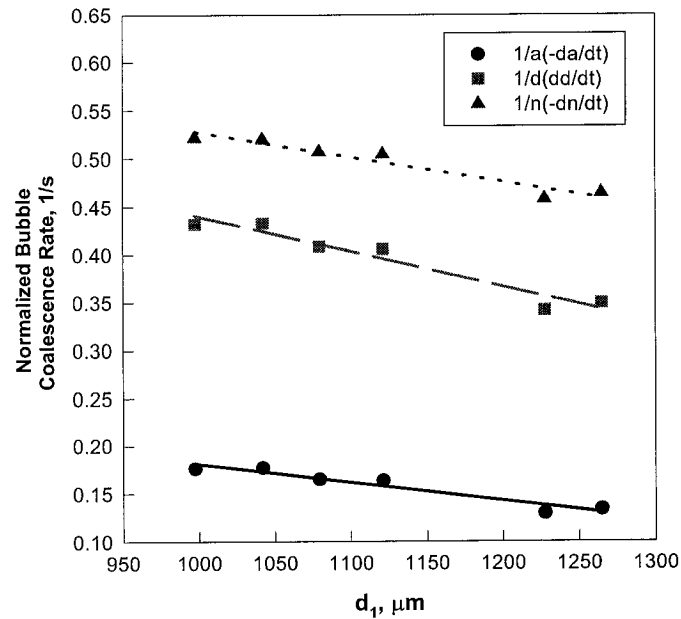


Fig. 5.10 Effect of bubble size on normalized coalescence rate characteristics (2 ppm,  $U_L=1.2$  m/s,  $\Phi_p=0.08$ ,  $\epsilon_S=16$  w/kg)  
 a) interfacial area b) bubble size c) bubble population density

with increasing initial bubble size. The three normalized coalescence rate expressions (interfacial area shrinking rate, bubble growth rate, and the bubble population decrease rate) depict an obvious dependence on initial bubble size (Fig. 5.8 and 5.10). In another word, when the bubble size is small, the bubble coalescence rate is fast. This is in agreement with Eq. (5-13) to (5-15) and the predictions of Lee et al. (1987), Prince and Blanch (1990) and Chesters (1991). However, no prior experimental verification of this factor has been reported in the literature in which coalescence-dominated conditions were ensured.

The 52 experimental points obtained using tap water were correlated using the stepwise linear regression program of the SAS software package (Cody, et al., 1997). It selects the most influential parameters first and progressively incorporates less significant ones until the statistical significant test requirements (F test at 95% confidence limits) are no more met.

The following correlation was found to predict the effect of various hydrodynamic factors on coalescence rates quite well,

$$-\frac{dn}{dt} = 27\Phi_p^{0.97} \varepsilon_p^{1.6} d^{-2.0} e^{-t_c/t_i} \quad (5-30)$$

The values of  $t_i$  and  $t_c$  were calculated using Eq. (5-20) and (5-22). The value of  $h_i$  was taken to be constant,  $10^{-5}$  m, as suggested by Ivanov and Dimitrov (1974) and Mobius and Miller (1998) whereas the value of  $h_c$  was calculated using Eq. (5-24) in order to account for the effect of hydrodynamic forces on this term.

A fairly good correlation coefficient was obtained ( $R^2 = 0.93$ ) over a relatively wide range of experimental conditions ( $\Phi_p = 0.007 - 0.37$ ,  $\varepsilon_p = 13 - 17$  W/kg,  $d_{32} = 800 - 8,400$   $\mu\text{m}$ ) and covers coalescence rates that vary by two orders of magnitudes (Fig.5.11).

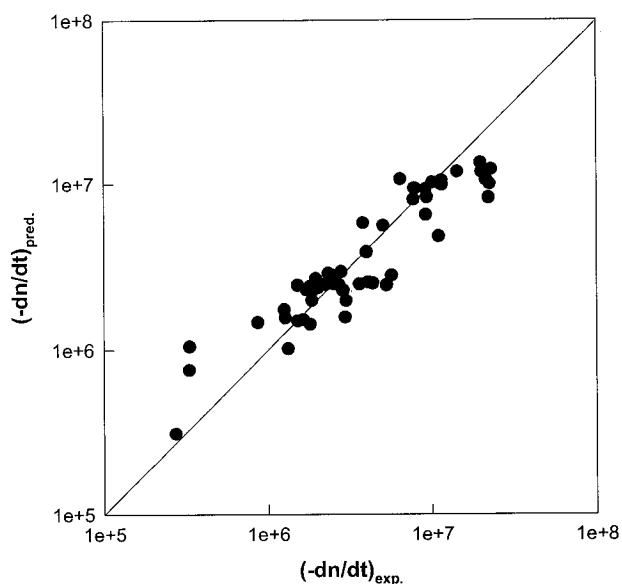


Fig. 5.11 Comparison of experimental bubble coalescence rate in tap water with model predictions (Eq. 5-30).

There are two cases (the experimental values are about  $3.3 \times 10^5$ ) that do not seem to correspond to the model fitted to the bulk of the data. If these two were eliminated as



outliers, the fitting result would be improved. Because of the absence of any coalescence-retarding agent, these data points were obtained using relatively large bubble diameters ( $d_{32} = 0.8 - 8.4$  mm) and their coalescence rate may be more suitably expressed using the model recently-developed model by Kamp, et al. (2001).

Their model is more applicable to the situation of large bubble (e.g. 2 - 25 mm bubble size range) where bubble deformation plays a more pronounced role. Using Eq. (5-30) to predict coalescence rates for bubbles larger than 5 mm was found to result in overestimating bubble coalescence rates. This is most probably caused by dimple formed between deformable bubbles resulting in slow thinning (Ivanov et al., 1985 and Li, 1996).

Although Eq. (5-30) has the same form as Eq. (5-17), the value of empirically obtained exponents differ significantly from those predicted by the theory. This is most probably caused by the inherent assumption of a monodisperse bubble size distribution equal to the Sauter mean diameters as well as by the fact that tap water exhibits some low-level coalescence retardation due to the presence of trace quantities of minerals.

## **5.2.2 Effect of Interfacial Characteristics on Bubble Coalescence Rates**

This section discusses the experimental results obtained in the presence of low SAA concentrations. They will be used to develop a better understanding of how bubble coalescence rate is retarded and the role played by various static and dynamic interfacial characteristics (such as concentration, static surface tension, Gibbs surface excess, and dynamic surface excess based on long-term approximation affect the coalescence rates).

### **5.2.2.1 Bubble Coalescence Retardation**

It is well known that the presence of surface active agents (SAA) retards bubble coalescence through their ability to modify the static and dynamic interfacial characteristics of the system. This is clearly shown by the results in Fig. 5.12 a, b and c. Compared to the results obtained with tap water, the normalized coalescence rates were found to decrease radically in the presence of even minute quantities of SDS. For example, in the case of  $d_{32} = 1.2$  mm the normalized rate of change of bubble population density was found to drop from 1.1 events per second (in the case of tap water) down to

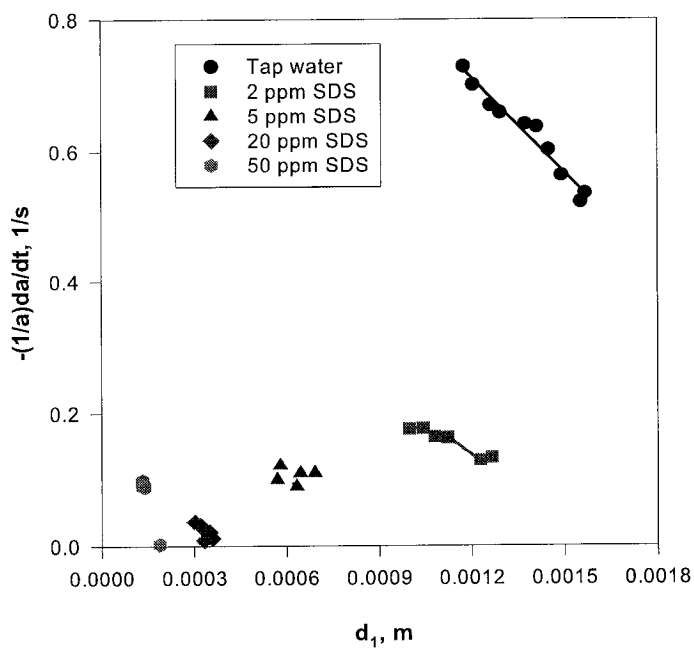


Fig. 5.12a Effect of SDS concentration on normalized bubble coalescence rate : interfacial area (0, 2, 5, 10, 50 ppm,  $\Phi_P = 0.08$ ,  $\epsilon_P = 16$  w/kg)

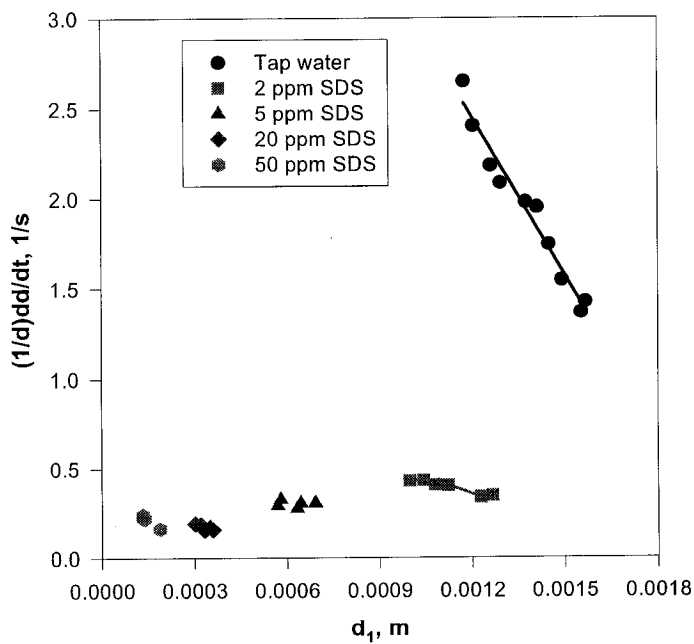


Fig. 5.12b Effect of SDS concentration on normalized bubble coalescence rate : bubble size (0, 2, 5, 10, 50 ppm,  $\Phi_P = 0.08$ ,  $\epsilon_P = 16$  w/kg)

$0.5 \text{ s}^{-1}$  in the presence of 2 ppm SDS. This represents a 2.2-fold reduction in the normalized coalescence rate. The coalescence rate is further reduced to  $0.2 \text{ s}^{-1}$  in the presence of 5 ppm SDS, which represents more than 1-order reduction in comparison to the case of water. Similar conclusions could be drawn in so far as the interfacial area shrinking rate or the bubble growth rate is concerned.

Shown in Fig. 5.8 and 5.10 for air-water, the three normalized coalescence rate expressions (interfacial area shrinking rate, bubble growth rate, and the bubble population decrease rate) were found to depict a strong dependence on initial bubble size. However, as can be seen from Fig. 5.12, the coalescence rate is dramatically reduced with increasing SDS concentration. This is in agreement with the bubble coalescence time findings of Marrucci and Nicodemo (1967), Oolman and Blanch (1986), and Zahradnik et al. (1995).

Similar trends were observed in the case of film thinning time encountered in the foam studies of Ivanov (1988) and Craig et al. (1993). In those investigations, the effect of surface active agents on coalescence rates and foam stability has been mainly accounted for through their ability to decrease static surface tension in the film thinning time expression (Eq. 5-22).

#### **5.2.2.2 Effects of Interfacial Characteristics on Bubble Coalescence Rate**

The importance of SDS concentration on bubble coalescence rate can best be visualized by considering the data presented in Fig. 5.13 a, b and c. In this set of data all hydrodynamic factors were kept constant (gas holdup of 0.2 and local turbulent energy dissipation rate of 16 w/kg which corresponds to  $U_{Lp} = 1.2 \text{ m/s}$ ) and the initial bubble size was close to 1 mm.

As can be seen from Fig. 5.13a, the spatial variation in specific interfacial area (i.e. the difference between locations 1 and 2) was found to decrease with increasing SDS concentration. Similar trends are observed in the case of Sauter mean bubble diameter and bubble population density (Fig. 5.13b and c). In other words, within the concentration range investigated, bubble coalesce is significantly retarded by the presence of SDS. This is clearly depicted in Fig. 5.14 where the influence of SDS on the

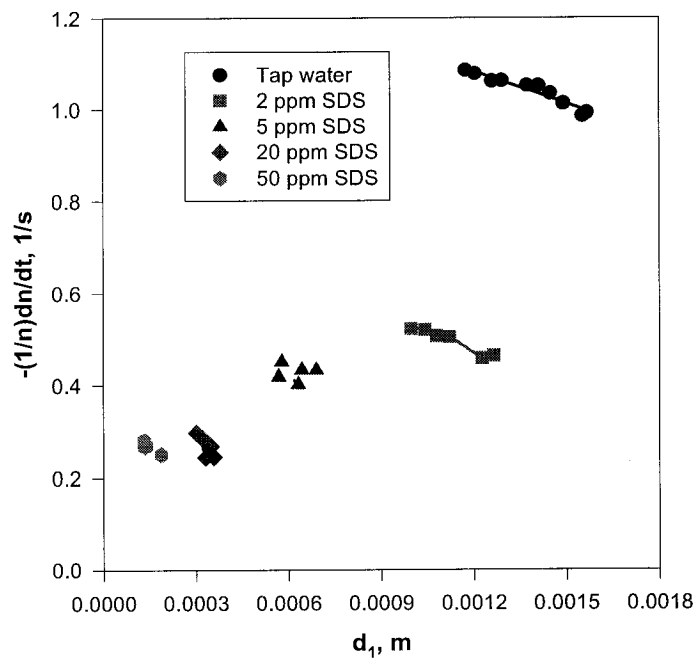


Fig. 5.12c Effect of SDS concentration on normalized bubble coalescence rate : bubble population density (0, 2, 5, 10, 50 ppm,  $\Phi_P = 0.08$ ,  $\epsilon_P = 16$  w/kg)

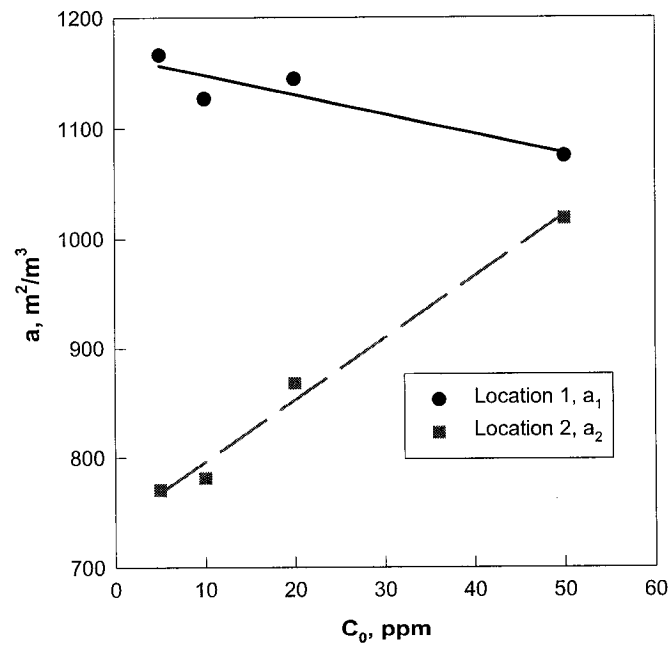


Fig. 5.13a Effect of SDS bulk concentration on the gas/liquid contacting characteristics : interfacial area ( $\Phi_P = 0.2$ ,  $\epsilon_P = 16$  w/kg,  $d_1 \approx 1000 \mu m$ )

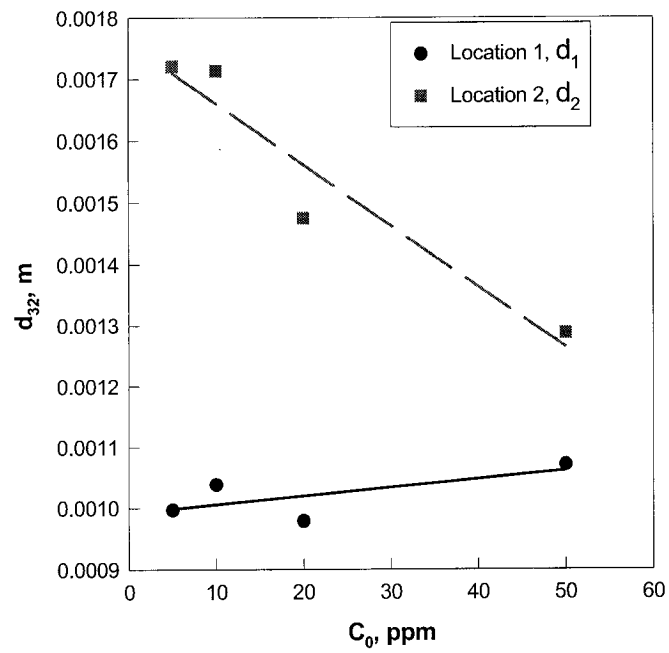


Fig. 5.13b Effect of SDS bulk concentration on the gas/liquid contacting characteristics : bubble size ( $\Phi_P = 0.2$ ,  $\varepsilon_P = 16$  w/kg,  $d_l \approx 1000$   $\mu\text{m}$ )

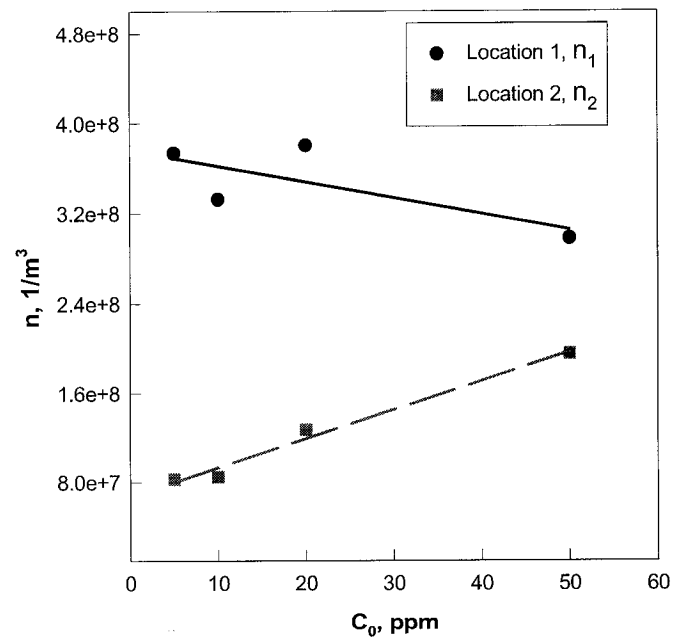


Fig. 5.13c Effect of SDS bulk concentration on the gas/liquid contacting characteristics : bubble population density ( $\Phi_P = 0.2$ ,  $\varepsilon_P = 16$  w/kg,  $d_l \approx 1000$   $\mu\text{m}$ )

three normalized coalescence rates is shown. As the bulk SDS concentration increases from 5 to 50 ppm, the interfacial area shrinking rate was found to be reduced by a factor of 7, whereas the bubble growth rate and the rate of change bubble population density were both reduced by a factor of 4 and 2 respectively.

The effect of interfacial characteristics on gas/liquid contacting in pure systems has traditionally been accounted for in the variation of the value of the static surface tension,  $\sigma$ . This parameter, however, can not satisfactorily explain the significant increases in specific interfacial area of contact encountered in the presence of very small concentrations of secondary constituents (such as alcohols, acids, electrolytes) such as those investigated by Divakarla (1983), Zlokarnik (1985), Al Taweel and Cheng (1996), and Jamialahmadi and Muller-Steinhagen (1992). These large increases in interfacial area of contact were achieved in conjunction with relatively small reductions in the static interfacial tension (even an increase in the value of  $\sigma_{sta}$  in the case of electrolytes) which resulted in the surface tension exponents being as high as  $-23.7$  in order to accommodate such observations (Al Taweel and Cheng, 1996). The need for using more sophisticated interfacial characteristics was highlighted by Zlokarnik (1985) for the case of complex industrial systems. In the case at hand (dynamic sparger in pipeline flow), the addition of 50 ppm SDS to water results in less than 40% reduction in the value of the static surfacetension (Table 4.2) yet, the associated bubble coalescence rates can be reduced by a factor as large as 28-fold.

To identify the interfacial characteristic that plays the most important role in controlling bubble coalescence processes, the following parameters were evaluated:

- Static surface tension  $\sigma_{sta}$ : which reflects the force per unit length (measured at equilibrium) trying to minimize the interfacial area of contact.
- Surface pressure  $\Pi$ : which yields a measure of reduction in surface energy due to the presence of SAA.
- Gibbs surface excess  $\Gamma_G$ : which represents the amount of SAA species adsorbed per unit area of interface at equilibrium, and it also implies the rate of change of surface energy with SAA concentration.

- Dynamic surface tension  $\sigma_t$ : which is the surface tension of a freshly created surface measured after a given time of contact. It represents a non-equilibrium state and a characteristic time is therefore needed for this parameter.
- Diffusivity and apparent effective diffusivity  $D$  and  $D_{app}$ : those parameters result from long-term approximation of SAA diffusion controlled process. However, as shown in section 4.1, its value is constant over the concentration range covered by the present investigation.
- Surface excess based on long-term approximation  $\Gamma_L$ : it stands for the quantity of surfactant molecules adsorbed upon the surface per unit area of interface in the process of that surfactant molecules are migrating from the subsurface onto the interface, so it is a dynamic surface excess, but it possesses a static value when applying in a certain time range of 0.08 – 6 s for SDS systems.

In order to find out how interfacial variables influence the bubble coalescence rate, the coalescence rates at the same hydrodynamic conditions and almost the same initial bubble size were plot against various interfacial parameters (Fig.5.14 - 5.18).

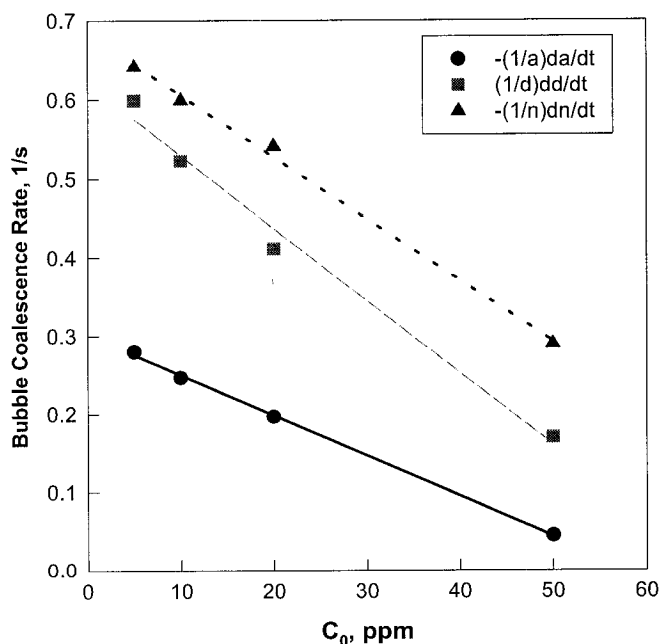


Fig. 5.14 Effect of bulk concentration on bubble coalescence rates ( $\Phi_p = 0.2$ ,  $\varepsilon_p = 16$  w/kg,  $d_l \approx 1,000 \mu\text{m}$ )

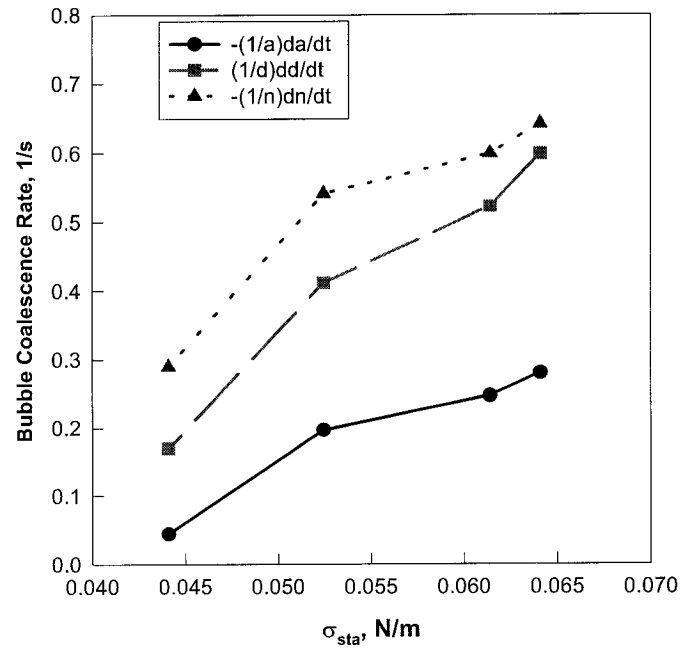


Fig. 5.15 Effect of static surface tension on bubble coalescence rates ( $\Phi_P = 0.2$ ,  $\epsilon_P = 16$  w/kg,  $d_1 \approx 1,000 \mu\text{m}$ )

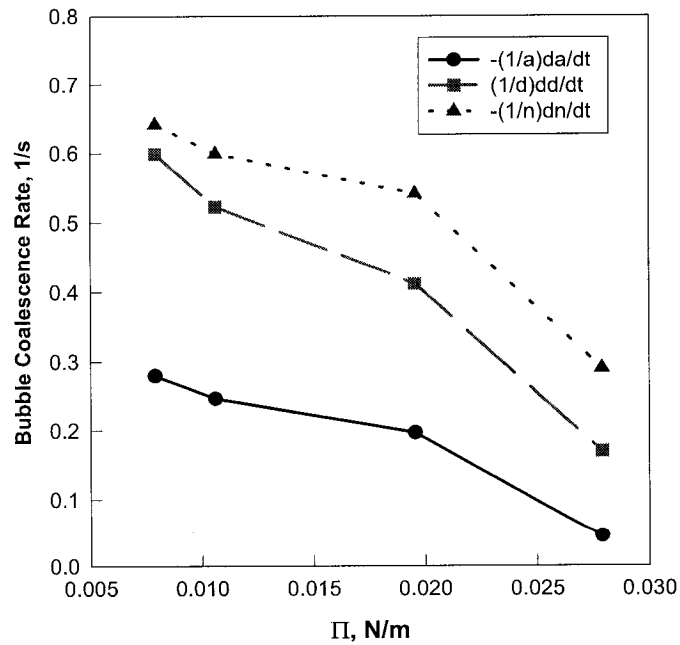


Fig. 5.16 Effect of surface pressure on bubble coalescence rates ( $\Phi_P = 0.2$ ,  $\epsilon_P = 16$  w/kg,  $d_1 \approx 1,000 \mu\text{m}$ )



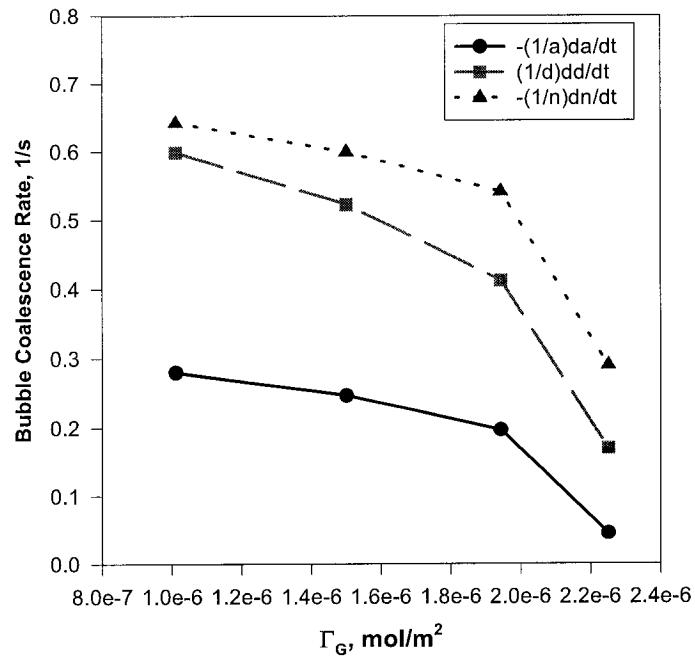


Fig. 5.17 Effect of Gibbs surface excess on bubble coalescence rates ( $\Phi_P = 0.2$ ,  $\epsilon_P = 16$  w/kg,  $d_i \approx 1,000 \mu\text{m}$ ,  $d_l \approx 1,000 \mu\text{m}$ )

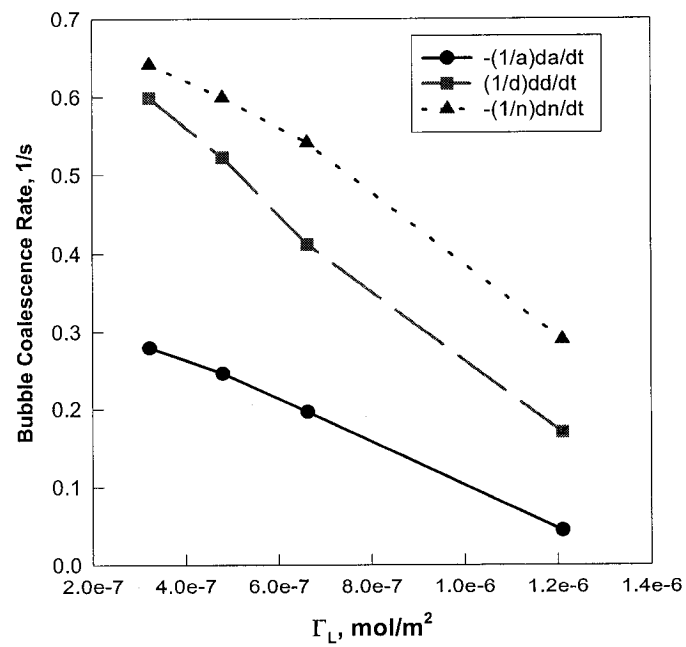


Fig. 5.18 Effect of surface excess on bubble coalescence rates ( $\Phi_P = 0.2$ ,  $\epsilon_P = 16$  w/kg,  $d_l \approx 1000 \mu\text{m}$ )

The data for water were not included in the plots due to the larger initial bubble size from that of the SDS solutions. As can be seen from Fig.5.14 to Fig 5.18, all normalized bubble coalescence rates are sensitive to the above-mentioned interfacial characteristics; that is to say that the bubble coalescence rate will decrease as  $C_0$ ,  $\Pi$ ,  $\Gamma_G$ ,  $\Gamma_L$  increases, or as  $\sigma$  decreases.

The static surface tension is often used to predict/correlate the effect of variation in interfacial characteristics; however, it is well known that the characteristic coalescence time is of the order of milliseconds whereas it takes much more than 3 s in order for SDS to approach its equilibrium value (Fig. 4.5). This thermodynamic parameter is thus not expected to yield a physically consistent explanation of the effect impurities have on the very rapid and dynamic bubble coalescence processes.

The Gibbs surface excess,  $\Gamma_G$ , is an indication of the amount of surfactant species adsorbed onto the gas-liquid interface at equilibrium and is derived from equilibrium measurements. It is thus not expected to be a good representative of the non-equilibrium bubble breakage and coalescence processes.

The surface pressure yields a good indication of the energy needed to deform bubbles where the interfacial concentration is reduced due to the increase of their surface area without the ability of new SAA to diffuse to the surface. However, it is, once again, based on equilibrium surface tension measurement and suffers, therefore, from the same problem as  $\sigma$  and  $\Gamma_G$ .

The dynamic interfacial characteristics of the system provide a good indication of the rate at which SAA material diffuses to and adsorbs on the interface. This factor is expected to play an important role in determining the coalescence rate of bubbles (Marrucci and Nicodemn, 1967; Sagert and Quinn, 1978; Drogaris and Weiland, 1983 and Xue, 1999). Unfortunately, the dynamic surface tension varies with the surface age and it is not possible to use a single value to characterize the interface unless the characteristic coalescence time is well known. Under the experimental conditions investigated, the

latter was calculated to range from 0.2 ms to 36 ms depending on the complicated hydrodynamics and interfacial characteristics. Attempts were therefore undertaken to use the effective diffusivity and diffusivity of SDS in aqueous solutions as an interfacial characteristic. However, as shown in Chapter 4, the diffusivity of SDS was found to be insensitive to the variations in the bulk concentrations of SDS ( $D = 8.42 \times 10^{-10} \text{ m}^2/\text{s}$ ) over the concentration range investigated. It can thus not be used as an indicator of the variation of interfacial characteristics with concentration.

The surface excess based on the long-term approximation,  $\Gamma_L$ , is obtained from dynamic measurements and may be a suitable candidate for expressing the effect of interfacial characteristics on bubble coalescence rates. As shown in Table 4.2, the value of  $\Gamma_L$  varies with SDS concentration but was found to be independent of surface age within the range of concentrations studied in the present investigation. It can thus be used as a single characteristic describing the effect of SAA diffusion/adsorption.

As mentioned before, a thin film is formed when two bubbles approach each other under the influence of the turbulent conditions present in the bulk of the liquid phase. The rate of thinning of the thin film between the bubbles is dependent on the balance between the attraction and repulsive forces, both of which are strongly influenced by the interfacial properties. The attraction forces stem mainly from van der Waals attraction, while the repulsive forces include double layer repulsive force (that is significant especially for electrolyte solutions such as that used in the present investigation). Several authors (Garrett, 1993; Christerson and Yaminsky, 1995; Rosen, 1996; Mobius and Miller, 1998) analyzed the coalescence process in foam by considering the interfacial viscosity, elasticity or visco-elasticity, Gibbs effect, and the Marogoni effect. Almost all of them agree that as the concentration of SAA at the interface increases, the disjoining force will increase and the coalescing process is retarded. Since the value of  $\Gamma_L$  increases with increasing SDS concentration, it accounts for the presence of more SAA entities on the surface of the bubbles and may, therefore, yield a good indicator of the repulsive forces. Those disjoining forces are known to contribute to slowing down the liquid thinning between the bubbles (Drogaris and Weiland, 1983; Pugh and Yoon, 1994; Weissenborn and Pugh, 1996; Pashley and Crag, 1997).

As a result of the above, bubble coalescence time will increase because of the slower film drainage rates. Since the contact time between the two colliding bubbles remains essentially constant, the ratio of coalescence time to contact time increases and the coalescence probability expressed by Eq. (5-16) decreases, thus resulting in a retardation of the bubble coalescence process.

### 5.2.3 Modeling Bubble Coalescence Rate in Industrially-Simulated Systems

The experimental results obtained in this investigation will be used to discern amongst those many parameters using the theoretical expression given in Eq. (5-13). This expression format was selected because it is based on the same concepts used in the physical interpretation of bubble coalescence in the case of pure systems, a situation which was found to apply well to the case of tap water (Eq. 5-30). The linear regression program of SAS was applied to air-SDS aqueous solutions, similar to Eq. (5-30), the correlating equation is as follows,

$$-\frac{dn}{dt} = 55\Phi_p^{2.0} \epsilon_p^{1.6} d^{-5.0} e^{-1.0t_c/t_i} \quad (5-31)$$

The regression coefficient is as low as 81%, moreover, the power for the bubble diameter is significantly higher than that in Eq. (5-30). It implies that if the bubble size increases doubly, the bubble coalescence rate will decrease 1-order of magnitude, which do not agree to the observation as shown in either Fig. 5.8 or Fig.5.10. The reason why Eq. (5-31) is not able to express the bubble coalescence rate of air-SDS aqueous solutions fairly might be that it is not sufficient for the surface tension as the only interfacial indicator taken into account in the bubble coalescence time.

As we know that the presence of SAA in the system is expected to increase the film drainage time and hence, affect the value of  $\lambda$ . To differentiate between coalescence efficiency in pure and contaminated systems, the coalescence efficiency in contaminated systems is designated as the effective coalescence efficiency,  $\lambda_{\text{Eff}}$ , expressed as

$$\lambda_{\text{Eff}} = \lambda * \text{correction factor} = e^{-tc/ti} e^{-X} \quad (5-32)$$

An exponential form, similar to that used to describe the effect of hydrodynamic parameters, was used to express the role of the interfacial characteristics in retarding bubble coalescence in order to keep the physical model consistent (i.e. that the coalescence efficiency is controlled by the ratio of the bubble contact time relative to the film drainage time).

This concept is similar to that used by Sagert et al. (1976) to account for the effect of stretching and collapsing on the film thinning time encountered as the foam drains. The first characteristic time,  $t_c/t_i$ , accounts for the effect of hydrodynamic factors (such as local energy dissipation, bubble diameter, and continuous fluid density) as well as for the effect of the static surface tension, on coalescence efficiency. These can be calculated using the Eq. 5-20 and 5-22. The second characteristic time,  $X$ , accounts for the coalescence retardation that takes place due to the additional interfacial forces generated due to the presence of SAA. By using the parameter  $X$  it may be possible to extend the usage of the expression obtain for pure systems to include industrial streams that exhibit complex interfacial characteristics.

Bubble coalescence rate can thus be expressed as,

$$-\frac{\partial n}{\partial t} = c_1 \lambda_{Eff}^{c_2} \Phi^{c_3} \varepsilon^{c_4} d^{c_5} = c_1 (e^{-t_c/t_i})^{c_2} (e^{-X})^{c_3} \Phi^{c_4} \varepsilon^{c_5} d^{c_6} \quad (5-33)$$

where  $c1-c6$  are empirical constants.

As demonstrated in Chapter 6, the non-dimensional interfacial characteristics can successfully be applied to describe the effect of SAA on the performance of the dynamic sparger, i.e. bubble dispersion, and may well be suitable for use to characterize the effect of the interfacial characteristics on bubble coalescence. Moreover, allow for the retention of the non-dimensional nature of the coalescence efficiency. The interfacial parameters  $C_0/C_{CMC}$ ,  $\Pi/\sigma_{water}$ ,  $F_G/\Gamma_{max}$ ,  $F_L/\Gamma_{max}$ , were selected to stand for  $X$  in Eq. (5-32) in order to assess the effect of SAA on bubble coalescence rate.

The 677 experimental data points (water and aqueous SDS solutions) were analyzed using the stepwise linear regression program of the SAS software package (Cody, et al., 1997). The following regression expressions were obtained,

$$-\frac{dn}{dt} = 0.50\Phi_p^{1.0}\varepsilon_p^{1.5}d^{-2.7}e^{-\left(0.79\frac{t_c}{t_i}+20\frac{C_0}{C_{CMC}}\right)} \quad (R^2 = 0.88) \quad (5-34)$$

$$-\frac{dn}{dt} = 0.56\Phi_p^{1.0}\varepsilon_p^{1.5}d^{-2.7}e^{-\left(0.73\frac{t_c}{t_i}+0.39\frac{\Pi}{\sigma_{Sta}}\right)} \quad (R^2 = 0.87) \quad (5-35)$$

$$-\frac{dn}{dt} = 0.54\Phi_p^{1.0}\varepsilon_p^{1.5}d^{-2.7}e^{-\left(0.69\frac{t_c}{t_i}+0.34\frac{\Gamma_G}{\Gamma_{Max}}\right)} \quad (R^2 = 0.87) \quad (5-36)$$

$$-\frac{dn}{dt} = 0.46\Phi_p^{1.0}\varepsilon_p^{1.5}d^{-2.7}e^{-\left(0.68\frac{t_c}{t_i}+1.82\frac{\Gamma_L}{\Gamma_{Max}}\right)} \quad (R^2 = 0.89) \quad (5-37)$$

All four regression expressions were found to a yield satisfactory fit ( $R^2 \geq 0.87$ ) for bubble coalescence data obtained over a wide range of experimental conditions (surfactant concentration of 0 - 50 ppm,  $0.008 < \Phi_G < 0.5$ ,  $4 < \varepsilon_p < 26$  w/kg,  $30 \mu\text{m} < d_{32} < 11,000 \mu\text{m}$ . This must be considered to be a very good fit considering that the bubble coalescence rates fitted by this correlation vary by five orders of magnitudes (Fig.3.19).

Because of the fact that the value of all 4 correlation coefficients were close to each other, it was not possible to discriminate amongst the four correlations and identify the most suitable interfacial characteristic. Although the interfacial concentration and surface activity of SDS solutions are not linearly proportional to its bulk concentration, this parameter is the simplest one to use. It was rendered dimensionless by dividing it by a convenient concentration that is often used as an indicator of saturation, namely the critical micelle concentration,  $C_{CMC}$ . The static surface tension is often used to predict/correlate the effect of variation in interfacial characteristics; however, it is well known that the characteristic coalescence time is of the order of milliseconds whereas it takes much more than 3 s in order for SDS to approach its equilibrium value (Fig. 4.5).

This thermodynamic parameter can be accounted for as a dimensionless ratio  $[(\sigma_{\text{Water}} - \sigma_{\text{Static}}) / \sigma_{\text{Water}} = \Pi / \sigma_{\text{Water}}]$ .

Since it is easy to measure and identify the values of the static parameters  $C_0/C_{\text{CMC}}$  and  $\Pi/\sigma_{\text{water}}$ , it is recommended that the correlations similar to those given by Eq. 5-33, 5-34 or 5-35 be used to predict the effect of SAA on bubble coalescence. This recommendation is based on purely statistical grounds since the use of  $C_0/C_{\text{CMC}}$ ,  $\Pi/\sigma_{\text{water}}$ , or  $\Gamma_G/\Gamma_{\text{max}}$ , does not take into account the fact that all these parameters are derived from equilibrium measurements and do not reflect the interfacial conditions taking place at the rapidly changing gas/liquid interface. The situations could be significantly different when the contaminants are more complex and significant interfacial viscoelasticity is encountered.

The dynamic interfacial characteristics of the system provide a good indication of the rate at which SAA material diffuses to and adsorbs on the interface. This is expected to play an important role in determining the coalescence rate of bubbles (Xue, 1999). Unfortunately, the dynamic surface time varies with the surface age and it is not possible to use a single value to characterize the interface unless the characteristic coalescence time is well known. Under the experimental conditions investigated, the latter was calculated to range from 0.2 ms to 36 ms. Attempts were therefore undertaken to calculate the effective diffusivity and diffusivity of SDS in aqueous solutions. However, as shown in Chapter 4, the diffusivity of SDS was not found to be sensitive to the variations in the bulk concentrations of SDS investigated ( $D = 8.42 \times 10^{-10} \text{ m}^2/\text{s}$ ). It can thus not be used as an indicator of the variation of interfacial characteristics with concentration.

The dynamic surface excess based on the long-term approximation,  $\Gamma_L$ , has been proposed to express the effect of interfacial characteristics on the bubble coalescence rates. As stated in Chapter 4 and Chapter 6,  $\Gamma_L$  is a better indicator to represent the interfacial characteristics in dynamic bubble breakage and coalescence. This is due to its ability to account for the diffusivity of the surface active species, gradient of the dynamic surface tension as well as for the bulk concentration of that species given in Eq. (4-20).

This advantage will emerge when comparing effects for different type of SAAs as will be discussed afterwards.

As stated in Chapter 2, available models could not be applied to either turbulent systems or impure systems. It is therefore interesting to note that, as shown in Fig. 5.19, the proposed model (Eq. 5-36) can correlate data that cover a very wide range of experimental conditions (64-fold increase in gas holdup, 6-fold variation in local energy dissipation rate, and 420-fold jump in bubble diameter). The ability of this parameter to account for the effect of interfacial characteristics is in line with its ability to correlate the sparger performance obtained using SDS solutions (Eq. 6-16 and 6-20).

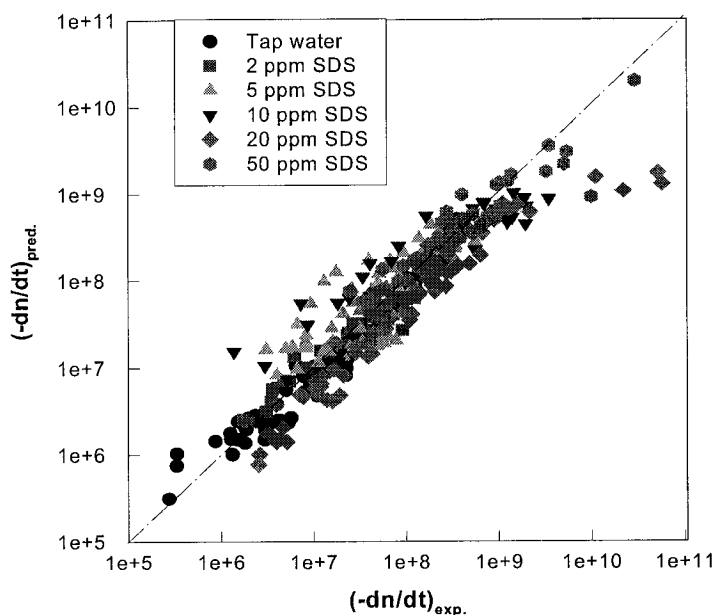


Fig. 5.19 Comparison of bubble coalescence rate between experiment and model by Eq.(5-37)

Correlations describing the coalescence rate expressed as the rate of the interfacial area decrease, and the rate of bubble size growth, can be derived from the above mentioned population density correlation by using Eq. (5-7) and Eq. (5-8).



There are very few investigations of the effect of different SAA systems on bubble coalescence rate under turbulent fluid flow conditions. The closest case is the experimental research conducted by Prince and Blanch (1990) in which they determined bubble coalescence rates in bubble columns filled with  $\text{Na}_2\text{SO}_3$  or  $\text{NaCl}$  aqueous solutions. Their results, expressed as bubble coalescence rates, (that is coalescing event per bubble per second,  $-(1/n) \cdot (dn/dt)$ ), are plotted in Fig. 5.20 along with the SDS data generated in this investigation. In all cases, the bubble coalescence rates were found to decrease as the bulk concentrations of the solutions increase.

As indicated by both experimental results and modeling prediction (Eq.5-30 and 5-33 to 5-36) results, small bubble and intensified hydrodynamics will lead to high coalescence rate, therefore 1 mm bubbles in pipe flow for SDS aqueous solution are supposed to exhibit higher coalescence rates than that of 3.8 mm bubbles in a bubble column filled with  $\text{Na}_2\text{SO}_3$  or  $\text{NaCl}$ . However, the coalescence retardation effectiveness of the various agents was found to change this fashion significantly. Thus, for example, the presence of 0.1 mM SDS can reduce bubble coalescence rate from around 0.8 1/s for water system down to 0.4 events per bubble per second whereas 4 mM  $\text{Na}_2\text{SO}_3$  or 90 mM  $\text{NaCl}$  are needed in order to accomplish the same effect. In another words, with the same SAA concentration, the bubble coalescence rate for SDS will be remarkably lower than that of either  $\text{Na}_2\text{SO}_4$  or  $\text{NaCl}$  system. This vast concentration difference (up to 900-fold) can be partially explained by the above-mentioned concepts since the diffusivity of  $\text{NaCl}$  is significantly larger than  $\text{Na}_2\text{SO}_4$  or SDS ( $15.5 \times 10^{-10} \text{ m}^2/\text{s}$  vs.  $11.4 \times 10^{-10} \text{ m}^2/\text{s}$  for  $\text{NaCl}$  and  $8.425 \times 10^{-10}$  for SDS). On the other hand, as shown in Fig. 4.9 of Chapter 4, the slopes of the dynamic surface tension vs.  $t^{-1/2}$  for high concentration of SDS solutions are generally larger than those of low concentrations, which implies that the surface tension gradients,  $d\sigma/dt^{-1/2}$ , are large at high SDS concentration that will require more time to overcome the resistance to film thinning. This is another reason why bubbles in higher concentrated solution coalesce slowly.

Although other interfacial parameters such as the bulk concentration, the static surface tension, the surface pressure and the Gibbs surface excess can well describe the coalescence rate as long as the coalescence efficiency is expressed in exponential format

of interfacial parameters, the physical meaning of the surface excess based on the long-term approximation,  $\Gamma_L$ , is projected to be of wider applicability since two dynamic factors,  $D$  and  $d\sigma/dt^{-1/2}$ , are taken into accounts in calculating the value of  $\Gamma_L$  (as shown in Eq. 4-20).

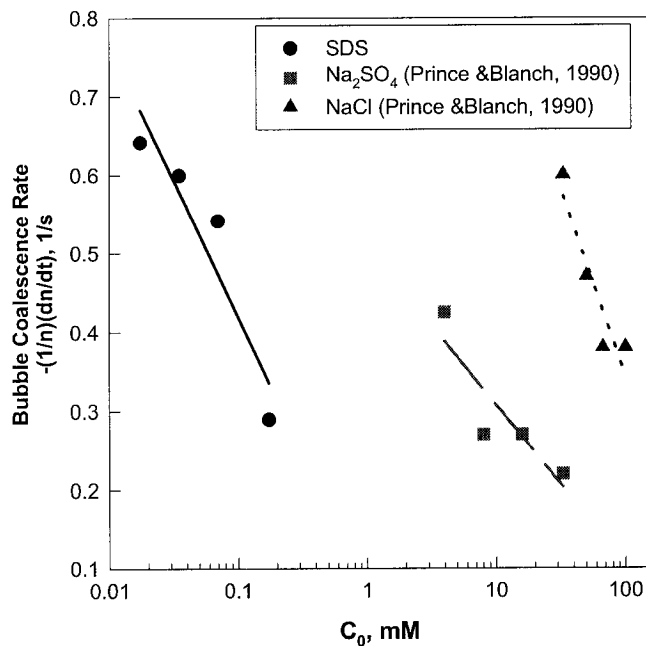


Fig. 5.19 Comparison of bubble coalescence rate among three surface active agents (For SDS: 1 mm bubble in pipeline flow,  $U_{LS}=1$  m/s; for Na<sub>2</sub>SO<sub>4</sub> and NaCl: 3.8 mm bubble in bubble column,  $U_{GS}=0.05$  m/s)

Larger values of either  $D$  or  $d\sigma/dt^{-1/2}$  yields larger  $\Gamma_L$  values which, in turn, predicts the generation of smaller bubble coalescence rate (Eq.5-36). One also realize that  $\Gamma_L$  includes not only  $D$  and  $d\sigma/dt^{-1/2}$  but also the bulk concentration  $C_0$ . The other advantage of using  $\Gamma_L$  is that at the same bulk concentration, different SAAs exhibiting different surface activities (expressed by  $D$  and  $d\sigma/dt^{-1/2}$ ) will explain how coalescence rate is hindered.

The exponents for the hydrodynamic factors (such as,  $\Phi_p$ ,  $\varepsilon_p$ ,  $d$ ) obtained in those four correlations (Eq. 5-33, 5-34, 5-35, 5-36) and in the water system (Eq.5-30) are similar; which implies that the effects of hydrodynamic factors are well defined in both systems.

However, they are a little different from those predicted by the theoretical model (Eq. 5-17). This is most probably caused by the inherent assumptions in the model of a monodisperse bubble size distribution, and the use of the experimentally determined Sauter mean diameter as a representative of this characteristic diameter.

Although the experiments were carefully designed in order to maintain the dominance of the bubble coalescence mechanism, the difficulties encountered in clearly identifying the interfacial characteristic controlling coalescence rate can be attributed to the dominance of the hydrodynamic factors (bubble diameters, energy dissipation rates, gas holdup) and the fact that the SDS system investigated yields little interfacial viscosities. The interference of electrical charge, stemming from the use of a cationic SAA, could also have had an effect that is not accounted for in the present analysis. It is therefore suggested that further investigations be undertaken using a wide range of surface active materials (such as alcohols, organic acids, non-ionic and ionic SAA) and broad concentrations in order to delineate this issue.

### 5.3. Conclusions

1. A comprehensive experimental investigation of bubble coalescence rate in turbulent pipe flow was undertaken using a broad range of experimental conditions (i.e.  $0.008 < \Phi_G < 0.5$ ,  $4 < \varepsilon_p < 26$ ,  $25 \mu\text{m} < d_{32} < 8,700 \mu\text{m}$ , and SDS concentration range 0 - 50 ppm).
2. Factors affecting bubble coalescence can be categorized into two groups, one pertains to hydrodynamics conditions (gas hold-up, energy dissipation rate, and bubble size) while the other deals with interfacial properties. The effect of all these factors on bubble coalescence was thoroughly explored. The bubble coalescence rate was found to increase as the gas hold-up and the energy dissipation rate increase, and decrease as the bubble size and the SAA concentration increase.
3. Different forms to express the bubble coalescence rate are summarized and their relationships are revealed.

4. Compared to tap water, the relative coalescence rates were found to decrease radically by the presence of a minute dosage of SAA. For example, the relative bubble coalescence rate could be 1-orderly diminished by addition of 5 ppm SDS.
5. A better understanding of the role interfacial characteristics plays in retarding bubble coalescence rate in gas/liquid turbulent flow was developed. The exponential format of interfacial parameters can prevail to characterize effect on bubble coalescence processes, which implies that the interfacial characteristics affect the bubble coalescence through influencing collision efficiency. Different interfacial parameters such as the static surface tension, surface pressure, Gibbs surface excess and surface excess based on long-term approximation are evaluated in regard to explain how SAA retards the bubble coalescence rate, and the last parameter might be better to serve the job.
6. A theoretical model for particle coalescence rate is simplified and adapted to current bubble coalescence rate in turbulent flow. It is not only applied to pure water system but also to impure industrial streams displayed surface activity. The equation obtained is in a good agreement with the experimental results.
7. Under the similar operating conditions, 0.1 mM SDS can prevent bubble coalescence to the same degree as either 4 mM  $\text{Na}_2\text{SO}_3$  or 90 mM NaCl solutions. It suggests that a proper selection of SAA would exceedingly cut additive consumption without impairing the gas-liquid contacting.

## CHAPTER 6 BUBBLE DISPERSION AND PERFORMANCE OF A NOVEL DYNAMIC SPARGER

### 6.1 Introduction

Gas-liquid contacting plays an important role in a multitude of environmentally related operations such as: absorption of impurities, stripping of residual volatiles from aqueous streams, air oxidation of water soluble components, supply of oxygen requirements in biological wastewater treatment, wastewater remediation by oxidation/ozonation, and the removal of suspended fine particles and insoluble oils by selective flotation of constituents (Grosz-Roll, 1972; Zlokarnik, 1985; Mikekiilineni and Kinickle 1985, Mutsakis, et al.,1989; Rader, et al.1989, Xu and Finch 1989, Shaw et al., 1994; Al Taweel et al. 1995).

Spargers are commonly used as means for dispersing the gas into bubbles in order to enhance contact between the phases. Unfortunately, most conventional sparger types generate relatively large bubbles that generate low interfacial area of contact between the phases. Gas dispersion is, therefore, often promoted through the introduction of additional mechanical energy that is used to further disperse the gas into smaller bubbles as well as to mix the liquids phase present in the contactor. Unfortunately, this approach is energy inefficient, in so far as bubble dispersion is concerned and its use results in the development of a broad residence-time-distribution and the consequent reduction in the mass transfer driving force (factors that reduce the overall effectiveness of the operation). On the other hand, the use of dynamic spargers in combination with pipeline processing can be quite advantageous because of their ability to achieve very high interfacial area of contact and maintain plug flow conditions. Furthermore, the latter approach provides the ability to optimize energy input according to process needs and generates very narrow residence time distributions.

Spargers are usually classified into two general categories, namely static and dynamic spargers. The former sparger type relies on buoyancy and/or shear forces to form bubbles and includes devices such as perforated plates and tubes, porous/sintered

distributors, slotted rubber sleeves. On the other hand, the dynamic spargers rely on the kinetic energy present in the liquid stream to breakup the gas phase into small entities. This group includes devices such as two-phase ejectors, and static mixers. Their use offers the following advantage (Kastánek et al. 1993; Chen and Al Taweel, 1994; Lee and Tsui, 1999):

- The ability to generate very high interfacial area of contact in the mixing zone results in accelerating mass-transfer and chemical reaction rates. This process intensification results in significant reduction in the mixer volume requirements,
- The ability to handle large throughputs in an energy-efficient manner,
- The absence of moving parts results in low maintenance requirements,
- Relatively low capital costs,
- Low axial dispersion, a factor that plays a major role as the equilibrium conditions are approached,
- Narrow residence time distributions, this is an important factor that facilitates the control of product quality and enhances selectivity in case of competing reactions and/or absorption,
- Some designs have the ability to control bubble sizes in response to variation in process requirements.

In the case of single-phase pipe spargers, the dominant breakage mechanism responsible for the formation of bubbles is the breakage of the gas jet formed at the tip of the sparger. The size of bubbles generated by this type of sparger is thus controlled by the kinetic energy of the gas jet relative to that of the surrounding liquid (which is controlled by gas flow rate and the diameter of the pipe sparger) and the surface tension of the system. On the other hand, the mechanism responsible for the formation of bubbles in two-phase spargers is the turbulent breakup taking place as the two-phase system passes through regions of high energy dissipation rates.

When a gas-liquid mixture is exposed to the action of turbulence, a dynamic equilibrium between bubble dispersion and coalescence processes takes place. Under the continuous flow conditions encountered in static mixing operations, small bubbles are formed in regions of high turbulence intensities but tend to coalesce as they migrate into regions of where energy dissipation rates are lower. The maximum stable bubble size in a turbulently flowing liquid was analyzed by Levich (1962); Prince and Blanch (1990) and Hesketh et al.(1991), and is given by Eq. (2-7) and Table 2.1.

This relationship demonstrates that the maximum bubble diameter decreases as the gas density  $\rho_G$ , liquid density  $\rho_L$ , or local energy dissipation rate are increased. However, the maximum bubble size will be larger at higher surface tensions. The above equation provides only a simple guideline about what the maximum stable bubble size in a flowing gas/liquid system because breakage efficiency (which is a function of the residence time in the hydrodynamic region responsible for breakup) is not taken into consideration. Better understanding of the mechanisms responsible for bubble generation is, therefore, needed in order to optimize the sparger performance. This was addressed in the experimental program discussed in Chapter 3, and the subsequent analysis of the results undertaken in this section.

## 6.2 Results and Discussions

The criterion by which the sparger's performance is to be evaluated depends on the nature of the environmental treatment process considered. In the case of operations controlled by mass transfer between the phases (e.g. ozonation, oxygen transfer, stripping of residual volatiles) the objective is to enhance the gas/liquid interfacial area of contact. On the other hand, in the case where spargers are to be used for the removal of suspended particles and oil droplets by flotation, the performance of the separation process is strongly influenced by the size of the bubbles formed as well as by their number density. Hence, the gas/liquid contacting performance of the sparger was evaluated on the basis of its ability to generate:

- small bubble sizes,  $a$ ,
- high bubble population density,  $n$ , and,

- large specific interfacial area of contact,  $a$ .

The three parameters  $a$ ,  $d_{32}$ , and  $n$  are not independent but are interrelated by Eq. (3-1), Eq. (3-2) and,

$$n = \frac{a}{\pi d_{32}^2} \quad (6-1)$$

All of these parameters were found to be strongly affected by several factors such as: the gas to liquid volumetric flow ratio in the sparger, gas to liquid volumetric flow ratio in the pipeline, pressure drop across the sparger and the interfacial characteristics of the system being treated.

### 6.2.1 Effect of Gas Holdup

The effect of the gas to liquid volumetric flow ratio in the pipeline (termed as  $Q_G/Q_L$  or  $U_G/U_L$  or gas holdup,  $\Phi_G$ ) on the interfacial area of contact, bubble size, and bubble population density is shown in Fig. 6.1a, b, and c for the air/aqueous MIBC system. The size of the bubbles generated at low G/L ratio values was found to be very small (less than 200  $\mu\text{m}$  at a pressure drop of 30 psi) at very low gas holdups but increased with increasing G/L ratios (Fig. 6.1b). The influence of gas holdup on the Sauter mean bubble diameter was pronounced in the case of pure water and decreases as the coalescence tendency of the system decreased (i.e. at higher additive concentration). This is caused by the small bubbles formed at the high energy dissipation rates encountered within the sparger tending to coalesce into larger entities under the lower energy dissipation rates encountered in the pipe flow region, a phenomenon which is promoted at larger gas holdups. The dramatic reduction bubble population density (Fig. 6.1c) is caused by the same mechanism. The combined effect of these factors results in the formation of a smaller number of large bubbles at higher gas to liquid ratios. As can be seen from Fig. 6.1a, this results in a net increase in the interfacial area of contact between the phases, a tendency which levels off (or is slightly reversed) at very high G/L ratios.



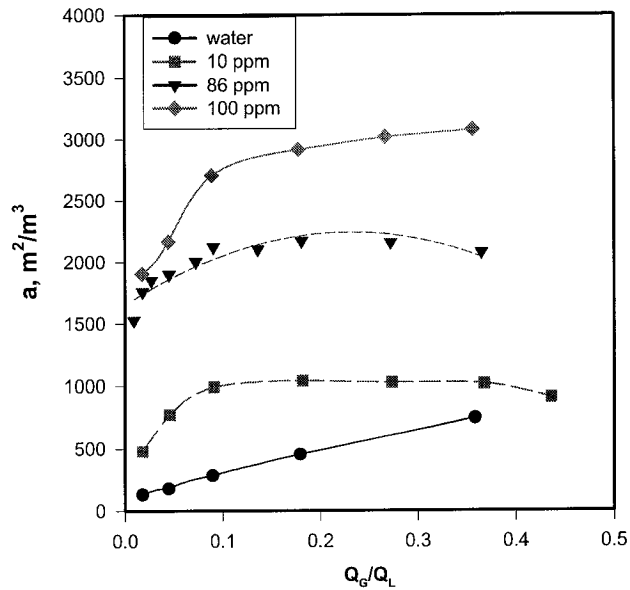


Fig. 6.1a Effect of gas-to-liquid volumetric flow ratio on performance of two-phase dynamic sparger in MIBC solutions ( $U_L = 1.4 \text{ m/s}$ ,  $\Delta p_{\text{Sparger}} = 30 \text{ ps}$ ) : interfacial area

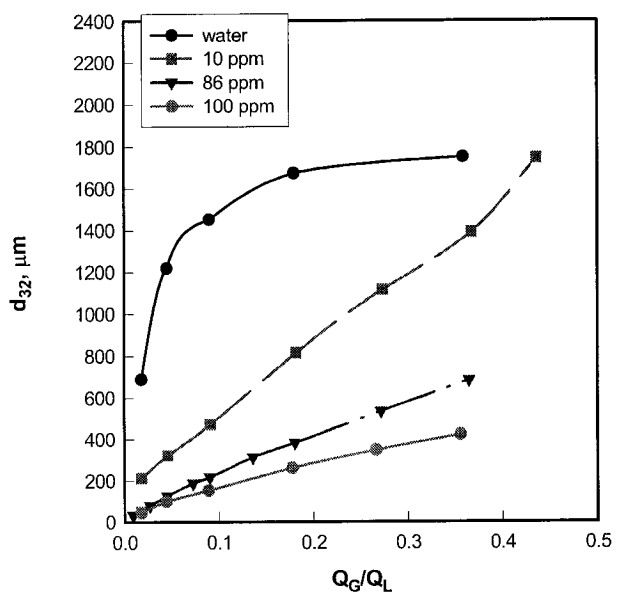


Fig. 6.1b Effect of gas-to-liquid volumetric flow ratio on performance of two-phase dynamic sparger in MIBC solutions ( $U_L = 1.4 \text{ m/s}$ ,  $\Delta p_{\text{Sparger}} = 30 \text{ psi}$ ) : bubble size

The point at which increasing gas holdup can detrimentally affect the sparger's performance is very dependent on the performance criterion considered (i.e.  $d_{32}$ ,  $n$ , or  $a$ ) as well as on the pressure drop across the sparger, and the coalescence tendencies of the system. For example, the bubble size and bubble number density are always adversely affected, i.e. decreased by increasing the value of G/L ratio whereas the interfacial area increases as the G/L ratio increase. Therefore optimum gas holdups were identified at values  $0.1 < Q_G/Q_L < 0.3$  depending on the above mentioned parameters. This is attributed to the bubbles being more likely to collide and coalesce to form larger bubbles at higher gas holdups.

Bubble population densities as high as 500 bubbles/mm<sup>3</sup> were obtained at very small gas-to-liquid flow ratios (0.02) and large pressure drops (50 psi). This population density, and the size of the bubbles formed (down to 30  $\mu\text{m}$ ), compares favorably with those obtained using conventional dissolved air flotation (DAF) systems. However, the use of two-phase dynamic spargers can greatly simplify the process and provide the ability of varying the size of the bubbles according to process needs. The dynamic sparger may therefore be advantageously used to overcome the bubble generation problems encountered in many DAF systems and to provide a degree of control that allows the generation of optimal bubble sizes. These are needed when the suspended particles require the production of bubbles larger than 30  $\mu\text{m}$  in order to provide adequate buoyancy forces for the particle-bubble complex (e.g. in the treatment of oily water).

The results obtained using SDS system (see Fig. 6.2a, b and c, ) show similar trends to those obtained using the MIBC system. At a constant local energy dissipation rate in the throat,  $\epsilon_{\text{Th}}$ , a larger number of bubbles is generated. However, these bubbles tend to coalesce as they move to the regions of lower energy dissipation rates prevalent in the divergent section of the sparger as well as in the 0.47 m section of the pipeline where the two-phase jet mixes with the main flow in the pipe. Consequently, the net effect is strongly affected by the coalescence tendencies prevalent in the system as well as how

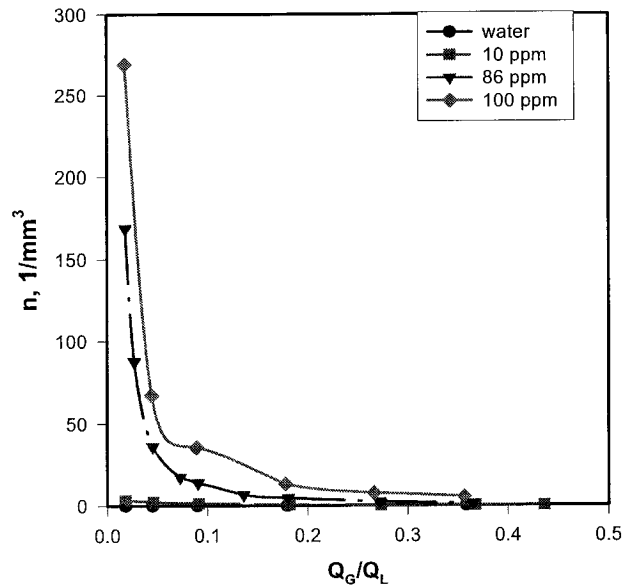


Fig. 6.1c Effect of gas-to-liquid volumetric flow ratio on performance of two-phase dynamic sparger in MIBC solutions ( $U_L = 1.4 \text{ m/s}$ ,  $\Delta p_{\text{Sparger}} = 30 \text{ psi}$ ) : bubble population density

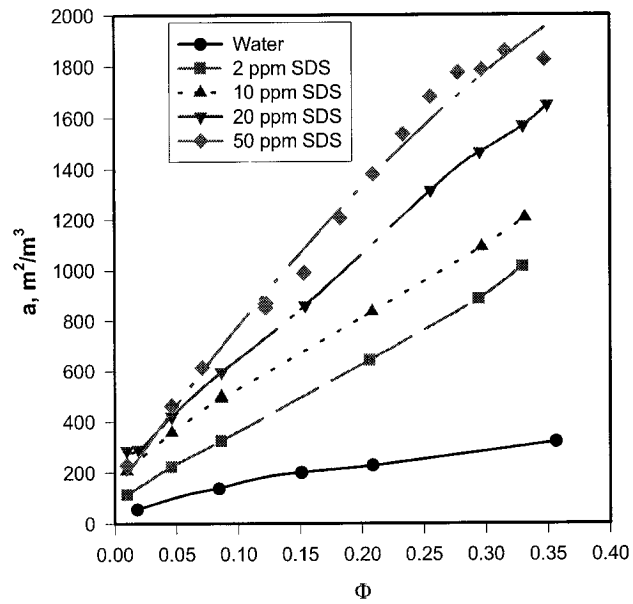


Fig. 6.2a Effect of gas holdup on performance of two-phase dynamic sparger with various concentrations of SDS solution ( $U_L = 1.1 \text{ m/s}$ ,  $U_{LS} = 0.1 \text{ m/s}$ ) : interfacial area

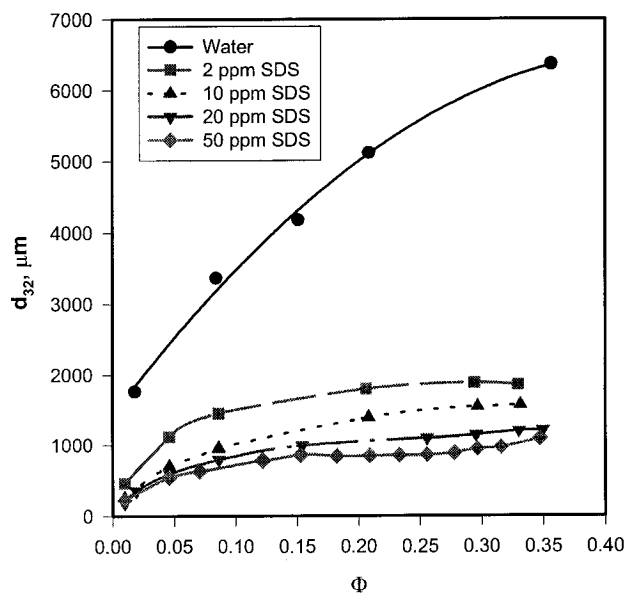


Fig. 6.2b Effect of gas holdup on performance of two-phase dynamic sparger with various concentrations of SDS solution ( $U_L = 1.1$  m/s,  $U_{LS} = 0.1$  m/s) : bubble size

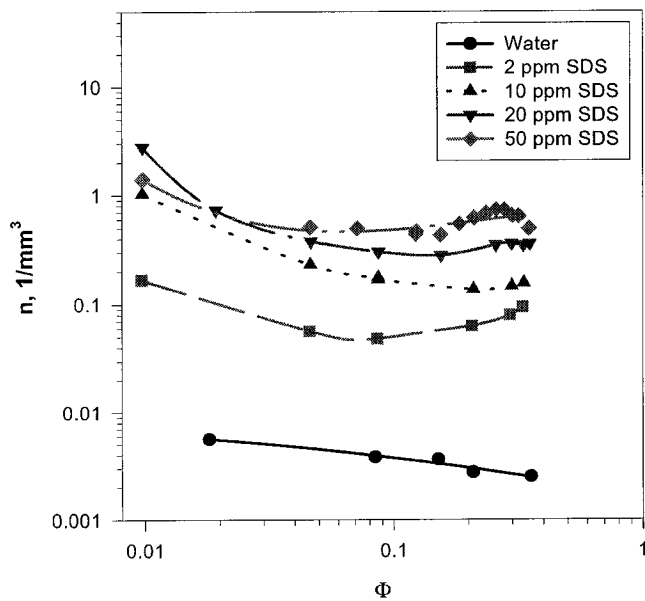


Fig. 6.2c Effect of gas holdup on performance of two-phase dynamic sparger with various concentrations of SDS solution ( $U_L = 1.1$  m/s,  $U_{LS} = 0.1$  m/s) : bubble population density

strongly the monitored parameter is affected by increasing coalescence rates. For example, as can be seen from Fig. 6.2a, b and c, the specific interfacial area and the Sauter mean bubble diameter were found to increase with increasing gas holdup whereas the bubble population density was found to decrease with increasing gas holdup. The slight increase in bubble population densities observed at relatively high SDS concentrations is most probably caused by the formation of smaller bubble diameters at larger gas holdups (due to a slight increase in the value of  $\epsilon_{Thr}$  which is based on the water content in the two-phase stream).

As can be seen from Fig. 6.1 (a, b and c) and 6.2 (a, b and c), the results obtained using the rapidly-coalescing system air/tap water are significantly different from those obtained in slowly-coalescent systems. This points out the importance of taking into consideration the effect of interfacial characteristics in gas dispersion. This is in agreement with the findings of Al Taweel and Cheng (1997).

The importance of the liquid flow rate within the dynamic sparger,  $U_{LS}$ , can best be visualized by considering the overwhelming difference in bubble dispersion performance depicted in Fig.6.3. Under the conditions shown in Fig.6.3-I, the sparger behaves as a static sparger in which bubble dispersion takes place extraneously. On the other hand, bubble dispersion takes place inclusively within the sparger under the conditions shown in Fig.6.3-II.

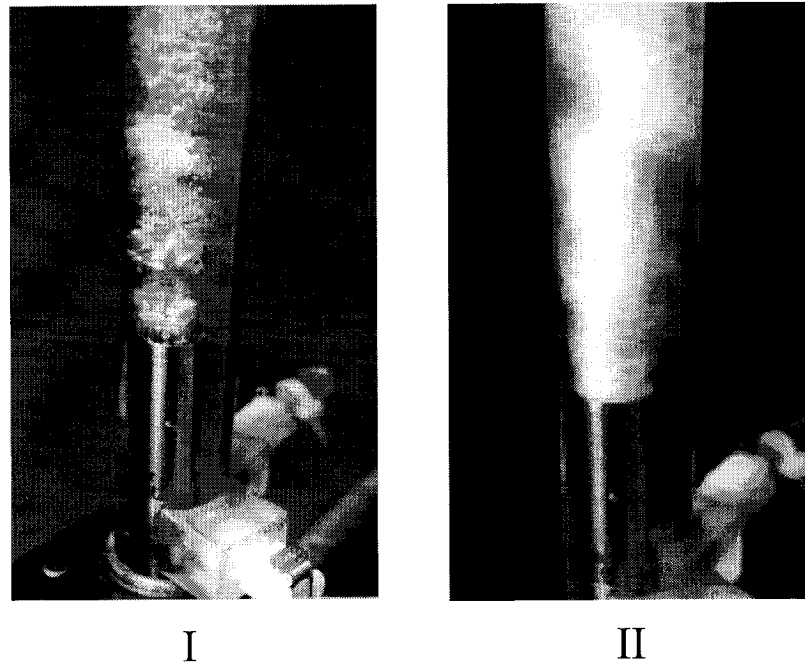


Fig. 6.3 Performance comparison between static and dynamic spargers ( $U_L = 1$  m/s,  
 $Q_G/Q_L = 0.3$ , 20 ppm MIBC)

I: Bubble produced by static sparger:  $d_{32} = 2,000$   $\mu\text{m}$

II: Bubble produced by dynamic sparger:  $d_{32} = 300$   $\mu\text{m}$

### 6.2.2 Effect of Local Energy Dissipation Rate in Sparger

As discussed in Chapter 3, the local energy dissipation rate in the sparger,  $\epsilon_s$  is directly related to the pressure drop across the sparger,  $\Delta P_s$ , as shown in Eq. (3-11), and it increases with increasing  $\Delta P_s$ . For a given gas-to-liquid flow ratio, an increase in  $\Delta P_s$ , or  $\epsilon_s$ , yields smaller bubbles, larger bubble population densities and bigger interfacial area of contact. This was found to be the case when the pressure drop across the sparger is increased from 15 psi to higher values (Fig. 6.4 a, b, c and Fig. 6.5 a, b, c). This finding is in agreement with the observation of Lee, et al. (1987) and Hesketh, et al. (1991b).

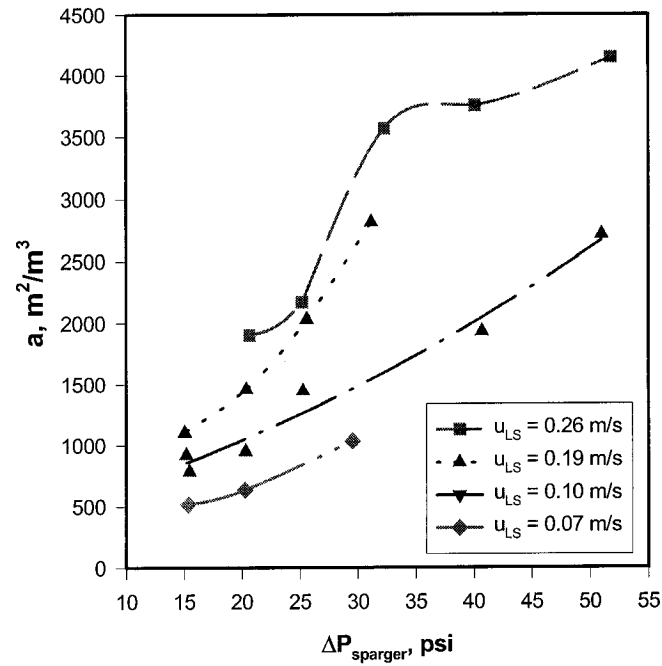


Fig. 6.4a Effect of pressure drop on performance of two-phase dynamic sparger ( $U_L = 1.1$  m/s,  $\Phi_G = 0.27$ , 20 ppm MIBC) : interfacial area

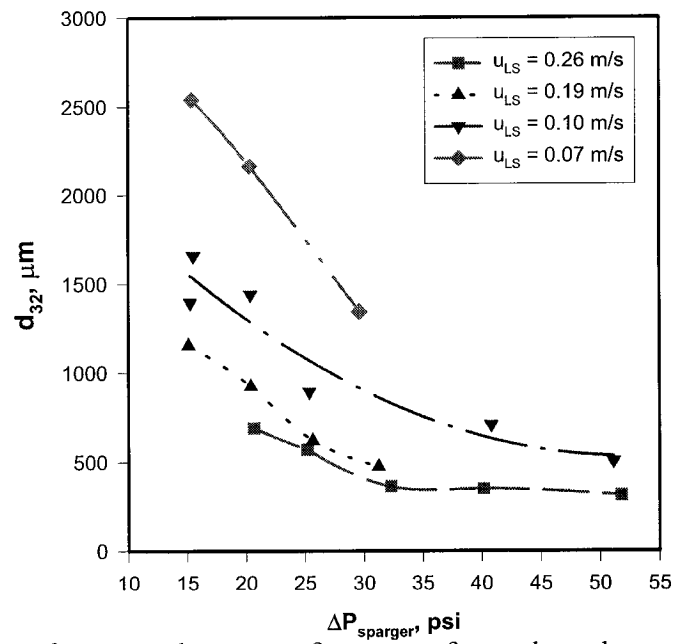


Fig. 6.4b Effect of pressure drop on performance of two-phase dynamic sparger ( $U_L = 1.1$  m/s,  $\Phi_G = 0.27$ , 20 ppm MIBC) : bubble size

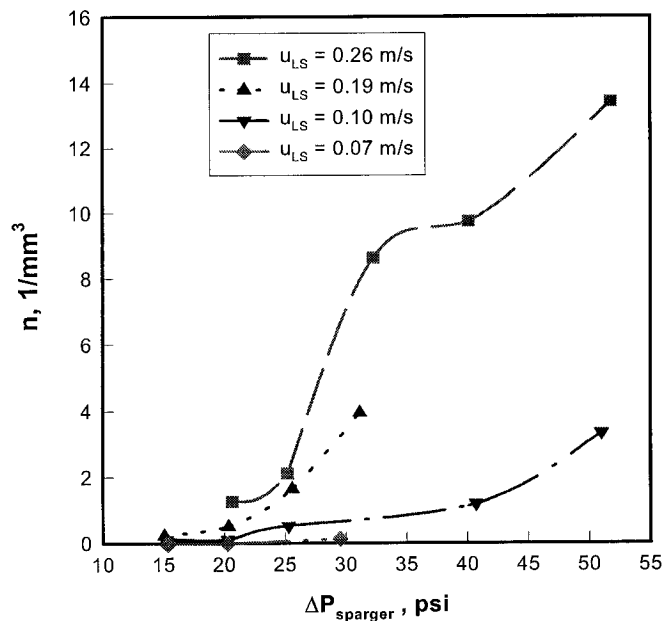


Fig. 6.4c Effect of pressure drop on performance of two-phase dynamic sparger ( $U_L = 1.1$  m/s,  $\Phi_G = 0.27$ , 20 ppm MIBC ) : bubble population density

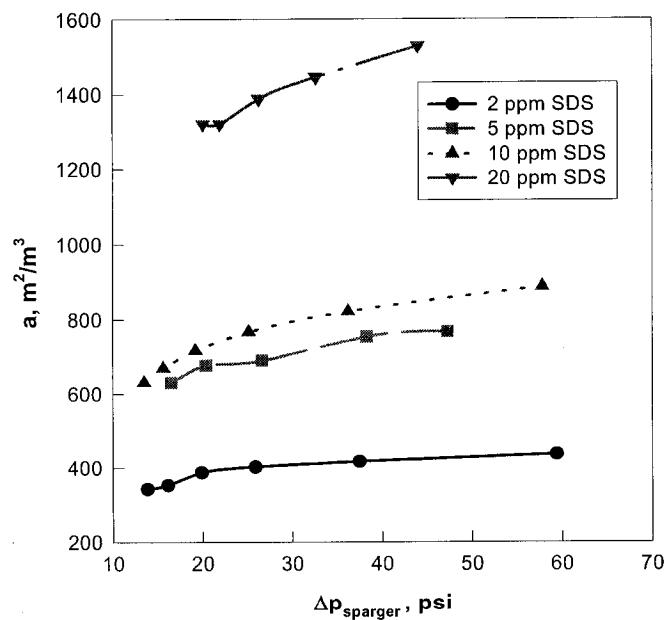


Fig.6.5a Effect of pressure drop on performance of two-phase dynamic sparger in various concentrations of SDS solution ( $U_L = 1.2$  m/s,  $U_{LS} = 0.2$  m/s,  $\Phi_G = 0.08$ ) :interfacial area



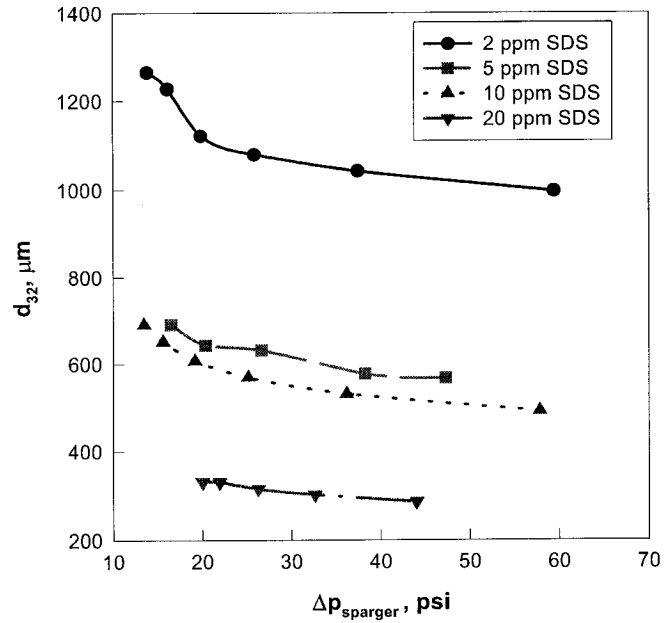


Fig.6.5b Effect of pressure drop on performance of two-phase dynamic sparger in various concentrations of SDS solution ( $U_L = 1.2$  m/s,  $U_{LS} = 0.2$  m/s,  $\Phi_G = 0.08$ )  
:bubble size

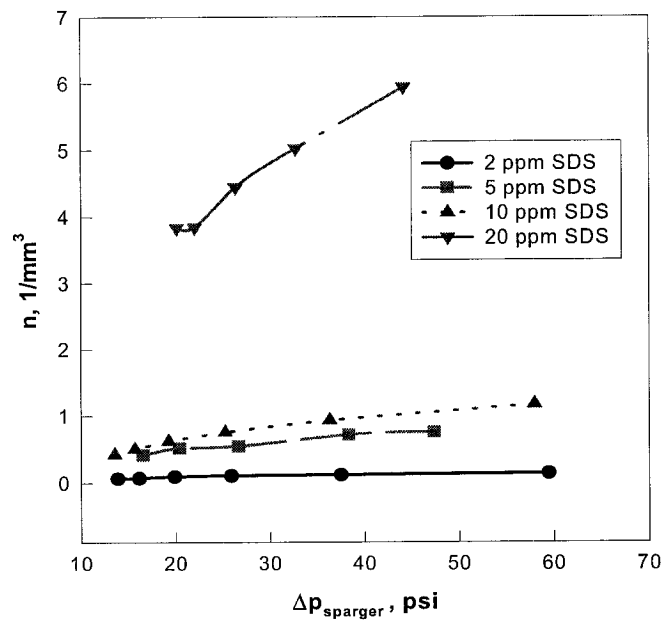


Fig.6.5c Effect of pressure drop on performance of two-phase dynamic sparger in various concentrations of SDS solution ( $U_L = 1.2$  m/s,  $U_{LS} = 0.2$  m/s,  $\Phi_G = 0.08$ )  
: bubble population density

The effect of pressure drop on bubble dispersion is most pronounced at higher  $U_{LS}$  values and has very limited effect on the bubble population densities at low sparger liquid flow rates (Fig. 6.4c). This is mainly caused by the tendency of the fine bubbles formed in the region of maximum energy dissipation to re-coalesce within the sparger as a result of increasing gas holdup encountered at lower  $U_{LS}$  values. For example, the gas holdup within the sparger could reach values as high as  $\Phi = 0.8$  under the lowest sparger liquid flow rates ( $U_{LS} = 0.07$  m/s), whereas it is about  $\Phi = 0.55$  when the sparger liquid velocity is increased up to  $U_{LS} = 0.26$  m/s. Consequently, coalescence of the microbubbles formed in the region of maximum energy dissipation is expected to be much smaller in the second case. Naturally, this effect is expected to be less pronounced the lower is the coalescence tendency of the system.

In order to understand the effect of the energy dissipation on gas liquid contacting properly it is necessary to consider the spatial variation within the contactor, particularly in industrially-relevant systems where coalescence tendencies can be significantly impacted (Al Taweel et al. 1991; Al Taweel and Cheng, 1995). The hydrodynamic conditions encountered within the sparger and those prevalent in the pipeline are quite different. Most of the energy dissipation in the present system is focused within the sparger (thereby resulting in very high  $\epsilon$  values) whereas the multi-phase flow in the pipeline encounters relatively little energy losses. The counteracting processes of bubble dispersion and coalescence (shown in Fig. 6.6) exist throughout the whole gas/liquid contacting system but are shifted in one direction or the other depending on the local value of  $\epsilon$  in the two regions. The bubbles will break up when they move into a higher  $\epsilon$  region; otherwise they tend to coalesce in a lower  $\epsilon$  region.

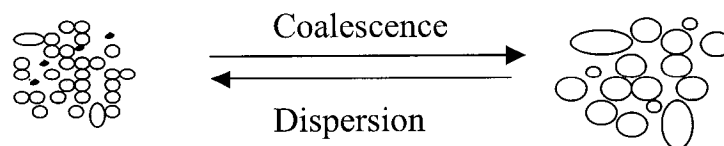


Fig. 6.6 Dynamic equilibrium between bubble dispersion and coalescence processes.

The results obtained suggest that in situations where the coalescence rate is slightly retarded by the presence of impurities (i.e. relatively high concentrations of MIBC and SDS), focusing of energy dissipation within a small fraction of the contactor's volume results in better gas liquid performance. As can be seen from Fig. 6.7 a, b and c, the higher the local energy dissipation rate within the throat, the better is the performance of the sparger. That is to say, smaller bubbles will be formed, larger interfacial area will be generated, and larger bubble population densities will be achieved. The variation of energy dissipation rate within the throat was achieved by mechanically adjusting the volume of the throat (or the cross sectional area of flow through the throat) in a fashion such that the total sum of energy consumed by the system is kept constant.

As the ratio of the local energy dissipation rate in the sparger, relative to that in the pipe, increases the interfacial area generated by the sparger is radically increased while the bubble size is dramatically decreased and the bubble population density is significantly increased (Fig. 6.7 a, b and c). For example, a 3-fold increase in the energy dissipation ratio was found to result in more than 6-fold increase in the specific interfacial area while the Sauter mean diameter is reduced by a factor of about 7 and the bubble number density jump up by a factor of more than 300. These benefits provide a guideline for the proper sparger design of dynamic spargers and the optimization of their operational conditions.

As shown in Fig. 6.5 a, b and c, the effect of the pressure drop is more pronounced the higher coalescence retardation is. This phenomenon can be ascribed to the augmentation of local energy dissipation rates within the sparger and the consequent shifting of the dynamic equilibrium between the bubble dispersion and coalescence processes towards the formation of smaller bubbles. Thus for example, using Eq. (2-7), the maximum bubble size generated within the sparger was estimated to be 5  $\mu\text{m}$  when the pressure drop across the sparger is 52 psi. The difference between the bubble size formed by the sparger and the equilibrium bubble size prevalent under any particular pipe flow conditions is thus expected to increase the larger is the pressure drop across the sparger. The importance of coalescence retardation therefore increases as the  $\Delta P_S$  increases. This observation is similar to those reported by Al Taweel and Cheng, 1995, and by Al Taweel

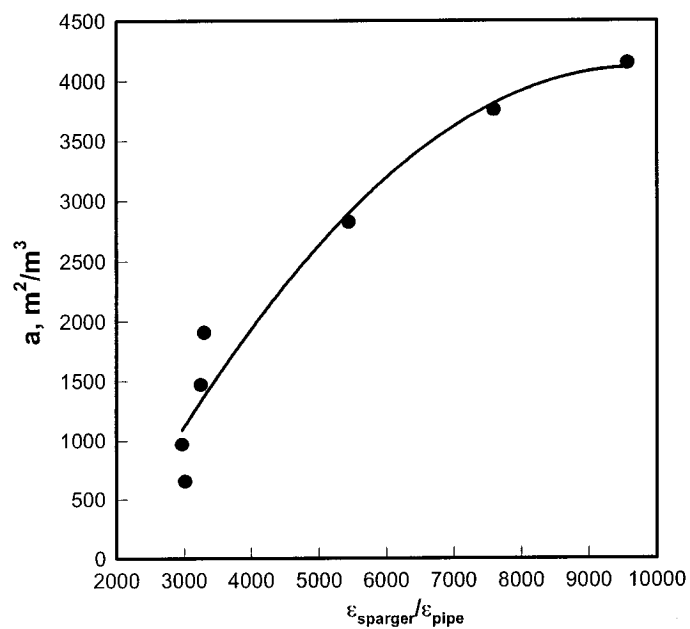


Fig. 6.7a Effect of local energy dissipation ratio  $\epsilon_{\text{sparger}}/\epsilon_{\text{pipe}}$  on performance of two-phase dynamic sparger ( $U_L = 1.2$  m/s,  $U_{LS} = 0.2$  m/s,  $\Phi_G = 0.08$ , 20 ppm MIBC)  
: interfacial area

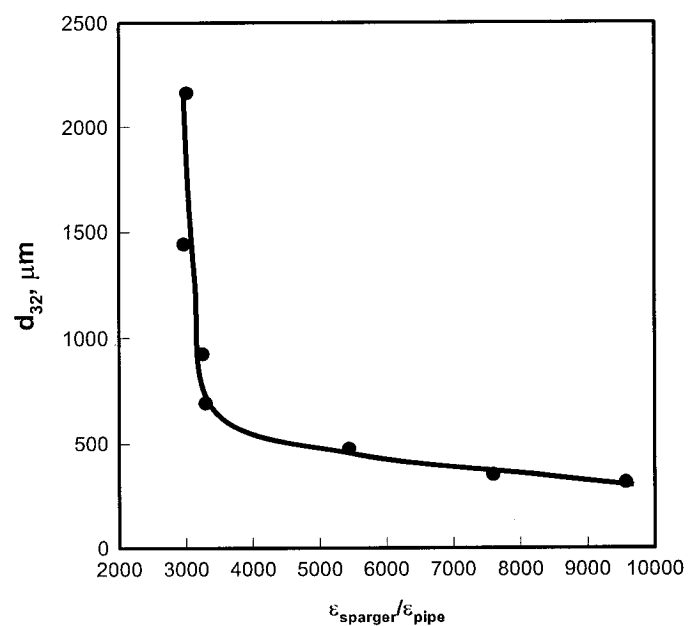


Fig. 6.7b Effect of local energy dissipation ratio  $\epsilon_{\text{sparger}}/\epsilon_{\text{pipe}}$  on performance of two-phase dynamic sparger ( $U_L = 1.2$  m/s,  $U_{LS} = 0.2$  m/s,  $\Phi_G = 0.08$ , 20 ppm MIBC)  
: bubble size

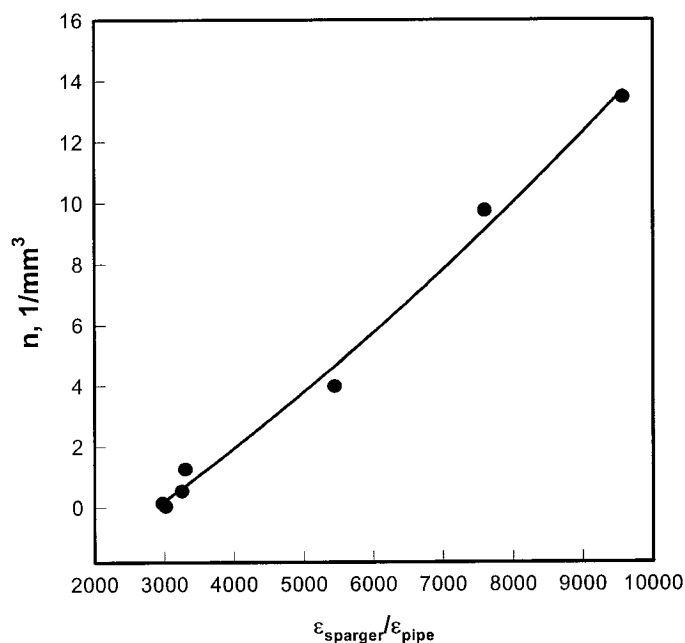


Fig. 6.7c Effect of local energy dissipation ratio  $\epsilon_{\text{sparger}}/\epsilon_{\text{pipe}}$  on performance of two-phase dynamic sparger ( $U_L = 1.2$  m/s,  $U_{LS} = 0.2$  m/s,  $\Phi_G = 0.08$ , 20 ppm MIBC)  
: bubble population density

et al., 1997. However, the maximum interfacial area obtained using the present sparger ( $5,300 \text{ m}^2/\text{m}^3$ ) is significantly higher than those reported by Al Taweel and Cheng ( $3,800 \text{ m}^2/\text{m}^3$ ) and the use of the dynamic sparger offers the possibility of on-line adjustment of the dispersion characteristics.

### 6.2.3 Effect of Interfacial Characteristics

It is known that the presence of impurities (e.g. as low as 10 ppm SAA) in gas/liquid systems usually results in lowering the static surface tension, a factor which facilitates bubble breakage (Hesketh et al., 1991) and profoundly retards bubble coalescence (Zlokarnik, 1985; Walter and Blanch, 1986; Prince and Blanch, 1990; Kastanek et al., 1993).

The effect of surfactant type and concentration on the interfacial area of contact, Sauter mean bubble size, and bubble population density are portrayed in Fig. 6.8 a, b and c and 6.9 a, b and c. They clearly show that much higher interfacial area of contact (i.e. a larger number of smaller bubbles) is obtained when systems depicting large coalescence retardation (simulated by using higher surfactant concentration in the aqueous phase) are encountered.

The importance of the above mentioned findings can not be over-emphasized since almost all multi-phase industrial streams contain a third component (such as alcohols, sugars, salts, organic acids, proteins, and clays, etc.) the presence of which is known to exhibit surface activity. The presence of these contaminants is known to retard bubble coalescence (Zlokarnik, 1985; Prince and Blanch, 1990; Gomaa et al., 1991; Jamialahmadi and Muller-Steinhagen, 1992; Al Taweel and Cheng, 1995) and the gas/liquid contacting characteristics of these industrial streams are therefore expected to be greatly different from those of the pure systems used in much of the multi-phase contacting R and D efforts. Furthermore, it is possible to say that the sparger investigated is particularly effective for facilitating inter-phase mass transfer to industrial streams where coalescence retardation is significant. Interfacial areas of contact as high as  $5,300 \text{ m}^2/\text{m}^3$  were achieved when slowly coalescing liquids (80 ppm MIBC) were contacted using large gas-to-liquid flow ratios (0.6 and high pressure drops 52 psi). Since coalescence is not fully suppressed in any of the experiments conducted in this investigation (due to the use of trace amounts of SAA) the system still exhibits some coalescence tendency. The gas/liquid contact characteristics (interfacial area, Sauter mean bubble size, bubble population density) reported in this investigation can thus be considered to be conservatively smaller than those encountered upstream from the point at which the interfacial area is measured due to the tendency of the small bubbles, formed in the throat section, to coalesce as they move within the divergent section of the sparger and the pipe section between the point of injection and that at which measurements are conducted. In spite of this, the results obtained are much higher than the  $1,000\text{-}2,000 \text{ m}^2/\text{m}^3$  reported for most intensive gas/liquid contactors (Lee and Tsui, 1999). The coalescence retardation characteristic of most industrial streams may thus be taken

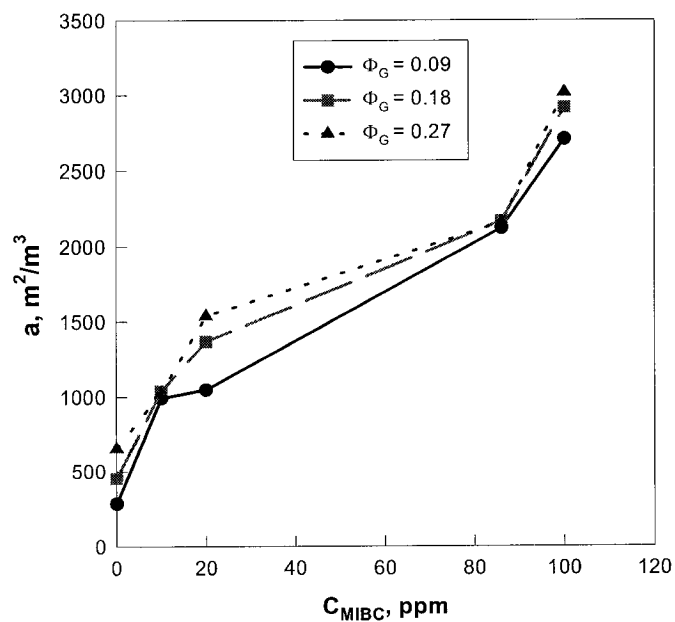


Fig. 6.8a Effect of MIBC concentration on performance of two-phase dynamic sparger ( $U_L=1.6$  m/s,  $U_{LS}=0.14$  m/s,  $\Delta p_{sparger}=30$  psi)  
: interfacial area

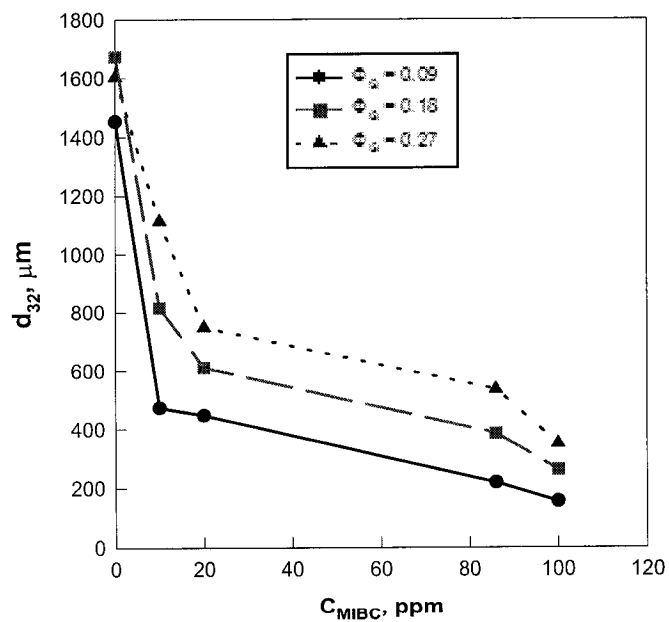


Fig. 6.8b Effect of MIBC concentration on performance of two-phase dynamic sparger ( $U_L=1.6$  m/s,  $U_{LS}=0.14$  m/s,  $\Delta p_{sparger}=30$  psi)  
: bubble size

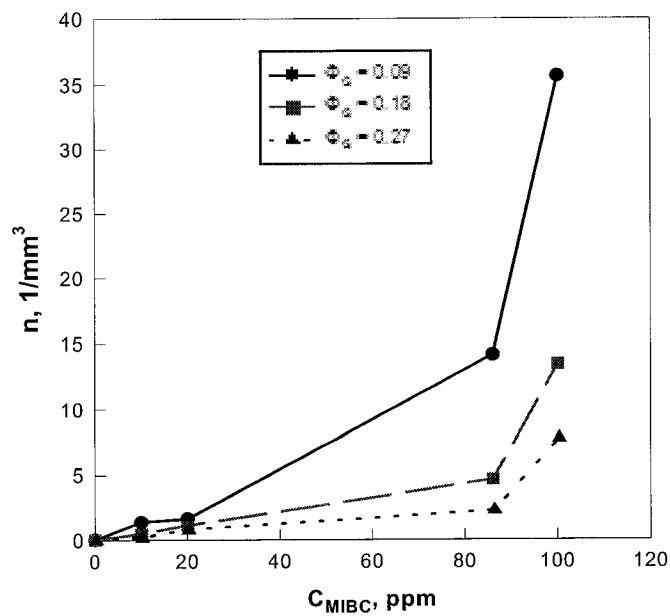


Fig. 6.8c Effect of MIBC concentration on performance of two-phase dynamic sparger ( $U_L=1.6$  m/s,  $U_{LS}=0.14$  m/s,  $\Delta p_{\text{sparger}}=30$  psi)  
: bubble population density

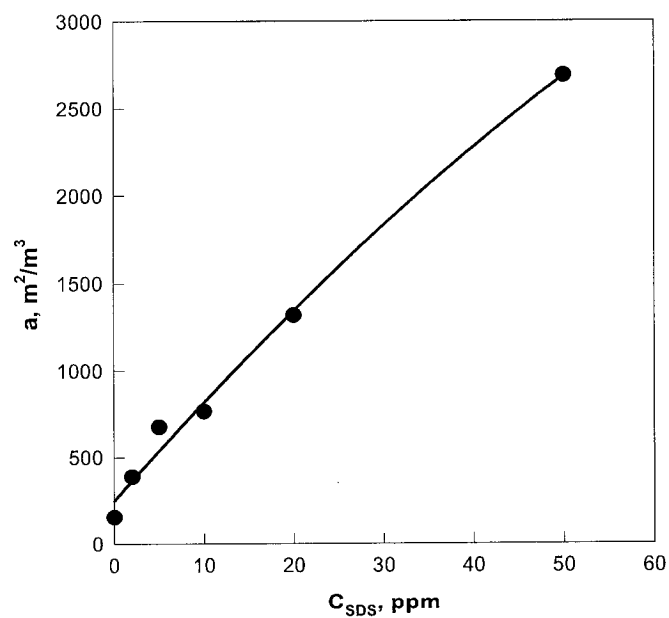


Fig. 6.9a Effect of SDS concentration on performance of two-phase dynamic sparger ( $U_L=1.2$  m/s,  $U_{LS}=0.2$  m/s,  $\Phi_G=0.08$ ,  $\Delta p_{\text{sparger}}=20$  psi)  
: interfacial area



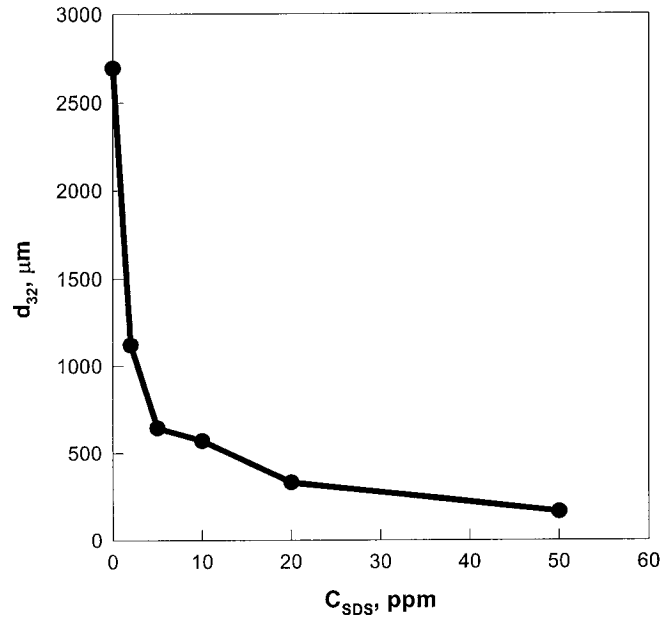


Fig. 6.9b Effect of SDS concentration on performance of two-phase dynamic sparger  
 ( $U_L=1.2$  m/s,  $U_{LS}=0.2$  m/s,  $\Phi_G=0.08$ ,  $\Delta p_{\text{sparger}}=20$  psi)  
 : bubble size

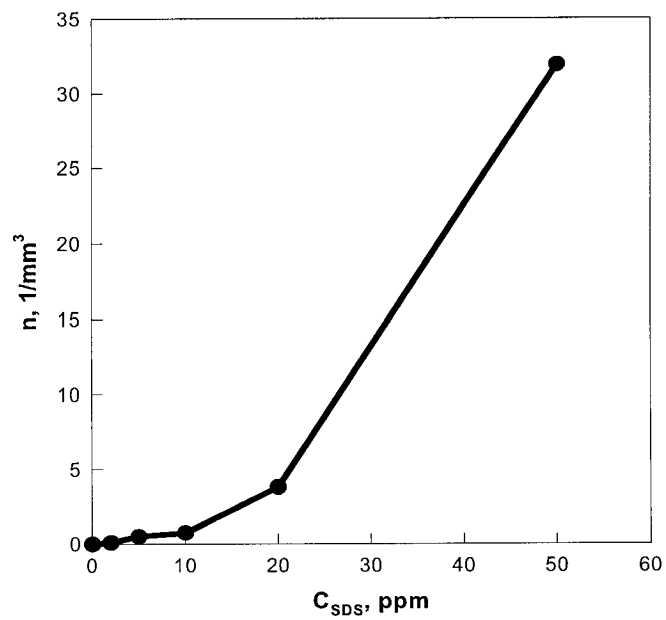


Fig. 6.9c Effect of SDS concentration on performance of two-phase dynamic sparger  
 ( $U_L=1.2$  m/s,  $U_{LS}=0.2$  m/s,  $\Phi_G=0.08$ ,  $\Delta p_{\text{sparger}}=20$  psi)  
 : bubble population density

advantage of to improve the efficiency by which energy is utilized to generate large interfacial area of contact between the phases.

Using the data discussed in the previous sections, an attempt was undertaken to identify the interfacial characteristic responsible for retarding bubble coalescence and enhancing the performance of dynamic sparger. The static surface tension,  $\sigma_{sta}$ , is the most common parameter used to quantify the surface activity of surfactants. As can be seen from Fig. 6.10 a, b and c, it is unlikely that  $\sigma_{sta}$  is a good characteristic since the results obtained identical hydrodynamic conditions tended to segregate into two separate groups, one for MIBC and another for SDS.

Much better agreement between the two SAA types was obtained using the Gibbs surface excess,  $\Gamma_G$  ( Fig.6.11a, b and c). The data obtained using two radically dissimilar surface active agents (one nonionic and the other cationic) could be treated as a singular group without excessive error over a wide SAA concentration range (SDS: 0 – 50 ppm and MIBC: 0 –100 ppm). This finding suggests that the value of the Gibbs surface excess,  $\Gamma_G$ , may be a good indicator of the bubble coalescence retardation tendency. This is in agreement with the findings of Cheng (1995) and Ramadan (1996). However, this hypothesis must be tested using a broad range of SAA types and concentrations before it can be used in a more general fashion. Although  $\Gamma_G$  can be easily determined for aqueous solutions containing salts, proteins, organic acids, clays, surfactants, etc., it suffers from the inability to fully account for the effect of interfacial viscoelasticity and does not account for the fact that bubble breakage/coalescence times are much smaller than those required for equilibrium conditions to be achieved at the interface (i.e. it does not account for the diffusivity of the interfacially active species).

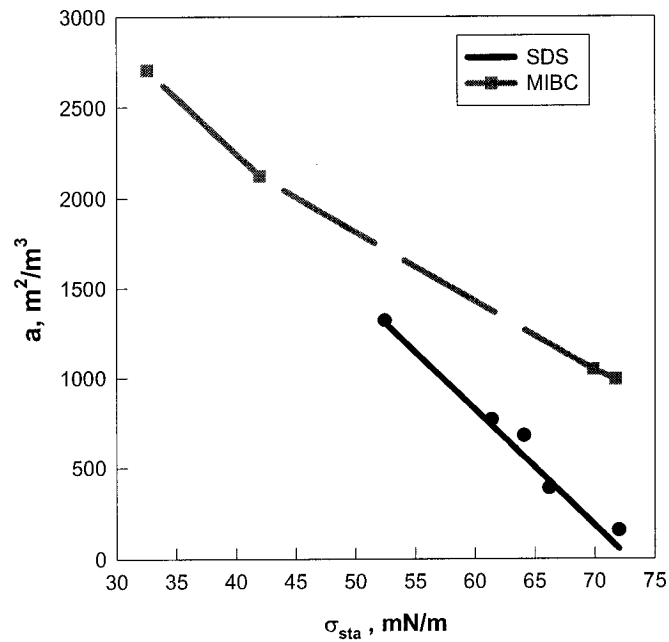


Fig. 6.10a Effect of static surface tension on performance of two-phase dynamic sparger in comparison between SDS and MIBC solutions at the similar operation conditions ( $U_L=1.2$  m/s,  $U_{LS}=0.2$  m/s,  $\Phi_G=0.08$ ,  $\Delta p_{\text{sparger}}=20$  psi) : interfacial area

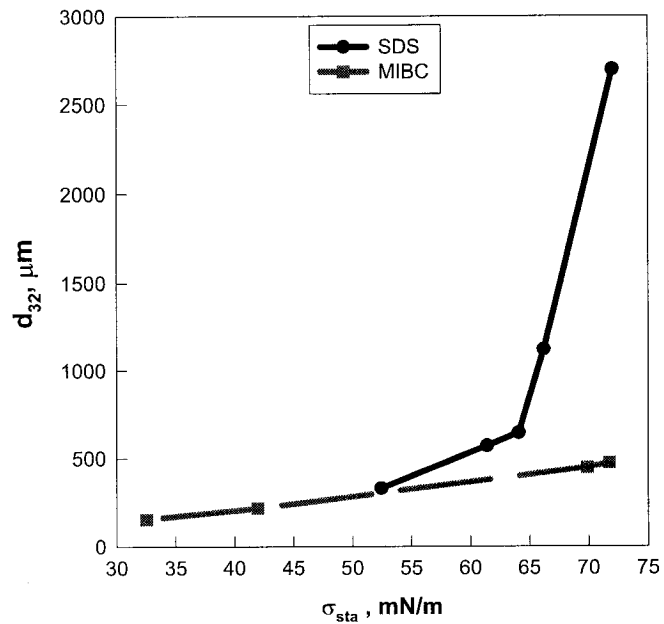


Fig. 6.10b Effect of static surface tension on performance of two-phase dynamic sparger in comparison between SDS and MIBC solutions at the similar operation conditions ( $U_L=1.2$  m/s,  $U_{LS}=0.2$  m/s,  $\Phi_G=0.08$ ,  $\Delta p_{\text{sparger}}=20$  psi) : bubble size

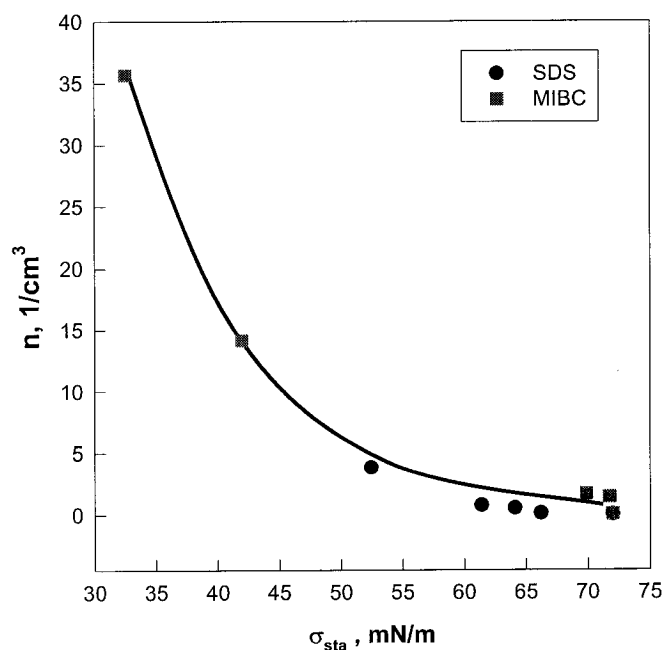


Fig. 6.10c Effect of static surface tension on performance of two-phase dynamic sparger in comparison between SDS and MIBC solutions at the similar operation conditions ( $U_L=1.2$  m/s,  $U_{LS} = 0.2$  m/s,  $\Phi_G = 0.08$ ,  $\Delta p_{sparger} = 20$  psi) : bubble population density

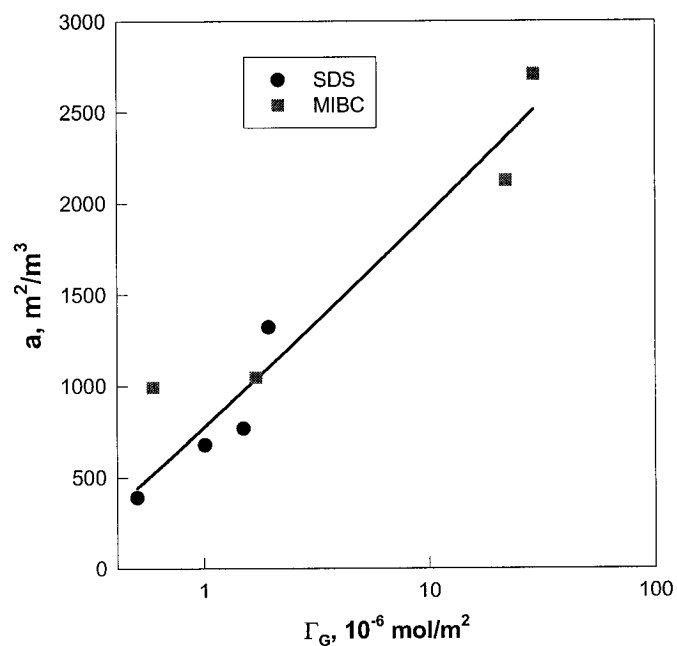


Fig. 6.11a Effect of Gibbs surface excess on performance of two-phase dynamic sparger in comparison between SDS and MIBC solutions at the similar operation conditions ( $U_L=1.2$  m/s,  $U_{LS} = 0.2$  m/s,  $\Phi_G = 0.08$ ,  $\Delta p_{sparger} = 20$  psi) : interfacial area

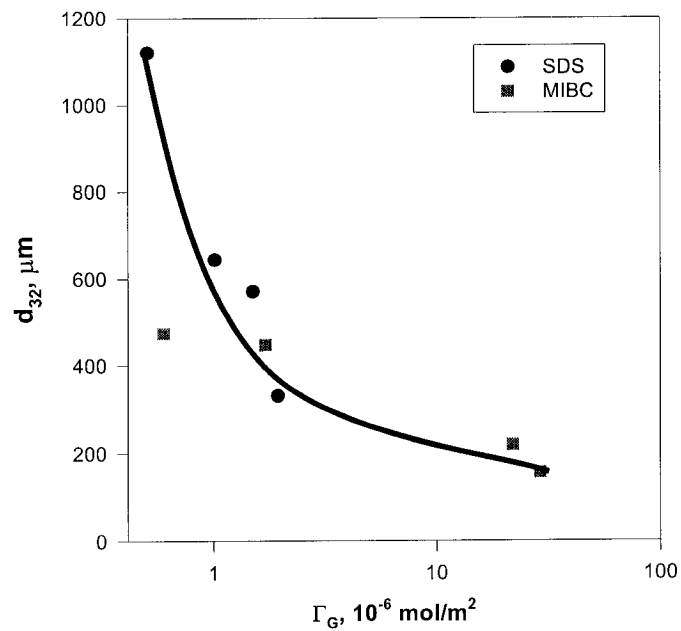


Fig. 6.11b Effect of Gibbs surface excess on performance of two-phase dynamic sparger in comparison between SDS and MIBC solutions at the similar operation conditions ( $U_L=1.2$  m/s,  $U_{LS}=0.2$  m/s,  $\Phi_G=0.08$ ,  $\Delta p_{\text{sparger}}=20$  psi) : bubble size

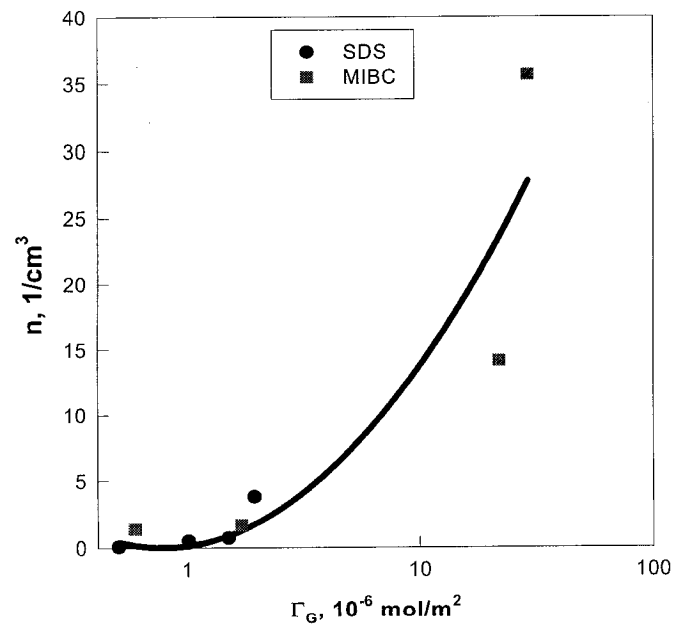


Fig. 6.11c Effect of Gibbs surface excess on performance of two-phase dynamic sparger in comparison between SDS and MIBC solutions at the similar operation conditions ( $U_L=1.2$  m/s,  $U_{LS}=0.2$  m/s,  $\Phi_G=0.08$ ,  $\Delta p_{\text{sparger}}=20$  psi) : bubble population density

### 6.2.4 Energy Consumption in Dynamic Spargers

There are three ways by which the energy input to a gas/liquid contactor can be considered. The first approach focuses on the overall amount of energy supplied to the mixer per unit time, which is termed as overall energy consumption,  $E$ . This term represents the power input of electric motors driving gas blowers or compressors, liquid pumps, and/or agitating devices. Such power input is usually related to overall mixer volume,  $V$ , and characterizes the energy demands of the respective mixer types. For the case at hand,

$$E = (Q_L + Q_G) * (\Delta p / \Delta L * L) + (Q_{LS} + Q_G) * (\Delta p_{sparger}) \quad (6-2)$$

where,

$L$	Length of pipe section	m
$\Delta p_{sparger}$	Pressure drop across sparger	Pa
$\Delta p / \Delta L * L$	Pressure drop along pipe section	Pa
$Q_L$	Overall liquid flow rate	m <sup>3</sup> /s
$Q_{LS}$	Liquid flow rate through the sparger	m <sup>3</sup> /s
$Q_G$	Gas flow rate	m <sup>3</sup> /s

The second approach focuses on the rate of energy dissipated per unit time and unit mass in the region where the gas is being dispersed. The whole volume is often used if mixing intensity is taken as essentially uniform throughout the contactor's volume. The energy dissipation rate per unit reactor volume in the pipeline contactor is thus given by,

$$\frac{E}{V} = \frac{E}{0.25 \pi D^2 \Delta L} \quad (6-3)$$

where,

$D$	Diameter of pipe	m
-----	------------------	---

The local rate of energy dissipated per unit mass of the liquid present in the mixer,  $\epsilon$ , is of primary importance when considering the mechanisms of bubble/drop dispersion and

coalescence in different mixer types. Assuming uniform conditions along the whole contactor yields,

$$\varepsilon = \frac{E}{V\rho_{Mix}} \quad (6-4)$$

where,

$$\rho_{Mix} \quad \text{Density of the mixture} \quad \text{kg/m}^3$$

The third approach applies only to the case of continuously flowing systems. It was introduced by Koglin et al. (1981) and Al Taweel and Walker (1983), and focuses on the power consumption needed to process a unit of the mixture processed. This parameter,  $E_{sp}$ , has the advantage of representing the concerns of mixing equipment users rather than those of equipment designer. It also allows for comparing the performance of mixing units with significantly different mixing times. The specific energy consumption rate  $E_{sp}$  can be calculated as two forms, the specific energy consumption rate per unit volume,  $E_{spv}$ , and the specific energy consumption rate per unit mass,  $E_{spm}$ .

$$E_{spv} = \frac{E}{V} * (\text{residence time}) \quad (6-5)$$

or,

$$E_{spm} = \frac{E}{\rho_{Mix} V} * (\text{residence time}) \quad (6-6)$$

This approach is somewhat analogous to the concept of the amount of oxygen transported to/from the liquid phase per unit of dissipated energy used extensively in the field of water/wastewater treatment (Al Taweel et al., 1997). This parameter is used to characterize the effectiveness of energy utilization in facilitating interfacial mass transport.

The efficiency by which various gas/liquid contacting devices utilize energy for the formation of interfacial area is graphically depicted in Fig. 6.12. The comparison is based on the value of  $E_{spm}$  to reflect the issues of interest to the users of the various

gas liquid contactors (the amount of energy consumed per unit mass of the stream processed). The residence time in the case of dynamic spargers combined with pipeline flow was calculated using,

$$\tau = \frac{V}{Q_{Mix}} \quad (6-7)$$

In the case of mechanically-agitated tanks, a conservatively small residence time of 2 minutes was assumed for the liquid phase. As can be seen, the interfacial areas obtained in all those contactors are strongly influenced by the type and the concentration of the coalescence retardants present in the system. However, the interfacial areas obtained using dynamic spargers at  $\Phi_G = 0.17$  are one order of magnitude higher than those obtained in mechanically-agitated tanks and traditional pipe nozzles operating at the same power input. The dynamic sparger was also found to be more efficient than some of the commonly used static mixers (such as Sulzer static mixers).

The benefits discussed above take into consideration neither the beneficial effects of the plug flow patterns in the sparger/pipeline contactor (and their impact on the average mass transfer driving force), nor the significant reduction in capital cost resulting from reduced volume requirements (in many cases the treatment can be undertaken while transporting the liquid to, or within, the treatment unit). These advantages rendered the use of such an approach attractive for remediating ineffective septic tanks (Gomaa et al., 1999).

The significant improvement in performance shown in Fig. 6.12 can be mainly attributed to the ability to design the gas/liquid contacting device (combined sparger/pipeline) in a fashion that takes advantage of the physical properties of the industrial system that is being processed. In particular, the design presented in this paper is based on the coalescence retardation characteristics that are rarely considered in conventional designs. By focusing energy dissipation rate into a small volume bubble breakage is promoted and very large interfacial areas of contact are developed. The coalescence retardation characteristic is then taken advantage of to maintain large



interfacial area in regions of low local-energy-dissipation rates. Very large average interfacial areas of contact can thus be achieved at relatively low energy consumption rates.

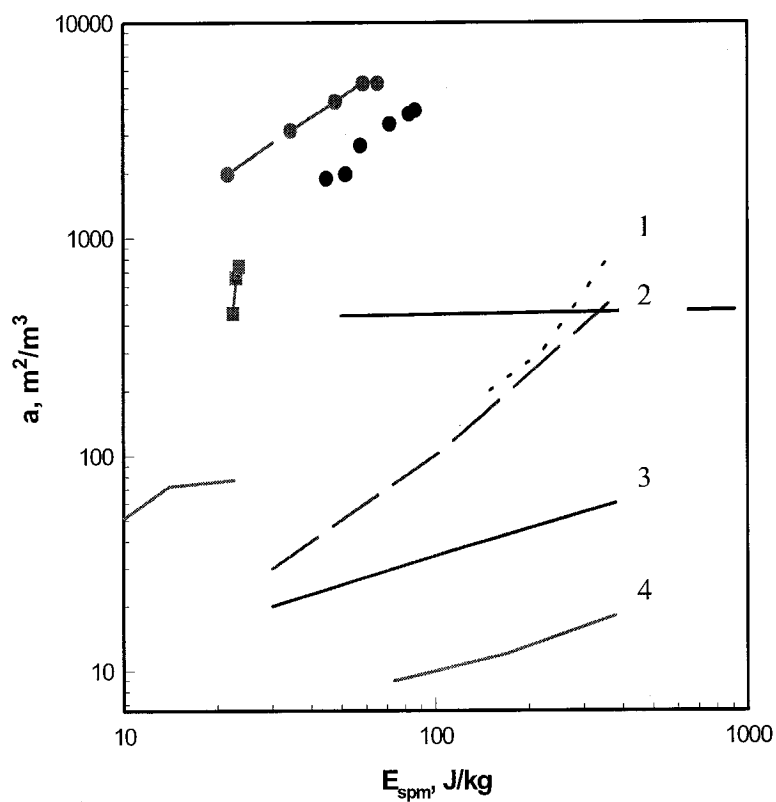
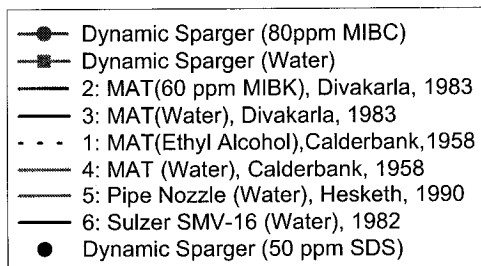


Fig. 6.12 Comparative evaluation of the performance of various gas/liquid contactors.



### 6.2.5 Correlation of experimental data

From the above discussion, it is evident that the performance of dynamic spargers is controlled mainly by three design/operating parameters (the pressure drop across the sparger, the gas-liquid flow ratio, the liquid flow rate through the sparger) and the coalescence characteristics of the system. Unfortunately, the interfacial characteristics of MIBC system were not extensively investigated; hence the experimental data of 294 points were correlated by using the following empirical equations based on the concentration of MIBC and the operational parameters

$$d_{32} = 1.57 \times 10^3 C_{\text{MIBC}}^{-0.40} \Delta p_s^{-0.35} Q_{\text{LS}}^{-0.26} (Q_G / Q_L)^{0.70} \quad (6-8)$$

$$R^2 = 0.93,$$

$$a = 5.82 \times 10^3 C_{\text{MIBC}}^{0.40} \Delta p_s^{0.35} Q_{\text{LS}}^{0.26} (Q_G / Q_L)^{0.32} \quad (6-9)$$

$$R^2 = 0.90,$$

$$n = 0.49 C_{\text{MIBC}}^{1.20} \Delta p_s^{1.05} Q_{\text{LS}}^{0.78} (Q_G / Q_L)^{2.10} \quad (6-10)$$

$$R^2 = 0.87.$$

A reasonably good fit was obtained for the three objective parameters although objectionable dimensional parameters appear in the equations. The correlation predicts that as the MIBC concentration increases the bubble size decreases, the interfacial area increase and the bubble population density increases. Similarly, as the pressure drop across the sparger increases, the local energy dissipation rate increases resulting in a decrease of the bubble size, larger interfacial area of contact, and significantly larger bubble population density. The liquid flow rate through the sparger was found to greatly affect the sparger performance because of its ability to influence the local energy dissipation rate in the sparger's throat. Finally, the gas/liquid volumetric flow ratio was found to exert a very strong influence on the sparger's performance mainly because of its influence on the coalescence rate within the divergent section of the sparger.

Because of the better understanding of the static and dynamic interfacial characteristics of dilute aqueous SDS solutions, an in-depth analysis of the effect of

various design, operational and systems parameters on the sparger performance was undertaken. An attempt was undertaken to correlate the three performance objective parameters (the specific interfacial area  $a$ , the Sauter mean bubble diameter  $d_{32}$  and the bubble population density  $n$ ) using two groups of variables. The first group represent operation/design parameters ( $U_{GS}$ ,  $U_{LS}$ ,  $U_{LP}$ ,  $\varepsilon_s$ ,  $\Phi_{GI}$ ,  $\Phi_S$ ) while the other group represent the system's interfacial characteristic represented by  $\sigma_{sta}$ ,  $C_0$ ,  $\Pi$ ,  $\Gamma_G$ , and  $\Gamma_L$ .

The 388 experimental data points obtained for the aqueous SDS system were analyzed using the stepwise regression analysis routine of by SAS program (Cody, et al., 1997). This program is capable of selecting the most significant parameters affecting the residual sum of squares and continues introducing various parameters selected from the specified input list in accordance with the order of their significance. The stepwise regression stops once the 95% significance limits have been reached. All the operation/design variables i.e. ( $U_{GS}$ ,  $U_{LS}$ ,  $U_{LP}$ ,  $\varepsilon_s$ ,  $\Phi_{GI}$ ,  $\Phi_S$ ) and interfacial variables  $C_0$ ,  $\sigma_{sta}$ ,  $\Pi$ ,  $\Gamma_G$ ,  $\Gamma_L$  were considered as factors that could potentially influence the sparger's performance.

The following correlation was obtained with a correlation coefficient  $R^2 = 0.94$ ,

$$d_{32} = 0.32U_G^{-0.26}U_{LS}^{-0.25}\Phi_S^{0.30}\varepsilon_S^{-0.41}C_0^{15}\Pi^{5.9}\Gamma_G^{-2.4}\Gamma_L^{-11} \quad (6-11)$$

This correlation could not apply to the case of pure water since  $C_0$ ,  $\Pi$ ,  $\Gamma_G$ ,  $\Gamma_L$  will tend to zero if the SAA concentration is zero. Furthermore, an increase of SDS dosage (which as shown in Chapter 4 leads to a monotonous rise of  $C_0$ ,  $\Pi$ ,  $\Gamma_G$  and  $\Gamma_L$ ) results in unreasonable variation in  $d_{32}$ .

If the interfacial property is simply taken as the value of the static surface tension,  $\sigma_{sta}$ , the following correlation was obtained,

$$d_{32} = 0.043U_{LS}^{-0.56}\Phi_S^{0.46}\varepsilon_S^{-0.33}(U_{GS}/U_{LP})^{0.046}\sigma_{sta}^{0.19} \quad (6-12)$$

This correlation incorporates the tap water data but the correlation coefficient is reduced to  $R^2=0.86$ .

In order to overcome above problems, all variables were converted into dimensionless parameters, so  $a$ ,  $d_{32}$ ,  $n$ ,  $U_{GS}$ ,  $U_{LS}$ ,  $U_{LP}$ ,  $\varepsilon_s$ ,  $\Phi_{G1}$ ,  $\Phi_S$  become  $U_{GS}/U_{LP}$ ,  $U_{LP}/U_{LS}$ ,  $U_{LP}/U_{LS}$ ,  $\Phi_{G1}$ ,  $\Phi_S$ ,  $\frac{a}{\varepsilon U_{LS}^3}$ ,  $\frac{\varepsilon d}{U_{GS}^3}$ ,  $\frac{n U_{LP}^3}{\varepsilon}$ , and  $C_0$ ,  $\Pi$ ,  $\Gamma_G$ ,  $\Gamma_L$  are properly transformed into

$C_0/C_{CMC}$ ,  $\Pi/\sigma_{\text{water}}$ ,  $\Gamma_G/\Gamma_{\text{max}}$ ,  $\Gamma_L/\Gamma_{\text{max}}$ . To render the expression applicable to water system, the exponential format for the interfacial characteristics is chosen yielding the following dimensionless parameters:  $\exp(C_0/C_{CMC})$ ,  $\exp(\Pi/\sigma_{\text{water}})$ ,  $\exp(\Gamma_G/\Gamma_{\text{max}})$ , or  $\exp(\Gamma_L/\Gamma_{\text{max}})$ . The other important reason for using this format is that it accounts for the observation that the performance of the sparger is strongly influenced by the coalescence-hindrance tendencies of the system. As was shown in Chapter 5, these were best expressed using the exponential format (Eq. 5-34 to Eq. 5-37). The reason overall sparger performance is controlled by the coalescence-hindering characteristic is the fact that the bubbles formed within the Sparger's throat will tend to coalesce as they move into regions of lower energy dissipation rates within the divergent parts of the sparger, or within the pipeline. In this regard, it is important to recall that the energy dissipation ratio  $\varepsilon_{\text{Throat}}/\varepsilon_{\text{pipe}}$  varied between 1,000 and 11,500 in the present investigation.

Three dimensionless parameters  $\frac{\varepsilon d}{U_{GS}^3}$ ,  $\frac{U_{GS}}{U_{LP}}$  and  $\frac{U_{LP}}{U_{LS}}$  were selected to represent the operation/design factors while only one non-dimensional parameter from the following four:  $C_0/C_{CMC}$ ,  $\Pi/\sigma_{\text{water}}$ ,  $\Gamma_G/\Gamma_{\text{max}}$ , and  $\Gamma_L/\Gamma_{\text{max}}$  was used to reflect the interfacial characteristics.

Stepwise regression was used to determine the value of the empirical exponents using 108 experimental points. The new correlations were found to correlate the data quite well,

$$\frac{\varepsilon d}{U_{GS}^3} = 8.1 \times 10^2 \left( \frac{U_{GS}}{U_{LP}} \right)^{-2.4} \left( \frac{U_{LP}}{U_{LS}} \right)^{-0.51} e^{-68 C_0 / C_{CMC}} \quad (6-13)$$

$$R^2 = 0.95,$$

$$\frac{\varepsilon d}{U_{GS}^3} = 1.1 \times 10^3 \left(\frac{U_{GS}}{U_{LP}}\right)^{-2.4} \left(\frac{U_{LP}}{U_{LS}}\right)^{-0.54} e^{-4.1\Pi / \sigma_{water}} \quad (6-14)$$

$$R^2 = 0.95,$$

$$\frac{\varepsilon d}{U_{GS}^3} = 1.4 \times 10^3 \left(\frac{U_{GS}}{U_{LP}}\right)^{-2.4} \left(\frac{U_{LP}}{U_{LS}}\right)^{-0.59} e^{-2.8\Gamma_G / \Gamma_{max}} \quad (6-15)$$

$$R^2 = 0.96,$$

$$\frac{\varepsilon d}{U_{GS}^3} = 1.2 \times 10^3 \left(\frac{U_{GS}}{U_{LP}}\right)^{-2.4} \left(\frac{U_{LP}}{U_{LS}}\right)^{-0.54} e^{-6.1\Gamma_L / \Gamma_{max}} \quad (6-16)$$

$$R^2 = 0.96$$

Although all four interfacial parameters yielded good fit to the data (e.g. Fig. 6.13 depicting Eq. 6-14), it may be easier to use Eq. 6-14 or 6-15 since they are based on parameters derived from static interfacial measurements without exhibiting the very large sensitivity associated with the use of Eq. 6-13 (Exponential constant of 68). Further investigation is needed in order to properly discriminate which interfacial characteristic controls coalescence retardation, and hence the performance of the dynamic sparger.

The use of a similar approach was found to correlate the specific interfacial area rather well.

$$\frac{a}{\varepsilon U_{LS}^3} = 3.5 U_{GS}^{-0.88} U_{LS}^{-2.7} \varepsilon_s^{-0.44} \left(\frac{U_{GS}}{U_{LP}}\right)^{1.2} e^{70C_{O_2} / C_{conc}} \quad (6-17)$$

$$R^2 = 0.89,$$

$$\frac{a}{\varepsilon U_{LS}^3} = 3.0 U_{GS}^{-0.82} U_{LS}^{-0.67} \varepsilon_s^{-0.46} \left(\frac{U_{GS}}{U_{LP}}\right)^{1.2} e^{4.2\pi / \sigma_{water}} \quad (6-18)$$

$$R^2 = 0.90,$$

$$\frac{a}{\varepsilon U_{LS}^3} = 2.8 U_{GS}^{-0.69} U_{LS}^{-2.7} \varepsilon_s^{-0.47} \left(\frac{U_{GS}}{U_{LP}}\right)^{1.1} e^{3.0\Gamma_G / \Gamma_{max}} \quad (6-19)$$

$$R^2 = 0.91,$$

$$\frac{a}{\varepsilon U_{LS}^3} = 2.2 U_{GS}^{-0.81} U_{LS}^{-2.7} \varepsilon_s^{-0.44} \left( \frac{U_{GS}}{U_{LP}} \right)^{1.2} e^{6.4 \Gamma_i / \Gamma_{max}} \quad (6-20)$$

$$R^2 = 0.91$$

Arguments concerning the best correlation approach to be used for describing the specific interfacial area of contact generated by the sparger are similar to those previously mentioned in association with the bubble diameter.

As shown in Chapter 4, information concerning the interfacial characteristics of aqueous MIBC solutions are rather limited and the dimensionless surface tension,  $\Pi/\sigma_{water}$ , is the only parameter that could be assessed for this system. The 108 experimental data points for the air- aqueous MIBC solutions (excluding water) were found to correlate well by the following correlation in terms of dimensionless bubble size ( $R^2 = 0.97$ , Fig. 6.14)

$$\frac{\varepsilon d}{U_{GS}^3} = 0.1 \left( \frac{U_{GS}}{U_{LP}} \right)^{-2.3} \left( \frac{U_{LP}}{U_{LS}} \right)^{0.5} e^{-1.7 \Pi / \sigma_{water}} \quad (6-21)$$

The fact that the data obtained using either SDS or MIBC systems could be well correlated (Eq. 6-14 and 6-21) suggested that it may be possible to correlate the whole data set with a single correlation. This was accomplished yielding the following correlation (see Fig. 6.15),

$$\frac{\varepsilon d}{U_{GS}^3} = 1.6 \times 10^5 \left( \frac{U_{GS}}{U_{LP}} \right)^{-2.1} \left( \frac{U_{LP}}{U_{LS}} \right)^{-2.9} e^{-8.8 \Pi / \sigma_{water}} \quad (6-22)$$

$$R^2 = 0.61$$

However, the very low correlation coefficient ( $R^2 = 0.61$ ) and segregation of SDS and MIBC data (see Fig. 6.15) suggest that other interfacial characteristics instead of the dimensionless surface tension may play a role. It can therefore be concluded that the effect of interfacial characteristics on the performance of dynamic sparger may be well predicted for various concentrations of the SAA using relatively simple parameters. However, further investigation is needed in order to completely identify the interfacial characteristic, or combination thereof, that can be used for a wide range of components.

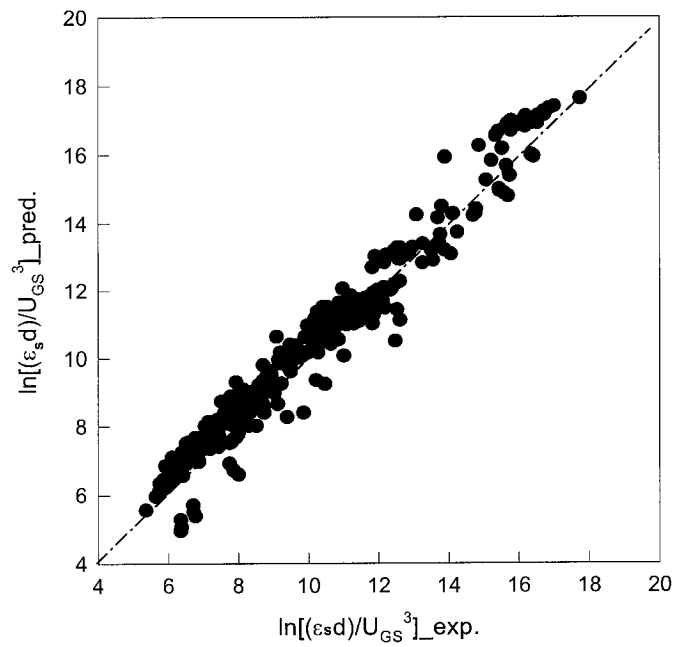


Fig. 6.13 Comparison of dimensionless bubble size between experiment and model by Eq.(6-14) for air-SDS aq. solutions

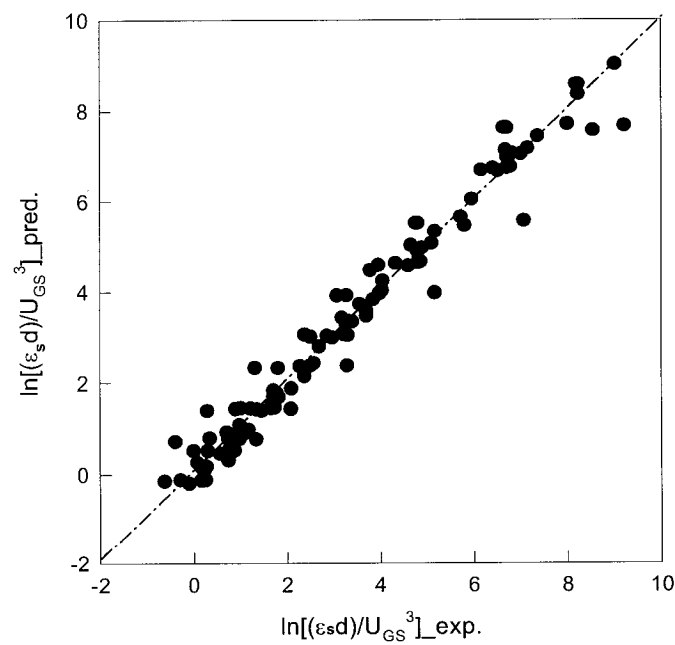


Fig. 6.14 Comparison of dimensionless bubble size between experiment and model by Eq.(6-21) for air-MIBC aq. solutions

A comparison between Fig. 10b and Fig. 11b, one could assume that the effect of the interfacial characteristics on the bubble dispersion can't be well represented by the dimensionless surface tension,  $\Pi/\sigma_{\text{water}}$ , and it might be better characterized by the Gibbs surface excess or the surface excess based on the long-term approximation. This is another recommendation for further investigation.

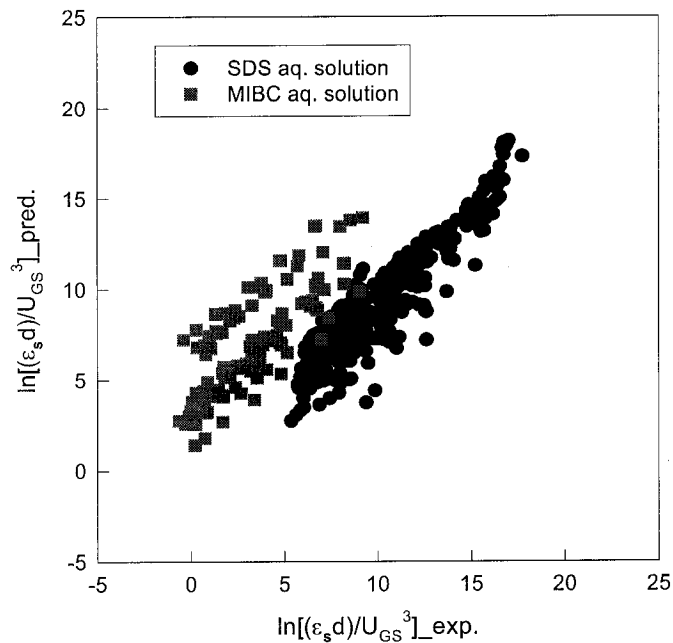


Fig. 6.15 Comparison of dimensionless bubble size between experiment and correlated equation by Eq.(6-22) for both air-SDS and air-MIBC aq. solutions

So far, it is possible to conclude that the specific interfacial area,  $a$ , and the Sauter mean diameter,  $d_{32}$ , can be predicted by combining the hydrodynamic variables  $U_{GS}$ ,  $U_{LS}$ ,  $U_{LP}$ ,  $\varepsilon_s$  and one of the interfacial properties  $C_0$ ,  $\Pi$ ,  $\Gamma_G$ ,  $\Gamma_L$ . However, there is no substantial reason to choose one correlation equation over the others since they all fit the current experimental data reasonable well. Due to the SAA concentration is most straightforward variable, the correlation equations including it could be chosen for convenience. The equations including the static surface tension could be selected since those data are not difficult to collect as well. But both cases have to be system



specific that is the above equation would be only applicable to SDS solutions. Both the Gibbs surface excess and surface excess based on long-term approximation are targeted to characterize the interfacial properties of assorted SAAs, thus they could be used to reveal SAA's effect on the interfacial area, the bubble size and the bubble population density. Through the discussion in Section 6.2.5, the equations containing  $\Gamma_G$  are more likely to be applicable to the systems contaminating non-SDS of various concentration ranges.  $\Gamma_L$  is another potential parameter since both surface excesses bear the similar physical interpretation on the interfacial characteristics.

### 6.3. Conclusions

1. The factors affecting bubble dispersion in a dynamic sparger were systematically investigated though the addition of trace quantities of MIBC and SDS.
2. The use of dynamic spargers results in the formation of large interfacial areas of contact (up to  $5,300 \text{ m}^2/\text{m}^3$ ) and small bubbles ( $d_{32}$  down to  $25 \text{ }\mu\text{m}$ ). This performance is controlled mainly by three design/operating parameters (the pressure drop across the sparger, the gas-liquid flow ratio and the liquid flow rate through the sparger) and the interfacial characteristics of the system being processed.
3. The efficiency by which dynamic spargers utilize energy for the formation of interfacial area was found to be one order of magnitude higher than that obtained in mechanically-agitated tanks and traditional pipe nozzles operating at the same power input per unit mass of the stream processed. The dynamic sparger was also found to be more efficient than some of the commonly used static mixers.
4. The interfacial area and the Sauter mean bubble size can be predicted by using correlation equations for MIBC and SDS aqueous solutions respectively. The surface excess offers better opportunities for taking the interfacial properties into account.
5. This sparger is particularly effective when used in conjunction with industrial effluents where the presence of secondary components (such as alcohols, organic acids, amines, proteins, salts, etc.) results in retarding bubble coalescence rate.

The dynamic sparger investigated also has the ability to control bubble sizes and interfacial areas in response to variation in process requirements. This can be accomplished without interrupting the operation.

## CHAPTER 7 OVERALL CONCLUSIONS AND RECOMMENDATIONS

1. The diffusion-controlled adsorption model is applicable to the adsorption of SDS aqueous solutions based on the available dynamic surface tension data. The analytical solution using long-term approximation fits the data quite well.
2. An accurate correlation of the static surface tension, and Gibbs surface excess of aqueous SDS solutions was developed in a rather wide concentration range of 0 – 10 mM. The static surface tension for aqueous MIBC solutions is also correlated.
3. Measuring dynamic surface tension could be a general method for analysis of interfacial characteristics of SAAs, since it is able to provide accurate estimates on static and dynamic properties, including static surface tension, surface pressure, Gibbs surface excess, diffusivity, and dynamic surface excess.
4. The surface excess based on the long-term approximation solutions is independent of the surface age over the range of 0.08 - 6 s due to a longer characteristic adsorption time than a characteristic diffusion time.
5. A comprehensive experiment was designed to investigate bubble coalescence rate in turbulent pipe flow at broad ranges of operation concentration ( $0.008 < \Phi_G < 0.5$ ,  $4 < \varepsilon_p < 26$ , and  $25 \mu\text{m} < d_{32} < 8,700 \mu\text{m}$ ) and SDS concentration (0 - 50 ppm) by measuring specific interfacial area at two locations (distance of 1.74 m) along the pipeline using a method of laser attenuation. Bubble coalescence rate increased as the gas hold-up or energy dissipation increased, but decreased as bubble size or SAA concentration increased.
6. More insight of a role the interfacial characteristics play in retarding bubble coalescence rate in gas/liquid turbulent flow is obtained by current studies. It is discovered that the effect of interfacial properties on the bubble coalescence is in

an exponential fashion, implying that interfacial characteristics affect bubble coalescence through influencing collision efficiency.

7. A theoretical collision model was adapted to calculate current bubble coalescence rate in turbulent pipe flow. Since it applied well to water systems, the model was then extended to contaminated systems by taking into account the ability of SAA to further reduce coalescence efficiency. The expanded model obtained by incorporating the factor of effective coalescence efficiency was capable of correlating the bubble coalescence data for water system and SDS solutions over a wide range of bubble coalescence rates (5 order of magnitudes).
8. How SAA retards bubble coalescence rate was examined by evaluating effects of various interfacial parameters including static surface tension, surface pressure, Gibbs surface excess, and surface excess based on long-term approximation. Although the dimensionless forms of these interfacial parameters are correlated with bubble coalescence rate for SDS aqueous solutions to the similar degrees, the surface excess based on the long-term approximation could prevail due to its revealing the underlying mechanism of coalescence hindrance.
9. Factors affecting bubble dispersion were investigated systematically through an experiment by adding either MIBC or SDS to simulate the industrial streams in a 25.4 mm I.D. and 6 m long pipe loop with liquid velocities of up to 3.2 m/s, and gas holdup varying between 0.008 and 0.5. The use of novel dynamic spargers resulted in the formation of large interfacial area of contact (up to 5,400 m<sup>2</sup>/m<sup>3</sup>) and small bubbles ( $d_{32}$  down to 25  $\mu$ m).
10. The efficiency that the dynamic spargers utilize energy to form interfacial area was one order of magnitude higher than those in mechanically agitated tanks and traditional pipe nozzles operating at the same power input per unit mass of stream processed.
11. Specific interfacial area and Sauter mean bubble diameter can be predicted by correlated equations for either MIBC or SDS aqueous solutions. It appears that

the surface excess based on current comparison results could represent the interfacial properties in terms of the bubble dispersion.

12. Further investigations are recommended by using various additives that exhibit not only surface activity, but also the other interfacial properties including surface viscosity, surface elasticity, and surface charge at broad ranges of concentration to find a prevailing interfacial parameter that is able to represent the interfacial properties of industrial streams.

## REFERENCES

- Abrahamson, J., "Collision Rates of Small Particles in a Vigorously Turbulent Fluid", *Chem. Eng. Sci.* **30**, 1371-1379 (1975)
- Acharya, A. and Ulbrecht, J.J., "Note on the Influence of Viscoelasticity on the Coalescence Rate of Bubbles and Drops", *AIChE J.*, **24**, 348 – 51, (1978)
- Aguta, R. M., Olsen, K.E., BØe, A., Saasen, A. and Aas, B. "Experimental investigation of Liquid Accumulation Effect During Orifice Gas Metering of Two-phase Flow", *Chem. Eng. J.*, **59**, 281-5 (1995)
- Aladyev, I.T., Kabakov, V.I. and Teplov, S.V. "Investigation of Ejectors with Two-Phase Flows of Water or Potassium", *Fluid Mechanics - Soviet Research*, **4** (5), 89-98 (1975)
- Allan, R.S., Charles, G.E. and Mason, S.G., "The Approach of Gas Bubble to a Gas-liquid Interface", *J. Colloid Sci.*, **16**, 150-65 (1961)
- Alvarez, J., "Gas-liquid Bioreactors: Maximum Stable Bubble Size", *Chem. Eng. J.*, **49**, B13-B16 (1992)
- Al Taweel, A. M. and Chen, C., "A novel static mixer for the effective dispersion of immiscible liquids", *Chem. Eng. Res. Des.*, **74**(A4), 445-450 (1996)
- Al Taweel, A.M. and Chen, C., "The Role of Dynamic Surface Tension in the Processing of Oilsands", Paper presented at the 75<sup>th</sup> Canadian Chemical Conference, Edmonton (May 1992)
- Al Taweel, A.M. and Cheng, Y.H., "Effect of surface tension on gas/liquid contacting in a mechanically-agitated tank with stator", *Chem. Eng. Res. Des.*, **73**(A6), 654-60 (1995)
- Al Taweel, A.M., and Landau, J., "Turbulence Modulation in Two-Phase Jets", *Int. J. Multiphase Flow*, **3**, 341-51 (1977)

- Al Taweel, A.M., Divakarla, R. and Gomaa, G., "Measurement of Large Gas-Liquid Interface Areas", *Can. J. Chem. Eng.*, **62**, 73-7 (1984)
- Al Taweel, A.M., Landau, J. and Picot, J.J., "Oxygen Transfer in Reciprocating Plate Columns", *AIChE Symp. Ser. No. 190*, 241 (1979)
- Al Taweel, A.M., Luo, J.-J. and Odedra, D., "Process Intensification in Gas/Liquid Reactors", Presented at the 50<sup>th</sup> Canadian Chemical Engineering Conference, Montreal, Canada (2000)
- Al Taweel, A.M., Luo, J.-J., Arora, S. and Goryunov, K., "Potential for Enhancing Bitumen Recovery in Hydrotransport Pipeline, Phase I: Sparger Performance", Technical Report submitted to Syncrude Canada Ltd. (April, 1998)
- Al Taweel, A.M., Walker, L.D. and Chen, C., "Dynamics of Dispersion and Coalescence". Paper presented at 73rd Canadian Chemical Conference and Exhibition (1990)
- Andrew, S. P. S. "Frothing in two-component Liquid Mixtures", *Int. Symp. on Distillation*, Rottenburg, P. A. (ed.), Institution of Chem. Engrs., London, 73-8, (1960)
- Arndt, E.A., "An Experimental Investigation of the Influence of Air Bubbles on the Acoustic Radiation Efficiency of Turbulent Shear Flow", Project Report No. 256, University of Minnesota, MN, (1987)
- Ayazi, S.P., Stavarindes, N.T. and Hoare, M., "Growth- independent Breakage Frequency of Protein Precipitates in Turbulency Agitated Bioreactors", *Chem.Eng.Sci.* **49** (16), 2647-56 (1994)
- Azbel, D. and Athanasios, I. L., "A Mechanism of Liquid Entertainment, Handbook of Fluids in Motion", N. Cheremisinoff, ed., Ann Arbor Sciences Publishers, Ann Arbor, MI, (1983)
- Azzopardi, B.J. "Gas-liquid Flows in Cylindrical Venturi Scrubbers: Boundary Layer Separation in the Diffuser Section", *Chem. Eng. J.*, **49**, 55-64 (1992)

- Azzopardi, B.J. "Liquid Distribution in Venturi Scrubbers: the Importance of Liquid Films on the Channel Walls", *Chem. Eng. Sci.*, **48** (15), 2807-13 (1993)
- Baird, M.H.I. and Rao, N.V.R., "Power Dissipation and Flow Patterns in Reciprocating Baffle-plate Columns", *Can. J Chem. Eng.*, **73**(4), 417-25
- Barigou, M. and Greaves, M., "Bubble Size Distributions in a Mechanically Agitated Gas-Liquid Cofactor", *Chem.Eng.Sci.* **47** (8), 2009-2025 (1992)
- Barnea, D., Hoffer, M.S., and Resnick, W., "Development of a Dynamic Circulation-Interaction Model for Mechanically Agitated, Liquid-liquid Reactors", *Chem. Eng. Sci.*, **34**, 901-11 (1979)
- Barnea, D., Shoham, O., and Taitel, Y., "Flow Pattern Transition for Vertical Downward Two Phase Flow", *Chem. Eng. Sci.*, **37** (5), 741-744 (1982)
- Batchelor, G.K., The Theory of Homogeneous Turbulence, 122 (1953).
- Batchlor, G.K., "The Stability of a Large Gas Bubble Rising Through Liquid", *J. Fluid Mech*, **184**, 399-422 (1987)
- Becher, P. and McCann, M.J., "Process of Emulsification. A computer Model", *Langmuir*, **7** (7), 1325-31 (Jul 1991)
- Beg, S.A., Hassan, M.M. and Chaudhry, M.A.S., "Effect of Sinuoidal Variation of Feed Concentration and Temperature on the Performance of a Packed-bed Biological Reactor - a Theoretical Study", *Chem. Eng. Technol.*, **19**, 43-9 (1996)
- Beltran, F.J., Gonzalez, M., Rivas, J. and Marin, M., "Oxidation of Mecoprop in Water with Ozone and Ozone Combined with Hydrogen Peroxide", *Ind. Eng. Chem. Res.*, **33**, 125-36 (1994)
- Beltran, F.J., Ovejero, G., Encinar, J.M. and Rivas, J., "Oxidation of Polynuclear Aromatic hydrocarbons in Water. 1. Ozonation", *Ind. Eng. Chem. Res.*, **34**, 1596-606 (1995)
- Beltran, F.J., Ovejero, G. and Rivas, J., "Oxidation of Polynuclear Aromatic Hydrocarbons in Water. 4. Ozone Combined with Hydrogen Peroxide", *Ind. Eng. Chem. Res.*, **35**, 891-8 (1996)



- Beltran, F.J., Ovejero, G., Garcia-Araya, J.F. and Rivas, J., "Oxidation of Polynuclear Aromatic hydrocarbons in Water. 2. UV Radiation and Ozonation in the Presence of UV Radiation", *Ind. Eng. Chem. Res.*, **34**, 1607-15 (1995)
- Benadda, B., Prost, M. and Otterbein, M., "A Study of Oxygen Absorption Kinetics in Ionic Cu(I) Aqueous Solutions", *Chem. Eng. Technol.*, **19**, 34-8 (1996)
- Beyerlein, S.W, Cossmann, R.K., and Richter, H.J., "Prediction of Bubble Concentration Profiles in Vertical Turbulent Two-Phase Flow", *Int. J. Multiphase Flow*, **11** (5), 629-41 (1985)
- Bhavaraju, S.M., Russell, T.W.F. and Blanch, H.W., "The Design of Gas Sparged Devices for Viscous Liquid Systems", *AIChE J.*, **24** (3), 454-66 (1978)
- Bisperink, C.G.J., Ronteltap, A.D., and Prins, A., "Bubble-size Distributions in Foams". *Advances in Colloid and Interface Science*, **38**, 13-32 (1992)
- Blass, E., "Formation and coalescence of bubbles and drops" *DECHEMA-Monographien*, **114**, 371-409 (1989)
- Blass, E., "Formation and Coalescence of Bubbles and Droplets", *Int. Chem. Eng.*, **30** (2), 206-21 (1990)
- Blinkov, V.N. and Jones, Jr., O.C., "Nucleation and Flashing of Initially Subcooled Liquids Following in Nozzles: 2. Comparison with Experiments Using 5-equation model for vapor", in *Dynamics Two-phase Flows*, ed. By Jones, O.C. and Michiyon, H., 637-63 (1992)
- Bojkov, B. and Luus, R., "Evaluation of the Parameters Used in Iterative Dynamic Programming" *Can. J. Chem. Eng.*, **71**, 451-8 (1993)
- Bonfillon, A., Sicoli, F., Langevin, D., "Dynamic surface tension of ionic surfactant solutions", *J. Colloid Interface Sci.*, **168**(2), 497-504 (1994)
- Borchardt, J.K. and Yen, T.F., "Oil-Field Chemistry: Enhanced Recovery and Production Stimulation", *ACS Symposium Series 396*, Developed from a Symposium at the 195th National Meeting of the American Chemical Society, Toronto, Ontario, Can., June 5-11, 1988, page 609 (1989).

- Borwankar, R.P., Wasan, D.T., "The kinetics of adsorption of surface active agents at gas-liquid surfaces", Chem. Eng. Sci., **38**(10), 1637-49 (1983)
- Bourne, J.R., Lenzner, J. and Petrozzi, S., "Micromixing in Static Mixers: An Experimental Study", Ind. Eng. Chem. Res., **31**, 1216-22 (1992)
- Bousfield, D.W., "Thinning of a Viscoelastic Film", Chem. Eng. Sci., **44** (3), 763-7, 1989
- Braginskii, L.N. and Belevitskaya, M.A., "Drop Breakup During Mechanical Stirring in Absence of Coalescence", Theoretical Foundations of Chemical Engineering (English Translation of Teoreticheskie Osnovy Khimicheskoi Tekhnologii), **24** (4), 351-7 (Mar 1991)
- Braginskij, L.N. and Belevetskya, M.A. "Effect of Viscosity on Drop Dispersion In Mixing Equipment" Teoreticheskie Osnovy Khimicheskoi Tekhnologii (English trans.) **25** (6), 698-706 (1991)
- Brodkey, R.S., "Limitations on a Generalized Velocity Distribution", AIChE J., 448-51 (1963)
- Brodkey, R.S., The Phenomena of Fluid Motions, 65, Addison-Wesley Publishing Company (1967)
- Brujan, E.-A., "The Effect of Polymer Assitive on the Bubble Behavior and Impulse Pressure", Chem. Eng. Sci., **48** (20), 3519-27 (1993)
- Bryson, A.W. and Hofman, D.L., "A population balance approach to the study of bubble behavior at gas-evolving electrodes", J. Appl. Electrochem., **19**(1), 116-9 (1989)
- Camp, T.R. and Stein, P.C., J. Boston Soc. Civil Eng. **30**, 219 (1943)
- Campanelli, J.R. and Cooper, D.G., "Interfacial Viscosity and The Stability of Emulsions", Can. J. Chem. Eng., **67**, 851-855 (1989)
- Campanelli, J.R. and Wang, X.H., "Comments on Modeling the Diffusion-Controlled Adsorption of Surfactants", Can. J. Chem. Eng., **76**, 51-57 (1998)
- Campbell, W.R., "Comments on the Paper: Liquid Circulation and Mixing Characteristics of Airlift Contactors", Can. J. Chem. Eng., **64**, 521-8 (1986)

- Casamatta, G. and Vogelpohl, A., "Modelling of Fluid Dynamics and Mass Transfer in Extraction Columns", *Ger. Chem Eng.* **8**, 96-103 (1985)
- Chang, C.H., Wang, N.-H.L. and Franses, E.I., "Adsorption Dynamics of Single and Binary Surfactants at the Air/Water Interface", *Colloids and Surfaces*, **62**, 321-32 (1992)
- Chang, C.S., Maa, J.R. and Yang, Y.M. "Dynamic Surface Effect and Nucleate Flow Boiling of Dilute Surfactant Solutions", *J. Chin. Inst. Chem. Eng.* **18**, 125-30 (1987).
- Chapin, F.J., "Calculator Program for Normal and Log-normal Distributions" *Chem. Eng.* 75-8 (1980)
- Chatzi, E, and Lee, J.M., "Analysis of Interactions for Liquid-Liquid Dispersions in Agitated Vessels", *Ind. Eng. Chem. Res.*, **26**, 2263-7 (1987)
- Chatzi, E.G., Boutris, C.J. and Kiparissides, C., "On-Line Monitoring of Drop Size Distributions in Agitated Vessels. 1. Effects of Temperature and Impeller Speed", *Ind. Eng. Chem. Res.*, **30**, 536-43 (1991)
- Chatzi, E.G., Gavrielides, A. D., and Kiparissides, C., "Generalized Model for Prediction of the Steady-State Drop Size Distributions in Batch Stirred Vessels", *Ind. Eng. Chem. Res.* **28**, 1704-11 (1989)
- Chatzi, E.G. and Kiparissides, C., "Steady-State Drop Size Distributions in High Holdup Fraction Dispersion Systems: Effect of the Degree of Hydrolysis of PVA Stabilizer", *Chem. Eng. Sci.*, **49**, 5039-52 (1994)
- Chatzi, E.G. and Kiparissides, C., "Drop Size Distributions in High Holdup Fraction Dispersion Systems: Effect of the Degree of Hydrolysis of PVA Stabilizer" *Chem. Eng. Sci.*, **49** (24B), 5039-52 (Dec 1994)
- Chatzi, E.G. and Kiparissides, C., "Steady-state Drop-size Distribution in High Holdup Fraction Dispersion systems" *AICHE.J.*, **41** (7), 1640-52 (1995)
- Chaudhari, R.V. and Hofmann, H., "Coalescence of Gas Bubbles in Liquid", *Review in Chemical Engineering*, **10** (2), 131-90 (1994).

- Chen, B.H. "Gas Hold-up and Liquid Flow Velocity in a Bubble Column Containing Screen Cylinders", *Can. J. Chem. Eng.*, **53**, 225-8 (1975)
- Chen, B.H., Yang, N.S. and Mcmillan, A.F., "Gas Holdup and Pressure Drop for Air-Water Flow through Plate Bubble Column", *Can. J. Chem. Eng.*, **64**, 387-92 (1986)
- Chen, C., "Dispersion and Coalescence in Static Mixer", Ph.D. thesis, Technical University of Nova Scotia, Halifax, Nova Scotia, Canada (1996)
- Chen, G.X., Afacan, A. and Chuang, K. T., "Effects of Surface Tension on Tray Point Efficiencies", *Can. J. Chem. Eng.*, **72**, 614-21 (1994)
- Chen, H.W., Hu, H., and Lee, T.Y., "Transient Crystallization and Crystal Size Distribution of Zeolite A" *Chem. Eng. Sci.*, **48** (21), 3683-91 (1993)
- Chen, J., "A Model of Coalescence Between Two Equal-sized Spherical Drops or Bubbles" *J. Colloid and Interface Sci.*, **107** (1), 209-20 (Sep.1985)
- Chen, J.-D., "A Model of Coalescence between Two Equal-Sized Spherical Drops or Bubbles", *J. Colloid Interface Sci.*, **107** (1), 209-20 (1985)
- Chen, J.-D., Hahn, P. S. and Slattery, J.C. "Coalescence Time for a Small Drop or Bubble at a Fluid-Fluid Interface", **30** (4), 622-30 (1984)
- Chen, L. and Lee, Y., "The Effects of a Surfactant on the Mass Transfer in Spray-Tower Extraction System", *Chem. Eng. J.*, **73**, 77-81 (1999)
- Chen, S.J. and Gilbert, R.G., "Mass Transfer and Mixing in the Kenics Aeration System", 69th AIChE Annual Meeting, Chicago, Illinois (Nov., 1976)
- Chen, Y and Fan, L.S., "Bubble breakage mechanisms due to collision with a particle in a liquid medium", *Chem. Eng. Sci.*, **44**, 117-32 (1989)
- Cheng, Y.H., "Bubble Generation by a Two - Phase Ejector", in *Column'96 -- Proceedings of the International Symposium on Column Flotation*, Edited by Gomez, C.O. and Finch, F.A., The Metallurgical Society of the Canadian Institute of Mining, Metallurgy and Petroleum, 3-11 (1996)

- Cheng, Y.H., "Gas-Liquid Contacting in Mechanically-Agitated Systems", Ph.D. thesis, Technical University of Nova Scotia, Halifax, Nova Scotia, Canada (1994)
- Cheng, Y.H., Mikhail, M.W., Salama, A.I.A. and Al Taweel, A.M., "Bubble Generation by a Two-phase Ejector", COLUMN '96, Proc. Int. Symp. Column Flotation, (1996)
- Chesters, A. K., "Modes of Bubble Growth in the Slow-formation Regime of Nucleate Pool Boiling", *Int. J. Multiphase Flow*, **4** (3), 279-302 (1978)
- Chesters, A.K., "The Modeling of Coalescence Processes in Fluid-Liquid Dispersions": A Review of Current Understanding, *Trans IChemE*, **69**, Part A, pp.259-270 (1991)
- Chhabrea, B.R. and Richardson, J.F., "Prediction of Flow Pattern for the Co-current Flow of Gas and Non-Newtonian Liquid in Horizontal Pipes", *Can. J. Chem. Eng.*, **62**, 449-54 (1984)
- Child, C. A., M. Sc. Thesis, Univ. of California, Berkeley, California (1982)
- Chisholm, D., Two-phase Flow in Pipelines and Heat Exchangers, Longman Inc., New York (1983)
- Chisti, Y., Kasper, M., and Moo-Young, M., "Mass Transfer in External - Loop Airlift Bioreactors Using Static Mixers", *Can. J. Chem. Eng.*, **68**, 45-50 (1990)
- Christenson, H.K. and Yaminsky, V.V., "Solute Effects on Bubble Coalescence", *J. Phys. Chem*, **99**, 10420 (1995)
- Clark, M.M, "Drop Breakup in a Turbulent Flow: I. Conceptual and Modeling Considerations", *Chem. Eng. Sci.* , **43**, 671-79 (1988)
- Clark, M.M., "Drop Breakup in a Turbulent flow: II. Experiments in a Small Mixing Vessel", *Chem. Eng. Sci.*, **43**, 681-92 (1988)
- Cliff, R, Grace, R.J and Weber, E.M., Bubbles, Drops, and Particles, Academic press, New York (1978)
- Clift, R. and Grace, R.J., "The Mechanism of Bubble Break-up in Fluidized Bed", *Chem. Eng. Sci.*, **27**, 2309-10 (1972)

- Coates, J. and Pressburg, B.S., "How to Analyze Two-Phase Flow", Chem. Eng., 153-6 (1959)
- Cody, R.P., Cody, R., and Smith, J., Applied Statistics and the SAS Programming Language, 4<sup>th</sup> edition, Prentice Hall (1997)
- Cohen, R.D., "Effect of Turbulence Damping on the Steady State Drop Size Distribution in Stirred Liquid-liquid Dispersions", Ind. Eng. Chem. Res., **30**, 277-9 (1991)
- Coker, A.K., "Understand Two-Phase Flow in Process Piping", Chemical Engineering Progress, 60-5 (1990)
- Colella, D., Vinci, D., Bagatin R., Masi, M. and Bakr, E.A., "A Study on Coalescence and Breakage Mechanisms in Three Different Bubble Columns", Chem. Eng. Sci., **54** (21), 4679-5354 (1999)
- Collins, S.B. and Knudsen, J.G., "Drop Size Distributions Produced by Turbulent Pipe Flow of Immiscible Liquids", AIChE J. **16**, 1072-80 (1970)
- Costigan, G. and Whalley, P.B., "Measurements of the Speed of Sound in Air-water Flows", Chem. Eng. J., **66**, 131-5 (1997)
- Coulaloglou, C.A. and Tavlarides, L.L., "Description of Interaction Processes in Agitated Liquid-Liquid Dispersions", Chem. Eng. Sci. **32**, 1289-97 (1977)
- Coulaloglou, C.A. and Tavlarides, L.L., "Drop size distributions and coalescence frequencies of liquid-liquid dispersions in flow vessels", AIChE J. **22**, 289 (1976)
- Coulaloglou, C.A., "Dispersed Phase Interactions in an Agitated Flow Vessel", Ph.D. thesis, Illinois Institute of Technology, Chicago (1975)
- Crabtree, J.R. and Bridgewater, J. "Bubble Coalescence in Viscous Liquids", Chem. Eng. Sci., **26**, 839-51 (1971)
- Cralg, V.S., Ninham, B.W., and Pashley, R.M., "Effect of Electrolytes on Bubble Coalescence", Nature, **364**, 317-9 (1993)
- Cramers, P.H.M.R., "Hydrodynamics and local mass transfer characteristics of gas - liquid Ejectors", Chem. Eng. J., **53**, 67-73 (1993)

- Curl, R.L., "Dispersed Phase Mixing: I. Theory and Effects in Simple Reactors", *AICHE J.*, **9**, 175-81 (1963).
- Daling, per S., Mackay, D., Mackay, N, and Brandvick, per J., "Droplet Size Distributions in Chemical Dispersion of Oil Spills: Toward a Mathematical Model", *Oil and Chemical Pollution*, **7**, 173-98 (1990)
- Danov, K.D., Ivanov, I.B., Gurkov, T.D., Borwankar, "Kinetic Model for the Simultaneous Processes of Flocculation and Coalescence in Emulsion Systems", *J. Colloid Interface Sci.*, **167** (1), 8-17 (1994)
- Dart, C.B. and Davis, M.E. "Catalysis for Environmentally Benign Processing", *Ind. Eng. Chem.*, **33**, 2887-99 (1994)
- Das, P.K., Hartland, S., "A Simple Correlation for Coalescence Rate-constant in Batch Turbulent Liquid-liquid Dispersions", *Chem. Eng. Comm.* **84**, 33-41 (1989)
- Das, P.K., Ramkrishna, D., and Narsimhan, G. "Effect of Mass Transfer on Droplet Breakup in Stirred Liquid-liquid Dispersions" *AICHE, J.*, **33** (11), 1899-902 (1987)
- Das, S.K., Biswas, M.N. and Mitra, A.K. "Friction factor for gas-non-Newtonian liquid flow in horizontal bends", *Can. J. Chem. Eng.*, **69**, 179-87 (1991)
- Das, S.K., Biswas, M.N. and Mitra, A.K., "Holdup for Two-Phase Flow of Gas-Non-Newtonian Liquid Mixtures in Horizontal and Vertical Pipes", *Can. J. Chem. Eng.*, **70**, 431-7 (1992)
- Das. K.P., and Kumar, R., "Coalescence of Drops in Stirred Dispersion. A White Noise Model for Coalescence", *Chem. Eng. Sci.*, **42** (2), 213-20 (1987)
- Datta, R., "Eddy Viscosity and Velocity Distribution in Turbulent Pipe Flow Revisited", *AICHE.J.*, **39** (7), 1107-12 (1993)
- Daugherty, R.L., Franzini, J.B. and Finnemore, E.J., Fluid Mechanics: with Engineering Applications, 8th ed., McGraw-Hill, New York, NY, 266-290 (1985)

- Davies, J.T., "A Physical Interpretation of Drop Sizes in Homogenizers and Agitated Tanks, Including the Dispersion of Viscous Oils", *Chem.Eng.Sci.*, **42** (7), 1671-76 (1987)
- Davies, J.T., Turbulence Phenomena ---- An Introduction to the Eddy Transfer of Momentum, Mass, and Heat, Particularly at Interfaces, 712, Academic Press, New York (1972)
- de Billerbeck, G.M., Condoret, J.S. and Fonnade, C., "Study of Mass Transfer in a Novel Gas-liquid Contactor: the Aero-ejector", *Chem. Eng. J.*, **72**, 185-193 (1999)
- de Bruijn, R.A., "Tipstreaming in Simple Shear Flows", *Chem. Eng. Sci.*, **48** (2), 277-284 (1993)
- de Nevers, N. and Wu, J.-L., "Bubble Coalescence in Viscous Fluid", *AICHE J* **17** (1), 182-6 (1971)
- Dean, R.B., "The Formation of Bubbles", *J. Appl. Sci.*, **15**, 446-51 (1944)
- Deckwer, W.D., "Phase Hold-ups and Mass Transfer, in Bubble Column Reactors", W.D. Deckwer and R.W. Field eds., John Wiley and Sons, 157-249 (1991)
- Degance, A.E. and Atherton, R.W., "Pressure-Drop Sample Calculations", *Chem. Eng.*, 101-8 (1970)
- Dejesus, J.M. and Kawaji, M., "Investigation of Interfacial Area Void Fraction in Upward, Cocurrent gas-liquid flow", *Can. J. Chem. Eng.*, **68**, 904-12 (1990)
- Dekee, D., Carreau, P.J. and Mardrski, J., "Bubble Velocity and Coalescence in Viscoelastic Liquid", *Chem. Eng. Sci.*, **41**, 2273-2283 (1986)
- Delichatsios, M.A., "Model for the Breakage Rate of Spherical Drops in Isotropic Turbulent Flow", *Physics Fluids*, **18** (6) 622-623 (1975)
- Dimitrova Al Khani, Sofka; Gourdon, Christophe; Casamatta, Gilbert, "Dynamic and Steady-State Simulation of Hydrodynamics and Mass Transfer in Liquid-Liquid Extraction Column", *Chem. Eng. Sci.*, **44** (6), 1295-1305 (1989)



- Dodd, P.W., Pandit, A.B., and Davidson, J.F., "Bubble Size Distribution Generated by Perforated Baffle Plates in Large Fermenters", 2nd International Conference on Bioreactor Fluid Dynamics, Cambridge, England, G2, 319-35 (1988)
- Doraiswami, R., "Analysis of Population Balance-IV, the Precise Connection Between Monte Carlo Simulation and Population Balances", *Chem. Eng. Sci.* **36**, 1203-1209 (1981)
- Doraiswami, R., "The Status of Population Balances", *Rev. Chem. Eng.* **3** (1), 49-95 (1985)
- Doraiswami, R., *Chem. Eng. Sci.* **26**, 1134-1136 (1971).
- Drogaris, G. and Weiland P., "Coalescence Behavior of Gas Bubbles in Aqueous Solutions of n-Alcohols and fatty Acids", *Chem. Eng. Sci.*, **38** (9), 1501-1506 (1983)
- Drogaris, G. and Weiland, P., "Influence of HCl on the Stability of Liquid Lamella between Two Colliding Bubble in Aqueous Solutions of n-fatty Acids", *Colloid Polym. Sci.*, (1983)
- Dukhin, S.S., Kretzschmar, G., Miller, R., ed., Dynamics of Adsorption at Liquid Interfaces. (Studies in Interface Science, Vol. 1), 60, Elsevier Science; New York (1995)
- Djuve, J., Pugh, R.J. and Sjoblom, J., "Foaming And Dynamic Surface Tension Of Aqueous Polymer/Surfactants Solutions 1: Ethyl(Hydroxyethyl) Cellulose And Sodium Dodecyl Sulfate", *Colloids Surf., A* **186**,189-202 (2001).
- Eastoe, J. and Dalton, J.S., "Dynamic Surface Tension and Adsorption Mechanisms of Surfactants at the Air-Water Interface", *Advances in Colloid and Interface Science*, **85** (2-3), 103-144 (2000)
- Egiebor, N.O., Zhou, Z.A. and Nyavor, K., "Development of a Particle-Bubble Collision Model for Flotation Column", *Dev. Chem. Eng. Mineral Process*, **5** (1/2), 21-42 (1997)

- Ehrhardt, G., "Flow Measurements for Wire Gauzes", *Int. Chem. Eng.* **23**, 455-465 (1983)
- Eisenberg, F.G. and Weinberger, C.B., "Annular Two-Phase Flow of Gases and Non-Newtonian Liquid", *AIChE J.*, **25** (2), 240-6 (1979)
- Elsayed, A.S. I. and Al Taweel, A.M., "Use of Population Balance to Describe Dispersion Properties in Multi-Phase Contactors", Technical Report Technical University of Nova Scotia (1993)
- Elton, G.A.H. and Picknett, R.G. "Coalescence of Aqueous Droplets with an Oil -Water Interface", *Proc. Int. Congress on Surface Activity*, Butterworths. London, **1** 288-294 (1957)
- Faeth, G.M., "Mixing, Transport and Combustion in Sprays", *Prog. Energy Combust. Sci.*, **13**, 293-345 (1987)
- Fainerman, V.B., Miller, R. and Joos, P., "The measurement of dynamic surface tension by the maximum bubble pressure method", *Colloid Polym. Sci.*, **272** (6), 731-9 (1994)
- Fang, J.P. and Joos, P., "Adsorption Kinetics of Cholesterol/SDS Mixtures at the Hexane / Water Interface", In Pillal, V. And Shah, D.O. ed., Dynamic properties of Interfaces and Association Structures, 57-79, (1996)
- Fernandes, R.C., Semiat, R., and Dukler, A.E., "Hydrodynamic model for Gas-Liquid Slug Flow in Vertical Tubes", *AIChE J.*, **29** (6), 981-89 (1983)
- Fontenot, K., and Schork, J., "Sensitive of Droplet Size and Stability in Monometric Emulsions", *Ind. Eng. Chem. Res.*, **32**, 373-85 (1993)
- Fordham, J.W.L., "Stereoregulated Polymerization in the Free Propagating Species", I. Theory. *J. Poly Sci.*, **39**, 321-334 (1959)
- Fordham, S., "Surface tension in systems not in equilibrium", *Trans. Faraday Soc.*, **50**, 593-8 (1954),
- Fort, I., Machon, V. and Kadlec, P., "Distribution of Energy Dissipation Rate in an Agitated Gas-Liquid System", *Chem. Eng. Technol.* **16**, 389-94 (1993)

- Franca, F. and Lahey Jr, R.T., "The Use of Drift-Flux Techniques for the Analysis of Horizontal Two-Phase Flows", *Int. J. Multiphase Flow*, **18** (6), 787-801 (1992)
- Frijlink, J. J., "Physical Aspects of Gassed Suspension Reactors", Ph.D. Thesis, Delft (1987)
- Frizell, K.W. and Arndt, R.E.A., "Noise Generation by Air Bubbles in Water: an Experimental Study of Creation and Splitting", Project Report No. 269, University of Minnesota, MN (1987)
- Gad-El-Hak, M. and Corrsin, S., "Measurements of the Nearly Isotropic Turbulence Behind a Uniform Jet Grid", *J. Fluid Mech.* **62**, 115-43 (1974)
- Gao, Z., Wang, Y., Shi, L. and Fu, J., "Theoretical and Experimental Studies on Bubble Diameter and Gas Holdup in Aerated Stirred Tanks", *Chin. J. Chem. Eng.*, **4** (4), 283-9 (1996)
- Garrett, P.R. and Ward, D., "A Reexamination of the Measurement of Dynamic Surface Tension Using the Maximum Bubble Pressure Method", *J. Colloid Interface Sci.*, **132** (2), 475-90 (1989)
- Gavrilyuk, S.L. and Fabre, J., "Lagrangian Coordinates for a Draft-Flux Model of a Gas-Liquid Mixture", *Int. J. Multiphase Flow*, **22** (3), 453-60 (1996)
- Gilbert, R.G. and Libby, D., "Field Testing for Oxygen Transfer and Mixing in Static Mixer Aeration system", Technical Report, Kenics, the 32nd Purdue Industrial Waste Conference (1977)
- Glasgow, L.A., "Sieve Plate Hole Pressure Fluctuations: Bubble Formation in Aerated Reactors", *AIChE J.*, **42** (5), 1495-9 (1996)
- Gomaa, H.G., Al Taweel, A.M., Luo, J.-J. and Yang, J., "Advances In Household Wastewater Treatment, in Proc. 2<sup>nd</sup> Intern. Conf. for Environmental Management and Technology", November, Cairo Egypt (1999)
- Gomaa, H.G., Landau, J. and Al Taweel, A.M., "Gas Liquid Contacting in Reciprocating Plate Columns: I Hydrodynamics", *Can. J. Chem. Eng.*, **69**, 228-39 (1991)

- Gordfrey, J.C., Obi, F.I.N., Reeve, R.N., "Measuring Drop Size in Continuous Liquid-liquid Mixers", Chem. Eng. Progress, 61-9 (1989)
- Goto, S. and Gaspillo, P.D. "The Effect of Static Mixer on Mass Transfer in Draft Tube Bubble Column and External Loop Column", Chem. Eng. Sci., **47** (13/14), 3533-9 (1992)
- Gourram-Badri, F., Conil, P., Morizot, G., "Measurements of Selectivity due to Coalescence between Two Mineralized Bubbles and Characterization of MIBC Action on Froth Flotation", Int. J. Miner. Process., **51**, 197-208 (1997)
- Grace, J.R., Wairegi, T. and Brophy, T., "Break-up of Drops and Bubbles in Stagnant Media", Can. J. Chem. Eng., **56**, 3-8 (1978)
- Grienberger, J., Untersuchung und modellierung von blasensaulen, Dissertation Universitat Erlangen-Nurnberg, Germany (1992)
- Groth, J. and Johansson, A.V., "Turbulence Reduction by Screens". J. Fluid Mech. **197**, 139-55 (1988)
- Grover, G.S., Rode, C.V. and Chaudhari, R.V., "Effect of Temperature on Flow Regimes and Gas Holdup in a Bubble Column", Can. J. Chem. Eng., **64**, 501-4 (1986)
- Gupta, S.K., "Breakage and Coalescence of Drops in Turbulent Stirred Dispersions", Dept. of Chemical Eng., Indian Institute of Science, Bangalore (India), Ph.D. thesis (1992).
- Hagesaether, L., Jakobsen, H.A. and Svendsen, H.F., "Theoretical Analysis of Fluid Particle Collisions in Turbulent Flow". Chem. Eng. Sci., **54**, 4749-55 (1999)
- Haller, H., Muschelknautz, E. and Schultz, T. "Venturi Scrubber Calculation and Optimization", Chem. Eng. Technol., **12**, 188-95 (1989)
- Hand, N.P., Spedding, P.L. and Ralph, S.L., "The Effect of Surface Tension on Flow Pattern, Holdup and Pressure Drop During Horizontal Air-Water Pipe Flow at Atmospheric Conditions", Chem. Eng. J., **48**, 197-210 (1992)
- Hartland, S., "Coalescence of a Liquid Drop at a Liquid-liquid Interface, III. Film Rupture", Trans. Inst. Chem. Eng., **45**(3) (1967)

- Hartland, S. and Jeelani, S.A.K., "Drainage in Thin Planar Non-Newtonian Fluid Films", *Can. J. Chem. Eng.*, **65**, 382 – 90 (1987)
- Hassan, T.M.I. and Robinson, C.W., "Mass-transfer-effective Bubble Coalescence Frequency and Specific Interfacial Area in a Mechanically Agitated Gas-liquid Contactor", *Chem. Eng. Sci.* **35**, 1277-89 (1980)
- Hatzikiriakos, S.G., Gaikwad, R.P. and Shaw, J.M., "Transitional Drop Size Distributions in Gas Agitated Liquid-Liquid Dispersions", *Chem. Eng. Sci.*, **45** (8), 2349-56 (1990)
- Hatzikiriakos, S.G., Gaikwad, R.P., Nelson, P.R. and Shaw, J.M., "Hydrodynamics of Gas-Agitated Liquid-Liquid Dispersions", *AIChE J.*, **36** (5), 677-84 (1990)
- Haunold, C., Cabassud, M., Gourdon, C., and Casamatta, G. "Drop Behaviour in a Kuhni Column for a Low Interfacial Tension System", *Can. J. Chem. Eng.* **68**, 407-14 (1990)
- Henriksen, H. K. and Ostergaard, K., "On the Mechanism of Bubble Break-up of Large Bubbles in Liquids and Three Phase Fluidization Beds", *Chem. Eng. Sci.*, **29**, 626-9 (1974)
- Henzler, H.J. "Design of Ejectors for Single-phase Material Systems", *Ger. Chem. Eng.*, **6**, 292-300 (1983)
- Herm-Stapelberg, H. and Mewes, D., "Pressure-drop Calculation in Three -Phase Slug Flow of Water, Oil, and Air", *Int. Chem. Eng.*, **34** (3), 295-314 (1994)
- Herringe, R.A. and Davis, M.R., "Structural Development of Gas-Liquid Mixture Flows", *J. Fluid Mech.*, **73**, Part 1, 97-123 (1976)
- Hesketh, R.P., "Bubble Breakage in Turbulence Liquid Flow", Ph.D. Dissertation, University of Delaware (1987)
- Hesketh, R.P., Etchells, A.W. and Russell, T.W.F., "Bubble Breakage in Pipeline Flow", *Chem. Eng. Sci.*, **46** (1), 1-9 (1991a)
- Hesketh, R P., Etchells, A.W. Russell, T.W.F., "Experimental Observations of Bubble Breakage in Turbulent Flow", *Ind. Eng. Chem. Res.*, **30**, 835-41 (1991b)

- Hesketh, R.P., Russell, T.W.F. and Etchells, A.W., "Bubble Size in Horizontal Pipelines", *AIChE J.*, **33** (4), 663-7 (1987)
- Hibiki, T. and Ishii, M., "Effect of flow-induced vibration on local flow parameters of two-phase flow", *Nucl. Eng. Des.*, **185** (2-3), 113-25 (1998)
- Hibiki, T. and Ishii, M., "Two-Group Interfacial Area Transport Equations at Bubbly-to-Slug Flow Transition", *Nucl. Eng. Des.*, **202** (1), 39-76 (2000)
- Hickman, K.E., Hill, P.G. and Gilbert, G.B., "Analysis and Testing of Compressible Flow Ejectors with Variable Area Mixing Tubes", *Transaction of ASME (Journal of Basic Engineering)*, 407-16 (June, 1972)
- Himmelblau, D.M. and Bischoff, K.B., Process Analysis and Simulation: Deterministic Systems, John Wiley and sons, Inc. (1968).
- Himmelblau, D.M., Process Analysis by Statistical Methods, John Wiley and Sons, Inc. (1970).
- Hinze, J.O. "Fundamentals of the hydrodynamic mechanism of splitting in dispersion processes", *AIChE J.*, **1**, 289-95 (1955)
- Hinze, J.O., Turbulence – An Introduction to Its Mechanism and Theory, McGraw-Hill, New York (1975).
- Hirt, D.E., Prud'homme, R.K., Miller, B. and Rebenfeld, L., "Dynamic surface Tension of Hydrocarbon and Fluorocarbon Surfactant Solutions Using the Maximum Bubble Pressure Method", *Colloid Surf.*, **44**, 101-17 (1990).
- Hoffer, M.S. and Resick, W., "A Study of Agitated Liquid/liquid Dispersions Part I", *Trans IChemE*, **57**, (1979)
- Hofmann, H., "Bildung und Koaleszenz von Blasen und Tropfen", *Chem. -ing. -Tech.* **60**, Nr.12, S.935-47, (1988)
- Holl, J.W., "An Effect of Air Content on the Occurrence of Cavitation", *J. Basic Eng.*, **82**, 941-6 (1960)
- Holmes, D.B., Voncken, R.M. and Dekker, J.A., "Fluid Flow in Turbulent-Stirred, Baffled Tanks-I Circulation Time", *Chem. Eng. Sci.* **19**, 201-8 (1964)

- Hong, O.P. and Lee, M.J., "Changes of the Average Drop Sizes During the Initial Period of Liquid-liquid Dispersions in Agitated Vessels", *Ind. Eng. Chem. Process Des. Dev.*, **24** (3), 868-72 (1985),
- Hong, P.O., and Lee, J.M., "Unsteady-State Liquid-Liquid Dispersions in Agitated Vessels", *Ind. Eng. Chem. Process Des. Dev.*, **22**, 130-5 (1983)
- Hosogai, K. and Tanaka, M. "Effect of Impeller Diameter on Mean Droplet Diameter in Circular Loop Reactor", *Can. J. Chem. Eng.*, **70**, 645-53 (1992)
- Howarth, W.J., "Coalescence of Drops in a Turbulent Flowfield", *Chem. Eng. Sci.* **19**, 33 (1964)
- Hsia, A.M. and Tavlarides, L.L., "Simulation Analysis of Drop Breakage, Coalescence and Micro Mixing in Liquid-liquid Stirred Tanks", *Chem. Eng. J.* **26**, 189-99 (1983)
- Hsu, S.-H., Lee, W.-H., Yang, Y.-M., Chang, C.H. and Maa, J.-R., "Bubble Formation at an Orifice in Surfactant Solutions under Constant-Flow Conditions", *Ind. Eng. Chem. Res.*, **39**, 1473-9 (2000)
- Hua, X.Y. and Rosen, M.J., "Dynamic Surface Tension of Aqueous Surfactant Solutions", *J. Colloid Interface Sci.*, **141** (1), 180-90 (1991)
- Hughmark, G.A., "Pressure Drop in Horizontal and Vertical Cocurrent Gas-Liquid Flow", *I & EC Fundamentals*, **2** (4), 315-20, In: Tilton, J.N., Fluid and Particle Dynamics, Chapter 6, 6: 1-54 (1963)
- Hulburt, H.M. and Akiyama, T., "Liouville equations for agglomeration and dispersion processes", *Ind. Eng. Chem., Fundam.*, **8**(2), 319-24 (1969)
- Hulburt, H.M. and Katz, S., "Problems in particle technology. A statistical mechanical formulation", *Chem. Eng. Sci.*, **19**, 555-74 (1964)
- Israelachvili, J., Intermolecular Forces, Academic Press, New York (1988)
- Israelachvili, J.N. and Pashley, R.M., "Molecular Layering of Water at Surfaces and Origin of Repulsive Hydration Forces", *Nature (London)*, **306** (5940), 249-50. (1983)

- Ivanov, I. B., Dimitrov, D. S., Somasundaram, S. and Jain, R. K., "Thinning of Film with Deformable Surfaces: Diffusion Controlled Surfactant Transfer", Chem. Eng. Sci., **40**, 137-50 (1985)
- Ivanov, I.B. Surfactant Science Series, Vol. 29: Thin Liquid Films: Fundamentals and Applications. Ed. 405 (1988)
- Ivanov, I.B., and Dimitrov, D.S., "Hydrodynamics of thin liquid films: Effect of Surface Viscosity on Thinning and Rupture of Foam Film", Colloid Polym. Sci., **252**, 982-90 (1974)
- Jaeger, P.T., v. Schnitzler, J. and Eggers, R., "Interfacial Tension of Fluid Systems Considering the Nonstationary Case with Respect to Mass Transfer", Chem. Eng. Technol., **19**(3), 197-202 (1996)
- Jameson, G.J. "Bubbles in Motion", Trans. I. Chem. E., **71**, Part A, 587-94 (1993)
- Jamialahmadi, M. and Muller-Steinhagen, H., "Effect of Alcohol, Organic Acid and Potassium Chloride Concentration on Bubble Size, Bubble Rise Velocity and Gas Hold-up in Bubble Column", Chem. Eng. J., **50**, 47-56 (1992)
- Jamialahmadi, M. and Muller-Steinhagen, H., "Effect of Electrolyte Concentration on Bubble Size and Gas Hold-up in Bubble Columns", Trans I. Chem. E., **68** (A), 202-4 (1990)
- Janssen, J.J.M., Boon, A., and Agterof, W.G.M. "Droplet Break-up in Simple Shear Flow in the Presence of Emulsifiers", Colloids and Surfaces A: Physicochemical and Engineering Aspects, **91**, 141-8 (1994)
- Jeelani, S.A.K. and Hartland, D., "Effect of Approach Velocity on Binary and Interfacial Coalescence", Trans. I. Chem. E., **69**, Part A, 271-81 (1991)
- Jeelani, S.A.K. and Hartland, S., "Prediction of Steady State Dispersion Height from Batch Settling Data", AIChE J., **31** (5), 711-20 (1985)
- Jeffreys, G.V. and Davies, G.A, In: Recent Advances in Liquid-Liquid Extraction, Manson, C. (ed.), 493. Pergamon Press, N.Y., (1971)



- Jeon, Y.M. and Lee, W.K., "A Drop Population Balance Model for Mass Transfer in Liquid-Liquid Dispersion. 1.Simulation and its Results", *Ind. Eng. Fundam.* **25**, 293-300 (1986)
- Joos, P., Fang, J.P. and Serrien, G., "Comments on Some Dynamic Surface Tension Measurements by the Dynamic Bubble Pressure Method", *J. Colloid Interface Sci.* **151**, 144-9 (1992).
- Joos, P. and Serrien, G., "Adsorption kinetics of Lower Alkanols at the Air/Water Interface: Effect of Structure Makers and Structure Breakers", *J. Colloid Interface Sci.*, **127** (1), 97-103 (1989)
- Joos, P., Vollhardt, D. and Vermeulen, M., "Interfacial Tension of Sodium Dodecyl Sulfate Solutions at the Hexane-Hater Interface", *Langmuir*, **6** (2), 524-5. (1990)
- Joshi, J.B., Elias, C.B. and Patole, M.S. "Role of Hydrodynamic Shear in the Cultivation of Animal, Plant and Microbial Cells", *Chem. Eng. J.*, **62**, 121-41 (1996)
- Ju, L.-K. and Sundararajan, A. "The Effect of Cells on Oxygen Transfer in Bioreactors: Physical Presence of Cells as Solid Particles", *Chem. Eng. J.*, **56**, B15-21, (1994)
- Kalinin, V.V. and Radke, C.J., "An Ion-binding Model for Ionic Surfactant Adsorption at Aqueous-fluid Interfces", *Colloids Surf., A.*, **114**, 337-50(1996)
- Kamp, A.M., Chesters, A.K., Colin, C. and Fabre, J., "Bubble Coalescence in Turbulent Flows: A Mechanistic Model for Turbulence-Induced Coalescence Applied to Microgravity Bubbly Pipe Flow", *Int. J. Multiphase Flow*, **27**, 1363-96 (2001).
- Kanel, J.S., "Effects of Some Interfacial Phenomena on Mass Transfer in Agitated Liquid-Liquid Dispersions", Ph.D. Dissertation, Georgia Institute of Technology, Atlanta, GA, (1990)
- Kasireddy, V.K. and Al Taweel, A.M., "An Improved Light Attenuation Technique for Measuring Large Interfacial Area", *Can. J. Chem. Eng.*, **68**, 690-3 (1990)
- Kastanek, F., Zahradnik, J., Kratochvil, J. and Cermak, J., Chemical Reactors for Gas-Liquid System, Translation Editor: Sharp, D. H., Ellis Horwood (1993)

- Kawase, Y. and Moo-Young, M. "Mathematical Models for Design of Bioreactors: Applications of Kolmogoroff's Theory of Isotropic Turbulence", Chem. Eng. J., **43**, b19-41 (1990)
- Kawase, Y. and Moo-Young, M. "Mathematical Models for Design of Bioreactors: Applications of Kolmogoroff's Theory of Isotropic Turbulence", Chem. Eng. J., **43**, b19-41 (1990)
- Kaweck, W., Reith, T., van Heuven, J.W., and Beek, W.J., "Bubble Size Distribution in the Impeller Region of a Stirred Vessel", Chem. Eng. Sci., **22**, 1519-23 (1967)
- Kay, B.H., "Determining the Characteristic of Fine Powder ", Chem. Eng., 239-249 (Nov.1966)
- Keitel, Gunter and Onken, Ulfert, "Inhibition of Bubble Coalescence by Solutes in Air / Water Dispersions", Chemical Engineering Science, **37** (11), 1635-8 (1982)
- Kennard, E.H., Kinetic Theory of Gases, Mcgraw-Hill, New York (1938)
- Kern, R., "How to Size Process Piping for Two-Phase Flow", Hydrocarbon Processing, 105-16 (1969)
- Killen, J.M., "An Experimental Investigation of the Influence of an Air Bubble Layer on Radiated Noise and Surface Pressure Fluctuations in Turbulent Boundary Layer", Project Report No. 202, University of Minnesota, MN (1981)
- Kim, J. O. and Kim, S. D., "Bubble Breakage Phenomena, Phase Hold-up and Mass Transfer in Three -Phase Fluidization Beds with Floating Bubble Breakers", Chem, Eng. Process, **28**, 101-11 (1990)
- Kim, J.W. and Lee, W. K., "Coalescence Behavior of Two Bubble Growing Side by Side", J. Colloid Interface Sci., **123**, 302-5 (1988)
- Kim, Y., Nikolov, A. D., Wasan, D. T., Diaz-Arauzo, H. and Shetty, C. S., "Demulsification of Water-in-Crude Oil Emulsions: Effects of Film Tension, Elasticity, Diffusivity and -Interfacial Activity of Demulsifier Individual Components and their Blends", J. Dispersion Science and technology, **17**, 33-53 (1996).

- Kimizuka, H., Abood, L.G., Tahara, T. and Kaibara, K., "Absorption kinetics of a surface-active agent at an interface", *J. Colloid Interface Sci.*, **40** (1), 27-34 (1972).
- King, R., Fluid Mechanics of Mixing: Modelling, Operations and Experimental Techniques, Kluwer Academic Publishers (1992)
- Kirkpatrick, R.D. and Lockett, M.J., "The Influence of Approach Velocity on Bubble Coalescence", *Chem. Eng. Sci.*, **29**, 2363-73 (1974)
- Klomp, E.D. and Sovran, G., "The Fluid Mechanics of Multiple-Venturi System and Their Application to Flow-Rate Metering", *Transactions of the ASME (Journal of Basic Engineering)*, 788-94 (Mar., 1972)
- Kocamustafaogullari, G. and Wang, Z. "An Experimental Study on Local Interfacial Parameters in a Horizontal Bubbly Two-Phase Flow", *Int. J. Multiphase Flow*, **17** (5), 553-72 (1991)
- Koglin, B., Pawlowski, J. and Schnoering, H. "Continuous emulsification with rotor/stator machines: effect of volume-related dispersion performance and residence time on fineness of emulsion", *Chem.-Ing.-Tech.*, **53** (8), 641-7. (1981)
- Koide, K., Yamazoe, S. and Harada, S., "Effect of Surface-Active Substances on Gas Holdup and Gas-Liquid Mass Transfer in Bubble Column", *J. Chem. Eng. Jpn.*, **18**, 287-92 (1985)
- Kolmogoroff, A., C.R. (Dokl.) Acad. Sci. USSR, 30, 301; 31, 538; 32, 16 (1941a).
- Kolmogoroff, A. N., "About the Breaking of Drops in Turbulent Flow", *Dokl. Akad. Nauk SSSR*, **66**, 825 (1941b)
- Kondur, R., and Shaw, J.M., "The Behavior of Large Gas Bubbles at a Liquid-Liquid Interface. Part 1: The Entrainment of Liquid Drops", *Proceedings of the International Symposium on Material Handling in Pyrometallurgy*, Hamilton, Ontario, August 26-30 (1990)
- Konno, M., Kosaka, N. and Saito, S., "Correlation of Transient Drop Sizes in Breakup Process in Liquid-Liquid Agitation", *J. Chem. Eng. Japan*, **26** (1), 37-40 (1993)

- Konno, M., Muto, T. and Saito, S. "Coalescence of Dispersed Drops in an Agitated Tank", *J. Chem. Eng. Jpn.*, **21** (4), 335-8 (1988)
- Koshy, A., Das, T. R. and Kumar, R., "Effect of Surfactant on Drop Breakage in Turbulent Liquid Dispersions", *Chem. Eng. Sci.*, **43** (3), 649-54 (1988)
- Koshy, A., Kumar, R., and Gandhi, S.K., "Effect of Drag-reducing Agents on Drop Breakage in Stirred Dispersions", *Chem. Eng. Sci.*, **44** (10), 2113-20 (1989)
- Kourio, M. J., Gourdon, C. and Casamatta, G., "Study of Drop-Interface Coalescence: Drainage Time Measurement", *Chem. Eng. Tech.*, **17**, 240-54 (1994).
- Krawczyk, M.A., Wasan, D.T., and Shetty, C.S., "Chemical Demulsification of Petroleum Emulsions Using Oil-soluble Demulsifiers", *Ind. Eng. Chem. Res.*, **30** (2), 367-75 (1991)
- Kubie, J. and Gardner, G. C., "Drop Sizes and Drop Dispersion in Straight Horizontal Tubes and in Helical Coils", *Chem. Eng. Sci.* **32**, 195 (1977)
- Kuboi, R., Komazawa, I. and Otake, T. "Collision and coalescence of dispersed drops in turbulent liquid flow", *J. Chem. Eng. Jpn.* **5**(4), 423-4 (1972)
- Kuboi, R., Komazawa, I. and Otake, T. "Collision and coalescence of dispersed drops in turbulent liquid flow", *J. Chem. Eng. Jpn.*, **5**(4), 423-4 (1972)
- Kudrewizki, F. and Rabe, P., "Model of the dissipation of mechanical energy in gassed stirred tanks", *Chem. Eng. Sci.* **41**, 2247-52 (1986).
- Kumar, S., Kumar, R., Gandhi, K.S., "A Simplified Procedure for Predicting Max.diameter in Stirred Vessels", *Chem.Eng.Sci.*, **48**, (17), 3092-6 (1993)
- Kumar, S., Kumar, R., Gandhi, K.S., "A Multi-Stage Model for Drop Breakage in Stirred Vessels", *Chem. Eng. Sci.*, **47** (5), 971-80 (1992)
- Kumar, S., Kumar, R., Gandhi, K.S., "A New Model for Coalescence Efficiency of Drops in Stirred Dispersions", *Chem. Eng. Sci.*, **48** (11), 2025-38 (1993)
- Laats, M.K. and Frishman, F.A., "Development of Technique and Investigation of Turbulent Energy at the Axis of a Two-Phase Turbulent Jet", *Fluid Dynamics*, **8**, 304-7 (1974)

- Lagisetty, J.S., Das, P.K., Kumar, R. and Gandhi, K.S., "Breakage of Viscous and Non-Newtonian Drops in Stirred Dispersions", Chem. Engng. Sci. **41**, 65-72 (1986)
- Lamb, H., Hydrodynamics, 6th ed., Cambridge University Press, England (1932)
- Landau, J., Gomma, H.G. and Al Taweel, A.M., "Measurement of Large Interfacial Areas by Light Attenuation", Trans. Inst. Chem. Eng., **55**, 212-5 (1977)
- Laso, M., de Brito, H., M.H., Bomio, P. and von Stockar, U. "Liquid-side Mass Transfer Characteristics of a Structured Packing", Chem. Eng. J., **58**, 251-8 (1995)
- Laso, M., Steiner, L., and Hartland, S., "Dynamic Simulation of Liquid-Liquid Agitated Dispersions-I", Chem. Eng. Sci. **42** (10), 2429-36 (1987)
- Laso, M., Steiner, L. and Hartland, S., "Dynamic Simulation of Agitated Liquid-Liquid Dispersions-II. Experimental Determination of Breakage and Coalescence Rates in a Stirred Tank", Chem. Eng. Sci., **42** (10), 2437-45 (1987)
- Lee, C., Herickson, I.E., and Glasgow, L.A., "Dynamics of Bubble Size Distribution in Turbulent Gas-Liquid Dispersions", Chem. Eng. Comm., **61**, 181-95 (1987)
- Lee, C.-H., Erickson, L.E. and Glasgow, L.A., "Bubble Breakup and Coalescence in Turbulent Gas-Liquid Dispersions", Chem. Eng. Comm., **59**, 65-84 (1987).
- Lee, J.C. and Tasakorn, P., "Characteristics of agitated tanks in relation to suspension polymerization", Proc. Eur. Conf. Mixing, 3<sup>rd</sup>. (1), York, United Kingdom, 157-70, (Apr. 1979)
- Lee, J.C., Tasakorn, P., and Belghazi, A., "Fundamentals of Drop Breakage in the Formation of Liquid-Liquid Dispersions", Chem. and Eng. Aspects, 43-55 (1984)
- Lee, S.-Y. and Tsui, Y. P., "Succeed at Gas/Liquid Contacting", Chem. Eng. Prog., 23-49 (July, 1999)
- Leja, J., Surface Chemistry of Froth Flotation, Plenum Pub Corp, 512 (1982)
- Lemlich, R., "A Boltzmann-Like Model for the Size Distribution of Bubbles or Droplets in a Well Mixed Dispersion", Chem. Eng. Commun., **16**, 153-7 (1982)

- Levich, V.G., Physicochemical hydrodynamics, Englewood Cliffs, N.J., Prentice-Hall, 109 (1962a)
- Levich, V.G., *ibid.*, 210 (1962b)
- Lewalle, J., Lawrence, L., Tavarides, and Jairazbhoy, V., "Modeling of Turbulent, Neutrally Buoyant Droplet Suspensions in Liquids", *Chem. Eng. Comm.*, **59**, 15-32 (1987)
- Lewis, D. A. and Davidson, J. F., "Bubble Splitting in Shear Flow", *Trans. Inst. Chem. Eng.*, **60**, 283-91 (1982),
- Lewis, D. A. and Davidson, J. F., "Bubble Sizes Produced by Shear and Turbulence in a Bubble Column", *Chem. Eng. Sci.*, **18** (1), 161-7, (1983)
- Li, D. and Slattery, J. C., "Experimental Support for Analyses of Coalescence", *AIChE J.*, **34** (5), 862-4 (1988)
- Li, D., "Coalescence between Small Rubbles: Effects of Bulk and Surface Diffusion", *Chem. Eng. Sci.*, **51**(14), 3623-30 (1996)
- Lin, S.H. and Yeh, K.L. "Cooling Water treatment by Ozonization", *Chem. Eng. Technol.*, **16**, 275-8 (1993)
- Lin, S.H., Ho, S.J. and Wu, C.L. "Kinetic and Performance Characteristics of Wet Air Oxidation of High-Concentration Wastewater", *Ind. Eng. Chem. Res.*, **35**, 307-14 (1996)
- Liu, S. and Li, D., "Drop Coalescence in Turbulent Dispersions", *Chem. Eng. Sci.*, **54**, 5667-75 (1999)
- Liu, T.J. and Bankoff, S.G., "Structure of Air-water Bubbly Flow in a Vertical Pipe—1. Liquid Mean Velocity and Turbulence Measurements, *Int. J. Heat Mass Transfer*", **36** (4), 1049-60 (1993)
- Lucassen, J., Hollway, F. and Buckingham, J.H., "Surface Properties of Mixed Solutions of Poly-L-Lysine and Sodium Dodecyl Sulfate, II. Dynamic Surface Properties", *J. Colloid Interface Sci.* **67**, 432-40 (1978).

- Lucassen-Reynders, E.H. and Kuijpers, K.A., "The Role of Interfacial Properties in Emulsification", *Colloids Surf.*, **65**, 175-84 (1992)
- Luo, J.-J. Al Taweel, A.M., Surry, K., Czarneck, J. and Ng, S., "Dynamic Spargers: Means for Improving Gas/Liquid Contacting", AIChE annual meeting, Miami, USA (1998)
- Luo, J.-J. and Al Taweel, A.M., "Dynamic Interfacial Characteristics of SDS Solutions", to be submitted for publication in *Can. J. Chem. Eng.* (2002)
- Luo, J.-J. and Al Taweel, A.M., "Performance Characteristics of a Novel Dynamic Sparger", submitted to publication in *Advances in Environmental Research* (2001b).
- Luo, J.-J. and Al Taweel, A.M., "Role of interfacial characteristics in turbulent bubble coalescence", Presented at the AIChE annual meeting, Reno, NV, USA (2001a).
- Luo, J.-J., Al Taweel, A.M. and Ng, Samson, "Potential for Enhancing Bitumen Recovery in Hydrotransport Pipeline, Phase II: Sparger Performance", Technical Report submitted to Syncrude Canada Ltd. (1998)
- Luo, J.-J., Arora, S.K., Al Taweel, A.M., Sury, K. and Czarnecki, J., "Factors Affecting the Size Of Air Bubbles Generated To Recover Bitumen In Syncrude's Low Energy Extraction Process", 47<sup>th</sup> Canadian Chemical Engineering Conference, Edmonton, Canada (1997)
- Mackay, G.D.M. and Mason, S.G., "The Gravity Approach and Coalescence of Fluid Drops at Liquid Interfaces", *Can. J. Chem. Eng.*, **41** (5), 203-12 (1963)
- Madavan, N.K., Deutsch, S. and Merkle, C.L. "Reduction of Turbulent Skin Friction by Microbubbles", *Phys. Fluids*, **27**(2), 356-63 (1984)
- Madavan, N.K., Merkle, C.L. and Deutsch, S. "Numerical Investigations into the Mechanisms of Microbubble Drag Reduction", Research Report, The Pennsylvania State University (1984)

- Malysa K., Lukenheimer, K., Miller, R. and Hempt, C., "Relationship between Foam Stability and Surface Elasticity Forces: Fatty Acid Solutions", *Colloids Surf.* **53**, 47-62 (1991).
- Manev, E. D., Vassilief, C. S. and Ivanov, I. B., "Hydrodynamics of Thin Films", *Colloid Polym. Sci.*, **254**, 99 (1976)
- Margulis, M.A. and Ditrjeva, A.F., "Dynamic of Coalescence of Bubble in Gas-Liquid System", *Theoretical Found. of Chem. Eng.*, 152-8, Plenum Publishing Corporation, Translated from *Teoreticheskie Osnovy Khimicheskoi Tekhnologii*, **17**, No.2, 220-5 (1991)
- Marrucci, G. and Nicodemo, L., "Coalescence of Gas Bubble in Aqueous Solutions of Inorganic Electrolytes", *Chemical Engineering Science*, **22**, 1257-65 (1967)
- Marrucci, G., Nicodemo, L. and Acierno, D., In "Co-Current Gas-Liquid Flow", ed. by Rhodes E. and Scott D.S., Plenum Press, New York, 95 - 108 (1972)
- Martin, W.W. and Adbelmessih, A.H. "Characteristics of Laser-Doppler Signals from Bubble", *J. Multiphase Flow*, **7**, 439-60 (1981)
- Mathews, J. "Low-pressure-steam Ejectors", *Chem. Eng.*, 155-8 (1987)
- McBride, C., Walter, J., Blanch, H. W. and Russell, T. W. F., "Bubble Coalescence and Break-up in Fermentation", *Adv. in Biotechnology, I: Scientific & Engineering Principles*, ed. Moo-Young, M., Robinson, C. W. and Vezina, C., **78**, 489 - 97 (1980)
- McManamey, W.J., "Sauter mean and maximum drop diameters of liquid-liquid dispersions in turbulent agitated vessels at low dispersed phase hold-up", *Chem. Eng. Sci.*, **34**(3), 432-4. (1979)
- Merkle, C.L. and Deutsch, S., "Drag Reduction by Microbubbles: Current Research Status", *AIAA Shear Flow Control Conference*, Boulder, Colorado, (March, 1985)
- Mersmann, A., "Gas-Liquid Reactors", *International Chemical Engineering*, **31** (3), 397-406 (1991)



- Middleton, J.C. "Motionless Mixers as gas liquid Contacting Devices", AIChE Annual Meeting, Miami (1978)
- Mihail, R. and Straja, S., "A Theoretical Model Concerning Bubble Size Distributions", Chem. Eng. J. **33**, 71-7 (1986).
- Miller, R., Fainerman, V.B. and Joos, P., "Dynamics of Soluble Adsorption Layer Studied by a Maximum Bubble Pressure Method in the Micro- and Millisecond Range of Time", Prog. Colloid Polym. Sci. **100**, 316-320 (1996).
- Miller, C.A. and Neogi, P., Interfacial Phenomena, Equilibrium and Dynamic Effects, Marcel Dekker, New York (1985)
- Miller, R, Joos, P. and Fainerman, V.B., "Dynamic Surface and Interfacial Tension of Surfactant and Polymer Solutions", Adv. Colloid Interface Sci., **49**, 249-302 (1994)
- Möbius, D. and Miller, R., ed. Drops and Bubbles in Interfacial Research, Elsevier Science, 299-317 (1998)
- Moo-Young, M. and Blanch, H.W., "Design of biochemical reactors: Mass transfer criteria for simple and complex systems", Adv. Biochem. Eng. **19**, 1-69 (1981)
- Moujaes, S. and Dougall, R.S., "Experimental Investigation of Concurrent Two Phase Flow in a Vertical Rectangular Channel", Can. J. Chem. Eng., **65**, 705-15 (1987)
- Mukerjee, P., Mysels, K.J. and Dulin, C.I., J. Phys. Chem., **62**, 1390 (1959)
- Muller, F.L. and Davidson, J.F., "On the Effects of Surfactants on Mass Transfer to Viscous Liquids in Bubble Columns", in 2nd International Conference on Gas/Liquid/Solid Reactor Engineering, Cambridge, UK, 291 (March, 1995)
- Muller, F.L. and Davidson, J.F., "On the Effects of Surfactants on Mass Transfer to Viscous Liquids in Bubble Columns", Trans I Chem E, **73**, Part A, 291-6 (April 1995)
- Muralidhar, R., "Drop Coalescence in Turbulent Liquid-Liquid Dispersions", Ph.D. thesis, Purdue University (1988)

- Mutsakis, M., Rader, R., Cross-Roll, F. and Maugweiler, W., "Better Absorption: Try a Static Mixer", Chem. Eng., 137-42 (July, 1989)
- Miyahara, T., Tsuchiya, K. & Fan, L.-S., "Effect of Turbulent Wake on Bubble/Bubble Interactions in a Gas/Liquid/Solid Fluidized Bed", Chem. Eng. Sci., **46**, 2368-73 (1991)
- Mysels, K.J., "Surface Tension of Solutions of Pure Sodium Dodecyl Sulfate", Langmuir, **2** (2), 423-8, (1986)
- Mysels, K.J., "Some Limitations in the Interpretations of the Time Dependence of Surface Tension Measured by the Maximum Bubble Pressure Method", Langmuir, **5**, 442-7 (1989)
- Nagaraj, N. and Gray, D.J., "Interfacial Area and Coalescence Frequency in Gas-Slurry Reactors", AIChE J., **33**, 1563-6 (1987)
- Nakoryakov, V.E., Kashinsky, O.N., Randin, V.V. and Timkin, L.S., "Gas-liquid Bubbly Flow in Vertical Pipes", J. Fluids Eng., **118**, 377-82 (1996)
- Nambiar, D.K.R., Kumar, R., Das, T.R., and Gandhi, K.S., "A New Model for the Breakage Frequency of Drops in Turbulent Stirred Dispersions", Chem. Eng. Sci., **47** (12), 2989-3002 (1992)
- Nicol, S.K., Engel, M.D., Teh, K.C., "Fine Particle Flotation in an Acoustic Field", Int. J. Miner. Process., **17**, 143-50 (1995)
- Nishikawa, M., Mori, F., Kayama, T., and Nishioka, S., "Drop Size Distribution in a Liquid-liquid Phase Mixing Vessel", J. Chem. Eng. Jpn., **24** (1), 88-94 (1991)
- Niyogi, D., Kumar, R., and Gandhi, K.S., "Modeling of Bubble-Size Distribution in Free Rise Polyurethane Foams", AIChE J., **38** (8), 1170-1184 (1992)
- Oolman, T.O. and Blanch, H.W., "Bubble Coalescence in Stagnant Liquid", Chem. Eng. Commun., **43**, 237-61 (1986a)
- Oolman, T.O. and Blanch, H.W., "Bubble Coalescence in Air-sparged Bioreactors", Biotechnol. Bioeng., **28**(4), 578-84 (1986b)
- Oran, E.S. and Boris, J.P., Numerical Simulation of Reactive Flow, Elsevier (1987)

- Otake, T., Tone, S., Nakao, K. and Mitsuhashi, Y., "Coalescence and Breakup of Bubbles in Liquids", Chem. Eng. Sci., **32**, 377-83 (1977)
- Ottmers, Delbert M. and Rase Howard F., "Characteristics of Single- and Multiphase-hole Orifice Plates for Gas-Liquid Reactions", Ind. Eng. Chem., Fundam., 106-10 (1964)
- Padmavathi, G. and Rao, K.R. "Effect of Liquid Viscosity on Gas Holdups in a Reversed Flow Jet Loop Reactor", Can. J. Chem. Eng., **70**, 800-2 (1992)
- Pal, R. and Masliyan, J., "Oil Recovery from Oil in Water Emulsions Using a Floatation Column", Can. J. Chem. Eng., **68**, 959-67 (1990)
- Pal, Rajinder, "Pipeline Flow of Unstable and Surfactant-Stabilized Emulsions", AIChE J., **39**, No.11, 1754-64 (1993)
- Pandit, A. B. and Davidson, J. F., "Bubble Breakup in Turbulent Liquid", International Conference on Bioreactor Fluid Dynamics, Cambridge, England, 109-20 (1986)
- Pandit, A.B., Kumar, P.S., and Kumar, M.S., "Improve Reactions with Hydrodynamic Cavitation", Chem. Eng. Prog., 43-50 (May, 1999)
- Parthasarathy, R. and Ahmed, N., "Sauter Mean and Maximum Bubble Diameters in Aerated Stirred Vessels", Trans IChemE, **72**, Part A, 565 - 72 (July 1994)
- Parthasarathy, R., Jameson, G.J. and Ahmed, N., "Bubble Breakup in Stirred Vessels - Predicting the Saunter Mean Diameter", Trans IChemE, **69**, Part A, 295 - 301, (July 1991)
- Pashley, R.M. and Craig, V.S., "Effect of Electrolytes on Bubble Coalescence", Langmuir, **13**, 4772-4 (1997)
- Perry, R.H. and Green, D.W., Perry's Handbook of Chemical Engineering, 6-111, McGraw-Hill (1997)
- Pham, T.M., Michel, J.M. and Lecoffre, Y., "A New Design of the Cavitation Susceptibility Meter: The Venturix, in Bubble Dynamica and Interface Phenomena", ed. by Blake, J.R., Boulton-Stone, J.M. and Thomas, N.H., Kluwer Academic Publishers, Birminhan, UK, 277-84 (1993)

- Phan-Thien, N. and Tanner, R.I., "Lubrication Squeeze-film Theory for the Oldroyd-B Fluid", *J. Non-Newtonian Fluid Mech.*, **14**, 327-35 (1984)
- Prince, M.J. and Blanch, H.W., "Bubble Coalescence and Break-Up in Air-Sparged Bubble Columns", *AIChE J.* **36** (10), 1485-99 (1990)
- Prins, A. and van't Riet, K., "Proteins and Surface Effects in Fermentation: Foam, Antifoam and Mass Transfer", *TIBTECH* **5**, 290-301 (1987)
- Pugh, R.J., Weissenborn, P., and Paulson, O., "Flotation in Inorganic Electrolytes – The Relationship between Recover of Hydrophobic Particles, Surface-Tension, Bubble Coalescence and Gas Solubility", *Int. J. Miner. Process.*, **51**, p.125-38 (1997)
- Pugh, R.J. and Yoon, R.H., "Hydrophobicity and rupture of thin aqueous films", *J. Colloid Interface Sci.*, **163** (1), 169-76 (1994)
- Radhakrishnan, V.R. and Mitra, A.K., "Pressure Drop, Holdup and Interfacial Area in Vertical Two-phase Flow of Multi-jet Ejector Induced Dispersions", *Can. J. Chem. Eng.*, **62**, 170-8 (1984)
- Radoev, B. P., Dimitrov, D. S. and Ivanov, I. B., "Hydrodynamics of Thin Liquid Films: Effect of the Surfactant on the Rate of Thinning", *Colloid & Polymer Sci.*, **252**, 50 - 5 (1974)
- Rajasekhar, D., "Hydrodynamics during the Flotation of Fine Coal", Ph.D. thesis, Technical University of Nova Scotia, Halifax, Canada (1983)
- Ramadan, A.M.M., "Physico-chemical Parameters Affecting Flotation Systems", Ph.D. thesis, Al-Azhar University, Egypt (1996)
- Ravera, F., Liggieri, L., Passerone, A., Steinchen, A., "Sorption kinetics at liquid-liquid interfaces with the surface-active component soluble in both phases", *J. Colloid Interface Sci.*, **163**(2), 309-14 (1994)
- Reynolds, A.J., Turbulent Flows in Engineering, John Wiley and Sons, (1974)

- Riberio, L.M, Regueiras, P.F.R, Guimaraes, M.M.L, Madureira, C.M.N, Cruz-Pinto, J.J.C, "The Dynamic Behavior Of Liquid-Liquid Agitated Dispersions- I. the Hydrodynamics", *Computers Chem. Eng.*, **19**, (3). 333-43 (1995)
- Rietema, K., Drew, T.B., Hoopes, J.W.Jr., Vermeulen, T., "Segregation in liquid-liquid dispersions and its effect on chemical reactions", *Advan. Chem. Eng.*, **5**, 237-302 (1964),
- Rincon-Rubio, L. M., Kumar, A. and Hartland, S., "Drop-Size Distribution And Average Drop Size in a Wirz Extraction Column", *Trans. IChemE*, **72**, Part A, 493-502 (1994)
- Risso, F., "The Mechanisms of Deformation and Breakup of Drops and Bubbles", *Multiphase Sci. and Tech.*, **12**, 1-50 (2000)
- Rod, V. and T. Misek, "Stochastic Modelling of Dispersion Formation in Agitated Liquid-Liquid Systems", *Trans IChemE*, **60**, 48-53 (1982)
- Rode, C. V., "Studies in Multiphase Reactors", Ph.D. Thesis, University of Poona (1990)
- Rommel, W., Meon, W., and Blass, E., "Review- Hydrodynamic Modeling of Droplet Coalescence at Liquid-Liquid Interfaces", *Separation Science and Technology*, **27** (2), 129-59 (1992)
- Rosen, M. J., Surfactants and Interfacial Phenomena, 2nd ed., 180, Wiley, New York (1996)
- Rosen, M.J. and Hua, X.Y., "Dynamic Surface Tension of Aqueous Surfactant Solutions, 2. Parameters at 1 s and at Mesoequilibrium", *J. Colloid Interface Sci.* **139**, 397-407 (1990)
- Ross, D., Cavitation, Pergamon Press, New York, 203-51 (1976)
- Ross, S.L. and Curl, R.L., Paper No. 29b, Joint Chem. Eng. Conf., 4th, Vancouver, Sept. (1973)
- Rotta, J.C., Turbulente Stromungen, B.G. Teubner, Stuttgart (1972)
- Rowe, P. N. and Partridge, B. A., "A Note on the Initial Motion and Break-up of Two Dimensional Air Bubble in Water", *Chem. Eng. Sci.*, **19**, 81-2 (1964)

- Ruckenstein, E. and Jain, R.K., "Spontaneous Rupture of Thin Liquid Films", *J. Chem. Soc. Faraday II* **70**, 132-47 (1974)
- Saffman, P.G. and J.S. Turner, *J. Fluid Mech.* **I**, 16 (1956)
- Sagert, N. H. and Quinn, M. J., "The Coalescence of H<sub>2</sub>S and CO<sub>2</sub> Bubbles in Water", *Can. J. Chem. Eng.*, **54**, 392-8 (1976)
- Sagert, N. H. and Quinn, M. J., The Coalescence of Gas Bubbles in Dilute Aqueous Solution, *Chem. Eng. Sci.*, 1087-95 (1978)
- Sagert, N. H. and Quinn, M.J., Gribbs, S. C. and Rosinger, E. L. J., "Bubble Coalescence in Aq. Solutions of N-alcohols", In Foams, Akers, R. J. (ed.), Academic Press, London, 147-62 (1976)
- Salcudean, M.E., "Effect of Flow Obstructions on Flow Transitions and Pressure Drop in Two-phase Flows", in Encyclopedia of Fluid Mechanism, III: Gas-liquid Flow, 715-70 (1988)
- Sampson, K.J. and D. Ramkrishna, *J. Colloid Interface Sci.*, **104**, 269-76 (1985)
- Sasaki, T., Hattori, M., Sasaki, J. and Nukina, K.. "Studies of aqueous sodium dodecyl sulfate solutions by activity measurements", *Bull. Chem. Soc. Jpn.*, **48**(5), 1397-403 (1975)
- Saxena, A.K., Schumpe, A, Nigama, K.D.P. and Deckwer, W.D., "Flow Regimes, Holdup and Pressure Drop for Two Phase Flow in Helical Coils", *Can. J. Chem. Eng.*, **68**, 553-9 (1990)
- Scheele, G.F. and Leng, D.E., "Experimental Study of Factors which Promote Coalescence of Two Colliding Drops Suspended in Water", *Chem. Eng. Sci.*, **26**, 1867-79 (1971)
- Scheludko, A., "Thin Liquid Films", *Adv. Colloid Interface Sci.*, **1**, 391 (1967)
- Schneider, G., "Static mixers as gas/liquid reactors", *Inst. Chem. Eng. Symp. Ser.*, **121** (Fluid Mixing 4), 109-19 (1990)
- Schramm, L. L., Emulsions: Fundamentals and Applications in the Petroleum Industry, ed., American Chemical Society, 145 (1992)

- Schramm, L. L., Foams: Fundamentals and Applications in the Petroleum Industry, ed., American Chemical Society (1994)
- Scott, S.D., "Properties of Cocurrent Gas-Liquid Flow", in Advanced Chemical Engineering, **4**, 200-73 (1963)
- Seidshazileh, K., "Effect of Interfacial Characteristics on Phase Inversion in Liquid Dispersions", Ph.D. Thesis, Dalhousie University (1999).
- Sevik, M. and Park, S. H., "The Splitting of Drops and Bubbles by Turbulent Fluid Flow", *Trans. Soc. Mech. Engng J. Fluids Engng.*, **95**, 53-60 (1973)
- Shah, B. H. and D. Ramkrishna, *Chem. Eng. Sci.* **28**, 389-99 (1973)
- Shaw, D.J., Introduction to Colloid and Surface Chemistry, Butterworths & Co. Ltd., London, 78 (1988)
- Shaw, J.M., and R. Konduru, "The Behavior of Large Gas Bubbles at a Liquid-Liquid Interface. Part 2: Liquid Entrainment", *Can. J. Chem. Eng.*, **70**, 381-4 (1992)
- Shaw, R. C., Czarnecki, J., Schramm, L.L. and Axelson, D., "Bituminous Froths in the Hot-Water Flotation Process", in Foam: Fundamentals and Application in the Petroleum Industry, Schramm, Laurier L. Ed., American Chemical Society, New York (1994)
- Sheeintuch, M. and Shvartsman, S. "Spatiotemporal Patterns in Catalytic reactors", *AIChE J.*, **42** (4), 1041-68 (1996)
- Shende, R.V. and Mahajani, V.V., "Kinetics of Wet Air Oxidation of Glyoxalic Acid and Oxalic Acid", *Ind. Eng. Chem. Res.*, **33**, 25-30 (1994)
- Sheu, E.Y., De Tar, M.M. and Storm, D.A., "Interfacial Properties of Asphaltenes", *Fuel* **71**, 1277-1281 (1992)
- Simon, M. and Fonade, C., " Experimental Study of Mixing Performance using Steady and Unsteady jets", *Can. J. Chem. Eng.*, **71**(4), 507-13 (1993)
- Singh, P.N. and Ramkrishna, D., "Solution of Population Balance Equations by MWR", *Comput. Chem. Eng.*, **1**(1), 23-31 (1977)

- Sircar, S., "Gibbsian Surface Excess for Gas Adsorption-Revisited", *Ind. Eng. Chem. Res.*, **38**(10), 3670-82 (1999)
- Sirijeerachai, G., "Population Balance Analysis of Multiphase Systems", Ph.D. thesis, Dalhousie University, Halifax, Nova Scotia, Canada (2002)
- Skelland, A.H. and Kane, J.S., "Transient Drop Size in Agitated Liquid-Liquid Systems as Influenced by the Direction of Mass Transfer and Surfactant Concentration", *Ind. Eng. Chem. Res.*, **31**, 2556-63 (1992)
- Skelland, A.H.P. and Kanel, J.S., "Simulation of Mass Transfer in a Batch Agitated Liquid-Liquid Dispersion", *Ind. Eng. Chem. Res.*, **31**, 908-20 (1992).
- Sleicher, C.A., "Maximum Stable Drop Size in Turbulent Flow", *AIChE J.*, **8**, 471 (1962)
- Smith, R.V., "Two-phase, Two-component Critical Flow in a Venturi", *Transactions of the ASME (Journal of Basic Engineering)*, 147-55 (1972)
- Smith, S.M., "Coalescence Phenomena, In Phase - Interface Phenomena in Multiphase Flow", Edited by Hewitt, G.F., Mayinger, F. and Riznic, J.R., Hemisphere Publishing Co., New York, 293-307 (1991)
- Smoluchowski, M., "The Thermodynamics of Molecular Phenomena", *Physik. Z.*, **13**, 1064 (1913)
- Snider, D.M. and Andrews, M.J., "The Simulation of Mixing Layers Driven by Compound Buoyancy and Shear", *Transactions of ASME*, **118**, 370-6 (1996)
- Sovova, H., "A Model of Dispersion Hydrodynamics in a Vibrating Plate Extractor", *Chem. Eng. Sci.* **38** (11), 1863-72 (1983)
- Sovova, H., "Breakage and Coalescence of Drops in a Batch Stirred Vessel-II", *Chem. Eng. Sci.* **36**, 1567-73 (1981)
- Sovova, H., "Drop Size Distributions by Power Functions of Breakage and Coalescence", *Collection Czechoslovak Chem. Commun.*, **47**, 2393-402 (1982)
- Sovova, H., "Polydisperse Model of the VPE Extractor Hydrodynamics", *Collection Czechoslovak Chem. Commun.*, **51**, 801-8 (1986)



- Sovova, H. and Prochazka, J., "Breakage and Coalescence of Drops in a Batch Stirred Vessel-I. Comparison of Continuous and Discrete Models", *Chem. Eng. Sci.* **36**, 163-71 (1981).
- Spedding, P.L. and Chen, J.J.J., "Hold-up in Multiphase Flow", in "Encyclopedia of Fluid Mechanism", III: Gas-liquid Flow, 504 (1988)
- Sprow, F.B., "Drop Size Distributions in Strongly Coalescing Agitated Liquid-Liquid Systems", *AIChE J.*, **13** (5), 995-8 (1967).
- Sridhar, T. and Potter, O. E., "Gas Holdup and Bubble Diameters in Pressurized Gas-Liquid Stirred Vessels, *Ind. Eng. Chem. Fundam.* **19**, 21-6 (1980)
- Stamatoudis, M., "The effect of continuous phase viscosity on the dynamics of liquid-liquid dispersions in agitated vessels", Ph.D. thesis, Illinois Institute of Technology, Chicago, (1977)
- Stenstrom M. K. and Gilbert R.G., "Effects of Alpha, Beta, and Theta Factors on the Design, Specification and Operation of Aeration Systems", *Water Res.*, **15**, 643-54 (1981)
- Stewart, C.W. "Bubble Interaction in Low - Viscosity Liquid", *Int. Multiphase Flow*, **21** (6), 1037-46 (1995)
- Subramanian, G., Ramkrishna, D., Fredrickson, A.G., and Tsuchiya, H.M., "On the Mass Distribution Model for Microbial Cell Populations", *Bull. Math. Biophys.* **32**, 521-37 (1970)
- Sun, T.-Y. and Faeth, G.M., "Structure of Turbulent Bubbly Jets - I. & II Methods and Centerline Properties", *Int. J. Multiphase Flow*, **12** (12), 99-126 (1986)
- Tadros, Th. F., "Fundamental Principles of Emulsion Rheology and Their Applications ", *Colloids Surf., A.*, **91** (Nov. 3), 39-55 (1994)
- Taitel, Y., Bornea, D., and Dukler, A.E., "Modelling Flow Pattern Transitions for Steady Upward Gas-Liquid Flow in Vertical Tubes", *AIChE J.*, **26** (3), 345-54 (1980).
- Tatterson, G.B., Fluid Mixing and Gas Dispersion in Agitated Tanks, McGraw-Hill Inc. (1991)

- Tavlarides, L. and Stamatoudis, M., "The Analysis of Interphase Reactions and Mass Transfer in Liquid-Liquid Dispersions", *Adv. in Chem. Eng.*, **11**, 199-273 (1981)
- Taylor, G. I., "The Instability of Liquid Surfaces when Accelerated in a Direction Perpendicular to Their Planes", *Proc. Royal Soc.*, **A201**, 192-6 (1950)
- Thomas, A.D., "New Analysis of non-Newtonian Turbulent Flow - Yield-power-law Fluids", *Can. J. Chem. Eng.*, **65**, 335-8 (1987)
- Thomas, R.M., "Brief Communication: Bubble Coalescence in Turbulent Flows", *Int. J. Multiphase Flow*, **7**(6), 709-17 (1981)
- Tjaberinga, W.J., Boon, A. and Chesters, A.K., "Model experiments and Numerical Simulations on Emulsification under Turbulent Conditions", *Chem. Eng. Sci.*, **48** (2), 285-93 (1993)
- Tobin, T., Muralidhar, R., Wright, H., and Ramkrishna, D., "Determination of Coalescence Frequencies in Liquid-Liquid Dispersions: Effect of Drop Size Dependence", *Chem. Eng. Sci.*, **45** (12), 3491-504 (1990)
- Tsuchiya, K., Ohsaki, K. and Taguchi, K., "Large and Small Bubble Interaction Patterns in a Bubble Column", *Int. J. Multiphase Flow*, **22**(1), 121-32. (1996)
- Uchida, T. and Iguchi, M., "Entrapment of Small Bubbles into Liquid By Breakup of a Bubble Escaping from the Bath Surface", *J. Materials Processing & Manufacturing Science*, **8** (3), 256-264 (2001)
- Ulrich, G.D. and Riehl, J.W., "Aggregation and Growth of Submicron Oxide Particles in Flames", *J. Colloid Interface Sci.*, **87** (1), 257-65 (1982)
- Valentas, K. J. and Amundson, N.R., "Breakage and Coalescence in Dispersed Phase System", *Ind. Eng. Chem. Fundam.*, **5**, 533 (1966)
- van der Welle, R., "Void Fraction, Bubble Velocity and Bubble Size in Two-Phase Flow", *Int. J. Multiphase Flow*, **11** (3), 317-45 (1985)
- van Hunsel, J. and Joos, P., "Steady-state dynamic interfacial tensions of 1-alkanols during mass transfer across the hexane/water interface", *Langmuir*, **3**(6), 1069-74 (1987)

- Vanýsek, P., "Ionic Conductivity and Diffusion at Infinite Dilution", in Perry's Chemical Engineering Handbook, Perry, R.H. and Green, D.W. eds., 5-98 (1997).
- Varadaraj, R., Bock, J., Valint, P., Zushma, S. and Brons, N., "Relationship between Fundamental Interfacial Properties and Foaming in Linear and Branched Sulfate, Ethoxysulfate, and Ethoxylate Surfactants", *J. Colloid Interface Sci.* **140**, 31-34 (1990).
- Varadaraj, R., Bock, J., Zushma, S., Brons, N. "Relationships Between Dynamic Contact Angle and Dynamic Surface Tension Properties for Linear and Branched Ethoxylate, Ethoxysulfate, and Sulfate Surfactants", *J. Colloid Interface Sci.*, **147** (2), 403-6 (1991).
- Varley, J., "Mixing Energies for Submerged Jet Gas-liquid Transfer", *Inst. Chem. Eng. Symp. Ser.*, 121 (Fluid Mixing 4), 121-36 (1990),
- Velev, O. D., Danov, K. D. and Ivanov, I. B., "Stability of Emulsions Under Static and Dynamic Conditions", *J. Dispersion Sc. and Tech.*, **18**, 625-45 (1997)
- Venkatesan, V.S., "Determination of Average Bubble Size and Its Distribution Using a Video Technique", Technical Report, Inst. of Technische Chemie I, Erlangen, Germany (1991)
- Verwey, E.J.W. and Overbeek, T.Th.G., Theory of Stability of Lyophobic Colloids, Elsevier, Amsterdam (1948)
- Villiermaux, J., "The Role of Energy Dissipation in Contacting and Mixing Devices", *Chem. Eng. Technol.*, **11**, 276-87 (1988)
- Vogler, E.A., "A Simple Mathematical Model of Time-Dependent Interfacial Tension", *J. Colloid Interf. Sci.*, **133**, 228-36 (1989).
- Vrij, A., " Possible Mechanism for the Spontaneous Rupture of Thin, Free Liquid Films", *Disc. Faraday Soc.*, **42**, 23-33 (1966)
- Vrtovsek, J., Recelj, T., and Golob, J., "Influence of Various Components on Bubble Coalescence in Gas-Liquid Dispersions", *Vestn. Slov. Kem. Drus.* **36**, 201-13 (1989)

- Walker, L.D., "Liquid-Liquid Dispersion Processes in Static Mixers", M. Sc. Thesis, Technical University of Nova Scotia, Halifax, NS, Canada (1984)
- Wallis, G. B., One-dimensional two-phase Flow, McGraw-Hill, New York (1969)
- Wallis, G.B. and Sullivan, D.A., "Two-phase Air-Water Nozzle Flow", Transactions of the ASME (Journal of Basic Engineering), 788-94 (Dec., 1972)
- Walter, J. F., "Bubble Break-up and Mass Transfer in Gas-liquid Contactors", Ph.D. Thesis, University of California, Berkeley (1983)
- Walter, J. H. and Blanch, H. W., "Bubble Break-up in Gas-Liquid Bioreactors: Break-up in Turbulent Flows", Chem. Eng. J., **32**, B7-17 (1986)
- Wang, C. Y. and Calabrese, R. V., "Drop Break up in Turbulent Stirred-Tank Contactors, Part II: Relative Influence of Viscosity and Interfacial Tension", AIChE J., **32**(4), 667-676 (1986).
- Wang, Y-C. and Brennen, C.E., "One-dimensional Bubbly Cavitating Flows through a Converging-diverging Nozzle", Transactions of the ASME, **120**, 166-70 (1998)
- Ward, A.F.H. and Tordai, L., "Time Dependence of Boundary Tensions of Solutions-The Role of Diffusion in Time Effect", J. Chem. Physics **14**, 453-359 (1946).
- Wasan, D. T., Shah, S. M., Aderanjani, N., Chan, M. S. and McNamara, J. J., "Observation on the Coalescence Behavior of Oil Droplets and Emulsion Stability in Enhanced Oil Recovery", Society of Petroleum Engineer J., 409-417 (1978)
- Wasan, D. T., Shah, S. M., Sampath, K., and Aderanjani, N., "The Role of Coalescence Phenomena and Interfacial Rheological Properties in Enhanced Oil Recovery: An Overview", J. Soc. Rheol., **23**, 181-207 (1979)
- Weisman, J., Duncan, D. Gibson, J. and Crawford, T., "Effects of Fluid Properties and Pipe Diameter on Two-Phase Flow Patterns in Horizontal Lines", Int. J. Multiphase Flow, **5**, 437-62 (1979)

- Weissenborn, P.K. and Pugh, R., "Surface Tension of Aqueous Solutions of Electrolytes: Relationship with Ion Hydration, Oxygen Solubility, and Bubble Coalescence", *J. Colloid Interface Sci.*, **184**, 550-63 (1996)
- Wilkinson, P. M. and van Dierendonck, L. L., "Pressure and Gas Density Effects on Bubble Break-up and Gas Hold-up in Bubble Columns", *Chem. Eng. Sci.*, **45**, 2309-15 (1990)
- Wilkinson, P. M., Schayk, A. V. and Spronken, L. P. M., "The Influence of Gas Density and Liquid Properties on Bubble Breakup", *Chem. Eng. Sci.*, **48** (7), 1 213-26 (1993)
- William, J.J.E. and Crane, R.I., "Particle Collision Rate in Turbulent Flow", *Int. J. Multiphase Flow*, **9**, 421-35 (1983)
- Witte, J.H. "Mixing shocks in two-phase flow", *J. Fluid Mech.* **36** (4), 639-55 (1969)
- Woolfrey, S.G., Banzon, G.M., and Groves, M.J., "The Effect of Sodium Chloride on the Dynamic Surface Tension of Sodium Dodecyl Sulfate Solutions", *J. Colloid Interface Sci.*, **112** (2), 583-7 (1986)
- Xu, Z., Finch, J.A., "Direct method for studying collector adsorption on minerals in mixed-mineral system", *Trans. Inst. Min. Metall., Sect. C* 105, (1996).
- Yang, J., "Efficient Gas-Liquid Contacting for Industrially-Relevant Systems", M.Sc. thesis, Technical University of Nova Scotia, Halifax, Nova Scotia, Canada (1995)
- Yang, Y. M. and Maa J. R., "Bubble Coalescence in Dilute Surfactant Solutions", *J. of Colloid Interface Sci.*, **98** (1), 120-5 (1984)
- Yuan, N., Du, J., Hu, H., Liu, Z. and Ding, F., "Dynamic Characteristics of Bubble Distribution Zone in Gas-Liquid Reactors", *Shiyu Xuebao*, 134-140 (1997)
- Yuu, S. and Toyoda, A. "Large-scale structures in a slit nozzle turbulent air jet". *J. Chem. Eng. Jpn.*, **22**(5), 497-504 (1989),

- Zahradnik, J., Fialova, M., Kastanek, F., Green, K.D. and Thomas, N.H. "The Effect of Electrolytes on Bubble Coalescence and gas Holdup in Bubble Column Reactors", *Trans I. Chem. E.*, **73**, part A, 341-6 (1995)
- Zahradnik, J., Fialova, M., Linek, V., Sinkule, J., Reznickova, J. and Kastanek, F., "Dispersion Efficiency of Ejector-Type Gas Distributors in Different Operating Modes" *Chem. Eng. Sci.*, **52**, 4499-4510 (1997)
- Zahradnik, J., Kuncova, G. and Fialova, M., "The Effect of Surface Active Additives on Bubble Coalescence and Gas Holdup in Viscous Aerated Batches", *Chem. Eng. Sci.* **54**, 2401-8 (1999).
- Zahradnik, J. and Ryler, M. "Design and Scale-up of Venturi-Tube Gas Distributors for Bubble Column Reactors", *Collect. Czech. Chem. Commun.*, **56**, 619-35 (1991)
- Zakharov, L.V., Ovchinnikov, A.A. and Nikolayev, N.A. "Modelling of the effect of turbulent two-phase flow friction decrease under the influence of dispersed phase elements", *Int. J. Heat Mass Transfer*, **36** (7), 1981-91 (1993)
- Zeitlin, M.A. and Tavlarides, L.L., "Dispersed phase reactor model for predicting conversion and mixing effects", *AIChE J.*, **18**(6), 1268-71 (1972)
- Zhang, Y.M. and Kavetsky, A., "Investigation of Particle Breakage Mechanisms in a Batch Ball Mill Using Back-calculation", *Int. J. Miner. Process.*, **39**, 41-60 (1993).
- Zhou, G. and Kresta, S.M., "Correlation of Mean Drop Size and Minimum Drop Size with Turbulence Energy Dissipation and the Flow in an Agitated Tank", *Chem. Eng. Sci.*, **53** (11), 2063-79 (1998)
- Zhou, Z.A., Xu, Z., Finch, J.A., Hu, H. and Rao, S.R., "Role of Hydrodynamic Cavitation in Fine Particle Flotation", *Int. J. Miner. Process.*, **51**, 139-49 (1997)
- Zhou, Z.A., Plitt, L.R. and Egtebor, N.O., "The Effects of Solids and Reagents on the Characteristics of Coal Flotation in Columns", *Minerals Engineering*, **6** (3), 291-306 (1993)

Zlokarnik, M., "Tower-Shaped Reactors for Aerobic Biological Waste Water Treatment",  
in Biotechnology, M. Zlokarnik and H. Brauer, eds., VCH, Weinheim, Germany,  
537-69 (1985)

Zuber, N. and Findlay, J. A., "Average Volumetric Concentration in Two-Phase Flow  
Systems", J. Heat Transfer, 453-68 (1965)